Progress in the Determination Of the Earth's Gravity Field

Extended Abstracts
For the meeting held in Ft. Lauderdale, Florida
September 13–16, 1988

Edited by
Richard H. Rapp

PROGRESS IN THE DETERMINATION OF THE EARTH'S GRAVITY FIELD

Extended Abstracts

for the meeting held in Ft. Lauderdale, Florida
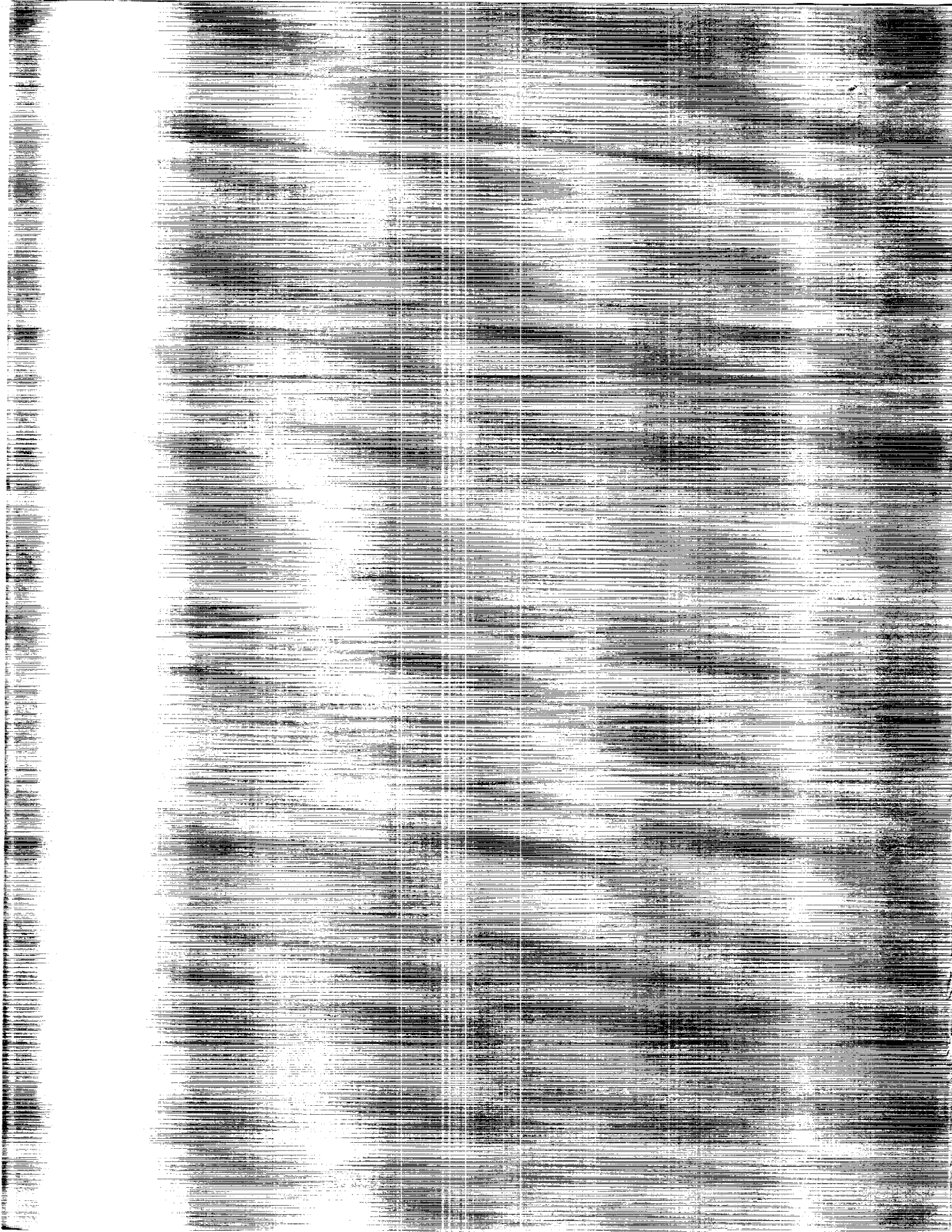
September 13-16, 1988

Edited by

Richard H. Rapp

Preface

This report contains the extended abstracts of the papers presented at the Chapman Conference on Progress in the Determination of the Earth's Gravity Field which was held at the Bahia Mar Hotel, Fort Lauderdale, Florida, September 13-16, 1988. This meeting was organized and sponsored by the American Geophysical Union. Chapman Conferences are topical meetings designed to permit organized and in-depth exploration of specialized subjects in a manner seldom possible at large meetings. The series of conferences was inaugurated by AGU in 1976 in honor of Sydney Chapman, who was "a trail-breaker in mathematics, physics, geophysics, astronomy, kinematic theory of gases, lunar effects in geophysics, and upper atmosphere physics." The meeting was co-sponsored by the International Association of Geodesy. Financial support for the meeting was provided by the National Aeronautics and Space Administration and the Air Force Geophysics Laboratory.

The meeting was divided into five different topic areas. Members of the program committee organized the sessions on the basis of invited and contributed papers. Members of the organizing committee were: B. Hager, C. Jekeli, R. Rapp, C. Reigber, R. Rummel, K.P. Schwarz, D. Smith, and B. Tapley, C. C. Tscherning, and V. Zlotnicki.

Table of Contents

Topic IV: Global Gravity Field Applications and Requirements in Geophysics and Oceanography

Topic V: Future Gravity Missions

Gravitational Model Improvement at the Goddard Space Flight Center

J. G. Marsh, F.J. Lerch, B. H. Putney, T. L. Felsentreger, B. V. Sanchez,
and D. E. Smith
Geodynamics Branch, Laboratory for Terrestrial Physics
NASA Goddard Space Flight Center, Greenbelt, Maryland

S. M. Klosko, E. C. Pavlis, J. W. Robbins, R. G. Williamson, O. L. Colombo,
D. D. Rowlands, W. F. Eddy, N. L. Chandler, and K.E. Rachlin
EG&G Washington Analytical Services Center, Inc., Lanham, Maryland

G. B. Patel, S. Bhati, and D. S. Chinn
Science Applications Research, Lanham, Maryland

ABSTRACT

Major new computations of terrestrial gravitational field models have been performed by the Geodynamics Branch of Goddard Space Flight Center [GSFC]. This development has incorporated the present state of the art results in satellite geodesy and have relied upon a more consistent set of reference constants than has heretofore been utilized in GSFC's GEM models. The solutions are complete in spherical harmonic coefficients out to degree 50 for the gravity field parameters. These models include adjustment for a subset of 66 ocean tidal coefficients for the long wavelength components of 12 major ocean tides. This tidal adjustment was made in the presence of 550 other fixed ocean tidal terms representing 32 major and minor ocean tides and the Wahr frequency dependent solid earth tidal model. In addition 5-day averaged values for Earth rotation and polar motion were derived for the time period of 1980 onward. Two types of models have been computed. These are "satellite only" models relying exclusively on tracking data and "combination" models which have incorporated satellite altimetry and surface gravity data. The satellite observational data base consists of over 1100 orbital arcs of data on 31 satellites. A large percentage of these observations have been provided by third generation laser stations [< 5 cm] . A calibration of the model accuracy of the GEM-T2 "satellite only" solution indicated that it was a significant improvement over previous models based solely upon tracking data. The rms geoid error for this field is 110 cm to degree and order 36. This is a major advancement over GEM-T1 whose errors were estimated to be 160cm. An error propagation using the covariances of the GEM-T2 model for the TOPEX radial orbit component indicates that the rms radial errors are expected to be 12 cm. The "combination" solution, PGS-3337, is a preliminary effort leading to the development of GEM-T3. PGS-3337 has incorporated global sets of surface gravity data and the Seasat altimetry to produce a model complete to [50,50]. A solution for the dynamic ocean topography to degree and order 10 was included as part of this adjustment.

INTRODUCTION

High precision ground based tracking of artificial satellites has provided an observational data set which has formed the basis for long-wavelength spherical harmonic models of the Earth's gravitational field. These data have been used at GSFC to calculate improved gravitational field models. Improvements in modeling the Earth's gravitational field are important for the calculation of artificial orbit trajectories, for point positioning, for studies

Global Gravity Model Development

Moderators: Byron Tapley

Richard Rapp

of the Earth's rheology, and for ocean circulation studies with satellite altimetry.

The TOPEX ocean topography satellite, which is planned for launch in 1991, requires that the contribution of the uncertainty in the geopotential model to the radial component of the orbital error budget be on the order of 10 cm. The best previously available "satellite only" model, GEM-L2 [Lerch et al., 1982], predicted radial errors for TOPEX on the order of 65 cm. Meeting the error budget for TOPEX is one of the motivating factors behind the current efforts to improve the overall gravitational field modeling capabilities.

The general philosophy adopted in this computation process has been to analyze the observational data in stages. Within each step of the process, individual data sets are separately evaluated and combined in order to extract optimum subset solutions. The initial emphasis has been placed upon the computation of "satellite only" models. The first such model, designated GEM-T1 [Marsh et al., 1988] , was the first preliminary GSFC model computed in this effort. Recently, a very significant augmentation of the satellite observational data base has permitted the compution of the GEM-T2 model. In an attempt to provide additional short wavelength gravitational information over the ocean areas and to provide an observational basis for the derivation of short wavelength geoid features, a preliminary model, PGS-3337 has incorporated the SEASAT altimeter data set along with surface gravimetry. The final model will be based upon the best combination of optical, laser, altimeter, satellite-to-satellite tracking, and surface gravity data.

TECHNIQUE

The primary software tools used at GSFC for precision orbit and geodetic parameter estimation are the GEODYN and SOLVE programs. The GEODYN program [Martin et al., 1987] uses fixed-integration-step , high-order Cowell predictor-corrector numerical integration techniques. The force models used in the analyses are: gravitation-Earth,luni-solar, and planetary, solar radiation pressure, atmospheric drag, and solid earth and ocean tides. Observation modeling included Earth precession and nutation, polar motion and earth rotation, and solid earth tidal displacements. The normal equations formed within GEODYN for the force and measurement model parameters are output to a file for inclusion in large parameter estimations and error analyses.

The SOLVE program selectively combines and edits the least squares normal equations to form the solutions for the parameters of interest. These programs are run on the GSFC Cyber 205 super computer.

TRACKING DATA

Tracking data from 17 and 31 satellites respectively, were used in the GEM-T1 and GEM-T2 gravitational modeling solutions. The satellite names, inclinations, data types and number of orbital arcs are summarized in Table 1. Orbital arc lengths were typically seven days for the optical data, 5 days for laser/Doppler data arcs with the exception of 30-day arcs used for Lageos. These solution were primarily based upon high quality laser ranging observations with single point accuracies now approaching 1 cm. The inclusion of a carefully selected sets of optical and electronic observations from a diverse set of spacecraft provided a valuable complement to the limited inclination coverage provided by the laser data.

4

GRAVITATIONAL MODEL AND OCEAN TIDAL SOLUTIONS

The solutions consisted of simultaneous adjustments for the spherical harmonic invariant geopotential coefficients and a subset of 66 ocean tidal coefficients for the long-wavelength components of 12 major ocean tides. The GEM-T1 gravity model is complete to [36,36], while the GEM-T2 model has been extended to include selected coefficients out to degree 50. A unified coordinate system was developed for the tracking stations based upon the laser coordinate system developed at GSFC from LAGEOS tracking [Smith et al., 1985].

CALIBRATION OF THE MODEL ACCURACY

The method for determining reliable error variances for the GSFC gravity model solutions employs both independent and dependent data subset solutions. Calibration techniques have been developed which yield a full field coefficient by coefficient estimate of the model uncertainties. The accuracy of the new GSFC gravity field models is more than a factor of two better than any previous models. The details of the data weighting and calibration techniques are presented in [Lerch et al., 1988]. Figure 1 presents the rms radial error for the TOPEX satellite predicted from the calibrated covariance matrices. The total rms error on TOPEX estimated for the GEM-T1 model is 25cm and 12 cm for GEM-T2.

CONCLUSIONS

The present GSFC gravitational and geodetic parameter solutions have been the result of a complete re-evaluation of previous solution design. A level of internal consistency and accuracy higher than that of any previous GSFC models has been achieved. Error calibration techniques have been developed which now permit the computation of realistic error estimates for the accuracy of the field and satellite ephemerides. In subsequent solutions planned for the next few years additional parameters such as time dependency in the geopotential and tracking station coordinates will be included. The inclusion of satellite altimetry from Geos-3, Seasat, and Geosat as well as the global set of surface gravity data will permit computations complete to [50,50] and beyond.

REFERENCES

Lerch, F.J., S.M. Klosko, and G.B. Patel, Gravity Model Development from Lageos, Geophys. Res. Lett., 9, 1263-1266, 1982.

Lerch, F.J., J.G. Marsh, S.M. Klosko, E.C. Pavlis, G.B. Patel, D.S. Chinn, C.A.Wagner, An Improved Error Assessment for the GEM-T1 Gravitational Model, Goddard Space Flight Center Technical Memorandum in preparation, presented at the Chapman Conference for Progress in the Determination of the Earth's Gravity Field, Ft. Lauderdale, Florida, September 12-16, 1988.

Marsh, J.G., et al., A New Gravitational Model for the Earth from Satellite Tracking Data: GEM-T1, J. Geophys. Res., 93, B6, 6169- 6215, 1988.

Martin, T.V., W.F. Eddy, D.D. Rowlands, and D.E. Pavlis, Vol. 1-5, GEODYN-II System Description, Contractor Report, EG&G, Lanham, MD, 1987.

Smith, D.E., et al., A Global Geodetic Reference Frame from LAGEOS Ranging [SL5-1AP], J. Geophys. Res., 90, 9221-9235, 1985.

Tapley, B.D., C.K. Shum, D.N. Yuan, J.C. Ries and B.E. Schutz, An Improved Model for the Earth's Gravity Field, presented at the Chapman Conference for Progress in the Determination of the Earth's Gravity Field, Ft. Lauderdale, Florida, 1988.

Table 1 — GEM-T2 TRACKING DATA SUMMARY

SAT. NAME	INCLINATION (DEG)	DATA TYPE*	ARCS GEM-T1	ARCS GEM-T2
ATS-6/GEOS-3	0/115.0	SST	-	26
PEOLE	15.0	L,O	6	6
COURIER-1B	28.3	O	10	10
VANGUARD-2	32.9	O	10	10
VANGUARD-2RB	32.9	O	10	10
D1-D	39.5	L,O	15	15
D1-C	40.0	L,O	14	14
BEC	41.2	L,O	89	89
TELESTAR-1	44.8	O	30	30
ECHO-1RB	47.2	O	-	32
STARLETTE	49.8	L	46	157
AJISAI	50.0	L	-	36
ANNA-1B	50.1	O	30	30
GEOS-1	59.3	L,O	91	121
TRANSIT-4A	66.8	O	-	50
INJUN-1	66.8	O	-	44
SECOR-5	69.2	O	-	13
BE-B	79.7	O	20	20
OGO-2	87.4	O	-	16
OSCAR	89.2	D	13	13
OSCAR-7	89.7	O	-	4
5BN-2	90.0	O	-	17
NOVA	90.0	D	-	16
MIDAS-4	95.8	O	-	50
LANDSAT-1	98.5	S-BAND	-	10
GEOS-2	105.8	L,O	74	74
SEASAT	108.0	D,L	29	29
GEOSAT	108.0	D	-	13
LAGEOS	109.9	L	58	85
GEOS-3	114.9	L	36	86
OVI-2	144.3	O	-	4
TOTAL			581	1130

*SST Satellite-to-Satellite Tracking

L   Laser ranging

O   Optical

D   Doppler

S-Band   Unified S-Band average range-rate

Figure 1 TOPEX PROJECTED RADIAL ERROR

RMS PER ORDER

GEM-T1 (TOTAL RMS =25.3)

PGS3429+ (TOTAL RMS = 11.7)

CENTIMETERS

ORDER
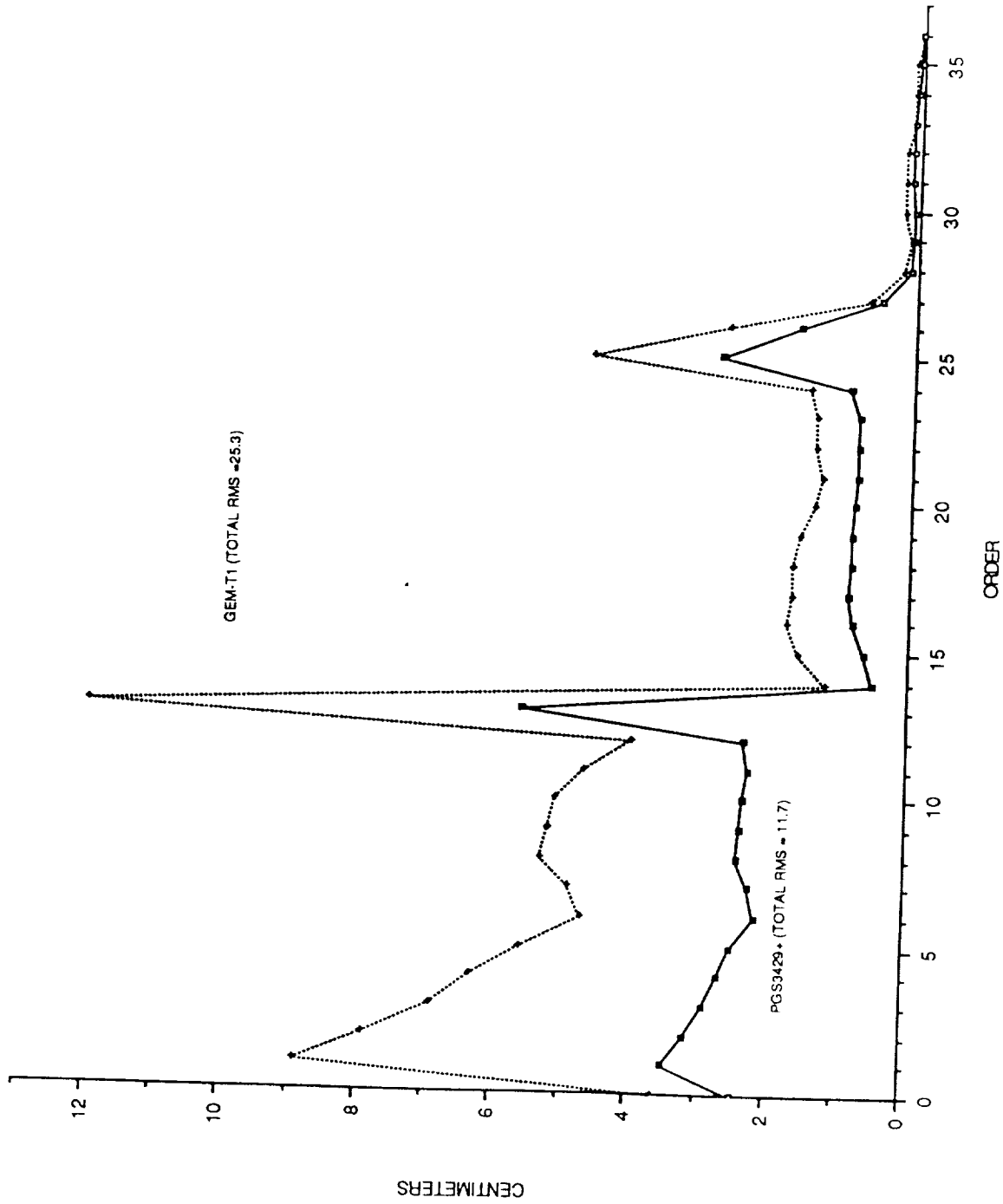
+ PGS3429 = (PRELIM. GEM-T2)

7

An Improved Model for the Earth's Gravity Field

B. D. TAPLEY, C. K. SHUM, D. N. YUAN, J. C. RIES AND B. E. SCHUTZ

Center for Space Research, The University of Texas at Austin, Austin, Texas

ABSTRACT

An improved model for the Earth's gravity field, TEG-1, has been determined using data sets from fourteen satellites, spanning the inclination ranges from 15° to 115°, and global surface gravity anomaly data. The satellite measurements include laser ranging data, doppler range-rate data, and satellite-to-ocean radar altimeter data measurements, which include the direct height measurement and the differenced measurements at ground track crossings (crossover measurements). Also determined was another gravity field model, TEG-1S, which included all the data sets in TEG-1 with the exception of direct altimeter data. The effort has included an intense scrutiny of the gravity field solution methodology. The estimated parameters included geopotential coefficients complete to degree and order 50 with selected higher order coefficients, ocean and solid Earth tide parameters, doppler tracking station coordinates and the quasi-stationary sea surface topography. Extensive error analysis and calibration of the formal covariance matrix indicate that the gravity field model is a significant improvement over previous models and can be used for general applications in geodesy.

1. INTRODUCTION

Significant progress has been achieved during the last decade in the determination of the spherical harmonic coefficients of the Earth's external gravitational potential. A substantial portion of this progress can be directly attributed to the advent of Earth-orbiting artificial satellites and to the ability to observe their motion from either ground-based or satellite-originated tracking data. While the satellite data primarily resolve the long and intermediate wavelengths (≥ 1500 km), global surface gravity measurements and the altimeter data are capable of recovering the shorter wavelength components of the Earth's gravity field. Recent trends in gravity model improvement have been driven, in part, by requirements for more accurate satellite orbits to achieve the objectives of the Crustal Dynamics Project and the recently approved NASA/CNES Topex/Poseidon mission. A joint effort to develop an improved model for the Earth's gravity field has been undertaken to develop a gravity model to meet the orbit accuracy requirement of the Topex/Poseidon mission. The gravity field solution will represent the first complete reiteration of the historical tracking data used to define the NASA Goddard Space Flight Center (GSFC) Earth Model series. The GSFC GEM-T1 [*Marsh et al.*, 1988] and the University of Texas (UT) TEG-1 fields, described in this paper, are preliminary versions of the Topex gravity field solution.

2. THEORY AND METHOD

The gravitational potential, U, due to the Earth's nonspherical mass distribution can be expressed as follows

$$U = \frac{GM}{r} \sum_{l=0}^{\infty} \sum_{m=0}^{l} \left[\frac{R_e}{r}\right]^l \bar{P}_{lm}(\sin\phi)\left[(\bar{C}_{lm}+\Delta\bar{C}_{lm})\cos m\lambda + (\bar{S}_{lm}+\Delta\bar{S}_{lm})\sin m\lambda\right]$$

where GM is the product of the gravitational constant and the total mass of the Earth and the atmosphere; R_e is the mean equatorial radius of the Earth; $\bar{P}_{lm}$ are the normalized Legendre associated function of degree l and order m; $\bar{C}_{lm}, \bar{S}_{lm}$ are the the normalized spherical harmonic coefficients whose values are functions of the mass distribution within the Earth and the atmosphere; $\Delta\bar{C}_{lm}, \Delta\bar{S}_{lm}$ are the time-varying components of $\bar{C}_{lm}$ and $\bar{S}_{lm}$ caused by tides; also are functions of the tidal coefficients, $C_{lm}^{\pm}$ and $S_{lm}^{\pm}$; and r,ϕ,λ are the Earth-fixed spherical coordinate system; r is the

radial distance, ϕ is the geocentric latitude and λ is the longitude measured from the Greenwich meridian.

The estimation of $\bar{C}_{lm}, \bar{S}_{lm}$, $C_{lm}^{\pm}, S_{lm}^{\pm}$ and other orbit and geophysical parameters can be accomplished using a modified least-squares estimation procedure. This estimation procedure, which provides adjustments to satellite orbit-dependent parameters and other geophysical and geodetic parameters, is given by *Tapley* [1973] and modified to include the simultaneous estimation of the relative weights for the individual satellite information arrays [*Yuan et al.*, 1988]:

$$\hat{x} = (H^T \hat{R}^{-1} H)^{-1} H^T \hat{R}^{-1} y \;\; ; \;\; \hat{R}_i = 1/k_i \, (y_i - H_i \hat{x})^{-1} \, (y_i - H_i \hat{x}) \cdot I$$

where $\hat{x}$ is the state parameter; $\hat{R}$ is the weighting matrix; I is the identity matrix; H_i is the partial derivative with respect to x for the ith data set; and k_i is the number of observations for ith dataset.

The system of equations given above can be solved iteratively using orthogonal transformation techniques [*Gentleman*, 1973]. The estimation process has been implemented in the University of Texas Orbit Processor (UTOPIA) software system [*Schutz and Tapley*, 1980]. The optimal weighting algorithm to combine satellite and nonsatellite information equations was installed in the Large Linear System Solver (LLISS). Vectorized versions of UTOPIA and LLISS are operational on the University of Texas System Center for High Performance Computing Cray X-MP/24 supercomputer. Reference orbits for each of these satellites were computed using UTOPIA with the best *a priori* gravity model and gravity field information equations were generated for each data set. The combination solution was performed using LLISS.

3. DATA AND MODELS

Fourteen satellites were selected for the current gravity model solution. Their orbital characteristics and data types are summarized in Table 1. The inclinations of these satellite orbits vary from 15° for Peole to 115° for Geos-3. The solution includes data at 90° for Oscar-14 and Nova-1. Data types include laser range, one-way range-rate, altimeter, altimeter crossover and surface gravity data. Detailed descriptions of the gravitational and nongravitational force models, the Earth orientation and time model, laser, doppler, direct altimeter and surface gravity measurement models are summarized in *Tapley et al.* [1987].

4. SOLUTION

The list of parameters which are simultaneously estimated with a relative weighting factor for each data set include: (1) geopotential complete to degree and order 50, plus selected coefficients; (2) GM, (3) ocean tides which include long period tides ($m = 0$, $l = 2,3$): Ssa, Sa, Mm, and Mf; diurnal tides ($m = 1$, $l = 2,3,4,5$): Q1, O1, P1, and K1; semi-diurnal tides ($m = 2$, $l = 2,3,4,5$): N2, M2, S2, K2 and T2 ($l = 2$); (4) quasi-stationary sea surface topography, complete to degree and order 15; (5) equipotential surface, W_o, or altimeter biases; (6) correction to significant wave height, $H_{1/3}$; (7) doppler and low inclination satellite laser station coordinates; (8) arc parameters for satellite orbits, which include position and velocity vectors, drag and solar radiation pressure coefficients, density correction parameters for selected satellites, and pass-dependent frequency biases for doppler satellites. Kaula's constraint equation [*Kaula*, 1966], which was inferred from surface gravity anomaly data, was used as an *a priori* constraint for degrees 19–50 of the geopotential. Two gravity models, TEG-1 and TEG-1S, were generated. TEG-1S did not include direct altimeter data.

5. ACCURACY EVALUATION

Efforts to evaluate and calibrate the accuracy of the UT gravity models were performed. Comparison of orbit fits using different gravity fields for Starlette, Ajisai, Seasat and Geosat were performed. It is shown that using TEG-1, a Starlette five-day orbit fit is at the ~20 cm level, Ajisai five-day orbit fit is at the ~15 cm level, and that a Seasat six-day orbit and a Geosat 17-day orbit have

Table 1. Satellite Data for the University of Texas Gravity Model, TEG-1					
Satellite	Launch Date	Data	Inclination	Eccentricity	Altitude (km)
Vanguard-1	1958	Optical†	34°	0.190	2318
Vanguard-2RB	1959	Optical†	33°	0.183	2318
Courier-1B	1965	Optical†	28°	0.016	1100
Geos-1	1965	Laser	59°	0.072	1600
BE-C	1966	Laser	41°	0.026	1130
DI-C	1967	Laser, Optical†	40°	0.053	1000
DI-D	1967	Laser, Optical†	39°	0.085	1200
Oscar-14	1967	Doppler	89°	0.005	1100
Geos-2	1968	Laser	106°	0.033	1400
Peole	1971	Laser, Optical†	15°	0.015	650
Geos-3	1975	Laser	115°	0.002	830
Starlette	1975	Laser	50°	0.020	900
Lageos	1976	Laser	110°	0.004	5900
Seasat	1978	Laser, Doppler, Altimeter and Crossover	108°	0.002	800
Nova-1	1980	Doppler	90°	0.002	1200
Geosat	1985	Doppler, Altimeter and Crossover	108°	0.000	800
Ajisai	1986	Laser	50°	0.001	1500
† Optical data currently withheld from gravity field solution					

Surface Gravity Data
1° × 1° terrestrial mean gravity anomaly from Ohio State University [Rapp, 1986]

crossover residuals at the ~25 cm level. Table 2 shows the summary for the Geosat orbit fits. Gravity field comparison using surface gravity data and a comparison of estimated TEG-1 ocean tidal parameters with solutions derived by other studies were also performed. Covariance matrices for TEG-1 and TEG-1S were calibrated to obtain estimates of errors associated with the gravity field using the consider covariance calibration technique [Yuan et al., 1988]. The predicted radial orbit errors using TEG-1 gravity field covariance matrix for Topex and Geosat are 13 cm and 24 cm, respectively (Table 3).

6. CONCLUSION

In this investigation, two gravity models, TEG-1 and TEG-1S, each complete to degree and order 50 plus resonant coefficients, were generated. Ground-based tracking data collected by 14 satellites, altimeter crossover and surface gravity data were used to determine the TEG-1S gravity field model. TEG-1 contains Seasat and Geosat direct altimeter data in addition to all the data in TEG-1S. The gravity field models were derived simultaneously with orbit, ocean tides, quasi-stationary sea surface topography, and other geophysical parameters as well as the relative weights for each data set. The fields were evaluated using both data included and data withheld from the solution. Formal covariance matrices were calibrated to reflect realistic error estimates of the gravity field. Evaluations based on orbit fits and gravity anomaly residuals indicate that the gravity models have achieved a significant advancement over previously existing gravity models.

Table 2. Gravity Field Accuracy Evaluation Using Geosat Orbit Fits			
$\bar{r}_o, \bar{v}_o, C_R$, daily C_D, density correction parameters adjusted			
Epoch 17-day orbits		TEG-1S (rms)	TEG-1 (rms)
86/12/7	Doppler (cm/sec)	0.67	0.62
	Crossover (cm)†	25	22
	Altimeter (cm)†	180	32
87/01/7	Doppler (cm/sec)	0.62	0.61
	Crossover (cm)†	24	25
	Altimeter (cm)†	180	32

† Data types used for residual prediction only; altimeter data smoothed to represent gravity spectrum to (50×50)

Table 3. Gravity Field Accuracy Evaluation Using Covariance Analysis		
Model	Predicted Topex Radial Orbit Error (cm)	Predicted Geosat Radial Orbit Error (cm)
GEM-T1	25	54
TEG-1	13	24
Topex orbit: 65° inclination, 1354 km altitude Geosat orbit: 108° inclination, 800 km altitude		

REFERENCES

Gentleman, W. M., Least square computations by Givens transformation without square roots, *J. Inst. Math. Applic.*, *12*, 1973.

Kaula, W. M., Test and combination of satellite determinations of the gravity field with gravimetry, *J. Geophys. Res.*, *71*(22), 5304–5314, November 1966.

Marsh, J. G., et al., A new gravitational model for the Earth from satellite tracking data: GEM-T1, *J. Geophys. Res.*, *93*(B6), 6169–6215, June 10, 1988.

Schutz, B. E. and B. D. Tapley, UTOPIA: University of Texas Orbit Processor, *IASOM TR-80-1*, Center for Space Research, The University of Texas at Austin, 1980.

Tapley, B. D, Statistical orbit determination theory, *Recent Advances in Dynamical Astronomy*, 396–425, B. D. Tapley and V. Szebehely, Eds., D. Reidel Publ. Co., Holland, 1973.

Tapley, B. D., B. E. Schutz, C. K. Shum, J. C. Ries and D. N. Yuan, An improved model for the Earth's gravity field, *Proc. IUGG 19th General Assembly*, Vancouver, Canada, August 1987.

Yuan, D. N., C. K. Shum and B. D. Tapley, Gravity field determination and error assessment techniques, presented at the Chapman Conference for Progress in the Determination of the Earth's Gravity Field, Ft. Lauderdale, Florida, September 12–16, 1988.

Progress in the Development
of High Degree Potential Coefficient Models

Richard H. Rapp

Department of Geodetic Science and Surveying
The Ohio State University, Columbus, OH 43210, U.S.A.

Abstract

A natural extension of the recent satellite derived potential coefficient models is the development of high degree (maximum 180 or 360) expansions. Such expansions are based on the combination of the satellite derived models with terrestrial gravity data and satellite altimeter data. Such models are useful for more precise geoid undulation computations, for simulation studies involving different typed of future missions (e..g. gradiometry), and as reference fields for different types of gravimetric computations. The attention to the effect of the terrain, ellipsoidal terms, and weighting. This paper reviews the basic methods used for the high degree solutions. Various correction terms are described and recent models are discussed and compared.

1. Introduction

Potential coefficient models derived from satellite orbital analysis have been determined up to various maximum degrees depending on data coverage and data accuracy. Recent models have been complete to degree 36 and 50. The normal equations from these models can be combined with surface gravity normal equations to produce a combination of the satellite and terrestrial data. In some solutions the highest degree will be equal to the highest degree in the satellite model. In other cases the solution can be carried to a higher degree that is determined by the size of the mean anomaly cell. Certain types of combination solutions require extensive normal equation formation and solution. Other methods use orthogonality relationships to merge the satellite and surface gravity data. Several high degree potential coefficient models have been developed in the past few years. The model of Wenzel (1985) used the GEML2 potential coefficient model with 1°x1° mean anomalies to obtain a solution to degree 200. Rapp and Cruz (1986a) used GEML2 with 1° data and optimal estimation theory to develop fields to degree 250. Using 30' mean anomalies, where available Rapp and Cruz (1986b) developed a model complete to degree 360. Since 30' mean anomalies are not available on a global basis the actual frequency content of the model is geographically dependent.

High degree models can also be tailored to fit existing gravity data in a given geographic region. The fitting is necessary when inaccurate, or no, terrestrial data was used in the original development of the model. Such tailored models have been described by Weber and Zomorrodian (1988).

High degree potential coefficient models have a number of different applications. Some are: a) the calculation of reference models for gravimetric predictions; calculation of geoid undulations; model for simulation studies involving future gravity field missions; study of the global spectra of the Earth's gravity field.

2. Future Prospects

The next group of high degree potential coefficient models will depend on new satellite alone solutions, acquisition of new terrestrial data, improved satellite altimeter analysis and improved theoretical and numerical formulation of the mathematical problem.

In terms of satellite models, the GEMT1 and GEMT2 models have been or will be available (Marsh et al, this volume). The GEMT2 model will be carried to degree 50 although not all coefficients will be estimated.

An effort is underway to improve the terrestrial data base collection. Activities are continually taking place at the Defense Mapping Agency Aerospace Center and the Bureau Gravimetrique International. At Ohio State the development of updated 30' and 1° mean anomaly data bases is underway. Major improvements are expected for the anomaly fields in Canada, United States, Africa, Scandinavian countries, and other regions. We now have for the first time an identification of geophysical predicted anomalies in the 1° data base is available.

The altimeter analysis now being done at Ohio State will produce a more reliable set of 30' mean gravity anomalies in the ocean area. The improved analysis will have the following changes:

a) additional bias removal form the altimeter data based on an adjustment in a 4°x4° area using a procedure developed by Knudsen;

b) use of the Levitus sea surface topography to reduce the altimeter values to the geoid;

c) use of much denser data than used in the 1984 solutions;

d) all programs moved to the Cray XMP2/8.

In our next combination solutions we will have the following improvements over the previous Ohio State models:

a) the surface free-air anomalies will be reduced to the geoid using the g_1 correction terms calculated by Wang (1988, this volume);

b) the full error covariance matrix of the GEMTX model will be used in the adjustment process;

c) ellipsoidal harmonics will be used to for the improved treatment of terrestrial gravity data;

d) the actual adjustment will be done with 30' mean gravity anomalies formed from a merger of terrestrial, altimeter derived, and a prioi (derived from GEMTX) anomalies.

3. Conclusions

High degree potential coefficient models can be estimated form a combination of satellite and terrestrial gravity information. The new above models, now being developed, can be used with improved analysis methods and improved data collection. New models should be available to degree 360 in 1989.

Gravity Field Determination and Error Assessment Techniques

D. N. YUAN, C. K. SHUM AND B. D. TAPLEY

Center for Space Research, The University of Texas at Austin, Austin, Texas

ABSTRACT

Linear estimation theory, along with a new technique to compute relative data weights, has been applied to the determination of the Earth's geopotential field and other geophysical model parameters using a combination of satellite ground-based tracking data, satellite altimetry data, and the surface gravimetry data. The relative data weights for the inhomogeneous data sets are estimated simultaneously with the gravity field and other geophysical and orbit parameters in a least squares approach to produce the University of Texas gravity field models. New techniques to perform calibration of the formal covariance matrix for the geopotential solution have been developed to obtain a reliable gravity field error estimate. Different techniques, which include orbit residual analysis, surface gravity anomaly residual analysis, subset gravity solution comparisons and consider covariance analysis, have been applied to investigate the reliability of the calibration.

1. INTRODUCTION

Significant progress has been achieved during the last decade used in the determination of spherical harmonic coefficients in the representation of the Earth's external gravitational potential. A substantial portion of this progress can be directly attributed to the advent of Earth-orbiting artificial satellites and to the ability to precisely observe their motion from either ground-based or satellite-originated tracking data. One of the basic requirements for determination of the Earth's gravity field model using ground-based tracking of artificial satellites is that observations of the orbital motions of satellites with various inclinations, as well as different altitudes, be used in the solution. The development of satellite-to-satellite range or range difference measurements, as well as satellite-to-ocean-surface radar altimeter measurements have provided new means for the determination of the Earth's gravity field. The current approach to the gravity field solution uses orbital analysis for multi-satellites with different inclinations and altitudes to obtain the long wavelength features (wavelength ≥ 1500 km) of the Earth's gravity field and to use radar altimetry and surface gravimetric data to determine the shorter wavelength components. The combination of satellite, altimetry and surface gravity data requires efficient data processing and optimal data weighting techniques. An optimal method for simultaneously estimating the model parameters and the appropriate data weight is developed in this study. The development of appropriate techniques to calibrate the formal covariance matrix associated with the estimated gravity field to obtain a realistic error estimate is another goal of this study.

2. METHODOLOGY FOR THE GRAVITY FIELD SOLUTION

The linearized observation equations for each data set can be expressed as follows

$$y_i = H_i x + \varepsilon_i \qquad i = 1, \ldots, N \tag{1}$$

where x is the state vector of dimension n, y_i is the observation residual vector of dimension k_i, H_i is the linearized observation-state relationship with dimension $k_i \times n$, k_i being the number of observations for data set i, and ε_i is the observation error for data set i. If it is assumed that the observation error, ε_i, is random with zero mean and specified covariance, i.e.,

$$E[\varepsilon_i] = 0 \qquad \text{and} \qquad E[\varepsilon_i \varepsilon_i^T] = R_i$$

References

Rapp, R.H., and J.Y. Cruz, The Representation of the Earth's Gravitational Potential in a Spherical Harmonic Expansion to Degree 250. Dept. of Geodetic Science and Surveying, The Ohio State University, Columbus, 1986a.

Rapp, R.H., and J.Y. Cruz, Spherical Harmonic Expansions of the Earth's Gravitational Potential to Degree 360 Using 30' Mean Anomalies, Report No. 376, Dept. of Geodetic Science and Surveying, The Ohio State University ,1986b

Weber, G., and H. Zomorrodian, Regional Geopotential Model Improvement for the Iranian Geoid Determination, Bulletin Geodesique, 62, 125-141, 1988

Wenzel, H.-G., Hochauflösende Kugelfunktionsmodelle für das Gravitationspotential der Erde, Wisseuschaftliche Arbeiten der Fachnichtung Vermessungswesen der Universitat Hannover, Nr. 137, Hannover, 1985

where R_i is an *a priori* diagonal covariance matrix of dimension k_i. Then the least squares estimate, $\hat{x}$ and $\hat{R}_i$, can be obtained by minimizing the performance index,

$$J = \sum_{i=1}^{N} (y_i - H_i x)^T R_i^{-1} (y_i - H_i x) + (\bar{x} - x)^T \bar{P}_0^{-1} (\bar{x} - x)$$

$$\text{Subject to} \quad R_i = \left[\frac{(y_i - H_i x)^T (y_i - Hx)}{k_i} \right] \cdot I \qquad i = 1, \ldots, N \tag{2}$$

where I is the $k_i \times k_i$ identity matrix. In Eq. (2), it is assumed that the *a priori* estimate for x is zero, e.g., $\bar{x} = 0$.

The solution of Eq. (2) is given as

$$\hat{x} = \left[\sum H_i^T \hat{R}_i^{-1} H_i + \bar{P}_0^{-1} \right]^{-1} \left[\sum H_i^T \hat{R}_i^{-1} y_i \right]$$

$$\hat{R}_i = \left[\frac{(y_i - H_i \hat{x})^T (y_i - H\hat{x})}{k_i} \right] \cdot I \qquad i = 1, \ldots, N \tag{3}$$

Assuming that $\hat{R}_i = \dfrac{R_i}{\hat{\lambda}_i}$, Eq. (3) can be reduced as follows

$$\hat{x} = \left[\sum_i \hat{\lambda}_i (H_i^T R_i^{-1} H_i + \bar{P}_0^{-1}) \right]^{-1} \left[\sum_i \hat{\lambda}_i (H_i^T R_i^{-1} y_i) \right] + \hat{\Lambda}_i \bar{P}_0^{-1}$$

$$\hat{\lambda}_i = \frac{k_i}{(y_i - H_i \hat{x})^T R_i^{-1} (y_i - H_i \hat{x})} \tag{4}$$

$$\hat{\Lambda}_{ii} = \frac{1}{\hat{x}_i (\bar{P}_{0_i}^{-1}) \hat{x}_i}$$

where $\hat{x}$ and $\hat{\lambda}_i$ in Eq. (4) can be estimated simultaneously so that the state vector $\hat{x}$, which includes orbit and geophysical parameters, the relative weighting parameter $\hat{\lambda}_i$ for each data set, and the scale factors, $\hat{\Lambda}_{ii}$, for the diagonal *a priori* covariance matrix, $\bar{P}_0^{-1}$, can be estimated in an iterative solution. The numerical technique to accumulate and solve Eq. (4) is based on a square-root-free formulation which decomposes information equations using orthogonal transformation [*Gentleman*, 1973]. The estimation process has been implemented in the University of Texas Orbit Processor (UTOPIA) [*Schutz and Tapley*, 1980]. The optimal weighting algorithm to combine satellite and nonsatellite information equations was installed in the Large Linear System Solver (LLISS). This algorithm is used to obtain the University of Texas TEG-1 gravity field solution [*Tapley et al.*, 1988].

3. CALIBRATION OF THE GRAVITY FIELD COVARIANCE MATRIX

One advantage of using the least squares technique for the determination of the Earth's gravity field and geophysical parameters is that the resulting covariance matrix will give an assessment of error estimates as well as the correlation of the errors between the derived parameters. However, the calibration of the formal covariance matrix is often necessary to provide a realistic estimate of the error. Several techniques to calibrate the gravity field covariance matrices are presented in the following paragraphs. A single calibration scale factor is applied to the covariance matrix in these

16

approaches. Some of the techniques can be extended to allow different calibration factors for low, intermediate and high frequency content of the gravity field.

Surface gravity data technique. This technique is valid only for the calibration of gravity field models which do not use terrestrial gravity data. In this investigation, the expected global mean variance of the gravity anomaly error based upon estimated errors in the geopotential coefficients, $\bar{C}_{lm}$ and $\bar{S}_{lm}$, can be computed and compared with the difference of the global mean power of the observed gravity anomaly and the global mean cross power between the observed and the computed anomaly. [*Kaula*, 1966].

Secular rate technique for zonal harmonics calibration. A technique to calibrate zonal harmonics can be achieved by computing the observed error in secular rates for the lumped zonal harmonics observed from long, continuous and precisely determined orbits (e.g., Lageos 12-year arc), and compared with the predicted error in secular rates by the covariance matrix. Calibration of zonal harmonics can be performed by computing the observed secular rate, and comparing to the predicted rates.

Subset gravity solution. Lerch et al. [1987] used this method for the calibration of the GEM-T1 gravity field model [*Marsh et al.*, 1988]. The advantage of this method is that it is possible to calibrate the gravity field covariance without using independent data, assuming the reference gravity field is perfectly calibrated.

Consider Covariance Technique. A new technique for calibration of the gravity field covariance matrix is to use consider covariance analysis which uses the formal covariance corresponding to the solution as the *a priori* statistical information of the consider parameters. Statistical assumptions for the technique are as follows:

$$\bar{c} = c + \beta \ ; \ E[\beta] = 0 \ ; \ E[\beta\beta^T] = \pi \ ; \ \bar{c} = E[c] = 0$$

c – consider global parameters (geopotential, ocean tides, etc.)

β – errors in the global parameters

π – *a priori* covariance matrix for the consider parameters

Major assumptions include that the major part of the observation residual of the calibrating data set is due to error in the global considered parameters, and that no correlation exists between the observation noise of the calibrating data sets and errors in *a priori* parameters, or $E[\beta\varepsilon^T] = 0$. The observation equation can be expressed as follows:

$$y \cong H_x x + H_c c + \varepsilon \ ; \ E[\varepsilon] = 0 \ ; \ E[\varepsilon\varepsilon^T] = R$$

x – deviation of satellite-dependent parameters

H_x – linearized observation-state relation with respect to x

H_c – linearized observation-state relation with respect to c

R^{-1} – weight matrix

The least squares solution can be expressed as follows:

$$\hat{x} = (H_x^T R^{-1} H_x)^{-1} H_x^T R^{-1} y$$

$$S \triangleq \frac{\partial \hat{x}}{\partial c} = -(H_x^T R^{-1} H_x)^{-1} H_x^T R^{-1} H_c$$

where S is the sensitivity matrix and y is the observation.

If the observation residual is $\delta y_i = y_i - H_i \hat{x} = Y_i - G(\hat{X}, y_i)$, then the predicted residual variance

$$E[\delta y_i^2] \cong \overline{H}_i \pi \overline{H}_i^T$$

where π = covariance matrix associated with c, $\overline{H} \triangleq H_{x_i}S + H_{c_i}$.

The calibration of the formal covariance matrix, π, is as follows:

$$\sum \delta y_i^2 = f \sum E[\delta y_i^2] \cong f \sum (\overline{H}_i \pi \overline{H}_i^T)$$

where f is the calibration factor for covariance matrix π, and $\sum \delta y_i^2$ is the sum of observation residual square.

4. RESULT

The consider covariance technique was used to calibrate the TEG-1 gravity field model [*Tapley et al.*, 1988]. The predicted radial orbit errors for Topex and Geosat using the calibrated covariance matrix are 13cm and 24 cm, respectively.

5. CONCLUSION

New methodologies were developed for the determination of the Earth's gravity field using satellite, altimetry and terrestrial gravity data. A linear estimation algorithm was developed to allow for the simultaneous solution of physical parameters, which include geopotential coefficients, tides and basin scale sea surface topography, and relative data weights associated with homogeneous and inhomogeneous data types. This algorithm was used to determine the University of Texas gravity field model, TEG-1 [*Tapley et al.*, 1988]. Several techniques were presented to calibrate the formal covariance associated with the estimated gravity field model and other physical parameters.

REFERENCES

Gentleman, W. M., Least square computations by Givens transformation without square roots, *J. Inst. Math. Applic.*, *12*, 1973.

Kaula, W. M., Test and combination of satellite determinations of the gravity field with gravimetry, *J. Geophys. Res.*, *71*(22), 5304–5314, November 1966.

Lerch, F., J. Marsh, S. Klosko, E. Pavlis, G. Patel, D. Chinn and C. Wagner, The GEM-T1 gravitational model: An error assessment using improved calibration methods, *GSFC report*, 1987.

Marsh, J. G., et al., A new gravitational model for the Earth from satellite tracking data: GEM-T1, *J. Geophys. Res.*, *93*(B6), 6169–6215, June 10, 1988.

Schutz, B. E. and B. D. Tapley, UTOPIA: University of Texas Orbit Processor, *IASOM TR-80-1*, Center for Space Research, The University of Texas at Austin, 1980.

Tapley, B. D, Statistical orbit determination theory, *Recent Advances in Dynamical Astronomy*, 396–425, B. D. Tapley and V. Szebehely, Eds., D. Reidel Publ. Co., Holland, 1973.

Tapley, B. D., C. K. Shum, D. N. Yuan, J. C. Ries and B. E. Schutz, An Improved Model for the Earth's Gravity Field, presented at the Chapman Conference for Progress in the Determination of the Earth's Gravity Field, Ft. Lauderdale, Florida, September 12–16, 1988.

AN IMPROVED ERROR ASSESSMENT FOR THE GEM-T1 GRAVITATIONAL MODEL

F.J. Lerch and J.G. Marsh
NASA/GSFC, Greenbelt, MD

S.M. Klosko and E.C. Pavlis
EG&G WASC, Lanham, MD

G.B. Patel and D.S. Chinn
STX, Lanham, MD

C.A. Wagner
NGS, Rockville, MD

ABSTRACT

Several tests have been designed to determine the correct error variances for the GEM-T1 gravitational solution which was derived exclusively from satellite tracking data. The basic method employs both wholly independent and dependent subset data solutions and produces a full field coefficient by coefficient estimate of the model uncertainties. The GEM-T1 errors have been further analyzed using a method based upon eigenvalue-eigenvector analysis which calibrates the entire covariance matrix. Dependent satellite and independent altimetric and surface gravity data sets, as well as independent satellite deep resonance information, confirm essentially the same error assessment.

OVERVIEW

The principal calibration technique (Lerch, 1985) is based upon the comparison of solutions (independent or dependent) which analyzes the consistency of the coefficient differences and the error estimates between the solutions as described in Table 1.

Calibrations utilizing each of the major data subsets within the solution yield very stable calibration factors which vary by approximately 10% over the range of tests employed. Measurements of gravity anomalies obtained from altimetry were also used directly as observations to show that GEM-T1 is calibrated. Based upon these calibrated error estimates, GEM-T1 is a significantly improved solution which to degree and order 8 is twice as accurate as earlier satellite derived models. By being complete to degree and order 36, GEM-T1 is much larger than earlier gravitational solutions calculated from direct satellite tracking and has significantly reduced aliasing effects that were present in previous models. The mathematical representation of the covariance error in the presence of unmodeled systematic error effects in the data is analyzed and an optimum weighting technique is developed for these conditions. This technique yields an internal self-calibration of the error model, a process which GEM-T1 is shown to approximate. This geopotential field with calibrated error estimates, predicts 25 cm (Table 2) for the radial RMS uncertainty of the TOPEX orbit. The TOPEX Mission has a requirement for 10 cm radial orbital modeling which is needed to support the oceanographic applications of a high quality spaceborne altimeter.

RESULTS

Taking full advantage of the "super-computing" environment available at NASA/Goddard Space Flight Center, many solutions have been compared providing a completeness of field testing heretofore impossible within earlier computing environments. The results show a model remarkably consistent in stability for the calibration of its errors. With the exception of a few known and understood high order resonance terms (and the limitations of the high altitude Lageos satellite providing data suitable

for the calibration of a full 36x36 field), the calibrations show a stability in error assessment at the 10% level for each of the major data subsets employed in this evaluation. The published coefficient uncertainties for GEM-T1 and its error covariance matrix are herein found to be reasonably well calibrated and reliable. For example, the average calibration factor (k) for GEM-T1 using nine major sets of data in Table 3 (excluding the anomalous result for LAGEOS data) gave k=0.99 (± .08) for the coefficient calibration and k=0.95 (± .09) for the eigenvector calibration. This is a gratifying result, particularly, since formal least squares error formulae based on random variables were employed with compensating downweighting factors to account for more general formulae involving error sources with unknown systematic effects. The mathematical validity of the error estimation techique for the gravity model was studied extensively and an optimal weighting technique with internal self-calibration of the error model was developed.

The authors would like to thank C.K. Shum, John Ries and Byron Tapley of the Center of Space Research, University of Texas, for their thoughtful reading and constructive comments in the preparation of this report. George Rosborough of the University of Colorado likewise made valuable comments. The authors would like to also thank Dick Rapp and Nick Pavlis of Ohio State University for their assistance in processing and helping us successfully utilize the surface gravimetry.

REFERENCES

Lerch, F.J., Error Spectrum of Goddard Satellite Models for the Gravity Field, Geodynamics Branch Annual Report-1984, NASA TM86223, August 1985.

Lerch, F.J., Marsh, J.G., Klosko, S.M., Pavlis, E.C., Patel, G.B., Chinn, D.S., and Wagner, C.A., An Improved Error Assessment for the GEM-T1 Gravitational Model, NASA TM----, in print, November 1988.

Lerch, F.J., Klosko, S.M., Wagner, C.A. and Patel, G.B., On the Accuracy of Recent Goddard Gravity Models, J. Geophys. Res., 90, (B11), pp. 9312-9334, 1985.

Marsh, J.G., et al., A New Gravitational Model for the Earth from Satellite Tracking Data: GEM-T1, J. Geophys. Res. 93, B6, 6169-6215, 1988.

TABLE 1

FORMULAE FOR ERROR CALIBRATION

TWO FIELDS F & $\overline{F}$

$$F \; : \; C_{l,m}, \quad S_{l,m}, \qquad \sigma\text{'s} \quad (\text{coeff. errors})$$

$$\overline{F} \; : \; \overline{C}_{l,m}, \quad \overline{S}_{l,m}, \qquad \overline{\sigma}\text{'s}$$

$$RMS_l \; (\Delta F) \;=\; \left[\; \sum_{m=0}^{l} \frac{\Delta C_{l,m}^2 + \Delta S_{l,m}^2}{2l+1} \; \right]^{\frac{1}{2}}$$

$$\sigma_l \;=\; \left[\; \sum_{m=0}^{l} \frac{\sigma_{(C_{l,m})}^2 + \sigma_{(S_{l,m})}^2}{2l+1} \; \right]^{\frac{1}{2}}$$

$$e_l^2 \;=\; E(RMS_l)^2$$

$$\;=\; \sigma_l^2 \;+\; \overline{\sigma}_l^2 \quad \text{when } F \text{ is independent of } \overline{F}$$

$$\;=\; \sigma_l^2 \;-\; \overline{\sigma}_l^2 \quad \text{when data in } F \subset \overline{F}$$

CALIBRATION FACTORS

$$k_l \;=\; \frac{RMS_l}{e_l} \qquad \text{for degree } l$$

$$k_{l,m} \;=\; \frac{RMS_{l,m}}{e_{l,m}} \qquad \text{for individual coeff. pair}$$

TABLE 2

Radial Orbital Errors (RMS)
for Three Day Arc Lengths
Using Calibrated Covariance Matrices

Geopotential Model	Radial RMS Error (cm)
GEM-L2	65
GEM-T1	25
GEM-T1 + Surface Gravimetry + Altimetry	17

TABLE 3

SUMMARY OF SOLUTION CALIBRATION FACTORS FROM GEM-T1 FIELD ASSESSMENTS

	COEFFICIENT CALIBRATION FACTOR	RMS WEIGHTED PROJECTED EIGENVECTOR CALIBRATION FACTOR ONTO GEM-T1
● (GEM-T1) vs (GEM-T1 minus DATA SUBSET)		
4-LASERS (GEOS 1,2,3, BE-C)	1.06	0.94
STARLETTE LASER	1.10	0.99
OSCAR + SEASAT DOPPLER	1.09	1.07
OPTICAL (11 SATS)	0.84	0.89
LAGEOS LASER	1.45	1.59
● GEM-T1 vs GEM-T1 + SURFACE GRAVITY	0.95	0.92
● GEM-T1 vs GEM-T1 + SURFACE GRAVITY + SEASAT ALTIMETRY	0.94	0.89
● GEM-T1 vs SURFACE GRAVITY + SEASAT + ALTIM	0.99	0.90
● GEM-T1 minus LAGEOS vs LAGEOS + SURFACE GRAVITY + SEASAT ALTIMETRY	0.95	0.88
● GEM-T1 vs GEM-T1 + Lumped Resonance Data	1.00	1.06
● GEM-T1 with 10 times the Data Weight vs GEM-T1 minus 4-LASERS with 10 times the Data Weight	2.75	2.45

A. H. W. Kearsley
R. D. Holloway

School of Surveying, University of New South Wales, Kensington, Australia

Abstract

We test the ability of three high-order geopotential models - OSU81, GPM2 and OSU86E - to recover the gravity anomaly field (Δg) in the Australian region. The region was divided into 2° x 2° blocks, and the mean and rms of the residual gravity ($\Delta g_{measured} - \Delta g_{modelled}$) found to estimate the fit of the model to the point gravity data. The results showed that OSU81 and GPM2 performed similarly, recovering the Δg with a mean value of < ± 5 mGal in 63% and 70% of the blocks, respectively. However, both these models achieved a fit of worse that ± 13 mGal in 6 to 7% of cases. These were in areas either on or near the coast, or in the Central Australian region, inferring that for a precise geoid slope determination in these regions, a detailed analysis of Δg in region is needed. On the other hand, OSU86E produced a very good result, having a mean fit of < ± 5 mGal in 80% of the blocks, and worse than ± 13 mGal in only 1% of cases. The rms values for this model were also improved over the other two models, indicating that for applications requiring highest precision, the preferred model is OSU86E.

1. Introduction

The growing interest in recovering orthometric heights from GPS has generated the need for models capable of recovering geoid features to finer detail. The past decade has seen the development of a series of models of increasing order, including two models taken to $n_{max} = 180$ (OSU79 and OSU81; Rapp, 1981), a model summed to $n_{max} = 200$ (GPM2; Wenzel (1985)), and most recently, two models taken to $n_{max} = 360$, OSU86E and OSU86F (Rapp, 1986). Geodesists have used these models extensively for geoid studies, mainly to determine the geoidal long to medium wavelength features and to provide the reference model for terrestrially-derived gravity anomalies used in, e.g., Stokes' integral, to find the short wavelength component of the geoid signal.

The ability of GPS to determine ellipsoidal height differences (Δh) over lines whose orthometric height differences (ΔH) are found by conventional levelling has provided, for the first time in history, high precision geometric determinations of ΔN, the geoid height change over the baseline. That is, for small deflections of the vertical

$$\Delta N = \Delta h - \Delta H \qquad (1)$$

ΔN will have a precision equivalent to $\sigma_{\Delta h}$, providing H is determined to 1st or 2nd order. This precision is thought to be of the order of 2 to 4 ppm of the line length. Networks in which Δh and ΔH have been precisely evaluated, therefore, provide valuable control data against which to compare gravimetric determinations of ΔN. We have recently performed a series of such comparisons, and have found that (Kearsley, 1988)

(i) the ability of a geopotential model to recover ΔN varies significantly, both with location and with n_{max},
(ii) the mean fit of ΔN from the geopotential model to the control ΔN constrains the precision obtainable from a full gravimetric solution

In the discussion which follows we test the fit of three models (OSU81, GPM2 and OSU86E) to the gravity anomaly field in the Australian region. Based upon earlier tests, we suggest how this mean fit may be used to estimate the ability of the model to recover ΔN in a particular region. Finally we recommend which model is most suitable for use as a reference in the Australian region.

2. Testing the Geopotential Models.

2.1 Description of Technique for Testing

In earlier tests we have compared the ΔN derived from OSU81 against control ΔN, derived from (1), where ΔH was found by conventional spirit levelling to 3rd-order or better, and Δh from GPS surveys (Kearsley, 1988, p. 6561). The comparisons showed that the ability of OSU81 to recover ΔN varied with both location, and with the upper limit of summation. The tests also showed that the best agreement does not necessarily occur when the geopotential model is taken to its maximum degree and order.

To test a model for its "fitness" - its ability to recover ΔN, in areas where observed ΔN are either non-existent or

sparse, we use the statistics of residual gravity δg, where

$$\delta g = \Delta g - \Delta g_L \qquad (2)$$

where Δg is the free air gravity anomaly from gravimetric survey and Δg_L is the gravity anomaly generated from the geopotential model. For these tests Δg_L was generated on $0.1°$ mesh across the Australian region. A value of Δg_L was estimated by interpolation at each gravity point in the Australian Gravity Data Base, and δg obtained by (2). The data set was then analysed in $2° \times 2°$ blocks, this approximating the area used in a spherical cap of integration in a full gravimetric evaluation. The δg_i were then analysed to obtain the mean ($m\delta g$) and root mean square ($rms\delta g$) for the population in the block.

This analysis was repeated for each of three recent geopotential models - OSU81, GPM2 and OSU86E. Each refers to GRS80 (Moritz, 1980) and their maximum degree and order are 180, 200 and 360 respectively.

2.2 Inferences to be drawn from statistics

From the few tests in Australia which compared ΔN_{Grav} against control ΔN a trend has appeared which relates $m\delta g$ to $m\delta N$. This trend is shown in Table 1, where $m_{\delta N}$ is the mean fit of ΔN for GPS lines in the region, in ppm of the line length, and $m_{\delta g}$ is the mean (bias) of the δg field in mGal, analysed over the $2°$ block containing the control data.

On the basis of this evidence we have inferred across Australia the likely value of $m\delta N$ from the $m\delta g$. This is of particular importance to precise geoid studies because, as we noted above, the geopotential model will constrain the potential precision of the full gravimetric solution if it is unable to sense the geoidal undulations at, say, the 4 to 6 ppm level or better.

3. Discussion of Results

The mean and rms of the δg population for the 256 $2° \times 2°$ blocks across the Australian continent were calculated for each of the three models tested.

3.1 Mean fit of Geopotential models to gravity data

The values of $m_{\delta g}$ have been placed into 4 bins, as shown in Table 1 . As is seen from this table, the bin limits were chosen because they appeared to be equivalent to the 5 ppm divisions in $m\delta N$.

The results have been summarised in the histograms in Figure 1, allowing a direct comparison between the three models.

Table 1 : Comparison of $m_{\delta g}$ with m_{dN}

Bin	$\pm\ m\delta g$ (mGal)	$\pm\ m\delta N$ (ppm)
1	0-5	0-5
2	5-13	5-10
3	13-21	10-15
4	>21	>15

(a) OSU81 and GPM2

For OSU81, 63% of blocks lay in bin 1, 30% in bin 2, 6% in bin 3, with 2% being worse than ± 21 mGal in their mean fit. From this we infer this model can recover ΔN, on average, to 10 ppm or better in 93%, or nearly

western coast, and in the centre of Australia. In
the first location, the model may reflect the fact that for the ocean regions, the Δg field used in the model was
collocated from geoid undulations derived from radar altimetry. This fact may also explain the high correlation
between bin 2 and 3 areas with the coastline. The bin 3 and 4 results in Central Australia are located of the Officer
and Amadeus Basins and the McDonnell Ranges (about 1500 m elevation), an area noted for the unusually high
signal variations in the Bouger anomaly field. These results suggest the 180 degree model insufficiently sensitive
to the gravity signal in this region.

The results for GPM2 were slightly improved over those for OSU81, reflecting the higher order of the former
model.

**Figure 1: Distribution of Mean Fit of Potential Model to Terrestrial Gravity
on $2° \times 2°$ blocks**

Number of $2°$ blocks = 256
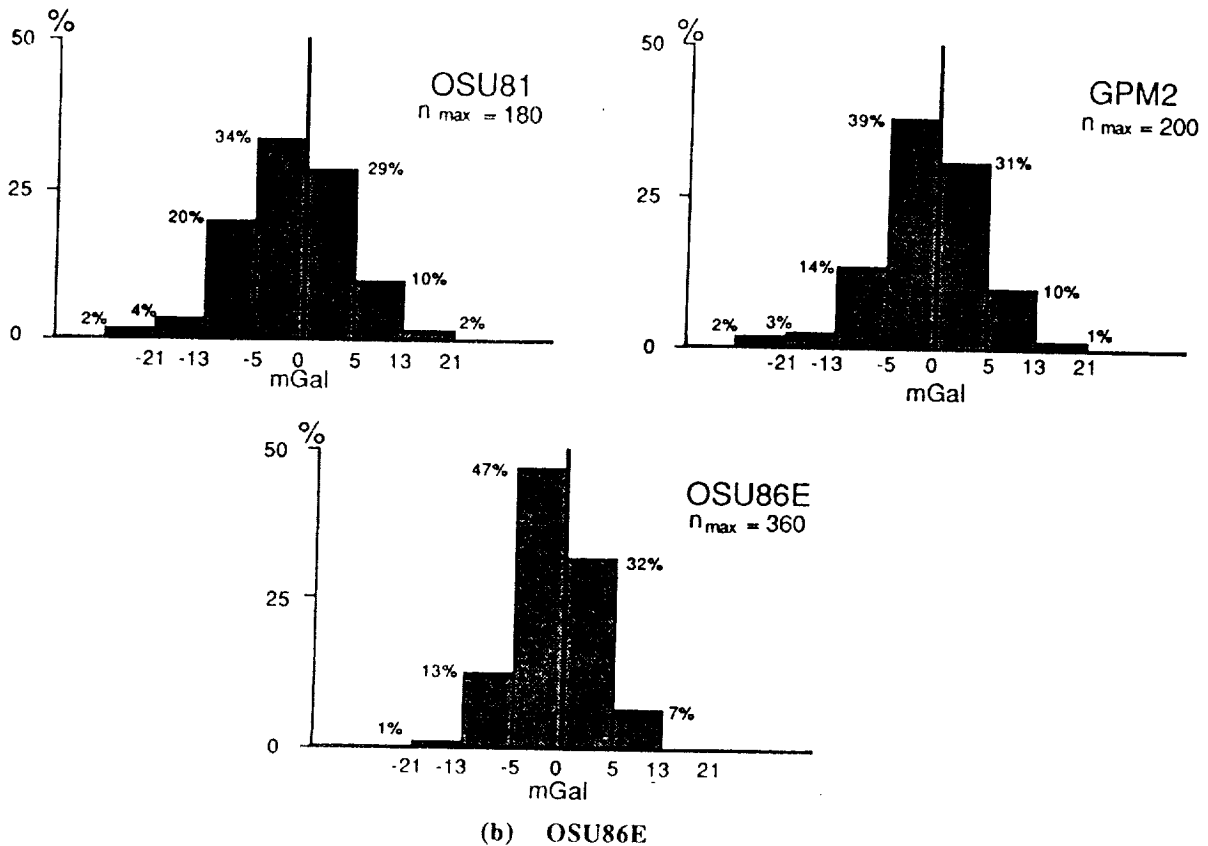
(b)   OSU86E

The results of this analysis are impressive. From Figure 1 we see that 79% of the blocks fell into bin 1, 20%
into bin 2, with 1% in bin 3. No blocks had a fit worse than ± 21 mGal. It appears that, for nearly 80% of
Australia OSU86E is capable of recovering ΔN to, on average, 5 ppm. In only three cases will the fit to ΔN be
worse than 10 ppm. It is strange that, in one of these cases OSU81 recovers Δg better than does OSU86E. There
still appears to be some correlation between bin 2 results and coastal regions, but the poor bin 4 results of OSU81
on the south western coast, and in Central Australia, have disappeared. These trouble spots now lie in bin 2.

It is obvious from this analysis that the mean fit, or bias , of this model with respect to terrestrial gravity has
improved greatly over both OSU81 and GPM2. This may be explained by the increased order of the model,
enabling it to capture shorter wavelength features in the gravity field. The numerical analysis adopted in this
solution, which used quadratures with a desmoothing procedure suggested by Colombo (1981) may also be partly
responsible, although the fact that OSU86E summed to 180 replicates almost exactly OSU81 taken to the same
order in the South Australian and West Australian test areas tends to discount this factor.

3.2   Root mean square of residual gravity anomalies

The other statistic of significance in this analysis is the rms, which gives some measure of the fluctuations of the

δg field from the geopotential model. The results of the computations are summarised in Table 2.

Table 2 Distribution of rms (Population 256)

Bin	Rms Range (mGal)	OSU81	GPM2	OSU86E
1	0-10	64 (25%)	62 (24%)	143 (56%)
2	10-20	142 (55%)	151 (59%)	96 (37%)
3	20-30	38 (15%)	32 (13%)	15 (6%)
4	>30	12 (5%)	11 (4%)	2 (1%)

As is seen from these figures and the summary, OSU81 and GPM2 perform nearly equally well, with 80% and 83% of blocks with rms of less than 10 mGal. As with the mean fit, the blocks of poorest representation are generally in the south western corner and in the centre, and along the east coast of Australia. Table 2 also shows how much the 360 degree model recovers the variations in the gravity field more faithfully. Over half the area is recovered with an rms of less than 10 mGal, while all but 7% of the blocks have an rms less than 20 mGal. Only 2 blocks modeled by OSU86E have an rms > 30 mGal.

Combining mean and rms for OSU86E

The above results confirm the integrity of OSU86E, already demonstrated in the test on the mean fit, in its ability to recover the gravity field across Australia. Indeed, when combining the mean and the rms results for OSU86E, we find that a large portion of the region have both small bias and rms values. Over 40% of the blocks analysed have a mean and an rms both of which lie in bin 1. Obviously the shorter wavelength features in these areas are well modeled by OSU86E. From Table 1 we infer that, in these regions, OSU86E will recover ΔN to better than 5 ppm, and that there may be little benefit in incorporating the short wavelength signal in ΔN obtained from the detailed analysis of surface gravity. Predictably, however, most of these areas lie across the inland, sparsely developed region of Australia. The areas which contain most development activity, the coastal regions, still exhibit less favourable recovery by this model and will apparently still require a full gravimetric solution for highest precision.

4. Conclusions

From these tests we see how the ability of a geopotential model to fit the gravity field across Australia improves with the increased order of the model Iit appears that this improvement is due almost entirely to the higher order of the model, and not to the different numerical technique used to solve for the potential coefficients. Finally, it appears that for 40% of the region, OSU86Ewill serve in the recovery of ΔN for all but the most exacting purposes. However for the coastal regions where most development activity occurs, a full gravimetric solution involving a detailed analysis of detailed gravity will be required for most higher-order surveying tasks.

References

Colombo, O.L., Numerical methods for harmonic analysis on the sphere, *Report No. 310*, Dept. Geod. Sci., The Ohio State University, Colombus, 1981.

Kearsley, A. H. W., Tests on the recovery of precise geoid height differences from gravimetry, *J. Geophys. Res.*, *93*(B6), 6559-6570, 1988

Moritz, H., Geodetic Reference System 1980, *Bull. Geod.*, *54.*(3), 395-405, 1980.

Rapp, R. H., The earth's gravity field to degree and order 180 using Seasat altimeter data, terrestrial gravity data and other data, *Rep. 322*, Dep. of Geod. Sci. and Surv., Ohio State.

Rapp, Richard H. and Cruz, Jaime, Y. Spherical harmonic expansions of the earth's gravitational potential to degree 360 using 30' mean anomalies, *Report No. 376*, Dept Geod. Sci. and Surv., The Ohio State University, Columbus, Ohio, 1986.

Wenzel, H.-G. Hochauflösende Kugelfunktionsmodelle für das Gravitationspotential der Erde, *Wissenschaftliche Arbeiten der Fachrichtung Vermessungswessen der Universität Hannover*, Hannover, 1985.

STABILIZED DETERMINATION OF GEOPOTENTIAL COEFFICIENTS
BY THE MIXED HOM-BLUP APPROACH

B. MIDDEL and B. SCHAFFRIN

Dept. of Geodetic Science, Stuttgart University, D - 7000 Stuttgart 1
Federal Republic of Germany

1. INTRODUCTION

For the determination of geopotential coefficients we can use data from ra-
ther different sources, e.g. satellite tracking, gravimetry or altimetry.
As each data type is particularly sensitive to certain wavelengths of the
spherical harmonic coefficients it is of essential importance how they are
treated in a combination solution. For example the longer wavelengths are
well described by the coefficients of a model derived by satellite tracking,
while other observation types such as gravity anomalies Δg and geoid heights
N from altimetry contain only poor information for these long wavelengths.
Therefore, the lower coefficients of the satellite model should be treated
as being superior in the combination. In our contribution we present a new
method which turns out to be highly suitable for this purpose due to its
great flexibility combined with robustness.

2. METHODS

In *B. Middel/B. Schaffrin (1987)* we introduced a method based on "robust
collocation", which according to *B. Schaffrin (1985,1986)* is the Best homo-
geneously Linear (weakly) Unbiased Prediction (hom-BLUP), as a promising
technique for the combination of terrestrial gravity data with spherical har-
monic coefficients from satellite tracking. With this method we obtain the
predicted coefficients, collected in the vector $\tilde{x}$, by

$$\tilde{x} = (P_S + P_T)^{-1} (P_S \xi_S + P_T \xi_T a) \tag{2.1}$$

where ξ_S contains the satellite coefficients and P_S is the corresponding
weight matrix. Vector ξ_T contains coefficients which we obtained by a least-
squares adjustment within a Gauß-Markov Model from terrestrial gravity data
and P_T is again the corresponding weight matrix. The terrestrial coefficient
set ξ_T is taken to be inferior with respect to the lower coefficients and by
comparison with the satellite coefficient set ξ_S we obtain the scalar factor
a to fit ξ_T to ξ_S. When the fitting factor is defined as a:=1 we obtain the
weighted mean of both data sets being, of course, the "geodetic collocation"
according to *H. Moritz (1973)*, which is the Best inhomogeneously Linear Pre-
diction (inhom-BLIP).

However hom-BLUP turned out to be robust against inconsistencies in ξ_T and
therefore, in this sense, superior to inhom-BLIP as we showed by applying
statistical tests in *B. Middel/B. Schaffrin (1988)*. Nevertheless we can
make this approach more flexible by splitting up the weaker coefficient set
ξ_T into groups of a special character. We allow them specific fitting fac-
tors collected in a vector $\underline{a}$ and name it "Mixed hom-BLUP", thus leading to
the following solution:

$$\tilde{x} = (P_S + P_T)^{-1} (P_S \xi_S + P_T \Xi_t \underline{a}) .$$ (2.2)

In this formulation the vector ξ_T is modified to a matrix Ξ_T where each column contains one group of coefficients at the respective places with zero entries otherwise.

3. NUMERICAL EXAMPLE

After this short description we now present some results of combination solutions up to degree 36 where we merged coefficients ξ_T, derived either from gravity anomalies or geoid heights or alternatively from a combination of them both, with GEM-L2 coefficients ξ_S up to degree 20, as described in F.J. Lerch et al (1982). For each combination we split up the weaker coefficient set ξ_t by degree and by order when using the Mixed hom-BLUP technique. In figures 3.1 to 3.3 we plotted the components of the vector $\underline{a}$ with respect to the group (i.e. degree or order) together with their confidence intervals of a significance level of 95%. In addition, the scalar factors a of inhom-BLIP and hom-BLUP were added.

Figures 3.1 show that we obtained with all methods different fitting factors a and therefore different results when we merge the GEM-L2 coefficients with coefficients ξ_T adjusted from gravity anomalies Δg. But it has to be mentioned that when using Mixed hom-BLUP and splitting ξ_T up by order most of the components of $\underline{a}$ are not significantly different from the scalar a of ordinary hom-BLUP since these values lie inside the 95% confidence interval.

The situation changes when we introduce coefficients ξ_T computed with geoid heights N. This data set is fully compatible with the GEM-L2 coefficients and therefore all fitting factors are very close to 1 as illustrated in figures 3.2. In this case we obtained nearly identical solutions with all the methods.

In figures 3.3 and 3.4 we present results which we obtained by a combination of GEM-L2 coefficients with coefficients which we adjusted from both data sets Δg and N. Figures 3.3 show that the scalar a is very close to 1 but with the Mixed hom-BLUP we obtained, in both cases of splitting, a-components far away from this value. Therefore, the solution with ordinary hom-BLUP leads to different results in both cases of splitting up the coefficients ξ_t. This can be very clearly seen in figure 3.4 where the degree variances of the different solutions have been plotted.

4. CONCLUSIONS

The use of "Mixed hom-BLUP", which we present in this contribution, leads to different solutions compared with "geodetic collocation" (inhom-BLIP) and "robust collocation" (hom-BLUP) if the combined data sets are not compatible. Due to the great flexibility and robustness of this method we expect that it is highly suitable for estimating geopotential coefficients when combining heterogeneous data sets.

a-factors for combination of GEM-L2 with ∆g (i=1)

inhom-BLIP
hom-BLUP
mixed hom-BLUP
conf. int. (sig. level 0.95)
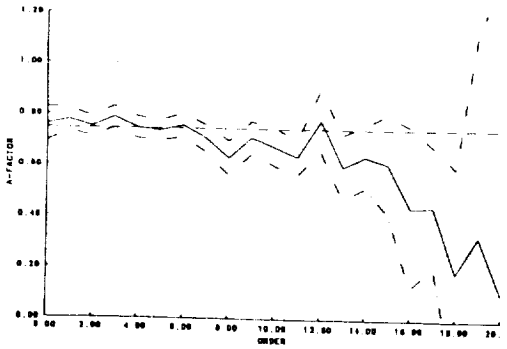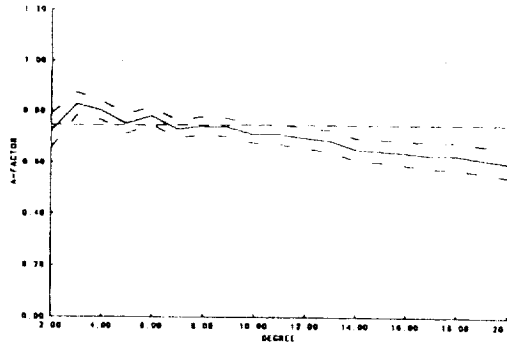
a-factors for combination of GEM-L2 with N (i=2)

inhom-BLIP
hom-BLUP
mixed hom-BLUP
conf. int. (sig. level 0.95)
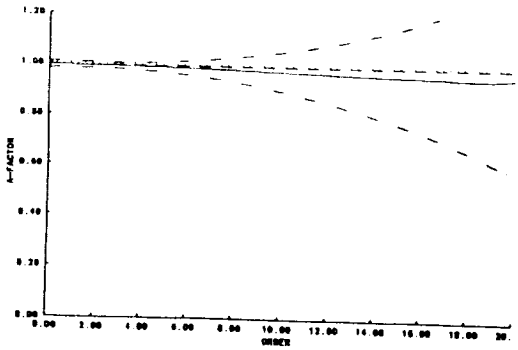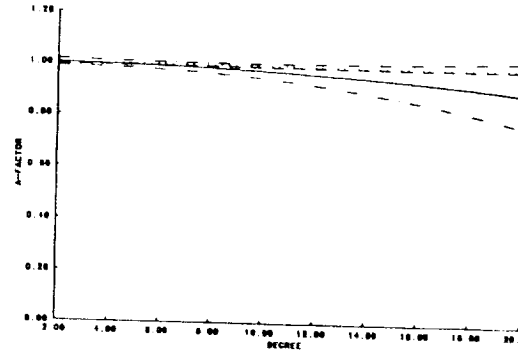
Figures 3.1

Figures 3.2

a-factors for combination of GEM-L2 with ∆g and N (i=3)

inhom-BLIP
hom-BLUP
mixed hom-BLUP
conf. int. (sig. level 0.95)
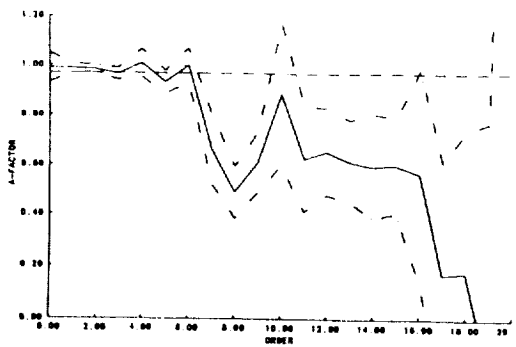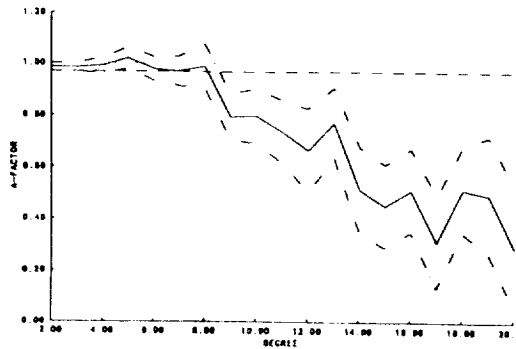
degree variances for combination of GEM-L2 with ∆g and N (i=3)
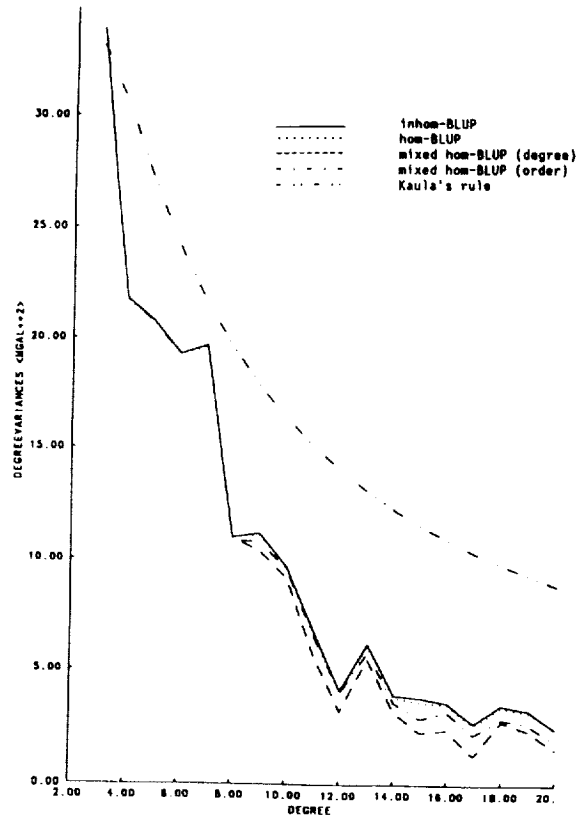
inhom-BLUP
hom-BLUP
mixed hom-BLUP (degree)
mixed hom-BLUP (order)
Kaula's rule

Figures 3.3

Figure 3.4

29

ACKNOWLEDGEMENT

5.   REFERENCES

Lerch, F.J. et al (1982): A refined gravity model from LAGEOS (GEM-L2); Geophys. Res. Letters 9 (1982), 1263-1266.

Middel, B. and B. Schaffrin (1987): Robust determination of the Earth's gravity potential coefficients; XIX. IUGG General Assembly, Proc. of the IAG Intersection Symp. on "Advances in Gravity Field Modelling", Vancouver/Canada 1987, Tome I, pp. 154-166.

Middel, B. and B. Schaffrin (1988): Testing the compatibility of different sets of geopotential coefficients; Proc. of 6th Int. Symp. "Geodesy and Physics of the Earth", Potsdam/GDR 1988.

Moritz, H. (1973): Least squares collocation; Deutsche Geodät. Komm. A-75, München 1973.

Schaffrin, B. (1985): Das geodätische Datum mit stochastischer Vorinformation; Deutsche Geodät. Komm. C-313, München 1985.

Schaffrin, B. (1986): On robust collocation; Proc. of the 1st Hotine-Marussi Symp. on Math. Geodesy (Rome 1985), Milano/Italy 1986, pp. 343-361.

Geopotential Coefficient Determination and the Gravimetric Boundary Value Problem - A New Approach

Lars E Sjöberg

The Royal Institute of Technology, Department of Geodesy, S-10044 Stockholm, Sweden

ABSTRACT

New integral formulas to determine geopotential coefficients from terrestrial gravity and satellite altimetry data are given. The formulas are based on the integration of data over the non-spherical surface of the Earth. The effect of the topography to low degrees and orders of coefficients is estimated numerically. Formulas for the solution of the gravimetric boundary value problem are derived.

1. INTRODUCTION

The long-wavelength features of the Earth's gravity field is best determined from dynamic satellite observations. For short-wavelength information terrestrial gravity anomalies (Δg) and satellite altimetry data play essential roles. A well-known method to determine geopotential coefficients from Δg is the integral method used by Rapp e. g. (1977). We present this method in section 2 followed by a new integral method in section 3.

2. RAPP'S INTEGRAL FORMULA

The determination of the harmonic coefficients according to Rapp requires that the data (Δg) is distributed continuously all over the surface of the Earth. Also it is assumed that the Earth's (disturbing) potential (T) can be developed into a harmonic series convergent down to the Earth's surface:

$$T = r_0 \gamma \sum_{n=2}^{\infty} (\frac{r_0}{r})^{n+1} \sum_{m=-n}^{n} A_{nm} Y_{nm} (\phi,\lambda), \qquad (2.1)$$

where γ is the mean surface gravity of the Earth, (r,ϕ,λ) are the geocentric, spherical coordinates of the computation point, $Y_{nm}(\phi,\lambda)$ is a fully normalized spherical harmonic and, for $r = r_0$,

$$A_{mn} = \frac{1}{4\pi r_0 \gamma} \iint_\sigma T \, Y_{mn} \, d\sigma, \qquad (2.2)$$

where σ is the unit sphere. Considering the "boundary condition" in spherical approximation (Heiskanen and Moritz 1967, p 87) one obtains the corresponding expansion for the gravity anomaly (Δg) :

$$\Delta g = \gamma \sum_{n=2}^{\infty} (n-1)(\frac{r_0}{r})^{n+2} \sum_{m=-n}^{n} A_{nm} Y_{nm} (\phi,\lambda) , \qquad (2.3)$$

from which formula the coefficients are given for $r = r_0$:

$$A_{nm} = \frac{1}{4\pi\gamma(n-1)} \iint_\sigma \Delta g \, Y_{nm} \, d\sigma . \qquad (2.4)$$

In principle r_0 is arbitrary, but is usually chosen as the equatorial radius of the selected reference ellipsoid. A practical obstacle in applying the integral formulas (2.2) and (2.4) is the necessity of reducing T and Δg to the sphere of radius r_0. For (2.4) Rapp (1984) used the Taylor series

$$\Delta g_{reduced} = \Delta g_{observed} - \frac{\partial \Delta g}{\partial h} \Delta h - \frac{1}{2} \frac{\partial^2 \Delta g}{\partial h^2}(\Delta h)^2 - ... , \qquad (2.5)$$

where $\Delta h = r - r_0$, and the derivatives were estimated from available series of harmonic coefficients.

3. THE NEW INTEGRAL APPROACH

Rewriting formula (2.1) on the form

$$T = R\gamma \sum_{n=2}^{\infty} (\frac{R}{r})^{n+1} \sum_{m=-n}^{n} C_{nm} Y_{nm}(\phi, \lambda),$$ (3.1)

where R is the radius of the minimum bounding sphere of the Earth, and considering Green's second identity for the functions T and U (Heiskanen and Moritz, 1967, p. 11):

$$\iiint_{\nu} (U\Delta T - T\Delta U)d\nu = \iint_{S} (U\frac{\delta T}{\delta n'} - T\frac{\delta U}{\delta n'}) dS,$$ (3.2)

where ν is the volume bounded by the surface S, which consists of the surface of the Earth (E) and the surface of the bounding sphere of radius R, and n' is the external normal to S with respect to ν, and setting U to

$$U = \{ (\frac{R}{r})^{n+1} + a_n (\frac{r}{R})^n \} Y_{nm}(\phi, \lambda),$$ (3.3)

where a_n is a non-zero constant with respect to position, the following general integral formula is derived in Sjöberg (1988):

$$C_{nm} = \frac{1}{4\pi R^2 \gamma (2n+1)a_n} \iint_{E} [U \{ \overline{\Delta g} - \frac{1}{\gamma} \frac{\delta g}{\delta r} T \} + T \frac{\delta U}{\delta r}] r^2 d\sigma,$$ (3.4)

where $\overline{\Delta g} = \Delta g - \gamma(\xi \tan \beta_1 + \eta \tan \beta_2)$, β_1 and β_2 are the terrain inclinations, and ζ and η are the corresponding deflections of the vertical. The integral is taken over the Earth's surface (E). Choosing $r = r_0 + \Delta h$ and $a_n = (R/r_0)^{2n+1} (n-1)/(n+2)$ one obtains (to order $\Delta h/r_0$):
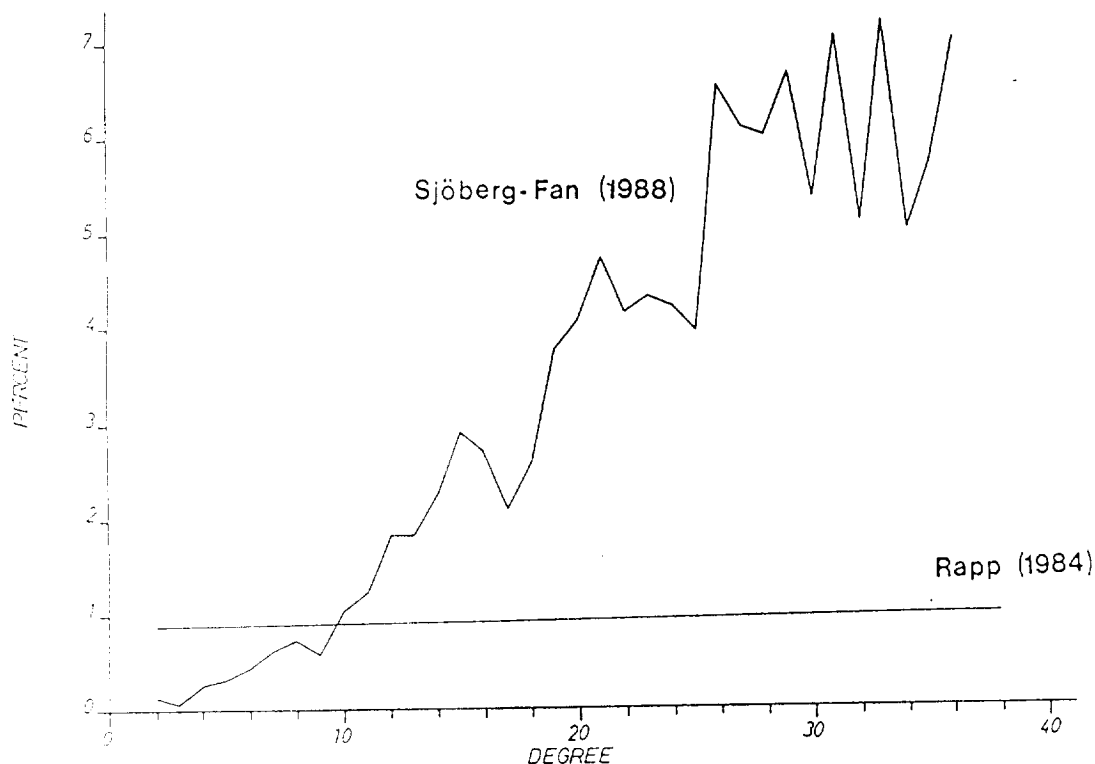
Fig. 1. The percentage terrain elevation effect by degree as computed by formula (3.6) and by Rapp (1984).

32

$$A_{nm} = (\frac{R}{r_o})^{n+2} C_{nm} = A_{nm}^0 + \Delta A_{nm}, \tag{3.5}$$

where A_{nm}^0 is given by (2.4) and

$$\Delta A_{nm} = \frac{n+2}{4\pi\gamma R r_o} \iint_E T \Delta h \, Y_{nm} \, d\sigma. \tag{3.6}$$

The percentage terrain corrections by degree determined by formula (3.6) are illustrated in Fig. 1. Details on the computations are given in Sjöberg and Fan (1988). For comparison the figure includes also terrain corrections from Rapp (1984).

Choosing $a_n = -(R/r_o)^{2n+1}$ one arrives at formula (3.5), but now with A_{nm}^0 given by (2.2) and

$$\Delta A_{nm} = \frac{1}{4\pi\gamma} (\frac{R}{r_o}) \iint_\sigma (\Delta g + \frac{2T}{R}) \frac{\Delta h}{r_o} Y_{nm}(\phi,\lambda) \, d\sigma. \tag{3.7}$$

Numerical computations show that this correction is within 2% for $n \le 50$. Again we refer to Sjöberg and Fan (1988) for details.

4. SOLUTIONS TO BOUNDARY VALUE PROBLEMS

Inserting (3.4) into (3.1) and assuming that summation and integration may change order one arrives at the following solutions for the height anomaly $\zeta_P = T_P/\gamma$:

Case I: $a_n = (R/r_o)^{2n+1} (n-1)/(n+2)$:

$$\zeta_P = \frac{R}{4\pi\gamma} \iint_\sigma [\{ S(\psi_{PQ},r_Q,r_P) - \Lambda(\psi_{PQ},r_Q,r_P) \} \overline{\Delta g_Q} + K(\psi_{PQ},r_Q,r_P) T_Q] \, d\sigma_Q, \tag{4.1}$$

where

$$S(\psi_{PQ},r_Q,r_P) = \frac{r_Q}{R} \sum_{n=2}^{\infty} \frac{2n+1}{n-1} (\frac{r_Q}{r_P})^{n+1} P_n (\cos \psi_{PQ})$$

$$\Lambda(\psi_{PQ},r_Q,r_P) = \frac{r_Q}{R} \sum_{n=2}^{\infty} \frac{n+2}{n-1} \{ 1 - (\frac{r_o}{r_Q})^{2n+1} \} (\frac{r_Q}{r_P})^{n+1} P_n (\cos \psi_{PQ})$$

and

$$K(\psi_{PQ},r_Q,r_P) = \frac{1}{R} \sum_{n=2}^{\infty} (n+2) (\frac{r_Q}{r_P})^{n+1} \{ 1 - (\frac{r_o}{r_Q})^{2n+1} \} P_n (\cos \psi_{PQ})$$

Case II: $a_n = -(R/r_o)^{2n+1}$:

$$\zeta_P = \frac{1}{4\pi\gamma} \iint_\sigma [\{ P(\psi_{PQ},r_Q,r_P) - L(\psi_{PQ},r_Q,r_P) \} T_Q + M(\psi_{PQ},r_Q,r_P) r_Q \overline{\Delta g_Q}] \, d\sigma_Q , \tag{4.2}$$

33

where

$$P(\psi_{PQ}, r_Q, r_P) = \sum_{n=2}^{\infty} (2n+1) \left(\frac{r_Q}{r_P}\right)^{n+1} P_n(\cos \psi_{PQ})$$

$$L(\psi_{PQ}, r_Q, r_P) = \sum_{n=2}^{\infty} (n-1) \left(\frac{r_Q}{r_P}\right)^{n+1} \left\{ 1 - \left(\frac{r_o}{r_Q}\right)^{2n+1} \right\} P_n(\cos \psi_{PQ})$$

and

$$M(\psi_{PQ}, r_Q, r_P) = \sum_{n=2}^{\infty} \left(\frac{r_Q}{r_P}\right)^{n+1} \left\{ 1 - \left(\frac{r_o}{r_Q}\right)^{2n+1} \right\} P_n(\cos \psi_{PQ}).$$

In the limit $r_Q \rightarrow r_o$ the formulas (4.1) and (4.2) approach (the extended) Stoke's formula and the Bruns-Poisson's formula, respectively.

5. DISCUSSION

As Figure 1 shows the terrain corrections of the new method (3.6) are more significant with increasing degree than those of Rapp (1984). This discrepancy might be explained by insufficient power in Rapp's derived derivatives of formula (2.5). The validity of the Earth surface integrals (4.1) and (4.2) should be further investigated. In any case they should have some interest for the determination of the external gravity field from surface data.

REFERENCES

Heiskanen, W. and H. Moritz, *Physical Geodesy*, W. H. Freeman and Co., 1967

Rapp, R. H., *OSU Report No. 251*, 1977.

Rapp, R. H., *OSU Report No. 361*, 1984.

Sjöberg, L. E., *Bull. Géod.*, 62, 93-101, 1988.

Sjöberg, L. E. and H. Fan, *Terrain Corrections to Geopotential Models*, 1988 (in preparation).

34

PRECISE SOLUTION FOR A FINITE SET OF SPHERICAL COEFFICIENTS FROM EQUIANGULAR GRIDDED DATA

Paul A. Zucker

The Johns Hopkins University, Applied Physics Laboratory, Laurel, MD 20707

INTRODUCTION

An important goal of geodesy is to determine the anomalous potential and its derivatives outside of the earth. Representing the surface anomalies by a series of spherical harmonics is useful since it is then possible to do a term by term solution of Laplace's equation and upward continuation. This paper addresses the problem of finding such a spherical harmonic series for anomaly values given on an equiangular surface grid. (This is a first step toward the more complicated problem of finding a function such that locally averaged values fit a grid of mean anomalies.) Three approaches to this fitting problem are discussed and compared: the discrete Fourier technique, the discrete integral technique, and a new approach by this author. The peculiar nature of the equiangular grid, with its increasing density of (noisy) data toward the poles, causes each method to exhibit a different type of difficulty. The new method is shown to be practical as well as precise since the numerical conditioning problems which appear can be successfully handled by such well-known techniques as a (simple) Kalman filter.

DISCRETE FOURIER METHOD

The discrete Fourier method [Dilts, 1985] uses a discrete Fourier series to represent both the longitude and latitude variation of the desired function. The data at the (i, j) grid point on a grid of N latitude and 2N longitude intervals can be uniquely represented by the double Fourier series,

$$f(\theta_i, \phi_j) = \sum_{q=-N}^{N} \sum_{m=-N}^{N} A_{qm} e^{iq\theta_i} e^{im\phi_j} . \tag{1}$$

The discrete Fourier method makes its modeling assumption at this point by choosing the function off the grid points to be given by this same double Fourier expansion. Comparison of the continuous spherical representation

$$f(\theta, \phi) = \sum_{n=0}^{L} \sum_{m=-N}^{N} C_{nm} \bar{P}_{nm}(\theta) e^{im\phi} \tag{2}$$

and expansion of the normalized Legendre polynomials

$$\bar{P}_{nm}(\theta) = \sum_{q=-n}^{n} B_q^{nm} e^{iq\theta} \tag{3}$$

to the function modeled as in Equation (1) then yields

$$\sum_{n=0}^{L} C_{nm} B_q^{nm} = \begin{cases} A_{qm} & \text{for } |q| \leq N \\ 0 & \text{otherwise.} \end{cases} \tag{4}$$

A solution exists for the upper limit L, equal to infinity. It can be expressed as

$$C_{nm} = \sum_{q=-N}^{N} Z_q^{nm} A_{qm} \tag{5}$$

where the "inverse" coefficients are obtained from

$$\frac{\pi}{2} \bar{P}_{nm}(\theta) |\sin\theta| = \sum_{q=-\infty}^{\infty} Z_q^{nm} e^{-iq\theta} \tag{6}$$

for θ between zero and 2π radians.

The shortcoming of this approach is the need for an infinite number of terms to solve Equation (4) for arbitrary A_{qm} (representing the data). Small amounts of noise in A_{qm} can lead to the presence of terms in the double Fourier expansion (Eq. (1)) which are not present in the gravity field and which have infinite derivatives at the poles. Truncation of the series is the strategy for coping with this difficulty. After truncation, the function will no longer match the gridded data, and the degree of discrepancy is not under the analyst's control.

DISCRETE INTEGRAL METHOD

The discrete integral approach has been widely used (see for example Colombo [1981]). It approximates the continuous inversion integral for the spherical coefficients by a discrete, weighted sum.

$$C_{nm} = \sum_{i=0}^{N} \sum_{j=0}^{2N-1} \bar{P}_{nm}(\theta_i) e^{-im\phi_j} W_i f(\theta_i, \phi_j) \tag{7}$$

The weights W_i are usually chosen to be the grid block areas. The difficulty with this approach is that the discrete $\bar{P}_{nm}(\theta_i)$ are not orthogonal on the equiangular grid. As a result, aliasing occurs, and the resultant spherical expansion does not match the gridded data. The expansion is truncated at degree N or less, and the amount of the discrepancy is thus only indirectly under the analyst's control. Comparison with the preceding technique is obtained by using the expansion of Equation (6) in the above expression (with the weights proportional to area and the interval extended to 2π):

$$C_{nm} = \sum_{q=-N}^{N} (Z_q^{nm} + Z_{q+2N}^{nm} + Z_{q-2N}^{nm} + \ldots)A_{qm} + \text{pole terms.} \qquad (8)$$

Comparison with Equation (5) shows that it corresponds to the leading term in the above expression. Thus, taking the degree of the discrete integral expansion to infinity does not appear to reproduce the gridded data.

NEW METHOD

The third method is newly presented by this author. It uses the Fourier representation of the data (Equation (1)) but makes its modeling assumption in the spherical domain. Comparison to the spherical expansion <u>only</u> <u>at</u> <u>the</u> <u>grid</u> <u>points</u> yields

$$\sum_{n=0}^{L} C_{nm}(B_q^{nm} + B_{q+2N}^{nm} + B_{q-2N}^{nm} + \ldots) = A_{qm}. \qquad (9)$$

This differs from Equation (4) since it is the result of a discrete comparison at the grid points (using the periodic nature of the discrete exponential) and not a comparison of continuous functions. If L is chosen equal to $N+|m|-2$ (except L=N for m=0), Equation (9) then becomes an invertible matrix equation (with E indicating the sum of the B terms):

$$EC = A \qquad \text{and then} \qquad C = E^{-1}A. \qquad (10)$$

Since the inverse yields a precise fit at the data points, the modeling assumption is that all the C_{nm}'s are zero for n greater than $N+|m|-2$. The continuous function resulting from using these C's in a spherical expansion thus reproduces the data and has a finite number of terms. Since L<2N the elements of the matrix E are easy to compute: at most two of the B terms in Equation (9) are non-zero. Even for terms of degree less than N, this solution is different from the discrete Fourier case, Equation (5), since (ZE) is not the identity.

The difficulty with this method is that the matrix E becomes ill-conditioned for large values of the order m. There are, however, many well-known and trustworthy techniques for dealing with such problems. A few such techniques are summarized below.

o   Perform the transformation of E to the identity in a column by column fashion, stopping when the conditioning becomes a problem. If this process is stopped at the column for degree N, the discrete Fourier approximation is obtained. Further steps toward finding E^{-1} constitute improved approximations.

37

o   Invert the matrix $(E+\delta I)$ for a small δ and use it instead of E^{-1}.

o   Use a simple Kalman filter

$$A = EC + V; \qquad C = E^T(EE^T + \gamma I)^{-1}A \qquad (11)$$

where the measurement noise, V, has variance $\gamma_1 I$ and the prior uncertainty on C is $\gamma_2 I$. Then $\gamma = \gamma_1/\gamma_2$ and is a small quantity.

o   Use a more complicated Kalman filter with detailed models for the noise and for the initial uncertainty.

All of these strategies yield results which are not overly sensitive to noise. By adjusting the parameters in these methods, the analyst can control how close the reconstructed function comes to the gridded data (allowing only for small deviations consistent with the noise model). Use of the Kalman filters also has the advantage of providing uncertainties in the estimated spherical coefficients.

SUMMARY

The problem of fitting a smooth function to data given on an equiangular spherical grid has been discussed. Two existing approaches were summarized and a new approach was presented. Each approach was found to possess an area of difficulty resulting from the properties of the equiangular grid. Well-known techniques (such as Kalman filtering) are available as practical strategies for dealing with the numerical conditioning in the new method. As a result, the new method is practical and capable of reproducing the gridded data to a precision consistent with the noise model.

REFERENCES

Colombo, O. L., Numerical Methods for Harmonic Analysis on the Sphere, Ohio State University Department of Geodetic Science Report 310, 1981.

Dilts, G. A., Computation of Spherical Harmonic Coefficients via FFT's, J. of Computational Physics, 57, 439-453, 1985.

MODELING OF THE EARTH'S GRAVITY FIELD USING THE NEW GLOBAL EARTH MODEL (NEWGEM)

YEONG E. KIM

Department of Physics, Purdue University, West Lafayette, IN 47907

W. Danny Braswell

Nichols Research Corporation, 4040 South Memorial Parkway, Huntsville, AL 35802

Traditionally, the global gravity field has been described by representations based on the spherical harmonic (SH) expansion of the geopotential (Heiskanen and Moritz, 1967). The SH expansion coefficients have been determined by fitting the Earth's gravity data as measured by many different methods including the use of artificial satellites. As gravity data has accumulated with increasingly better accuracies, more of the higher order SH expansion coefficients have been determined (Lerch et al., 1985; Reigber et al., 1985; Rapp, 1987, references therein; Marsh, 1988). The SH representation is useful for describing the gravity field exterior to the earth but is theoretically invalid on the Earth's surface and in the Earth's interior (Heiskanen and Moritz, 1967). Further, the smaller-scale detailed structure of the mass distribution is not reflected in SH representations.

It is well known that there is not a unique distribution of mass which gives rise to a given gravitational potential. Because of this nonuniqueness, other geophysical data such as topographic information and seismic observations must be combined with the gravity data to constrain the possible solutions to those which are geophysically meaningful.

Since some knowledge of the mass distribution in the interior of the Earth is emerging from seismic studies (Dziewonski and Anderson, 1981; Dziewonski and Woodhouse, 1987, references therein) and rather detailed knowledge of the earth's crust and surface is increasingly available in many places, it is desirable to introduce a new physical representation of the mass distribution for the entire Earth which can be refined to accommodate new and more accurate data as it becomes available and which can describe many different component properties and processes of the entire Earth system on both global and regional bases. A new global Earth model (NEWGEM) (Kim, 1987 and 1988a) has been recently proposed to provide a unified description of the Earth's gravity field inside, on, and outside the Earth's surface using (1) the Earth's mass density profile as deduced from seismic studies, (2) elevation and bathymetric information, and (3) local and global gravity data. Using NEWGEM, it is possible to determine the constraints on the mass distribution of the Earth imposed by gravity, topography, and seismic data.

As the zeroth-order approximation for NEWGEM, the ellipsoidal layer (EL) model (Kim and Klepacki, 1987; Kim, 1987) is used. In the EL model the Earth is assumed to consist of n ellipsoidal layers plus a core ellipsoid, with layer densities inferred from the Preliminary Reference Earth Model (PREM) (Dziewonski and Anderson, 1981). EL models have previously been investigated in ellipsoidal coordinates (Moritz, 1968; and references therein) and also in spherical coordinates (Jeffreys, 1976; Moritz, 1973; references therein). The EL model in NEWGEM utilizes cartesian coordinates since analytic solutions for the gravitational potential outside and inside an ellipsoidal layer of uniform density are available in that coordinate system (Kim and Klepacki, 1987; Kim, 1987 and 1988a).

As the first-order correction for NEWGEM, three-dimensional global variations of the mass density profile for the Earth's crust (oceans and continents) and also mass irregularities due to isostasy and the Earth's large -scale interior heterogeneity as observed from seismic data (Dziewonski and Woodhouse, 1987; references therein) are considered. These global corrections are being implemented by dividing the Earth's interior into many small spherical shell segments, each with it's own density. The corrections necessitated by the earth's varying topography are being included using the 5 minute by 5 minute worldwide elevation and bathymetric data base, ETOPO5, available from the National Geophysical Data Center. The total contribution to the gravitational acceleration (both magnitude and direction) at a location can be computed by summing the contributions of each cell. These global corrections will be added to the gravity field of the EL model. The resulting total gravity field will be compared to the International Gravity Standardization Net (IGSN) 1971 (Morelli et al., 1971) and also to the gravity field deduced form ground-based tracking of artificial satellites, GEM-T1 (Marsh et al., 1988).

Recently, the first order global corrections for lateral density variations have been estimated and shown to provide a consistent explanation of signature (attractive or repulsive) and magnitude of apparent anomalies observed in borehole and seafloor gravity measurements carried out as precision tests of Newton's gravitational law (Kim, 1988b).

Higher order corrections to NEWGEM can obtained by calculating the local and/or regional corrections with an additional subdivision of spherical shell segments in the local and /or regional volumes (limited area and depth) without disturbing the zeroth and first order description of the entire Earth system exterior to the local and or regional volumes under consideration. This is one of the advantages of NEWGEM, its capacity to be improved and upgraded indefinitely on local, regional, or global scales as more accurate data (local, regional and/or global) becomes available. This allows the investigation of local and/or regional gravity piecewise but yet as an integral part of the entire Earth system.

Density distributions in NEWGEM will be fine-tuned by requiring reasonable agreement between the NEWGEM gravity field and local gravity data such as the absolute gravity data of the United States (Peter, Moore, and Beruff, 1986). The NEWGEM gravity field will also be constrained to agree with SH expansion models at high altitudes.

NEWGEM is useful in investigating a variety of geophysical phenomena. It is currently being utilized to develop a geophysical interpretation of Kaula's rule (Kaula, 1968; Lambeck, 1976; Kaula, 1977; Cook, 1980). In this investigation, the zeroth order NEWGEM is being used to numerically integrate spherical harmonic expansion coefficients and simultaneously determine the contribution of each layer in the model to a given coefficient. The numerically determined SH expansion coefficients are also being used to test the validity of SH expansions at the surface of the earth by comparing the resulting SH expansion gravity model with exact calculations of the gravity at the Earth's surface.

References

Cook, A.H. (1980). *Interiors of the Planets*, Cambridge University Press, New York.

Dziewonski, A.M. and D.C Anderson (1981). Preliminary Reference Earth Model, *Physics of the Earth and Planetary Interiors*, 25, 297-356.

Dziewonski, A.M. and J.H. Woodhouse (1987). Global Images of the Earth's Interior, Science, Vol. 236, 37-48 (3 April 1987).

Heiskanen, W.A. and H. Moritz (1967). *Physical Geodesy*, Freeman, San Francisco.

Jeffreys, H. (1976). *The Earth*, 6th edition, Cambridge University Press, Cambridge.

Kaula, W.M. (1968). *An Introduction to Planetary Physics: The Terrestrial Planets*, John Wiley, New York.

Kaula, W.M. (1977). Geophysical Inferences from Statistical Analysis of the Gravity Field, *Dep. Geod. Sci. Rep.*, 250, 199, Ohio State University.

Kim, Y.E., D.J. Klepacki, and W.J. Hinze (1987). New force or model-dependent effect in the mine gravity measurements?, Physics Letters B195, 245-253.

Kim, Y.E. and D.J. Klepacki (1987). Newton's Theorem and geophysical determination of in-situ densities from gravity measurements?, *Purdue Nuclear Theory Group Preprint PNTG-87-11*, Purdue University, Indiana.

Kim, Y.E. (1987). Reference level ellipsoids for ellipsoidal layer model of the rotating earth, *Purdue Nuclear Theory Group Preprint PNTG-87-12*, Purdue University, Indiana.

Kim, Y.E. (1988a). New ellipsoidal layer model of the rotating earth and reference ellipsoids, EOS, Vol. 69, No. 16, April 19, 1988, p. 330 (paper G42-08).

Kim, Y.E. (1988b). Apparent anomalies in borehole and seafloor gravity measurements, *Purdue Nuclear Theory Group Preprint PNTG-88-9*, Purdue University, Indiana.

Lerch, F.J., S.M. Klosko, G.B. Patel, and C.A. Wagner (1985). A gravity model for crustal dynamics (GEM-L2), J. Geophys. Res. 90, 9301-9311.

Marsh, J.G. (1988). An enhanced "satellite-only" gravitational model: GEM-T2, EOS Vol. 69, No. 16, April 19, 1988, p. 329, (paper G41-08).

Marsh, J.G. (1988). An improved model of the Earth's gravitational field: GEM-T1, NASA Technical Memorandum 4019, NASA Scientific and Technical Information Division, 354 pages.

Morelli, C., C. Gantar, T. Honkasalo, R.K. McConnell, I.G. Tanner, B. Szabo, U. Uotila, and C.T. Whalen (1971). The international gravity standardization net 1971: I.A.G., 39 ter rue Gay Lussac, 75005 Paris, 194 p.

Moritz, H. (1968). Density distributions for the equipotential ellipsoid, Report No. 115, Department of Geodetic Science, Ohio State University; Mass distributions for the equipotential ellipsoid, Bollettino di Geofisica Teorica ed Applicata, Vol X, No. 37 (March 1968), p. 58-65.

Moritz, H. (1973). Ellipsoidal mass distributions, Report No. 206, Department of Geodetic Science, Ohio State University.

Peter,G., R.E. Moose, and R.B. Beruff (1986). New U.S. absolute gravity program, EOS, Vol. 67, no. 51, p. 1393, December 23, 1986.

Rapp, R.A. (1987). Status of the geopotential, *Rev. Geophys.* 25, 864-866.

Reigber, C., G. Balmino, H. Mueller, W. Bosch, and B. Moynot (1985). GRIM gravity model improvement using LAGEOS (GRIM3-L1), J. Geophys. Res. 90, 9285-9299.

Gravity Field Measuring Techniques

Moderators: Christopher Jekeli

Klaus-Peter Schwaz

A FRAMEWORK FOR MODELLING KINEMATIC MEASUREMENTS IN GRAVITY FIELD APPLICATIONS

K.P. Schwarz and M. Wei

Department of Surveying Engineering, The University of Calgary

N90-20524

ABSTRACT

To assess the resolution of the local gravity field from kinematic measurements, a state model for motion in the gravity field of the earth is formulated. The resulting set of equations can accommodate gravity gradients, specific force, acceleration, velocity and position as input data and can take into account approximation errors as well as sensor errors.

1. PROBLEM STATEMENT

The last few years have seen major advances in kinematic methods of gravimetry. Shipborne gravimetry, already a reliable tool, will be further enhanced by using accurate position and velocity information from differential GPS. Airborne gravimetry in either the fixed wing aircraft or helicopter mode experienced a resurgence over the last few years and is at the point where it provides gravity information of acceptable accuracy for wavelengths down to 10 or 15 km. Airborne gravity gradiometry has entered the testing stage and holds great potential for short wavelength resolution. Compared to even fifteen years ago, there is now a variety of sensors on the market and it appears that a judicious combination will yield information on different parts of the gravity spectrum. To assess different sensor configurations, a model is needed which allows the combination of kinematic measurements from gravity gradiometers, dynamic gravity meters, inertial sensors, differential GPS, laser altimeters, precise pressure altimeters and similar devices. The model must allow for the interaction of gravitational and inertial measurements and must be able to take sensor biases and measurement noise into account. The formulation of such a model using state space techniques is the topic of this extended abstract. A detailed derivation with a comprehensive list of references will be published in the near future.

2. THE STATE SPACE MODEL OF KINEMATIC GEODESY

Newton's second law for motion in the gravitational field of the Earth, expressed in an inertial frame of reference (i), will be taken as the starting point

$$\ddot{r}_i = f_i + \bar{g}_i \tag{1}$$

where r_i is the position vector from the origin of the inertial frame to the moving object and $\ddot{r}_i$ is the second time derivative of this vector, f_i is the specific force vector, and $\bar{g}_i$ is the vector of all gravitational accelerations acting on the moving object.

The set of nonlinear second-order differential equations (1) can be transformed into a set of first-order equations of the form

$$\begin{pmatrix} \dot{r}_i \\ \dot{v}_i \end{pmatrix} = \begin{pmatrix} v_i \\ f_i + \bar{g}_i \end{pmatrix} . \tag{2}$$

In general, measurements will not be taken in an inertial frame of reference but in an arbitrary body frame (b). They can, be transformed into an inertial reference frame by

$$f_i = R_{ib} \, f_b \tag{3}$$

where R_{ib} is a three-dimensional orthogonal matrix transforming f_b from the body frame (b) to the inertial frame (i). Note that the subscripts denote the direction of the rotation, not the element in the matrix. It is obvious from equation (3) that measurements f_b can only be used if R_{ib} is known

44

or can be measured. Thus, a set of three first-order differential equations for the rotation rates R_{ib} has to be added to equation (2). They are of the form

$$\dot{R}_{ib} = R_{ib} \, \Omega_b^{ib} \tag{4}$$

where Ω_b^{ib} is the skew-symmetric matrix of angular velocities.

Similarly, gravitation is usually not given in an inertial frame but in the Conventional Terrestrial frame, which will be denoted by (e) in the following. We thus have the transformation

$$\bar{g}_i = R_{ie} \, \bar{g}_e \, . \tag{5}$$

Since the rotation rate of the Earth can be considered constant for the applications discussed here, no additional equations for R_{ie} have to be added. Using equations (3) to (5) in (2) leads to the state equations

$$\dot{x}_i = \begin{pmatrix} \dot{r}_i \\ \dot{v}_i \\ \dot{R}_{ib} \end{pmatrix} = \begin{pmatrix} v_i \\ R_{ib} \, f_b + R_{ie} \, \bar{g}_e \\ R_{ib} \, \Omega_b^{ib} \end{pmatrix} \tag{6}$$

describing rigid-body motion in three-dimensional Euclidean space by three rotational and three translational parameters.

The implicit assumption in equation (6) is that gravitation $\bar{g}_e$ is known. In that case, the measurement of the specific force f_b and the rotation rates R_{ib} is sufficient to determine position, velocity, and attitude as functions of time. If gravitation is not known as a function of time, additional measurements are necessary. They can be of two types, inertial or gravitational. In the first case, v_i is determined independently, in the second case $\bar{g}_i$ is obtained. In both cases, gravitation and inertia can be separated in the second set of equations in (6). Thus, in principle, position, velocity, attitude and gravitation can be obtained by measuring f_b, R_{ib} and either v_i or $\bar{g}_i$ independently. The second case which is that of gravity gradiometry will now be discussed.

To transform equation (6) into a system that also admits gravity gradiometer measurements, a set of equations describing the change of the gravitational vector with time has to be added. It is obtained by differentiating equation (5)

$$\dot{\bar{g}}_i = \dot{R}_{ie} \, \bar{g}_e + R_{ie} \, \dot{\bar{g}}_e = R_{ie} \, (\Omega_e^{ie} \, \bar{g}_e + \dot{\bar{g}}_e)$$

where

$$= R_{ie} \, (\Omega_e^{ie} \, \bar{g}_e + G_e \, v_e) = \Omega_i^{ie} \, \bar{g}_i + G_i \, (v_i - \Omega_i^{ie} \, r_i) \tag{7}$$

$$G_e = \frac{\partial \bar{g}_e}{\partial r_e} = \frac{\partial^2 V_e}{\partial r_e \, \partial r_e} \tag{8}$$

is the matrix of second-order gradients of the gravitational potential V_e. The state vector which includes gradient measurements of type (7) is therefore of the form

$$\dot{x}_i = \begin{pmatrix} \dot{r}_i \\ \dot{v}_i \\ \dot{R}_{ib} \\ \dot{\bar{g}} \end{pmatrix} = \begin{pmatrix} v_i \\ R_{ib} \, f_b + \bar{g}_i \\ R_{ib} \, \Omega_b^{ib} \\ \Omega_i^{ie} \, \bar{g}_i + G_i \left(v_i - \Omega_i^{ie} r_i \right) \end{pmatrix} \tag{9}$$

3 CHANGE OF COORDINATE FRAME AND LINEARIZATION

In many cases, results are required in an earth-fixed coordinate frame and transformation of equations (9) into such frames are needed. They obviously involve the representation of the corresponding states in a rotating frame. The transformations are somewhat tedious and are given here without proof for the conventional terrestrial frame (e) and for the local-level frame (l).

In the first case, we get

$$\dot{x}_e = \begin{pmatrix} \dot{r}_e \\ \dot{v}_e \\ \dot{R}_{eb} \\ \dot{g}_e \end{pmatrix} \begin{pmatrix} v_e \\ R_{eb}\,f_b - 2\Omega_e^{ie}\,v_e + g_e \\ R_{eb}\,\Omega_b^{eb} \\ \left(R_{eb}\,G_b\,R_{be} - \Omega_e^{ie}\,\Omega_e^{ie}\right)v_e \end{pmatrix}$$

(10)

where g_e is the gravity vector. The transformation into the local-level frame 1, using curvilinear (φ, λ, h)-coordinates, follows along similar lines, and results in the state vector

$$\dot{x}_l = \begin{pmatrix} \dot{r}_l \\ \dot{v}_l \\ \dot{R}_{lb} \\ \dot{g}_l \end{pmatrix} = \begin{pmatrix} D v_l \\ R_{lb}\,f_b - \left(2\Omega_l^{ie} + \Omega_l^{el}\right) v_l + g_l \\ R_{lb}\,\Omega_b^{lb} \\ \left(R_{lb}\,G_b\,R_{bl} - \Omega_l^{ie}\,\Omega_l^{ie}\right)v_l - \Omega_l^{el}\,g_l \end{pmatrix}$$

(11)

where

$$D = \begin{pmatrix} 1/R & 0 & 0 \\ 0 & 1/(R\cos\varphi) & 0 \\ 0 & 0 & 1 \end{pmatrix}$$

The state equations derived up to this point are all nonlinear. The first step towards the solution of the differential equation system is usually linearization about a reference trajectory. The reference trajectory is obtained by introducing a gravity model into equation (9) and by integrating the gravity corrected measurements. Equation (9) can be written in the general form

$$\dot{x} = f\,\{r,\,v,\,w,\,\bar{g}\,\}$$

(12)

where w denotes the angular velocities in the Ω^{ib} and the Ω^{ie} matrices. Subscripts have been omitted for convenience. It can be rewritten as

$$\dot{x}^o + dx^o = f\,\{r^o + dr,\,v^o + dv,\,w^o + dw,\,\bar{g}^o + dg\,\}$$

(13)

where the superscript o denotes the reference trajectory and d the perturbation. By separating the reference trajectory

$$\dot{x}^o = f\,\{r^o,\,v^o,\,w^o,\,\bar{g}^o\,\}$$

(14)

from equation (12) and considering only first-order perturbations, the following set of equations is obtained

$$
\begin{pmatrix} d\dot{r} \\ d\dot{v} \\ d\dot{w} \\ d\dot{g} \end{pmatrix} = \begin{pmatrix} F_{11} & F_{12} & F_{13} & F_{14} \\ F_{21} & -- & -- & -- \\ F_{31} & -- & -- & -- \\ F_{41} & -- & -- & F_{44} \end{pmatrix} \begin{pmatrix} dr \\ dv \\ dw \\ dg \end{pmatrix} \tag{15}
$$

which is a set of linear homogeneous state equations of the form

$$
\dot{x} = Fx \quad . \tag{16}
$$

The matrices F_{11} to F_{33} are well known from the literature. F_{41} to F_{44} are obtained by developing the perturbation solution for g. In the local-level frame, we get the reference solution

$$
\dot{g}^o = \{ G^o (r^o) - \Omega^{ie}(r^o) \, \Omega^{ie}(r^o) \} \, v^o + \Omega^{el}(r^o) \, \bar{g}^o(r^o) \tag{17}
$$

and the perturbation solution

$$
d\dot{g} = \{ G^o - \Omega^{ie}\Omega^{ie} \} \, dv + dG \, v^o - \Omega^{el} \, dg - d\Omega^{el}g^o \tag{18}
$$

where

$$
dG = (G - G^o) + \left\{ \frac{\partial G^o}{\partial r} dr + \frac{\partial G^o}{\partial v} dv + \frac{\partial G^o}{\partial w} dw \right\} \tag{19}
$$

Using equations (18) and (19) in (15) will give the desired solution.

4   SENSOR ERROR MODEL

The linearized model given by equation (16) is the kinematic description of rigid body motion in the gravity field of the Earth. Except for approximation errors, it is a rigorous model. If sensors are used to determine the trajectory and the gravity vector, the above model has to be augmented by a set of error states for each of the sensors used and by system noise. The resulting equations will be of the general form

$$
\begin{pmatrix} \dot{x}_1 \\ \dot{x}_2 \end{pmatrix} = \begin{pmatrix} F_1 & 0 \\ 0 & F_2 \end{pmatrix} \begin{pmatrix} x_1 \\ x_2 \end{pmatrix} + Gu \tag{20}
$$

where x_1 contains the states in equation (15) and x_2 the error states, and where F_1 and F_2 are the corresponding dynamics matrices, and Gu describes the system noise. The F_2-matrix has a block-diagonal structure because the error states of the individual sensors are uncorrelated.

The error states are modeled in a stochastic manner by random biases, random walk models, or simple Gauss-Markov processes. Some judgement is required to decide whether a specific error source is modeled into x_2 or into Gu. If real-time estimation is performed with the model (20), a small state vector is often desirable.

ACKNOWLEDGEMENTS

Synopsis of Early Field Test Results from the Gravity Gradiometer Survey System

S. Brzezowski,[*] D. Gleason,[+] J. Goldstein,[*] W. Heller,[*] C. Jekeli,[+] and J. White[*]

The Analytic Sciences Corporation, Reading, Massachusetts
+*The Air Force Geophysics Laboratory, Hanscom AFB, Massachusetts*

ABSTRACT **N90-20525**

Initial airborne and surface testing shows that the earth's gravity gradients can be usefully measured both from an aircraft and an automotive vehicle.

1. BACKGROUND

The Gravity Gradiometer Survey System (GGSS) is a mobile unit that measures the five independent gradients of Earth's gravity vector. The system includes three gradiometer instruments and ancillary inertial hardware mounted on a local-level stabilized platform, a navigation system, and electronic support equipment. The entire apparatus is housed in a van that has the capability of surveying along roadways or of operating while being carried in a C-130 cargo airplane. Data processing includes an initial stage of demodulation, filtering, self-gradient corrections, acceleration sensitivity compensations and accounting for other environmental influences. Secondary postprocessing to obtain gravity component estimates includes bias estimation (using cross-over constraints and tie-point data), followed by along-track integration and downward continuation (for the airborne case) performed as an optimal, minimum variance estimation process. The tests to assess the survey accuracy of the GGSS were conducted primarily in the Texas-Oklahoma Panhandle area where the terrain is very smooth while the gravity signature is moderately pronounced. About 120 tracks were flown at nearly constant altitude (about 1000 m above ground) in a regular grid of north-south, east-west tracks. Each track is 315 km long with a nominal spacing of 5 km between tracks. In addition, surface testing was conducted which included two traverses performed on the same highway route.

2. AIRBORNE TEST DATA RESULTS

From the airborne GGSS test data collected in spring of 1987, a total of 56 distinct tracks were considered by the gradiometer operator to be appropriate for further analysis. Upon examination, the need to edit the data for erratic flight trajectory, loss of signal, and excessive noise was apparent and resulted in the elimination of 21 tracks from further processing. The resulting "edited" 35 tracks show sporadic occurrences of mostly-isolated spikes in the measured gradients. The spikes were removed by detection with a matched filter and deconvolving with the impulse response of the demodulator filter.

Based on their length and orientation with respect to the other edited tracks, 20 of the 35 tracks were selected for estimating gravity disturbances. The gradient data along these tracks were resolved into an appropriate local-level reference frame. Five-minute by five-minute gravity disturbances along each track were then estimated using a Kalman

smoothing algorithm. The smoother included error models for the GGSS white noise floor [as identified from Power

Spectral Densities (PSDs)], the gradient bias uncertainty (based on track length and PSD), and the uncertainty associated

with each tiepoint (rms uncorrelated error of 2.0 mgal). Single-track spectral analysis indicated that the GGSS contrib-

uted noise power ranging from 350 to 1700 E^2/Hz (double-sided PSD). Gravity disturbance estimates were compared

with corresponding quantities derived from an available five-minute by five-minute mean gravity disturbance truth

dataset. The truth values were interpolated along each GGSS track using a four-point bilinear smoother. Along the best

tracks, the vertical component of the gravity disturbance vector could be recovered with an rms error of about 5 mgal for

tiepoints over 200 km apart. The rms accuracy improved to 2 to 4 mgal when the tiepoint spacing was reduced to about

90 km.

Thirteen of the foregoing 20 tracks were situated in sufficiently close proximity (Figure 1) to permit investigation

of the increased accuracy obtainable for multi-track analysis. The TASC template algorithm (Refs. 1, 2) was used to

perform gravity disturbance estimation within the areas bounded by the intersections of the 13 tracks. The template

algorithm was used with the Clinton-Sherman Attenuated White Noise Statistical Gravity Model (Ref. 3), data-derived

error models for the GGSS measurements, and the rms uncertainty of the tiepoint values. A summary comparison of

these multi-track estimates with corresponding surface truth values is presented in Table 1. The two distinct cases

considered were 1) tiepoints at the ends of each track, and 2) tiepoints only at the centers of the boundary tracks. For

each case, the actual rms error agreed well with the predicted rms errors provided by the template algorithm covariance

equations (Ref. 4).
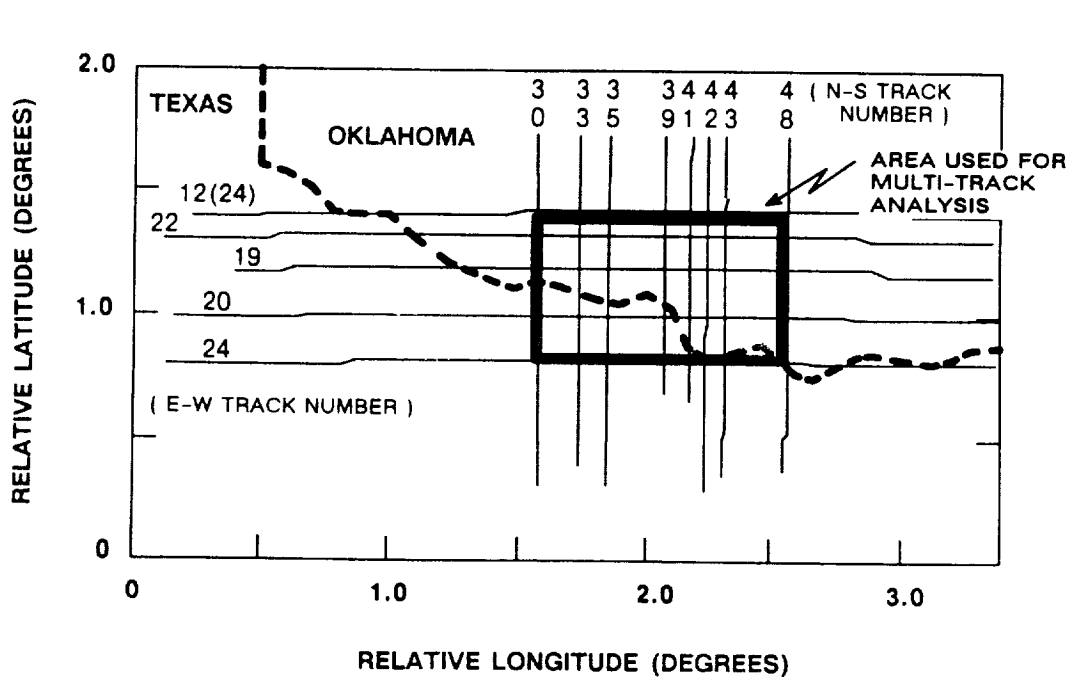
Figure 1. Tracks and area selected for multi-track analysis.

Table 1. Summary of multi-track comparisons.

CASE	RMS ERROR: ALL POINTS (mgal)		RMS ERROR: NON-TIE POINTS (mgal)		WORST CASE ACTUAL ERROR (mgal)
	PREDICTED	ACTUAL	PREDICTED	ACTUAL	
Tiepoints at Ends of Each Track	1.93	1.64	2.33	2.16	3.72
Tiepoints at Centers of Boundary Tracks	4.34	3.27	4.53	3.44	8.77

Deflections of the vertical were estimated along several of the tracks using line integration at altitude. In Figure 2, GGSS estimates for two selected tracks are compared with surface truth data derived using Vening-Meinesz integration. Source data consisted of a two-degree "square" inner zone containing 1'x1' mean anomalies, a middle zone having a six-degree by eight-degree outer perimeter with 5'x5' mean anomalies and an outer zone consisting of 30'x30' mean anomalies over the rest of the earth. The data was provided by DMA.
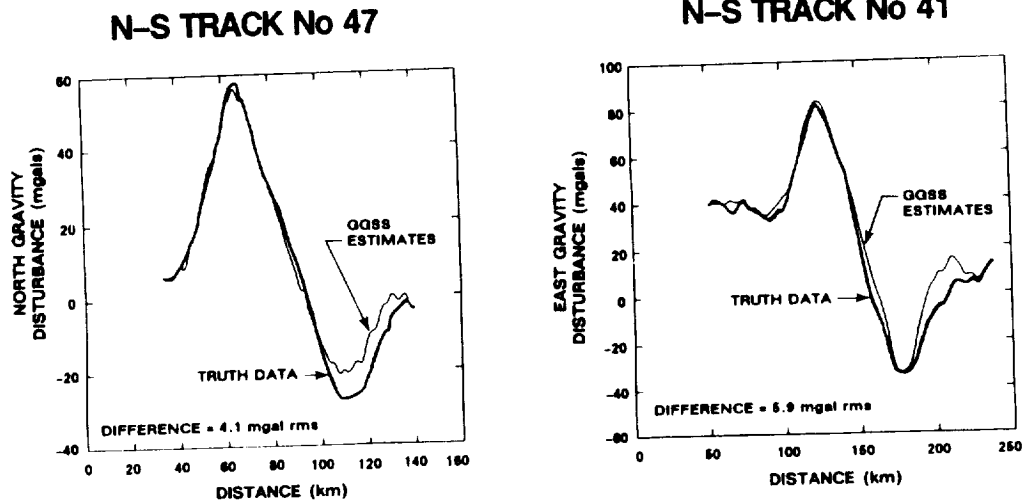
Figure 2. Horizontal gravity disturbance components at the surface.

3. SURFACE TEST DATA RESULTS

Surface GGSS testing was performed along a 53 km section of paved road near the Clinton-Sherman airfield. Two tracks of repeat traverse data (one taken on 6 June 1987 the other on 9 June) were processed by the gradiometer operator. The data quantities of interest available for each track were: time, fifth-wheel aided inertial latitude and longitude, altitude, heading, and the inline and cross gradients for each of the instruments in the triad. As with the airborne data, isolated spikes were present in the gravity gradients.

In addition to spike removal, navigation system performance was analyzed to assure that position misregistration errors of the relatively high frequency surface gradient field were not mistaken as GGSS noise (Ref. 5). Kalman-Smoothed estimates of all three components of the gravity disturbance vector were performed. The vertical and

along-track components are presented in Figure 3. For the repeatability analysis shown in Figure 3, the tiepoint spacing

for the deflection of the vertical data was 46 km and the rms accuracy was 0.5 arcseconds. Vertical disturbance tiepoints,

spaced at 52.8 km, were assigned an rms accuracy of 2.0 mgal.
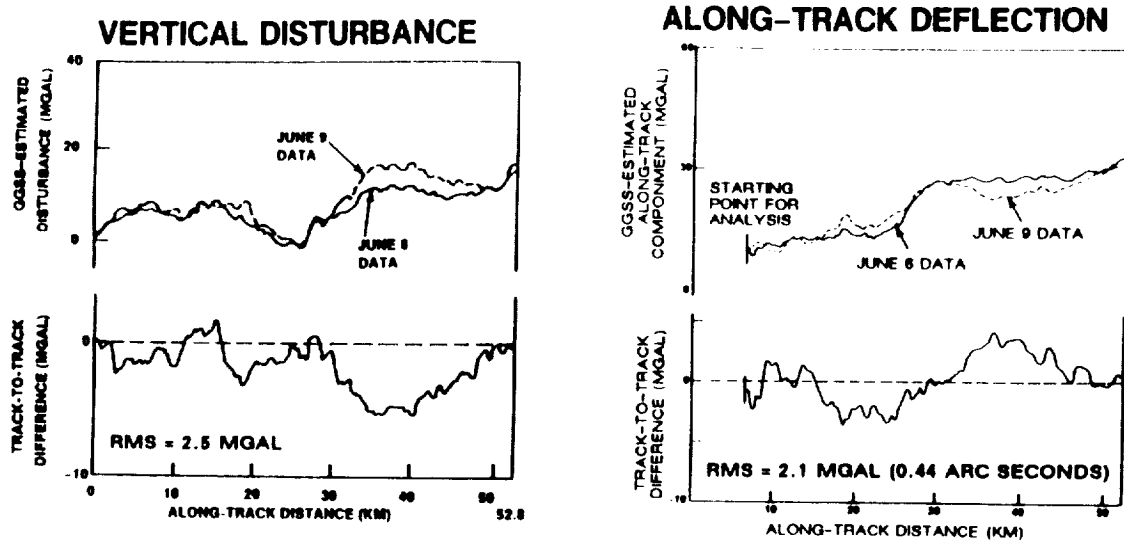
Figure 3. Kalman-smoothed gravity disturbance estimation for individual surface tracks.

4. CONCLUSIONS

Although the amount of data yielded by the tests was modest, it was sufficient to demonstrate that the full gravity

gradient tensor had been successfully measured from moving platforms both in the air and on the surface. The measure-

ments were effectively continuous with spatial along-track resolution limited only by choice of integration lengths taken

to reduce noise. The airborne data were less noisy ($800 \, E^2$/Hz typical) than were GGSS measurements taken at the

surface ($5000 \, E^2$/Hz typical). Single tracks of surface gravity disturbances recovered from airborne data were accurate

to 3 to 4 mgal in each component of gravity when compared to 5'x5' mean gravity anomalies over a 90 km track. Multi-

track processing yielded 2 to 3 mgal when compared to 5'x5' mean anomalies. Deflection of the vertical recovery over a

distance of 150 km was about one arcsecond.

REFERENCES

1. White, J.V., and Goldstein, J.D., *Gravity Gradiometer Survey Data Processing*, The Analytic Sciences Corpo-
ration, **Technical Report AFGL-TR-84-0198**, July 1984, ADA156165.

2. Goldstein, J.D., and White, J.V., *A Template Approach to GGSS Data Reduction*, Thirteenth Moving-Base
Gravity Gradiometer Review, U.S. Air Force Academy, CO, Feb 1985.

3. White, J.V., *A Statistical Gravity Model for Northern Texas*, The Analytic Sciences Corporation, **Technical
Report AFGL-TR-84-0037**, Nov 1984, ADA160474.

4. Brzezowski, S.J., and Heller, W.G., *Gravity Gradiometer Survey Errors*, **Geophysics**, Oct 1988, pp. 1355-1361.

5. Shipp, R.F., and Heller, W.G., *Navigation/Stabilization Requirements for Airborne/Surface Gravity Grad-
iometer Survey Missions*, Paper presented at AIAA Guidance and Control Conference, Seattle, WA, Aug 1984.

Gravity Field of the Western Weddell Sea:
Comparison of Airborne Gravity and Geosat Derived Gravity

R.E. Bell[1], J.M. Brozena[2], W.F. Haxby[1] and J.L. LaBrecque[1]

[1]Lamont-Doherty Geological Observatory, Palisades, NY 10964
[2]Code 5110, Naval Research Laboratory, Washington, DC 20375-5000

Introduction

Marine gravity surveying in polar regions has typically been difficult and costly, requiring expensive long range research vessels and ice-breakers. Satellite altimetry can recover the gravity field in these regions where it is unfeasible to survey with a surface vessel. Unfortunetly, the data collected by the first global altimetry mission, Seasat, was collected only during the austral winter, producing a very poor quality the gravity field for the southern oceans, particularly in the circum-Antarctic regions. The advent of high quality airborne gravity (Brozena, 1984; Brozena and Peters, 1988; Bell, 1988) and the availability of satellite altimetry data during the austral summer (Sandwell and McAdoo, 1988) has allowed us to recover a free air gravity field for most of the Weddell Sea. This paper will briefly review the derivation of the gravity field from both aircraft and satellite measurements before presenting along track comparisons and shaded relief maps of the Weddell Sea gravity field based on these two data sets.

Airborne Collection and Reduction

The airborne gravity was collected using the Naval Research Laboratory's Airborne Gravity Surveying System. This system includes a Lacoste-Romberg air-sea gravimeter, a short pulse radar altimeter, a pressure altimeter and two GPS sets, a TI 4100, a P-code receiver and a Magnovox T-set, a CA-code receiver. To extract the geologically interesting free air anomaly (A_{FAA}) from the total accelerations recorded by the gravimeter (A_M) the position of the aircraft in three components must be well determined. The relationship between the total measured acceleration field (A_M) and the free air anomaly (A_{FAA}) is described by the equation:

$$A_M = A_{FAA} + A_{aircraft} + A_{Eotovs} + A_{Theo} + A_{FAC}$$

where $A_{aircraft}$ is the acceleration associated with the vertical motion of the aircraft, A_{Theo} is the gravity on the ellipsoid, A_{Eotovs} is the correction necessary for all gravity measurements made from a platform moving across a rotating earth and A_{FAC} is the free air correction necessary to reduce the airborne measurement to the geoid. In contrast, to marine surveys where the maximum correction is 75 mgal, the amplitudes of these corrections far exceed the amplitudes of the gravity anomalies associated with such large features as seamounts, fracture zones and sedimentary basins (Figure 1).

A_{FAA}	$A_{Aircraft}$	A_{Eotvos}	A_{Theo}	A_{FAC}
+/- 400 mgal	+/- 600 mgal	+/- 1500 mgal	~980000 mgal	~150 mgal
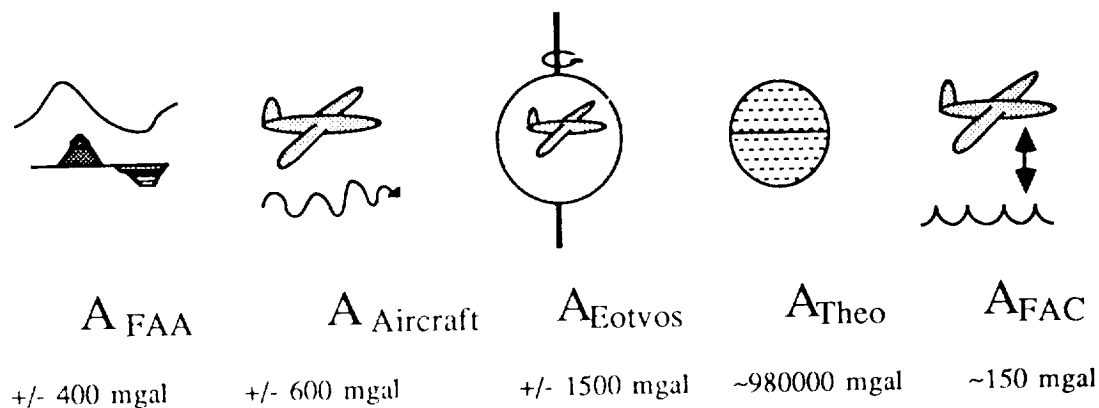
Figure 1. Schematic illustrating the components of the total acceleration field A_M measured by a gravimeter mounted aboard an aircraft and the possible amplitude range of each component.

The GPS receivers are used to monitor the horizontal velocities and the aircraft horizontal position necessary for A_{colovs} and A_{Thoo} while the radar and pressure altimeters are used to monitor the aircraft's vertical position. The vertical positions measured by the altimeters were used to calculate the vertical acceleration field of the system (A_{aircraft}) and the free air correction (A_{FAC}). For the 12000 km of data collected in the 1987 field season, the pre-adjustment crossover errors were 4.59 mgal for 84 crossings and improved to 2.25 mgal after along track adjustment.

Satellite Data Collection and Reduction

Extracting the gravity field from the Geosat data involves first editing the individual sea surface height profiles, adjusting profiles to minimize crossover errors, gridding the data to produce a geoid and finally calculating the gravity field. Each track was edited to remove the data crossing land and regions where the σ_n for 7 points exceeds 10 cm, a criterea which removes most of the noisy data across multi-year ice. After the tracks are edited, the repeat orbits are averaged to produce a mean profile. The crossover errors for these adjusted mean profiles are reduced to a minimum using an iterative least squares approach. Finally, gravity anomalies are calculated from the gridded altimetric geoid using Fourier transform methods.

The strength of the satellite data in the Weddell Sea is that it provides the very dense data coverage and the regular track spacing. In the central Weddell 3 to 4 orbits are averaged to produce the mean profile. However close to the limit of the satellite coverage, notably across the ice covered margin of the western Weddell, often only one orbit was available, resulting in a deterioration of the gravity field recovery.

Merging the Airborne and Satellite Gravity Fields

The two gravity data sets are quite complimentary as the airborne survey fills in a large hole in the satellite coverage where the altimetry was quite poor while the Geosat data provides the only ground truth available for the airborne gravity survey (Figure 2). No major offset exists between the two data sets. The two were merged so that in the extreme western and southern sections of the Weddell Sea the airborne gravity was used as in this region generally only one satellite pass was available to calculate the mean profile and the number of crossing tracks was small. In the central and northern Weddell Sea the satellite data was used in preference to the airborne data as in this region the satellite tracks are much denser than the airborne tracks. Figure 3 shows shaded relief maps of the gridded Geosat gravity field and the combined satellite and aircraft gravity field. The prominent features are the north-south trending continental margin edge effect and the regularly spaced fracture zone lineations trending northeast-southwest in the southern Weddell and northwest-southeast in the northern Weddell. An important result of this work is the dramatic relocation of this north-south trending continetal margin. Earlier bathymetric maps, based on sparse data, placed the shelf edge over 100 km to the east of the location now required by the prominent edge effect in the airborne gravity field. The strongly lineated gravity anomalies mapped in the satellite field are suggestive of major reorganization in the Weddell Sea spreading system at approximately 80 my (Haxby, 1988).

Airborne Gravity Tracks   Geosat Tracks
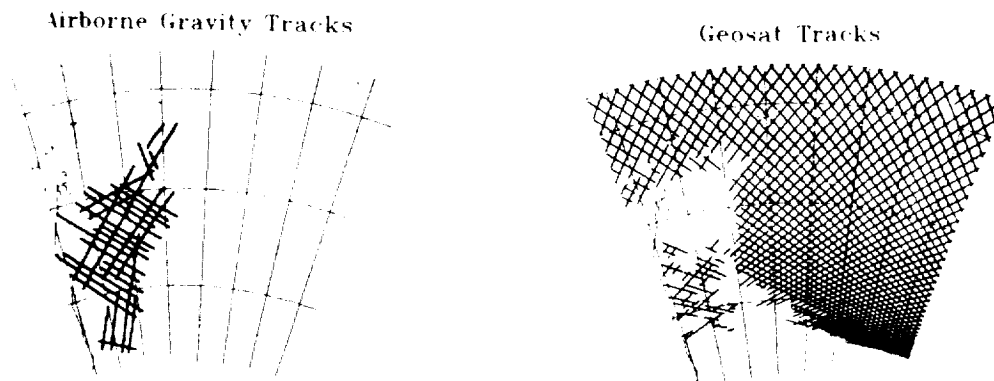
Figure 2. Track spacing the for 1987 airborne gravity survey (left) and for the Geosat mission (right). The limits of the map are 62°W to 23°W and 75°S to 58°S.
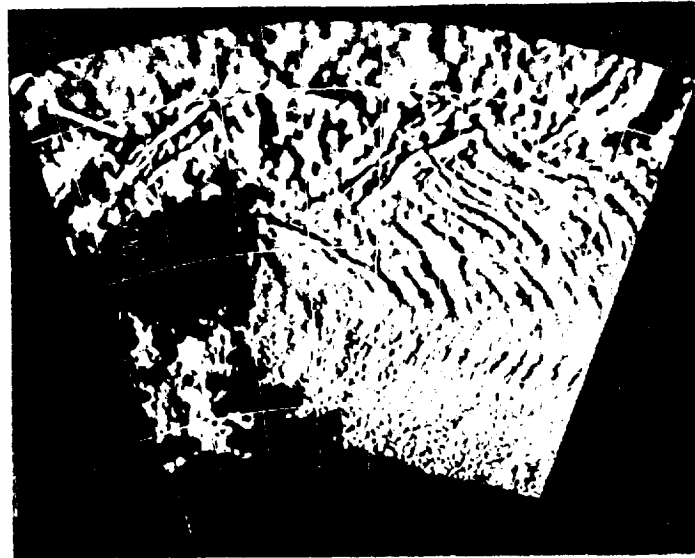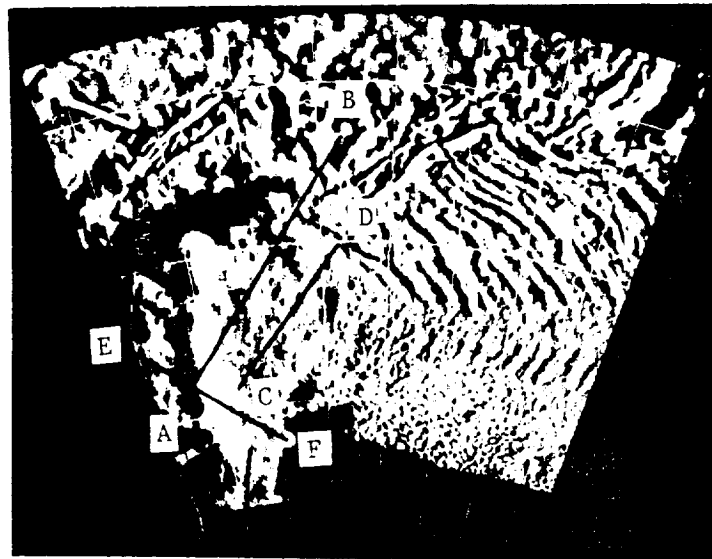
Figure 3. Shaded relief maps of the gravity field derived from the Geosat gridded geoid (upper) and the satellite data set merged with the gridded airborne gravity (lower). The illumination is from the east and the limits of the map are 62°W to 23°W and 75°S to 58°S. The lines on the merged image are the profiles presented in Figure 4.

In addition to revealing important structural features in the Weddell Sea, the merging of the two data sets has permitted us to document the validity of these two techniques in a region where no other gravity data exist. A series of along track comparisons are shown in Figure 4 where the solid line is the airborne data and the double line is the Geosat data resampled along the airborne flight lines. The agreement between the two data sets is remarkably good particularly along line A-B. Along this line the RMS difference between the two is 7.26 mgal for 723 points. Both systems recover the relatively long wavelength shelf edge anomaly and the short wavelength features (~15 km) just south of the Orkney Plateau at the northern end of the line. Line C-D also illustrates the agreement between these two methods across the 20 mgal step associated with an age discontinuity in the oceanic crust. The difficulty in using the satellite altimeter in regions of thick ice is clear in line E-F where the Geosat solution diverges from the airborne solution at the base of the shelf, a region where the ice is known to the thick.
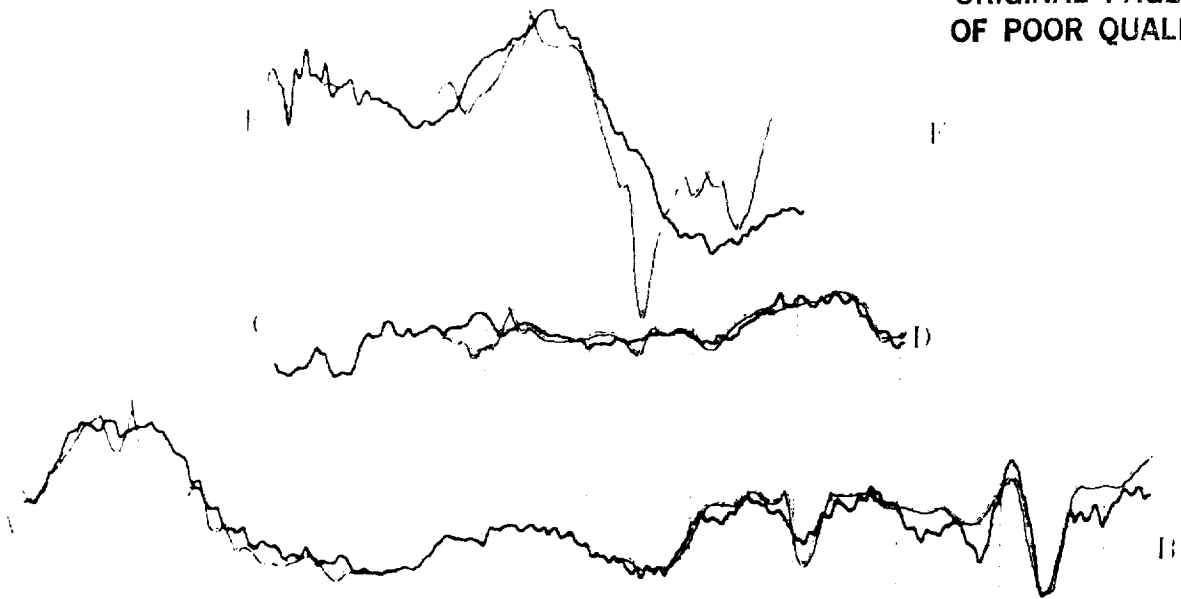
Figure 4. Along track comparisons of airborne gravity (solid line) and Geosat derived gravity (double line). The location of each profile is plotted on the accompanying image in Figure 3. The gridline spacing is 100 km on the horizontal axis and and 10 mgal on the vertical axis.

In conclusion, the gravity field of the Weddell Sea has been mapped using both the NRL airborne gravity system and Geosat altimetric gravity. The resultant map clearly delineates the western and southern margins of the Weddell Sea, well defined in the airborne results and large fracture zones signatures in the central Weddell, recorded by the altimetric gravity anomalies. These two data sets were compared in areas of overlap where gravity anomalies computed from gridded Geosat sea surface height were resampled along the airborne tracks. The RMS difference between the two data sets for 5483 points was 13.05 mgal with a mean of 1.60 mgal. Along track comparisons reveal that these two data sets resolve very similar wavelength features. Fracture zone signatures with widths of 15 km and amplitudes of 20 mgal are detected by both systems. The airborne system has the advantage of being able to collect data in regions of multi-year ice and focus on regions of interest while the Geosat data provides a very regular, regional coverage of the ice free region.

References

Bell, R. E., High Resolution Marine and Airborne Gravity Surveys: Applications to Rifted Margins, PhD Dissertation, Columbia University, 1988.

Brozena, J.M. and M.F. Peters, An Airborne Gravity Study of Eastern North Carolina, *Geophysics*, 53, 245 - 253, 1988.

Brozena, J.M., A Preliminary Analysis of the NRL Airborne Gravity System, *Geophysics*, 49, 1060 - 1069, 1984.

Haxby, W.F., Organization of Oblique Sea Floor Spreading into Discrete, Uniformly Spaced Ridge Segments: Evidence from Geosat Altimeter Data in the Weddell Sea, *EOS, (Fall AGU volume)* 1988.

Sandwell, D.T. and D.C. McAdoo, Marine Gravity of the Southern Ocean and Antarctic Margin from Geosat, 93, 10389 - 10396, *Journal of Geophysical Research*, 1988.

Terrestrial Gravity Instrumentation In The 20th Century:

A Brief Review

H. D. VALLIANT

LaCoste and Romberg Gravity Meters Inc., Austin, Tx 78759

At the turn of the century, only pendulum apparatuses and torsion balances were available for general exploration work. Both these early techniques were cumbersome and time-consuming. Although portable, torsion balances weighed up to 72 kg (160 lbs) (Steiner, 1926) and required an observing hut for protection from sun and wind. They were extremely sensitive to close-by terrain effects which had to be measured with painstaking detail to a radius of 100 m (30 ft) around the instrument (Heiland, 1933). Often the terrain had to be physically smoothed to a distance of 10 m (3 ft). Accuracy of pendulum measurements suffered because time standards of the day were pendulums themselves. The period of the roving pendulum could only be compared with that of another pendulum at a fixed site, or with a spring chronometer calibrated against a pendulum at a fixed site. This requirement was one factor that gave rise to the need for broadcast time signals and partly accounts for the early association between astronomy, time standards and geophysics. Vening Meinesz (1929) developed the technique of making shipboard observations with pendulums.

It was no wonder that the development of the gravity meter was welcomed with a universal sigh of relief. By 1935 potential field measurements with gravity meters supplanted gradient measurements with torsion balances. The invention of the so-called zero-length spring mechanism by Dr. Lucien LaCoste (1934) has been the basis for gravity meter (and long period seismometer) design for more than fifty years. Gravity meters of this type were erroneously labeled "astatic" because they were capable of achieving infinite sensitivity. Astatic gravity meters soon replaced "static" gravity meters and were developed through the years for a wide variety of applications, including: measurements on land, in bore-holes, under water, on the sea-surface and in the air. Measurements from a moving platform were made possible with the discovery by LaCoste (1967) that an overdamped, infinitely sensitive gravity meter could provide an instantaneous response and large dynamic range. With the help of modern electronics "static" gravity meters were also developed (Jacoby, 1970) for less precise dynamic applications and within the past five years (Hugill, 1984) for precise stationary observations.

Potential field measurements are generally characterized by three types:

1) **Absolute:** Measurements are made in fundamental units, traceable to national standards of length and time at each observation site.

2) **Relative with absolute scale:** Differences in gravity are measured in fundamental units traceable to national standards of length and time.

3) **Relative:** Differences in gravity are measured with arbitrary scale.

The free-fall apparatus is an example of the first type. Pendulums offer an example of both types 1 and 2, depending on how they are used. If the length of the pendulum is determined, the measurement is absolute; if the length of the pendulum is assumed to be constant, the measurement is relative with absolute scale. The gravity meter is an example of type 3. As gravity meters require a known gravity difference for calibration, various relative (type 2) pendulum apparatuses, capable of precisions up to 20 ppm, were employed until around 1970. The longevity

of pendulums was made possible with the development of broadcast time signals and later with portable precise crystal clocks. Measurements performed on the North American and European Gravity Standardization networks with the Gulf Pendulums (Gay, 1940), USA, Cambridge Pendulums (Jackson, 1961), UK, and the Canadian Pendulums (Valliant, 1971), amongst others, continue to contribute to the adjusted values of these gravity networks.

Absolute gravity measurements were originally performed as laboratory experiments at fixed sites. Sakuma (1963) in France, Preston-Thomas (1960) in Canada, Cook (1967) in the UK and Tate (1966) in the USA were among the early contributors in this field. A major breakthrough came when Faller and Hammond (1974) developed a portable free-fall apparatus in the early 70's. This apparatus not only improved upon the accuracy achieved with pendulums, but also provided absolute observations. The free-fall apparatus soon superceded pendulums for establishing gravity standards.

Improvements in the design of gravity meters since their introduction has led to a significant reduction in size and greatly increased precision. Weight decreased from 34 kg (75 lbs) in 1939 to about 3.6 kg (8 lbs) in modern instruments. As the precision increased from about 100 μGals to a few μGals, applications expanded to include the measurement of crustal motion, the search for non-newtonian forces, archeology, and civil engineering. The development of peripheral devices (Valliant et al, 1986) to automatically null the gravity meter contributed to this increased precision. Apart from enhancements to the "astatic" gravity meter, few developments in hardware were achieved. One of these was the vibrating string gravity meter (Gilbert, 1949) which was developed in the 1950's and was employed briefly for marine and borehole applications. Another is the cryogenic gravity meter (Goodkind et al, 1968) which utilizes the stability of superconducting current to achieve a relative (type 3) instrument with extremely low drift suitable for tidal and secular gravity measurements. An advance in performing measurements from a moving platform was achieved with the development of the straight-line gravity meter (LaCoste, 1983). In this invention, the proof-mass of the gravity meter is constrained to move in a vertical straight line, thereby eliminating the cross-coupling of horizontal accelerations into the vertical; a problem inherent in beam type gravity meters. The latter part of the century also saw the rebirth of gradient measurements which offers advantages for observations from a moving platform. Definitive testing of the Bell gradiomenter was recently reported (Jekeli, 1988).

REFERENCES

Cook, A.H., A new absolute determination of the acceleration due to gravity at the National Physical Laboratory, England. Phil. Trans. Royal Soc., London. A, 261, 211-252, 1967.

Faller, J.E., and Hammond J.A. A new portable absolute gravity instrument. Bulletin d'-Information, 35, Bureau Gravimetrique Intl., 143-148, 1974.

Gay, M.W. Relative gravity measurements using precision pendulum equipment, Geophysics, 5, 176-191, 1940.

Gilbert, R.L.G., A dynamic gravimeter of novel design. Proc Phy Soc, B, LXII, 445-454, 1949.

Goodkind, J.M., and W.A. Prothero Jr. A superconducting gravimeter, Rev Sci Instr., 39, 1257, 1968.

Heiland, C.A. Directions for the use of the Askania torsion balance. American Askania Corp., Houston, Tx., The Maple Press Co., York, Pa. 1933.

Hugill, A.L. The design and construction of a gravity meter with automatic readout. Ph.D. dissertation, Flinders University, Australia, 1984.

Jacoby, H.D. The new Askania seagravimeter GSS-3. In Advances in Dynamic Gravimetry, W.T. Kattner ed. Proc of the Symposium on Dynamic Gravimetry, Ft. Worth Tx., 1970.

Jekeli, Christopher. The gravity gradiometer survey system (CGSS).EOS, 105, 116-117, 1988.

LaCoste, L.J.B. A new type long period vertical seismometer. Physics 5, 178-180, 1934.

LaCoste, L.J.B. Measurement of Gravity at sea and in the air. Rev. of Geophysics, 5, 477-526, 1967.

LaCoste, Lucien. LaCoste and Romberg straight line gravity meter. Geophysics, 48, 606-610, 1983.

Jackson, J.E. The Cambridge pendulum apparatus. Geophysical Journal Royal Astronomical Soc. 4, 375-388, 1961.

Preston-Thomas H., L.G. Turnbull, E. Green, T.M. Dauphinee, and S.N. Kalra. An absolute measurement of the acceleration due to gravity at Ottawa. Can. J. Phys. 38, 824-852, 1960.

Sakuma, A., Etat actuel de la nouvelle determination absolue de la pesanteur au Bureau International des Poids et Mesures. Bull. Geodesique, 69, 249-260, 1963.

Steiner, George. Questions and answers in regard to the original Eotvos torsion balance. The Rein Co. , Houston, Tx, 1926.

Tate, D.R. Absolute value of g at the National Bureau of Standards NBS. Jour of Res, 70C, 2, 1966.

Valliant, H.D. The Canadian pendulum apparatus, design and operation. Pub Earth Physics Br., DEMR, Ottawa, Canada, 41, 4, 1971.

Valliant, H.D., C. Gagnon, and J.F. Halpenny. An inherently linear electrostatic feedback method for gravity meters. JGR, 91, 10463-10469, 1986.

Vening Meinesz, F.A. Theory and practice of pendulum observations at sea. Technische Boekhandel en Drukkerij, J. Waltman, Jr., Delft, 1929.

GENERAL REFERENCES

Dobrin, M.B. Introduction to geophysical prospecting. McGraw-Hill, 1975.

Heiskanen W.A. and F.A. Vening Meinisz. The earth and its gravity field. McGraw-Hill, 1958.

Howell, B.F. Jr. Introduction to Geophysics. McGraw-Hill. 1959.

Valliant, H.D. ed. Pendulum Papers. Dominion Observatory, 1975. (An anthology of papers about pendulums bound in two volumes. Available from the Geophysics Library of the Geological Survey of Canada, Ottawa, Canada. Referenced as QB335.P214)

Valliant, H. D. and N. Courtier, Comprehensive bibliography of absolute gravity and related topics. Internal Report 84-7 of the Earth Physics Branch DEMR, Ottawa, Canada, 1984

The Rapid Geodetic Survey System (RGSS)

J.R. Huddle

Litton Guidance and Control Systems Division, Woodland Hills, California

ABSTRACT

The RGSS is a system employing a high-accuracy gimbaled inertial platform. It provides a cost-effective capability for accurate direct measurement of the change in position, elevation, gravity intensity and deflection of the vertical from an initial point. The RGSS is an adaptation of the production version of the U.S. Army Position and Azimuth Determining System (PADS). Several hardware and software enhancements to improve the performance of the system, primarily for gravity vector survey, have occurred over the last few years. The basic principles for the control of error in the survey measurements due to noise and systematic error are discussed below. Actual acceptance test results for the RGSS which indicate an inherent capability of the system to measure change in the deflection of the vertical to a few-tenths of an arcsecond over survey periods of one to two hours using careful survey techniques are also presented. Finally a simple method to extend the capability of the system for longer duration surveys is indicated.

1. Introduction

The RGSS depicted in Figure 1 is based upon the Litton high-accuracy gimbaled LN-15 platform which employs 2 two-degree-of-freedom low drift rate G300-G2 gas spin bearing gyros and 3 low-noise A-1000 accelerometers. The full system includes a digital computer, control and display unit, power supply and tape recording unit. In a typical single traverse survey the system is aligned at the initial point, a process which brings the instrument coordinate system into coincidence with the local east, north and vertical geodetic coordinates, and is also provided with initial values of position, elevation and if available, the gravity disturbance vector. The system is then moved by land vehicle or helicopter to a new point where it is stopped to allow the real-time survey measurements to be recorded and system corrections to be made. It is well-known[1] that these corrections using the observable error in system computed velocity at the stops (called "ZUPTS"), effectively counteract the error effects of system noise sources during the travel periods, including the dominant source which is the change in the gravity disturbance vector. Additionally when the survey vehicle encounters the final point of the traverse, misclosures in the real-time position and elevation are used in a post-survey adjustment to remove the effects of accelerometer scale factor error and misalignment which are not observable with the velocity error observations at vehicle stops.

The manner in which the change in deflection of the vertical is measured with the RGSS is depicted schematically in Figure 2. At the initial point, the level accelerometers are aligned parallel to the reference ellipsoid. The Schuler-tuned inertial platform then maintains the parallel orientation of the level accelerometers with respect to this ellipsoid as it is moved across the surface of the earth. Consequently when the survey vehicle is stopped and there is no acceleration, any change to the deflection of the geoid from the ellipsoid can be observed with the level accelerometers.

2. Theory for Control of Error in a Vertical Deflection Survey

Any source of erroneous change in tilt of the level accelerometers will cause an error in measuring the change in the deflection of the vertical. Acceleration measurement error during the travel periods cause identical error in survey position and platform tilt. However, it has been well-documented[2] that the zero velocity updates and post-survey adjustment can control position error and consequently tilt, to the 10-cm (0.003 arcsec) level for short surveys. Hence it turns out that the principal source of erroneous tilt occurs due to the gyro drift rate integrated over the duration of the survey. Accelerometer noise and vehicle vibration are an additional
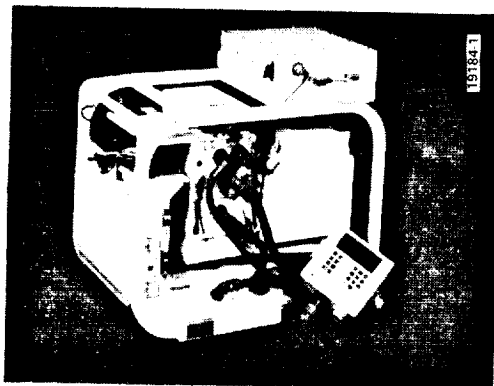
Figure 1. Rapid Geodetic
Survey System
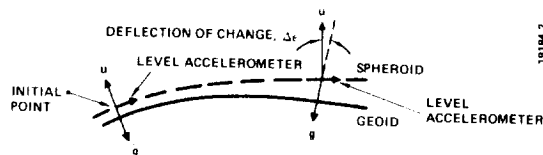
Figure 2. Measurement of
Deflection Change

direct source of deflection measurement error at vehicle stops but can be substantially reduced by averaging over the stopping period. When the terminal point of the survey is encountered, the reference deflection change over the survey derived from astronomic points can be used to remove a substantial amount (depending on the ratio of total survey time to drift rate correlation time) of the integrated drift rate which causes real-time deflection measurement error at the intermediate survey points.[1] For example, a drift rate of 0.0005 arcsec/sec (1σ) with correlation time of 2 hours causes an accumulated tilt of 1.35 arcsec (1σ) for a 1 hour survey. After adjustment, the peak residual error occurs at the mid-point (0.5 hour) of the survey and is only 0.23 arcsec (1σ).

3. System Test Results

Acceptance tests for the RGSS[3] were conducted in August of 1986. Two types of test courses were employed. The first course was a straight north-south traverse performed in a land vehicle which took approximately 1.2 hours to traverse with travel periods of 1 to 1.25 minutes and stop periods of 2 minutes. The repeatability of the results for four traverses for the two deflection components are shown in Figures 3 and 4. The real-time measurements have been linearly-smoothed using astronomic reference points accurate to approximately 0.2 arcsec. Reference deflection values of similar accuracy are shown at three points along the traverse.

The second traverse is "L-shaped" lying north-south and east-west. Repeatability of the linearly-smoothed results and their relationship to astronomic reference values are shown in Figures 5 and 6. The total traverse times were 1.5 and 1.9 hours with vehicle travel times of 3 minutes and stop periods of 2 minutes.

In collection of these survey measurements extreme care was taken in the installation of the equipment in the land vehicle to minimize vibration disturbances to the inertial instruments which can induce bias shifts. Also for the "L-shaped" traverse, an outer gimbal was employed to maintain the outer case of the inertial system fixed with respect to the instrument cluster despite vehicle heading changes. This procedure minimizes any changes in environmental influences which can also induce instrument bias shifts.

4. Performance Improvement

There is interest in enhancing the capability of the RGSS so that it can accurately measure the deflection change over longer duration traverses. Figure 7 depicts the stability of the inertial platform tilt for a static 3-hour laboratory test run. Clearly if measurements of the slopes of the tilt histories were periodically available, it would be possible to obtain improved estimates of the tilt over the full duration of the test. This is easy to do in the course of an actual survey by extending the stop periods slightly so as to observe the tilt change.

Figure 8 illustrates the significant theoretical performance improvement obtainable by such a procedure relative to the single point smoothing procedure. An exponentially-correlated drift of

61
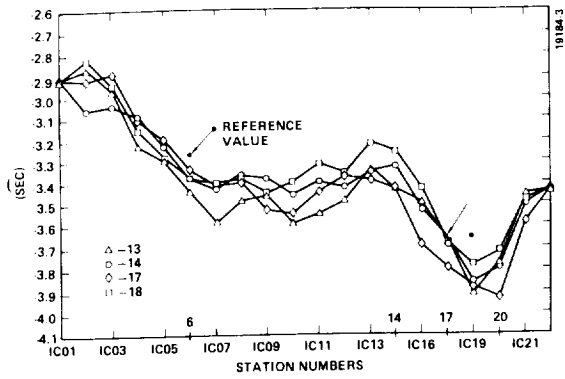
Figure 3. Meridional Deflection, Straight 10-Mile Traverse
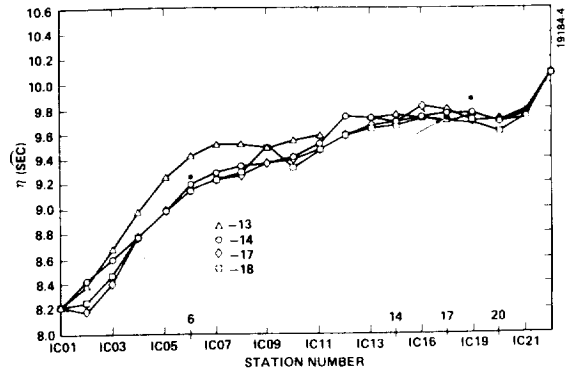
Figure 4. Prime Vertical Deflection, Straight 10-Mile Traverse
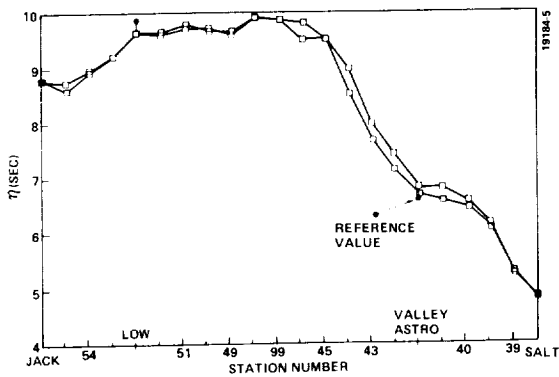
Figure 5. Prime Vertical Deflection, RGSS Test Line
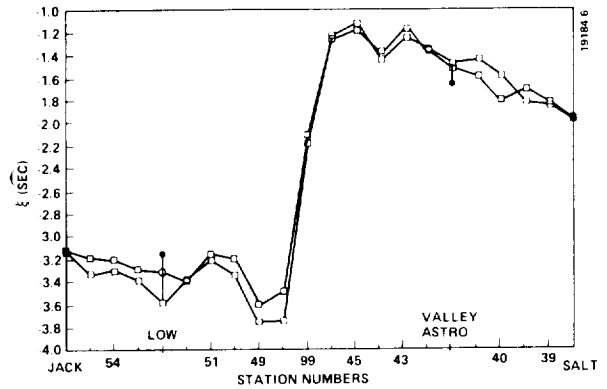
Figure 6. Meridional Deflection, RGSS Test Line
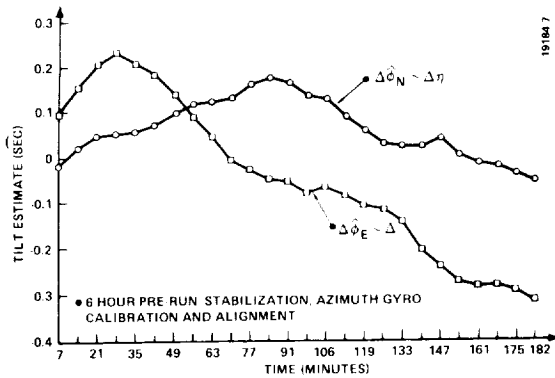
Figure 7. Platform Stability for Static Laboratory Test
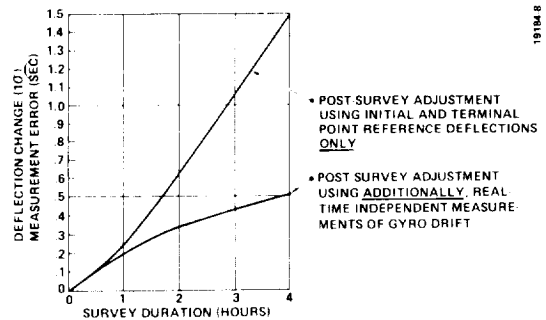
Figure 8. Peak (1σ) Error in Deflection Change Measurements versus Time Between Initial and Terminal Points of Survey Traverse

62

0.0005 arcsec/sec (1σ) with a 2-hour correlation time has been assumed for these results along with the assumption that an independent measurement of drift rate to an accuracy of 0.0005 arcsec/sec (1σ) is available every 6 minutes during the survey traverse.

References

1. Huddle, J.R. "Theory and Performance for Position and Gravity Survey with an Inertial System," AIAA Journal of Guidance and Control, Vol. 1, No. 3, May-June, 1978, Pp. 183-188.

2. Proceedings of International Symposia on Inertial Technology for Surveying and Geodesy, First at Ottawa, Canada in October, 1977; Second at Banff, Canada, June 1981; Third at Banff, Canada in September, 1985.

3. Roof, E.F., A number of private correspondences in 1987 and 1988.

First Year's Results and Field Experience With the Latest JILA Absolute Gravimeter

G. Peter, R.E. Moose, and C.W. Wessells

National Geodetic Survey, Charting and Geodetic Services
NOS, NOAA, Rockville, Maryland 20852

Abstract

One of the six absolute gravity instruments developed and built by the Joint Institute for Laboratory Astrophysics (JILA) between 1982 and 1985 has been tested under a variety of environmental conditions between May 1987 and 1988. Of the 30 sites visited during this period, 10 were occupied more than once. These reobservations indicate repeatability between 1 and 4 microgals.

1. Introduction

The National Geodetic Survey (NGS), in cooperation with the Defense Mapping Agency, Hydrographic and Topographic Center (DMAHTC), has been testing the field performance of one of the latest JILA absolute gravimeters, JILAG#4. Absolute gravity has been observed in eight east coast states; California; on the Hawaiian islands of Kauai, Maui, and Oahu; on Bermuda; and at Gatineau, near Ottawa, Canada. Rather than seeking rapid station occupations and sites with marginal environmental stability, the emphasis was placed on getting the best repeatability. Based on the laboratory performance of these instruments [Niebauer 1987 and Niebauer et al., 1986], it was expected that under ideal conditions repeatability of better than ±3 microgal could be obtained. To achieve such repeatability, a set of procedures for site selection, data collection, quality control, and corrections for the effects of environmental changes has been developed.

2. Site Selection

In addition to broad geological considerations, site selection was guided by three principal criteria. To provide a solid foundation for the instrument and to avoid the problem of groundwater table changes on gravity, we looked for buildings set on nonporous bedrock. In addition, buildings were selected in which vibrations introduced by human activity were judged to be relatively low. The instrument was set up in a room at or below ground level, where temperature fluctuations were also expected to be minimal.

It was found that few of these desired environmental conditions could be adequately prejudged. A good, after the fact, measure of the vibrations was the scatter of the individual drops from the mean in the given drop-sets. At the quietest sites, the standard deviation of the drop-sets was in the 5-10 microgal range, at the noisiest sites in the 50-70 microgal range (given 250 drops for a set). The most common range was 15-30 microgal.

However, even at the noisiest sites, the mean of the successive drop sets stayed in the 5-10 microgal range. The principal problematic vibration sources were air conditioning equipment, and at our island sites, the oceanic microseisms.

Inadequate temperature stability was the most likely cause for the up to 15 microgal differences among the means of successive drop sets at some of the seismically quietest sites. Large temperature variations, particularly when the temperatures climbed to 27 C° - 29 C°, could have affected the laser lock mode frequencies and the initial position of the dropped object. In addition, cooling down at night several times caused the bottoming of the mass of the superspring, causing unacceptable drop-to-drop scatter.

Changes of the groundwater table can be a major source of error in repeat gravity observations. Presently at three of our sites where the influence of groundwater table variation is a concern, the water table is monitored and corrections are applied to compensate for the consequent mass variations. The majority of the remaining sites are free from this effect. The few sites at which the groundwater table cannot be monitored will not be used for the investigation of the temporal changes of gravity.

3. Field Observations and Quality Control

The current field observations consist of the collection of drop sets (containing 250 drops) at 2 hour intervals for 2 days. The histograms of these drop sets approach Gaussian, and the drop set means are well defined. To minimize the change of the frequencies of the laser lock modes due to environmental effects, the laser lock mode is switched after every drop set. Environmental corrections are added either to each drop, the drop set means, or to the mean of all drop sets. The 2-day-long observations at a station minimize the errors left in the data after the application of the corrections.

To eliminate outliers caused by high random noise events, each drop set first is screened, and all drops exceeding three standard deviations from the mean are rejected. Although rarely more than three drops are rejected, the mean of the drop sets often changes by 3 microgals due to this process. After this quality control process, the corrections are added and the weighted mean of all drop sets is computed (using the variance of the drop-sets as weight) to obtain the gravity value of a station.

4. Corrections

The largest environmental correction is for the solid Earth tide, which is computed by the gravimeter controller using Longman's [1959] formulation. In post processing, this correction is replaced by the more accurate formulation of Tamura [1982], which eliminates the 3 to 4 microgal errors of the

previous program. The atmospheric attraction and loading are corrected for by using the approach of VanDam and Wahr [1987], the U.S. Standard Atmosphere [Boedecker et al., 1979], and regional pressure [Rabbel and Zschau, 1985] for absolute station pressure reference. This correction can amount to as much as 5 microgals. To correct for the effect of ocean loading, unpublished programs of T. Sato and H. Hanada and of D. Agnew have been adapted. At some coastal sites, the computed amplitudes had to be reduced to match the observed signal. While this correction to the individual drop sets had varied between 2 to 10 microgals, the actual change to the computed gravity value was usually a few tenths of microgals at the interior and 2-3 microgals at the coastal sites. Because, by coincidence, the repeat observations were made in the same season, the water table changes to date have resulted in only about 2 microgal corrections. The effect of the seasonal peak-to-peak change at the Herndon site would have been 13 microgals. We also corrected the observed gravity values for the changes of the Earth's rotational axis by converting the gravity value to the mean pole position. The magnitude of this correction for the half Chandler period is about ±9 microgals.

Instrumental corrections involved laser aging and laser temperature effects, and conversion to the same measurement height in case of repeat observations. While laser frequency drift due to aging is well defined, imprecise temperature corrections could contribute 2 microgals to the overall error budget, which in the majority of cases was under 6 microgals. This uncertainty estimate includes the 0.03 microgal/cm vertical gradient determination error.

5. Instrumental Problems

So far, the JILAG#4 gravimeter has undergone a major checkup twice a year. The instrument was taken apart, and repairs, replacements, readjustments and calibrations were made. Field problems included: 1) partial vacuum loss due to failure in the portable power supply; 2) electronic component failures, short circuits, and readjustments involving the dropping chamber and super spring controllers and the dropped object wiring harness; 3) data and time loss due to bottoming of the mass of the super spring and due to drift of the reference level (carriage lock position), both caused by excessive temperature changes (larger than ±3 C').

6. Results

Site description and absolute gravity values may be obtained from NGS by writing to the authors. Details on the absolute gravity program and on the first year's results are available in Peter et al. [1988] and in Peter et al. [in press]. The National Geodetic Survey now uses absolute gravity observations in conjunction with GPS and VLBI observations to monitor vertical crustal motion.

References

Boedecker, G., E. Reinhart, and B. Richter, 1979, Proceedings, XVII IUGG General Assembly, Canberra, Australia 16.

Longman, I.M., 1959, J. Geophys. Res., 64, 2351.

Niebuer, T.M., 1987, PhD. Dissertation, University of Colorado, 155 pp.

Niebauer, T.M., J.K. Hoskins, and J.E. Faller, 1986, J. Geophys. Res., 91, 9145.

Peter, G., R.E. Moose, and C.W. Wessells, NOAA, NGS Internal Report, Unpublished.

Peter, G., R.E. Moose, C.W. Wessels, J.E. Faller, and T.M. Niebauer, J. Geophys. Res., In press.

Rabbel, W., and J. Zschau, 1985, J. Geophys. Res., 56, 56.

Tamura, Y., 1982, Publications of the International Latitude Observatory, Misuzawa, Japan, 16, 200.

VanDam, T.M. and J.M. Wahr, 1987, J. Geophys. Res., 92, 1281.

GPS-Aided Gravimetry at 30 Km Altitude from a Balloon-Borne Platform

ANDREW R. LAZAREWICZ
Air Force Geophysics Laboratory, LWG, Hanscom AFB, MA 01731

ALAN G. EVANS
Naval Surface Weapons Center, K-13, Dahlgren, VA 22448

N90-20530

ABSTRACT

A balloon-borne experiment, flown at 30 Km altitude over New Mexico, was used to test dynamic differential GPS tracking in support of gravimetry at high-altitudes. The experiment package contained a gravimeter (Vibrating String Accelerometer), a full complement of inertial instruments, a TI-4100 GPS receiver and a radar transponder. The flight was supported by two GPS receivers on the ground near the flight path. From the 8 hour flight, about a forty minute period was selected for analysis. Differential GPS phase measurements were used to estimate changes in position over the sample time interval, or average velocity. In addition to average velocity, differential positions and numerical averages of acceleration were obtained in three components. Gravitational acceleration was estimated by correcting for accelerations due to translational motion, ignoring all rotational effects.

INTRODUCTION

The primary objective of this flight (named DUCKY II, flown in October 1985) was to test the differential GPS tracking system; the secondary objective was to improve on the gravity field measurement shown to be feasible with the previous flight (named DUCKY Ia, flown in October 1983). As with DUCKY Ia, a great deal of data were collected, organized, inspected and analyzed by several different groups. Overall, the flight, data collection and analysis went very well, but a few problems did complicate the data analysis sufficiently that the full promise of this experiment was not fulfilled. Nevertheless, we did succeed in demonstrating GPS tracking and improving the quality of the gravity measurements from DUCKY Ia.

TEST DESCRIPTION

The principal limitation in high-altitude gravimetry, as concluded from the flight of DUCKY Ia, is high accuracy tracking. Since all accelerometers measure only acceleration and cannot distinguish between gravitational acceleration and kinematic acceleration, it is critical to add sensors to aid in separating the two. There are only two known ways in which this can be done: 1) External tracking to directly determine kinematic acceleration; or 2) Gravity gradiometry to directly detect gravitational acceleration. External tracking works by measuring position, velocity and acceleration relative to the tracking device, which is fixed, usually in a non-inertial frame. We chose external tracking via GPS because it is a lot simpler, and it has the potential to resolve a few mGal accelerations with available technology. DUCKY II did have inertial sensors, and when properly combined with GPS, highly accurate tracking data is possible.

GPS tracking for DUCKY II was accomplished using three DMA versions of the TI 4100 receivers. One in flight and two on the ground. The two ground stations were picked to minimize distance between ground receiver and balloon. For the flight, one ground station was placed at AFGL Det. 1, near the launch site; and the other was placed on the roof of the Post Office in Lovington, NM, near the expected landing area. The data from the flight

68

receiver was telemetered and analyzed in real-time, just as the ground stations; only the hard line was replaced with a radio link.

At the time of flight, GPS was a pilot program, with only six satellites in orbit. GPS will not be a mature service until at least the late 1980's or early 1990's. When GPS is fully operational, this experiment could be repeated, with good satellite coverage and geometry, from launch to landing. As GPS time was limited, we intended to put the best coverage at altitude; future flights will cover the ascent - a time of high interest. The ascent time covers 25 to 30 Km of vertical distance, and gravitational acceleration and gradient data would be most interesting. Currently, we have demonstrated that this system works.

GPS DATA PROCESSING

The data processing is shown diagrammatically in Figure 1. First, a rough estimate of absolute position was obtained using a Kalman Filter with pseudorange measurements. Next, the combined L_1 and L_2 frequency pseudorange measurements and change in range from phase measurements were combined to obtain an average estimate of the pseudorange at the first data time. Here, change in range Doppler measurements were subtracted from succeeding pseudoranges for the entire satellite pass and averaged to obtain a more accurate estimate of the pseudorange at the initial start GPS solution time. Next, the pseudorange values were used to obtain the initial number of wavelengths between double differenced phase measurements. The double-differenced phase measurements were obtained by first differencing between the two receivers. Then, the phase measurements were differenced between two satellites, where for this set of data PRN 11 was the reference satellite. Using data from four satellites (PRNs 6, 9, 11 and 12), the relative position of the balloon was obtained at each 6 second time mark. This relative positioning procedure corrects the absolute positioning estimates, discussed above.

The average velocity was determined next using only the very accurate L_1 change in phase measurements. The standard Doppler procedure was used to obtain change in range values. Using the relative positioning values obtained above for the correction partials, average position changes were estimated over each data interval. Finally, the accelerations, most importantly the vertical accelerations, were obtained using a basic numerical difference between successive average velocity values divided by the time interval. These accelerations represent the acceleration due to all forces and are represented in the geodetic coordinate frame.

TEST RESULTS

GPS estimates of vertical acceleration were first obtained between the two static receivers at Holloman and Lovington sites. Here, the Doppler procedure for obtaining average velocity over a 6 sec interval was used and numerically differentiated to obtain vertical acceleration. Here, the estimates had a numerical standard deviation of 39.3 mGals. When averaged over the 15 minute interval of data available to the two sites (and the balloon) an error of only 0.087 mGals was obtained. Even though the receivers were in a low noise static mode rather than a slightly higher noise low dynamic mode, this is still a very good indication that GPS is sufficiently precise to obtain accurate gravity estimates.

The GPS data was then processed for the balloon with respect to both static sites. However, since Holloman had such a small amount of simultaneous data with the balloon, only the results of the balloon with

69

respect to Lovington are presented. The data was processed as described above. The relative vertical position as a function of time is presented in Figure 2. During this time period, the balloon moved with average velocities of about 9 m/s in the North direction and about 17.5 m/s in the East direction. The cyclic vertical motion was due to gas in the balloon expanding and contracting as the balloon changed altitude and correspondingly temperature. Doppler estimates of vertical velocity were obtained and numerically differentiated to produce the vertical acceleration given in Figure 3. This can be compared with the Vibrating String Accelerometer (VSA) measurements given in Figure 4.

In order to obtain a gravity value, the 30 km altitude of the balloon trajectory, modeled gravity as a function of height was obtained and removed from the GPS accelerations. Also, Eotvos and Earth rotation corrections were made. A constant value was found for the difference between the corrected GPS accelerations and the raw accelerometer measurements. The value obtained was 90 mGal. This value, if all computations were done correctly, should theoretically be due to the difference between the modeled gravity and actual gravity at a 30 km altitude. However, there appears to be a bias that has not been accounted for.

SUMMARY

The two flights completed in this program have demonstrated that gravimetry is possible at 30 Km altitudes. Although the original goal of 1 mGal accuracy has not been reached, much has been learned from the test. The key is GPS differential tracking, which has been demonstrated with this flight. The results of the static GPS acceleration estimates indicate that GPS has sufficient accuracy to obtain satisfactory acceleration estimates. However, the results of the dynamic high altitude portion of the test indicate that a bias is in the data. With the information available from the test, it has been difficult to isolate this bias. That is, the bias could be in the gravimeter, the gravity model, or computational corrections. It is recommended that further testing be performed in a controlled manner close or on the Earth's surface to further validate the accuracy of the GPS/gravimeter procedure. As the GPS constellation increases in number, this work will become much easier in planning and scheduling flights. If and when the next flight occurs, we should have good tracking throughout the ascent and flight; certainly that dataset would be unique as the only vertical profile over 30 Km.

ACKNOWLEDGEMENTS

GPS ACCELERATION

Fig. 3. Balloon Z-acceleration from GPS differences with Lovington.

VSA ACCELERATION
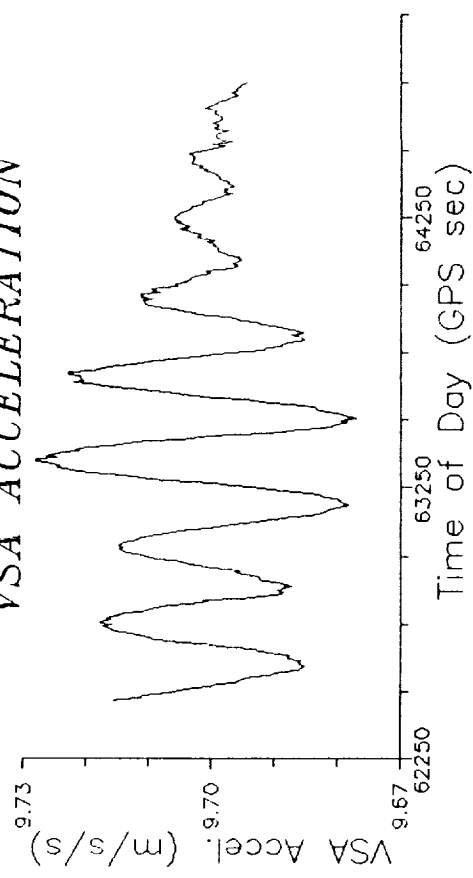
Figure 4. Balloon Z-acceleration as directly measured by the gravimeter.

Fig. 1. Flow diagram for GPS data for analysis of acceleration.
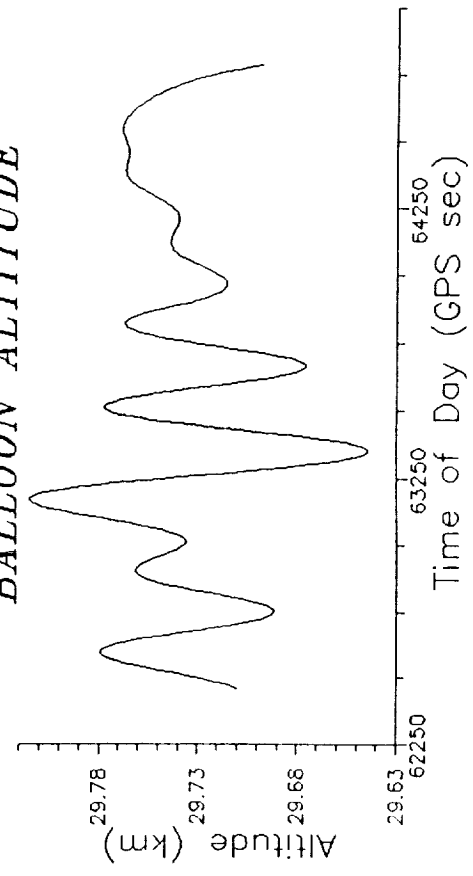
BALLOON ALTITUDE

Fig. 2. Balloon altitude from GPS differences with Lovington, NM.

Critique of the Vertical Gradient of Gravity

Sigmund Hammer
Department of Geology and Geophysics
University of Wisconsin-Madison

Growing interest by Geodesists and Theoretical Physicists in high precision studies of the earth's gravitational field warrant a critical review of precision requirements to yield useful results. Several problems are now under consideration. All of these problems involve, more or less, the precise value of the vertical gradient of gravity.

Elevation corrections for gravity mapping.

The major present use of the so-called Free-Air Vertical Gravity Gradient is to calculate elevation corrections of gravity station data for gravity maps. It is standard practice to use the "normal" gradient value 0.3086 mgls/meter (0.09406 mgls/ft). This ignores the fact that published data demonstrate that the value of the earth's vertical gravity gradient varies at least plus or minus five percent (± 5%). In high topography (say 4000 meters – 12,000 feet) this produces sea-level anomaly values that may be in error more than fifty milligals (50 mgls).

Errors of this magnitude on official published gravity maps are not tolerable. The often-heard argument that this is not an error but a real part of the anomaly, is not valid. It produces inconsistent anomaly values for stations observed at different elevations - such as ground and airborne.

Vertical gradient measurement

The measurement of the vertical gradient of gravity (V) is expressed by the equation

$$V + e_V = (\Delta g + e_g)/(\Delta H - e_H)$$

where e_V, e_g and e_H represent errors in the data. The fractional errors in these factors are

$$e_V/V = (1 + e_g/\Delta g)/(1 - e_H/\Delta H) - 1$$

A plot of this equation is shown in Fig. 1.
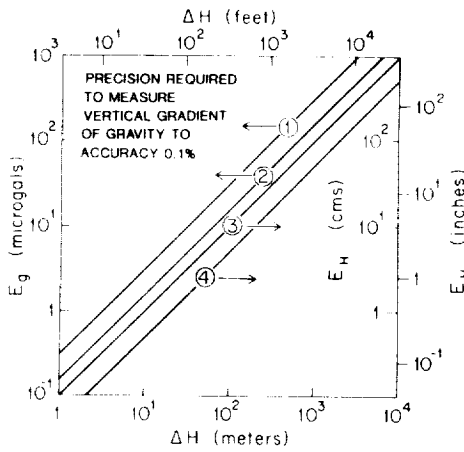
Fig. 1   Curve 1 $e_H/\Delta H = 0$
         Curve 3 $e_g/\Delta g = 0$
         Curves 2 & 4 $e_g/\Delta g = e_H/\Delta H$
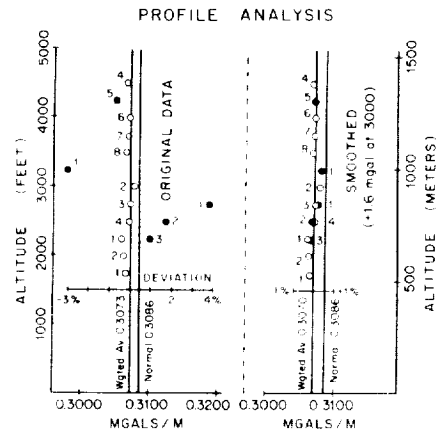
Fig. 2   Airborne
         Vertical Gradient
         (Discussed below)

The precision requirements versus elevation range of observation from Figure 1 are tabulated below

Table 1 Precision required to measure the vertical gradient to 0.1%

Method	ΔH Meters	e_g (μgal)		e_H (cms)	
		(a)	(b)	(c)	(d)
TRIPOD	3	0.9	0.46	0.15	0.3
TOWER	100	31	15	5	10
AIRBORNE	1000	309	154	50	100

(a):   Zero error in ΔH

(b) & (c):   Equal errors$\dfrac{E_g}{\Delta g}$ and $\dfrac{E_H}{\Delta H}$

(d):   Zero error in Δg

It is apparent that present instrumentation cannot achieve the necessary precision on a portable tripod with elevation range of, say, three meters

(10 feet). Tall buildings and towers, with elevation ranges up to several hundred meters can achieve the necessary precision but are seldom available where needed. Upward continuation of ground based gravity survey data are difficult to evaluate. An example of an airborne vertical gradient measurement, which achieves the desired accuracy, is shown in Fig. 2 above.

The data in Fig. 2 were observed at six elevations, up to 5500 feet, (1600+ meters) which provided fifteen (15) internal gradient values. Most of these data were in excellent agreement (open circles in the left hand section). Five discordant points (blackened circles) all involve data at a single level. A smoothing correction of +1.6 mgls to that value eliminates the scatter as shown in the right hand section. The RMS error of the smoothed gradient data is 0.1% (± 3 E°).

Borehole gravity

Many borehole gravity surveys in oil and gas wells have been published. The borehole data which penetrated the Greenland ice sheet are of great interest. The possibility of deep ocean profiles also has been proposed. An active new purpose of these data is to improve the accepted value of the gravitational constant, usually designated as G or γ which is the least accurate of all fundamental physical constants. For this purpose the density of the formation penetrated, as well as the gravity gradient, and various corrections require accuracies of better than 0.1%. This needs to be reported in detail for each case.

The actual value of the vertical gradient at the borehole site is also involved. The observed gravity variation in a borehole is

$$\Delta g = (V - 4\Pi G \sigma)\Delta H - (TC_1 - TC_2)$$

where TC is the calculated correction for surface topography and non-

uniform subsurface formation layering at the two end points for the

gravity measurement, Δg. Solving for G we have

$$G = [V - \frac{\Delta g}{\Delta H} + \frac{\Delta TC}{\Delta H}]/4\Pi\sigma$$

The use of the "normal" value 0.3086 mgls/m (0.09406 mgls/ft) for the

free-air gradient value (V) at the site may involve very large errors in

the "observed" value of G.

CONCLUSION

The principal conclusion from this review is that the essential

absence of Free Air Vertical Gravity Gradient control and actual values of

gravimeter calibrations require serious attention. Large errors in high

topography on official published gravity maps also cannot be ignored.

Post Script

Since oral delivery of this paper at the recent Chapman Gravity

Conference in Fort Lauderdale, Florida, I have had access to a manuscript

report on a related topic (Romaides et al 1988). This is a detailed

report on gravity observations in a 600 meter television tower and

procedures to calculate the comparative vertical gravity profile by upward

continuation of ground based gravity survey data which were especially

designed for the purpose. Precision of data and analysis is a major

feature of the paper. Calibration of the LaCosts-Romberg gravimeter,

which was used for the study, is also detailed. If and when published

this report will provide a significant up-date for the present paper.

References

Romaides, Jekeli, Lazarewicz, Eckhardt and Sands, "A Detection of Non-Newtonian Gravity", Air Force Geophysics Laboratory, Hanscom AFB, MA 01731-5000 (No date).

Hammer, Sigmund, "Signals" Letter to the editor: Geophysics: The Leading Edge, Vol. 7, No. 1, January 1988, page 8.

Hammer, Sigmund, "Density Determinations by Underground Gravity Measurements - Sequel", Geophysics, Vol. XXX, No. 6, December 1965, pp. 1133-1134.

Methods for the Appoximation of the Gravity Field

Moderators: Reiner Rummel

C.C. Tscherning

76

Methods for Local Gravity Field Approximation

R.V. SAILOR, K.S. TAIT, AND A.R. LESCHACK

The Analytic Sciences Corporation, Reading, Massachusetts

ABSTRACT

The most widely known modern method for estimating gravity field values from observed data is least-squares collocation. Its advantages are that it can make estimates at arbitrary locations based on irregularly spaced observations, and that it makes use of statistical information about errors in the input data while providing corresponding information about the quality of the output estimates. Disadvantages of collocation include the necessity of inverting square matrices of dimension equal to the number of data values and the need to assume covariance models for the gravity field and the data errors. Fourier methods are an important alternative to collocation. They have the advantage of greater computational efficiency, but require data estimates to be on a regular grid and do not use or provide statistical accuracy information.

The GEOFAST algorithm is an implementation of collocation that achieves high computational efficiency by transforming the estimation equations into the frequency domain where an accurate approximation may be made to reduce the workload. The forward and inverse Fast Fourier Transforms (FFT) are utilized. We have demonstrated the accuracy and computational efficiency of the GEOFAST algorithm using two sets of synthetic gravity data: marine gravity for an ocean trench region including wavelengths longer than 200 km; and local land gravity containing wavelengths as short as 5 km. We discuss these results along with issues such as the advantages of first removing reference field models before carrying out the estimation algorithm.

1. INTRODUCTION

Algorithms for estimating gravity field quantities should be theoretically sound, accurate, and computationally efficient. In characterizing and describing such algorithms, the issues we consider include the specific geodetic quantity or quantities to be computed or estimated, the general approach (deterministic or statistical), the type or types of measurement data to be used, the geographic distribution of points at which geodetic quantities are observed and are to be computed, and the approximations (if any) made in the computation algorithm. The class of *least-squares collocation methods* is *statistical* in nature; *general* in terms of the quantities to be estimated, the measured data to be used, and the geographical distribution of data and computation points; and, in principle, *exact* if assumed covariance models are reasonable.

GEOFAST is an approach to implementing collocation with high efficiency by carrying out computations in the spatial frequency domain. It assumes the availability of two-dimensional gridded data; it uses stationary statistical gravity field models; it computes minimum-variance estimates of gravity field quantities; and it achieves high computational efficiency of the order of N log N operations, where N is the number of measurement points. This efficiency depends on the use of a critical approximation which, in practice, introduces little loss of accuracy. Furthermore, the user has control of the tradeoff between accuracy and computational efficiency.

2. THE GEOFAST ALGORITHM

The GEOFAST algorithm provides an efficient computational solution to the minimum-variance estimation equations of collocation:

$$\underline{x} = C_{xz} (C_{zz})^{-1} \underline{z} \tag{1}$$

where $\underline{z}$ is a data vector of dimension N, C_{zz} (of dimension N by N) is the sum of its autocovariance plus measurement noise, $\underline{x}$ is a vector of estimates (of dimension M), and C_{xz} is the cross-covariance matrix (of dimension M by N) between the estimated and measured quantities. Direct solution of equation (1) involves on the order of $N^3 + MN$ operations, limiting the feasible applications of collocation methods where data sets of thousands of measurements are involved.

This workload can be reduced to the order of N log N, if the following assumptions are valid: measured values are given, and estimates are required, at the same points on a rectangular grid, and covariances are a function of relative position only (shift invariance). In practice, shift invariance is equivalent to the assumption of stationary statistics. These assumptions impose a special structure on the matrices appearing in equation (1): they are block Toeplitz. The special properties of block Toeplitz matrices are essential to the GEOFAST algorithm.
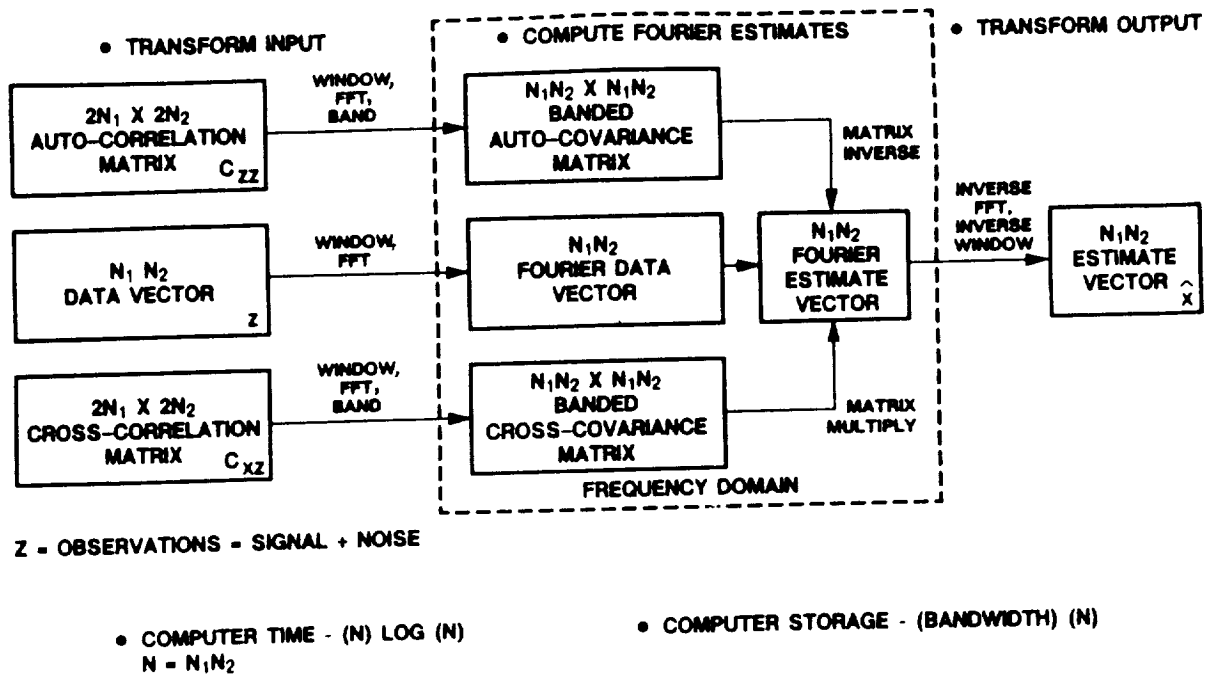
Figure 1. Outline of the GEOFAST algorithm.

Transformation of equation (1) to the spatial frequency domain is carried out efficiently through the use of the Fast Fourier Transform (FFT), leading to an equivalent estimation equation in the transformed variables $\underline{x}'$ and $\underline{z}'$:

$$\underline{x}' = C'_{xz}(C'_{zz})^{-1}\underline{z}' \tag{2}$$

In practice, the first step of the GEOFAST algorithm, as illustrated in the left-hand column of Figure 1, is the transformation of the data vector $\underline{z}$ and the matrices C_{zz} and C_{xz} into the frequency domain. The transformations, however, are not exact; approximations essential to the computational economy of the GEOFAST algorithm are incorporated. In effect, the C_{zz}' and C_{xz}' matrices that would be the exact transforms are replaced by banded approximations, and a compensating data windowing is applied in the computation of $\underline{z}'$. The second stage of the GEOFAST algorithm, shown in the central box of Figure 1, is the approximate solution of the banded version of equation (2) through the use of an iterative technique. In effect, this is equivalent to the

78

computation of $\underline{x}'$. The final step (right-hand column of Figure 1) is the inverse FFT from $\underline{x}'$, the frequency-domain solution, to $\underline{x}$, the spatial domain solution, incorporating the inverse of the windowing operation that was part of the transformation from $\underline{z}$ to $\underline{z}'$.

User control of tradeoffs between accuracy and computing time in the GEOFAST algorithm involves the selection of parameters governing the *bandwidth* retained in the approximations to the matrices C_{zz}' and C_{xz}', and the number of iterations carried out in the iterative solution of the approximate frequency-domain equations. In actual applications, reasonable parameter choices result in an accurate and highly efficient algorithm.

3. FIRST TEST DATASET — MARINE GRAVITY

For the first set of tests, gridded values of gravity anomaly and deflection of the vertical were generated for a 36 deg by 36 deg area in the western Pacific that includes a significant ocean trench, using the Rapp (1981) worldwide spherical harmonic expansion to degree and order 180. The GEOFAST algorithm is used to compute components of the deflection from the gravity anomaly data; comparison with the deflection components computed originally from the spherical harmonic model (regarded as truth data) provides a measure of algorithm performance. To quantify the effects of using high-order reference fields, the same spherical harmonic model can be used to generate a set of anomalies and deflections, but for degrees 91 through 180 only. Using GEOFAST with this high-frequency field is equivalent to removing a degree-and-order-90 reference field from the data prior to processing. Other parameters explored in the testing include data extent, grid spacing, GEOFAST bandwidth, choice of covariance models, and measurement noise level.
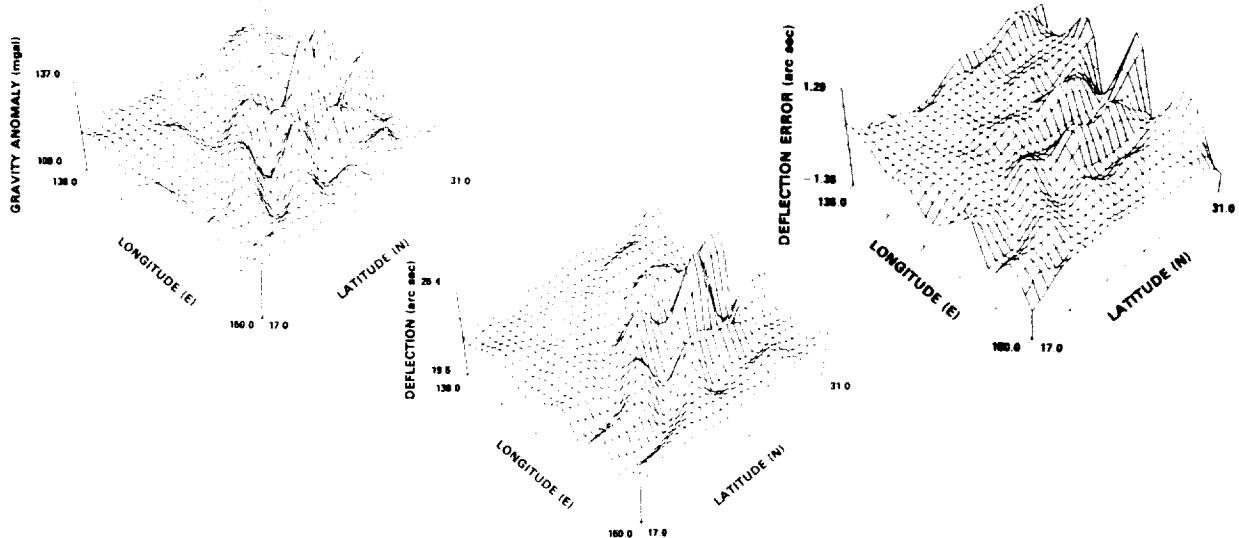
Figure 2. Input data and results for GEOFAST test. Input gravity anomalies are shown at the left; synthetic deflection truth data are shown in the center; errors in the estimated deflection appear on the right.

A typical test is illustrated in Figure 2. The gravity anomaly data (in this case with the degree-90 reference field removed) at 0.5 deg grid spacing are shown on the left; these are used as input to GEOFAST. Deflection data computed by GEOFAST for the same grid, assuming an attenuated white noise covariance model (with correlation distance of 0.5 deg), will be compared to the synthetic "truth data" shown in the middle. The resulting deflection error field appears on the right. Some test results are summarized in Table 1, which shows the effects of the bandwidth parameter, m_B, and the grid spacing (0.25 or 0.50 deg) on accuracy and computing time. Table 2 summarizes the effects of measurement noise on estimation accuracy. To a first approximation, measurement noise (in this case, white noise) contributes additively to estimation error variance. The

Table 1. Summary of GEOFAST Test Results.

Resolution		Bandwidth		Error (arcsec)		
Grid (deg)	Points	MB	Time* (min)	Mean	Sigma	Maximum
0.25	3600	0	4	0.001	0.15	0.70
0.25	3600	4	30	0.003	0.09	0.31
0.50	900	0	1	0.003	0.17	0.59

Table 2. Effects of Measurement Error on GEOFAST Performance.

Grid (deg)	Measurement Error rms (mgal)	Noise-Induced Error rms (arcsec)	Total Estimation Error rms (arcsec)
0.25	0	0.00	0.15
	1	0.03	0.15
	2	0.07	0.17
	5	0.16	0.22
0.50	0	0.00	0.17
	1	0.04	0.17
	2	0.08	0.19
	5	0.20	0.26

effects of removing a reference field from the measured data were explored in another set of tests. A typical result is that the error standard deviation is reduced by a factor of more than five by removing the reference field.

4. SECOND TEST DATASET — LAND GRAVITY

The second set of tests was designed to investigate the performance of GEOFAST on local data sets containing high-frequency information. Synthetic data were generated, using a mass dipole model originally formulated for the gravity gradiometer testing program. The statistical properties of the data are consistent with those for an actual test area in north Texas. As in the marine gravity tests, synthetic truth data were generated in the form of gravity anomalies and deflections of the vertical, for each point of a 5 km grid covering a square 500 km on a side. GEOFAST is used to estimate the east component of the deflection from the anomaly data; comparison with the directly generated deflection values provides a measure of the algorithm's performance. These tests use a covariance model with a correlation distance of 10 km. Estimation regions ranging from 40 to 150 km on a side are selected from the interior of a 150 km square located centrally within the original 500 km area, with resulting error standard deviations between 0.4 and 1.9 arcsec. The estimation accuracy would be improved by using a finer grid spacing.

5. SUMMARY

The GEOFAST algorithm, described briefly above, is used to estimate deflection of the vertical from gravity anomaly to an rms accuracy of better than 0.2 arcsec with modest computer cost. Conventional implementations of collocation require considerably more computing effort. GEOFAST provides a user tradeoff between computing cost and estimation accuracy. In a typical application reducing the accuracy requirement from 0.1 to 0.2 arcsec reduces computing time by a factor of eight. Other test results confirm the importance of removing a high-order reference field from the data before applying the algorithm. For example, removing a degree-90 reference field from the synthetic marine gravity data reduces estimation errors by a factor of five.

The GEOFAST algorithm can be applied to current real-world problems involving the reduction of gradiometer or altimeter data. Potential application areas include the production of accurate maps for marine crustal and lithospheric studies.

80

The Use of High-Resolution Terrain Data in Gravity Field Prediction

E. Groten, M. Becker, H.-J. Euler, W. Hausch, Th. Kling

Institut für Physikalische Geodäsie, Technische Hochschule Darmstadt, F.R.G.

Abstract

The aim of this paper is to develop, test and, to some extent, compare different types of gravity prediction methods for local and regional gravity evaluation. Four different test areas have particularly been selected in view of different prediction requirements. Also different parts of the spectrum of the gravity field were considered.

1. Introduction

From modern seismic tomography and other results it is known that lateral density variations have been underestimated in the past. Consequently, gravity variations at the surface of the earth are difficult to predict. On the other hand, modern photogrammetric and altimetric measurements give way to very detailed models of the terrain for estimating gravity in continental areas. Four different areas were selected in order to test various aspects of regional and local gravity modeling. Different mathematical tools have been used in order to test their ability to predict gravity under various conditions.

2. Description of prediction tests

Test area one comprises a 500 by 300 km area in Northern Argentina, Southern Bolivia and Northern Chile in the high Andes. Based on a recent terrestrial gravity survey (Goetze et al., 1988) which could be assumed to be free of errors in that comparison a study of the accuracy of Rapp's (1981, 1986) global gravity models was possible in a zone where very scarce surface gravity data was available to the global models. The area is a typical subduction zone and was recently studied in detail by Isacks (1988). This is one of the few areas where the geophysical structure is relatively well known from seismic results even though details of the gravity field are not well known. Nevertheless, the comparison was based on a regular Airy-Heiskanen model using a compensation depth of 40 and 50 km, respectively. The investigation in terms of isostatic anomalies was done in order to reduce the effect of erroneous elevation data and local effects. The two data sets could be assumed to be independent of each other. Basically, wave lengths up to degree n = 180 were considered. The comparison was made in terms of free air, Bouguer and isostatic gravity. The comparison indicates a surprisingly good agreement of large scale phenomena whereas smaller phenomena of the gravity field reveal discrepancies of the order of ± 10 mgal, as expected.

A second test area is characterized by alpine overthrust, leading to strongly varying anomalous regression of free air gravity with elevation. Therefore, Nettleton type prediction does not lead to good free air or Bouguer gravity estimates as in the case of homogeneous parts of the Northern Alps. The area was chosen in order to demonstrate the difficulties associated with overthrust and similar density variations in mountain areas

81

which can make local gravity prediction quite erroneous unless precise geo-
logical information is available. But there are few areas where detailed
density information is available where gravity is unsurveyed. In the area
under consideration the density values determined by the Nettleton method
differ about 0.1 to 0.2 gr/cm^3 from that determined by geological means.
For details see (Kling et al., 1987).

The overwhelming part of the investigation is related to the <u>third</u>
area in the Odenwald close to the Rhinegraben where extremely dense (from
ten to fifty meter grid spacing) terrain data were available. The area is
dominated by paleocoic mountains and deep (4 km) sediments, in the graben
zone, and magmatic rocks of different kind leading to quite discontinuous
and significant density variations. Fig. 1 shows a small part of the third
test area on the eastern Rhinegraben shoulder (Odenwald) where the majority
of the prediction tests were carried out. In order to get a meaningful
illustration a grid distance of 100 m was chosen instead of 10 to 50 m as
was used in the computations themselves. The figure should illustrate the
type of topography for which gravity prediction, based on various mathe-
matical techniques, was carried out using high-resolution terrain, sparse
density and a few gravity data. As mean gravity values for blocks of a few
kilometer side length are of primary interest to geodesy the smoothing or
"smearing" effects inherent in least-squares adjustment of terrain models
with respect to relatively few gravity data is not too perturbing.

The <u>fourth</u> test area is located off central Italy close to Sardinia
island in the Tyrrhennian Sea which is characterized by extremely thin (10
km) lithosphere. Various types of gravity data including altimetric results
were available. Mainly terrain, regional density and gravity data were used
for prediction based on various types of spectral analysis.
As a relatively dense gravity net was available the application of
various mathematical procedures could be tested. Flat twodimensional
Fourier methods (FFT) were used to represent local digital terrain models.
Freeden's (1982) well known spherical spline techniques were modified in
order to solve strictly local prediction and transformation (conversion of
gravity into potential etc.) problems. Pellinen's (1964) classical methods
by which he solved Molodensky's linear integral equation approach using
terrain data was adapted to regionally varying coefficients for the linear
regression of free air gravity with elevation. As a great variety of geo-
physical parameters such as (1) thickness and density variations in the
crust, (2) various types of Moho depths, (3) thickness and density variati-
ons in the lithosphere, (4) thickness of sediment layers etc. have been
derived for Western Europe from seismic and gravity data this information
(which is usually not available for gravity prediction in unsurveyed areas)
could be fully exploited for our test areas (2) to (4). These parameters
clearly reveal variations of totally different wave lengths s down to s <
30 km. Consequently, by fully exploiting modern digital terrain models
errors of > 5 mgal in smooth hill areas occur which do not average out over
distances of 10 to 20 km unless geophysical detail information is
available. Deviations from standard isostatic and similar models are of
non-isotropic and non-random character so that stochastic or similar re-
gression techniques can only be used reliably if trends can be well estima-
ted from existing (scarce) gravity or similar information.

3. CONCLUSIONS

This study which focuses on four primary aspects of modern prediction of gravity in unsurveyed or weakly determined areas reveals the efficiency and limitations of gravity prediction using high-resolution terrain models. It also shows the accuracy of global gravity models in (almost) "unsurveyed" areas characterized by strongly varying irregular gravity fields. It demonstrates the consequences of lateral density variations in the crust and lithosphere. By comparing these results with prediction results earlier derived by others or by us it becomes clear that quite favorable prediction results obtained e.g. in the Northern Alps where homogeneous density prevails should be generalized with great care or should better not be generalized at all. The necessity to supplement global gravity models to be deduced from satellite gradiometry for degrees n $\leq$ 180 by other measurements was shown. In spite of the fact that static models prevail in modeling local and regional gravity for harmonics of degrees 180 $\leq$ n $\leq$ 1800 the use of strong correlation of free air gravity with terrain is perturbed by a great variety of significant local and regional effects.
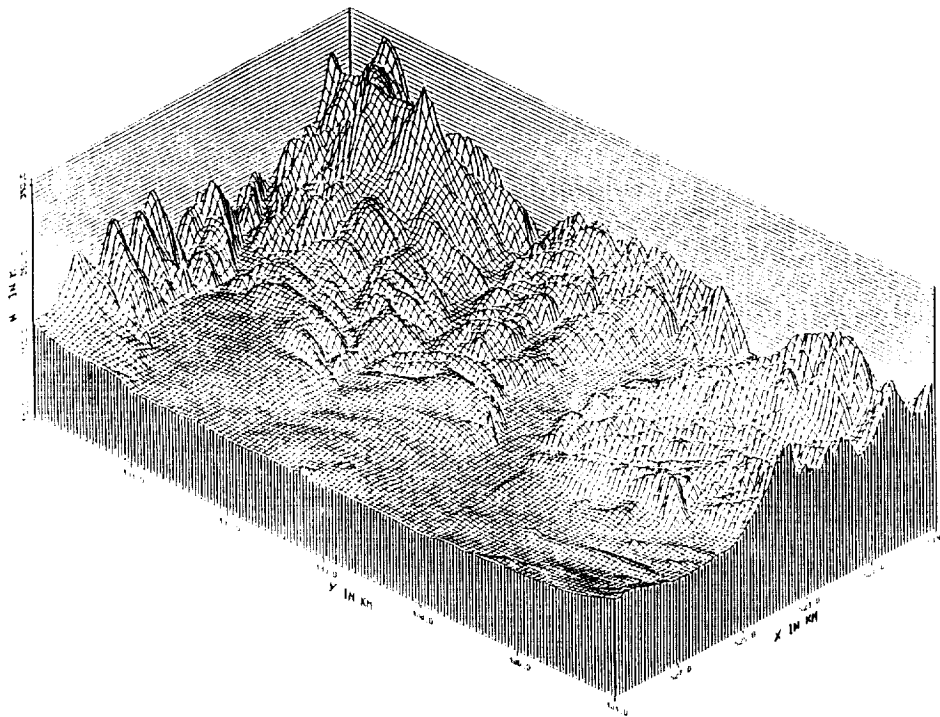
Fig. 1 Typical digital terrain model in third test area

83

REFERENCES

Freeden, W., On the permanence property in spherical spline interpolation, The Ohio State University, Department of Geodetic Science, Rep. No. 341, Columbus, 1982

Götze, H.-J., S. Schmidt and S. Strunk, Central Andean gravity field and its relation to crustal structures , Lecture Notes in Earth Sciences, Vol. 17, H. Bahlburg, Ch. Breitkreuz, P. Giese (Eds.), The Southern Central Andes, Springer Verlag Berlin Heidelberg New York, 1988

Isacks, B.L., Uplift of the central Andean plateau and binding of the Bolivian Orocline, JGR 93, 84, 3211-3231, 1988

Kling, Th., M. Becker, H.-J.-Euler and E. Groten, Studien zur detaillierten Geoidberechnung, Deutsche Geodätische Kommission, Reihe B, H. 285, München 1987

Mostanpour, M.M., Einheitliche Auswertung krustenseismischer Daten in Westeuropa. Darstellung von Krustenparametern und Laufzeitanomalien, Berliner Geowiss. Abh., Verlag Dietrich Reiner, Berlin 1984

Pellinen, L.P., Expedient formulae for computation of earth's gravitational field characteristics from gravity anomalies, Bull. Géodésique No. 72, pp.327-333, 1964

Rapp, R.H., The earth's gravity field to degree and order 180 using SEASAT altimeter data, terrestrial gravity data, and other data, Dept. of Geodetic Science and Surveying, Ohio State Univ. Columbus, Rep. No. 322, 1981

Rapp, R.H., and J.Y. Cruz, Spherical harmonic expansions of the earth's gravitational potential to degree 360 using 30' mean anomalies, Dept. of Geodetic Science and Surveying, Ohio State Univ., Columbus, Rep. No. 376, 1986

The Role of Topography in Geodetic Gravity Field Modelling

R Forsberg (Geodetic Institute, Gamlehave Alle 22, DK-2920 Charlottenlund, Denmark).

M G Sideris (Department of Surveying Engineering, The University of Calgary, Calgary, Alberta, Canada T2N 1N4)

Abstract: Masses associated with the topography, bathymetry, and its isostatic compensation are a dominant source of gravity field variations, especially at shorter wavelengths. On global scales the topographic/isostatic effects are also significant, except for the lowest harmonics. In practice, though, global effects need not be taken into account as such effects are included in the coefficients of the geopotential reference fields. On local scales, the short-wavelength gravity variations due to the topography may, in rugged terrain, be an order of magnitude larger than other effects. In such cases, explicit or implicit terrain reduction procedures are mandatory in order to obtain good prediction results. Such effects may be computed by space-domain integration or by FFT methods. Numerical examples are given in the paper for areas of the Canadian Rockies.

In principle, good knowledge of the topographic densities is required to produce the smoothest residual field. Densities may be determined from sample measurements or by gravimetric means, but both are somewhat troublesome methods in practice. The use of a standard density, e.g., 2.67 g/cm³, may often yield satisfactory results and may be put within a consistent theoretical framework.

The independence of density assumptions is the key point of the classical Molodensky approach to the geodetic boundary value problem. The Molodensky solutions take into account that land gravity field observations are done on a non-level surface. Molodensky's problem may be solved by integral expansions or more effective FFT methods, but the solution should not be intermixed with the use of terrain reductions. The methods are actually complimentary and may both be required in order to obtain the smoothest possible signal, least prone to aliasing and other effects coming from sparse data coverage, typical of rugged topography.

Introduction

The two aspects of the role of the topography, namely the direct attraction of masses of the terrain and the uneven surface on which terrestrial measurements are made, are from a theoretical point of view completely different problems. The first assumes a density model, while the second – the Molodensky theory – in principle is free of any density assumptions. Using terrain reductions a computational smoothing of the gravity field is attempted, making interpolation and prediction from scattered data points more precise. Molodensky's theory makes the classical geodetic boundary value problem solutions "correct" on the uneven topographic surface; applying the Molodensky correction terms to gravity implies no smoothing at al.. The methods are therefore complimentary and should be used together whenever feasible.

Terrain reductions

The terrain reductions may be classified under global or local models. On global scales, topographic-isostatic reductions must be used according to some idealized isostatic models. The simple model coming closest to geophysical reality is the Vening Meinesz model, which is a modified Airy model taking into account the elasticity of the crust, permitting short-wavelength loads to remain uncompensated. Some areas of the earth are, however, notably deviating from the simple models, as for example trench areas and midoceanic ridges. For a review

of computation of global topographic-isostatic effects, which may be done efficiently by fast spherical harmonic expansions, see Rummel et al. (1988).

The global topographic-isostatic reductions have only limited use in geodetic gravity field modelling, but are very useful for identifying anomalously compensated areas. The real impact of terrain reductions come on the local scale, where they strongly diminish aliasing from undersampling of the rapidly varying, height-correlated gravity anomalies in rugged topography.

On a local scale, isostatic effects need not be considered. Instead, a residual terrain model reduction (RTM), where only the topographic deviations from a smooth mean topography are considered, may be used with advantage. The smooth mean height surface h_r may be obtained from the topographic heights h by a moving average filter over suitable caps, say 1° in size. In this case, RTM-reduced gravity anomalies will resemble isostatic anomalies (Forsberg, 1984). Removing the complete effect of topography relative to a constant mean elevation level for a given area, as often done in practice, may be considered a special case of the RTM reduction. The total computational removal of all topography down to the geoid, i.e. the complete Bouguer reduction, is not useful in geodetic gravity field modelling because of very large indirect effects on the geoid.

The general form of a terrain effect on any gravimetric quantity expressable as a linear functional L(T) of the anomalous potential T is of the general form

$$L_p(T_m) = G \iint_E \int_{h_r}^{h} L_p(\tfrac{1}{\ell}) dx dy dz, \quad \ell = \sqrt{(x-x_p)^2 + (y-y_p)^2 + (z-h_p)^2} \qquad (1)$$

where E is the infinite x-y plane (planar approximation). Integrals like (1) may in practice be evaluated by prism integration or by expansions in convolutions, permitting use of FFT techniques. For details see Forsberg (1984, 1985) or Sideris (1985). Formally T_m is the potential generated by the selected terrain mass model. When computations are done consistently in a remove-restore technique, i.e. modelling the reduced potential

$$T^c = T - T_m \qquad (2)$$

by subtracting terrain effects from input data, and restoring terrain effects in predictions, then in principle density ρ need not be known. However, meaningful results are only obtained when ρ is close to the real word values.

The question of density

Estimation of good insitu densities is often quite difficult. Only the surface of topography is available for sampling, and measurements of bulk densities on rock samples tend to show high variability even within the same geological formation. For sedimentary rocks, questions of porosity, water saturation, and compaction present special problems. Typical density values encountered in practice range from below 2.0 g/cm³ in moraine hills up to 3.3 g/cm³ in (rare) gabbroic intrusive areas. However, the standard density 2.67 g/cm³ represents a surprising good value in many cases (granities, gneisses, old sediments), and its use have been justified by many empirical investigations (Dobrin, 1976). Where significantly lower density values need to be used (e.g., young sediments), topographic relief is usually also lower and good density values are therefore less critical.

For local applications a good alternative to density measurements is the estimation of ρ through studies of correlation of gravity with topographic heights ("the Nettleton method"). This method may be put within a consistent framework in least-squares collocation, estimating one or more density parameters alongside the gravity field modelling itself. For details, see Sünkel (1981).

Molodensky's problem

The first order Molodensky solution to the geodetic boundary value problem consists of a series expansion of the form

$$\zeta(P) = \sum_{n=0}^{\infty} \frac{1}{2\pi\gamma} \iint\limits_{E} \frac{g_n(Q)}{[(x_Q-x_P)^2+(y_Q-y_P)^2]^{\frac{1}{2}}} \, dx_Q dy_Q \tag{3}$$

with

$$g_0(Q) = \Delta g(Q) \tag{4}$$

$$g_1(Q) = -(h_Q-h_P) \frac{1}{2\pi} \iint\limits_{E} \frac{\Delta g(x,y)-\Delta g(x_Q,y_Q)}{[(x_Q-x)^2+(y_Q-y)^2]^{3/2}} \, dxdy \tag{5}$$

For a review, see Moritz (1980) or Sideris (1987). Depending on the terrain roughness, higher-order terms may be quite significant. Their computation requires repeated applications of the harmonic continuation integral (5), which may be formulated as a sequence of convolutions and evaluated efficiently by FFT methods. For examples see Sideris (1987).

When used on free-air anomalies, formula (5) is known to be closely related to the classical terrain correction c (Moritz, 1980). The relationship comes from noting that in rugged topography free-air anomalies show a correlation with terrain height of the form $\Delta g = \Delta g_B + 2\pi G \rho h$ where Δg_B is the simple Bouguer anomaly. Unfortunately the use of c (requiring density information) rather than g_1 (independent of ρ) have been the source of much confusion, and the practice is not recommended. It is thus preferable to evaluate (5) with terrain-reduced gravity data Δg^c. The corresponding "reduced" Molodensky terms g_n^c will be smaller, and the convergence of (3) improved. If terrain reductions are not used then, on the one hand, gravity data must be given densely enough to sufficiently sample even the shortest topographic-induced wavelengths, and, on the other hand, higher-order Molodensky series terms should be considered. Dense gravity data are hardly ever available in practice.

An example: Kananaskis area, Canadian Rocky Mountains

The Kananaskis area west of Calgary is a mountainous area with topography ranging from 1400 m to 3400 m. A number of astronomic deflections of the vertical and GPS-derived geoid undulations are available along the main valley area, in addition to gravity data space every 5 to 10 km in the surrounding region, and a dense digital terrain model. Results for a FFT gravity field modelling example are given below; for more results on terrain corrections for gravity and gradiometry in the same area, see Tziavos et al. (1988).

For the terrain reduction of the available data, a 100 m x 100 m and 1 km x 1 km DTM was used. A smooth height surface with resolution of 70 km was generated by averaging. The statistics of the data, removing topographic effects relative to the mean height surface, is shown below. Predictions were not attempted without terrain reductions, as individual gravity anomaly values could change up to 100 mgal close to the prediction points, depending on whether the observation happened to be made on top of a mountain or at the bottom of a valley. In other words, the observed Δg-field is seriously undersampled without some kind of terrain reduction.

Data type	Δg (mgal)		ξ (arcsec)		η (arcsec)		ζ (m, relative to northernmost GPS-point)	
No. of points	473		15				10	
Statistics	mean	std.dev.	mean	std.dev.	mean	std.dev.	mean	std.dev.
Observed values	20.5	57.2	1.37	3.37	.95	6.28	1.15	.46
Terrain effects	-14.9	47.2	.86	2.97	-.22	5.74	.27	.21
Reduced data	35.4	29.8	.51	1.60	1.16	2.15	.88	.25

For the FFT prediction, gravity anomalies were gridded on a 1.5'x2.5' grid in a $2.5^\circ \times 3^\circ$ region. A similar 1.5'x2.5' height grid was obtained by gridding gravity station heights for representing the uneven surface to which observations refer, in order to be able to use FFT techniques for computing the first-order Molodensky corrections g_1^c. The procedure of gridding station heights rather than averaging the detailed DTM is preferable, because the height distribution of gravity stations does not necessarily follow the averaged topography; gravity stations tend to be located in valleys rather than mountaintops.

The results of predictions with and without a spherical harmonic reference field (OSU86F to degree 180), and with and without the Molodensky terms, are shown below. Considering the rough topography, results are very satisfactory. The influence of the Molodensky term seems to be completely masked by other error sources, illustrating the high degree of smoothness locally provided by the terrain reductions.

Kananaskis: Prediction results (observed minus predicted) for various solution types

Solution with		ξ (arcsec)		η (arcsec)		ζ relative (m)	
180x180 reference field	Molodensky g_1 terms	mean	std.dev.	mean	std.dev.	mean	RMS
No	No	.92	.65	.31	.57	.09	.24
No	Yes	.91	.69	.33	.60	.09	.25
Yes	No	1.92	.66	-1.57	.48	.09	.17

References

Dobrin, M B: Introduction to Geophysical Prospecting. McGraw-Hill, New York, 1976.

Forsberg, R: A study of Terrain Reductions, Density Anomalies and Geophysical Inversion Methods in Gravity Field Modelling. Reports of the Department of Geodetic Science and Surveying, No. 355, The Ohio State University, Columbus, Ohio, 1984.

Forsberg, R: Gravity Field Terrain Effect Computations by FFT. Bulletin Géodésique, Vol. 59, pp. 342-360, 1985.

Moritz, H: Advanced Physical Geodesy. H. Wichmann Verlag, Karlsruhe, 1980.

Rummel, R, R H Rapp, H Sünkel and C C Tscherning: Comparison of Global Topographic/Isostatic Models to the Earth's Observed Gravity Field. Reports of the Dep. of Geodetic Science and Surveying, No. 388, The Ohio State University, 1988.

Sideris, M: A Fast Fourier Transform method for computing terrain corrections. Manuscripta Geodaetica, Vol. 10, No. 1, pp. 66-71, 1985.

Sideris, M G: Spectral Methods for the Numerical Solution of Molodensky's problem. UCSE Rep. 20024, Dept. of Surveying Engineering, University of Calgary, 1987.

Sünkel, H: The estimation of free-air anomalies. Rep. 315, Dept. of Geodetic Science and Surveying, The Ohio State University, 1981.

Tziavos, I N, M G Sideris, R Forsberg and K P Schwarz: The effect of the Terrain on Airborne Gravity and Gradiometry. Journal of Geophysical Research, Vol. 93, No. 38, pp. 9173-9186, 1988.

THE INVERSE GRAVIMETRIC PROBLEM IN GRAVITY MODELLING

F. Sansò*, C.C. Tscherning   **N90-20535**

Istituto di Topografia Fotogrammetria e Geofisica, Politecnico Milano, Italy

1.

One of the main purposes of geodesy is to determine the gravity field of the earth in the space outside its physical surface [13]. This purpose can be pursued without any particular knowledge of the internal density even if we don't know the exact shape of the physical surface of the earth, though this seems to entangle the two domains, as it was in the old Stoke's theory before the appearance of Molodensky's approach [10].

Nevertheless even when large, dense and homogeneous data sets are available, it has always been recognized that subtracting from the gravity field the effect of the outer layer of the masses (topographic effect) yields a much smoother field, which allows for computations with a much lower approximation error [16].

This is obviously more important when we have a sparse data set, so that any smoothing of the gravity field helps in interpolating between the data without raising the modelling error [3]: this approach is nowadays generally followed also because it has become very cheap in terms of computing times since the appearance of spectral techniques [14].

2.

As we know the mathematical description of the IGP is dominated mainly by two principles, which in loose terms can be formulated as follows:

1) the knowledge of the external gravity field determines mainly the "lateral" variations of the density;

2) the deeper is the density anomaly giving rise to a gravity anomaly, the more improperly posed is the problem of recovering the former from the latter.

For a sphere, of radius normalized to 1, the relation between harmonic coefficients of the external gravity field $u(P) = \Sigma\ u_{nm}Y_{nm}(\sigma_P)$ and of the internal density $\rho(Q) = \Sigma\ \rho_{nm}(r_Q)Y_{nm}(\sigma_Q)$ is described by the formula

$$u_{nm} = \frac{1}{2n+1}\ \int_0^1 \rho_{nm}(r)\ r^{n+2}\ dr \quad . \tag{1}$$

Several applications of (1) derived from fixing the radial variations of ρ: e.g. the single layer case is considered as well as harmonic or quasi-harmonic densities, which correspond to suitable variational problems.

3.

The statistical relation between ρ and n (and its inverse) is also investigated in its general form, proving that degree cross-covariances have to be introduced to describe the behaviour of ρ, i.e.

$$\sigma_{\rho,n}(r_1, r_2) = \frac{1}{2n+1}\ \sum_m\ \rho_{nm}(r_1)\ \rho_{nm}(r_2) \quad : \tag{2}$$

the general relation between such functions and the usual degree variances of the potential

89

$$\sigma^2_{u,n} = \frac{1}{2n+1} \Sigma_n u^2_{nm} \quad ,$$

is

$$\sigma^2_{n,m} = \frac{1}{2n+1} \int_0^1 \int dr_1 \, dr_2 \, \sigma_{\rho,n}(r_1,r_2) \, (r_1 \cdot r_2)^{n+2} \tag{3}$$

The meaning of Kaula's rule is investigated in this framework proving that it demonstrates, within a layered model, the presence of a white noise in the lateral variations of the outermost layer; this is interpreted as the effect mainly of the rough signal due to topographic masses and their compensation.

4.
Furtheron the problem of the simultaneous estimate of a spherical anomalous potential and of the external, topographic masses is addressed criticizing the choice of the mixed collocation approach, as presented in [12]. This approach in fact fixes the relation between internal covariance of ρ and n in such a way that it has been proved to be wrong in practical cases [5].
A reasonable improvement is found when the modelling of the density is constant on a scheme of overlapping blocks, since this allows the construction of suitable crosscovariance models. This approach is now undergoing a practical investigation.
The paper will be published in full length by the Danish Geodetic Institute in the book in honour of the 60th birthday of Torben Krarup.

REFERENCES

[1] Barzaghi R., Sansò F.: Remarks on the inverse gravimetric problem; Boll. di Geod. e Sc. Aff., n. 2, 1986.

[2] Barzaghi R., Sansò F., Tscherning C.C.: Choice of norm for the density distribution of the Earth; Geophys. J. R.A.S., 87:1, 1986.

[3] Forsberg R.: Gravity surveying and terrain corrections in Greenland; Proc. of Int. Meeting on Potential Fields in Rugged Topography; Lausanne, July 1985.

[4] Forsberg R., Knudsen P., Tscherning C.C.: Description of GRAUSOFT package; in preparation, 1988.

[5] Hein G., Sansò F., Strykowsky G., Tscherning C.C.: On the choice of norm and base functions for the solution of the inverse gravimetric problem; Pres. 17 Conference on Mathematical Geophysics, Blanes, June 1988.

[6] Kaula W.M.: Theory of Satellite Geodesy; Blaisdell Pub. Co., Waltham, Mass., 1966.

[7] Lions J.L., Magenes E.: Problèmes aux limites non homogènes et applitions; Dunod, Paris, 1968.

[8] Phillips R.J., Lambeck K.: Gravity field of the terrestrial planets: long wavelength anomalies and tectonics; Rev. of Geoph. and Sp.Phys., vol. 18, n. 10, 1980.

[9] Sansò F.: Internal collocation; Memorie dell'Accademia dei Lincei, Vol. XVI, n. 1, 1980.

[10] Sansò F.: Recent advances in the theory of geodetic boundary value problem; Rev. of Geophysics and Space Physics, n. 3, 1981.

[11] Sansò F., Tscherning C.C.: Mixed collocation: a proposal; Quaterniones Geodaesiae, Univ. Thessaloniki, 3,1:1982.

[12] Sansò F.: Statistical methods in physical geodesy; in "Mathematical and Numerical Techniques in Physical Geodesy", Ed. H.Suenkel, Lecture Notes in Earth Sciences, vol. 7, Springer-Verlag, Berlin Heidelberg, 1986.

[13] Sansò F.: Talk on the theoretical foundations of physical geodesy; in "Contribution to geodetic theory and methodology", Publ. of Dept. of Surveying Eng., Univ. Calgary, 60006, Calgary, June 1987.

[14] Sideris M.G.: Computation of gravimetric terrain corrections using FFT techniques; Dept. Surveying Eng., Univ. Calgary, UCSE Rep. 20007, Calgary, 1984.

[15] Suenkel H.: Local gravity field approximation; in "Contributions to geodetic theory and methodology", Dept. Surveying Eng., Univ. Calgary, 60006, Calgary, June 1987.

[16] Suenkel H.: The gravity field in Austria; Presented at XIX Gen. Assembly IUGG/IAG, Vancouver, 1987.

[17] Tscherning C.C., Suenkel H.: A method for the construction of spheroidal mass distributions consistent with the harmonic part of the earth's gravity potential; Manuscripta Geodaetica, vol. 6, 1981.

[18] Tscherning C.C., Strykowski G.: Quasi-harmonic inversion of gravity field data; Pres. 5 Int. Seminar on Model Optimization in Exploration Geophysics, Berlin, Feb. 1987.

FFT—Local Gravimetric Geoid Computation

Dezső Nagy, Geophysics Division, Geological Survey of Canada, Ottawa, Canada
and
Rudolf J Fury, National Geodetic Survey, NOS/NOAA, Rockville, Md. USA

Abstract

Model computations show that changes of sampling interval introduce only 0.3 cm changes, whereas zero padding provides an improvement of more than 5 cm in the FFT generated geoid. For the GPS survey of Franklin County, Ohio, the parameters selected as a result of model computations, allow large reduction in local data requirements while still retaining the *cm* accuracy when tapering and padding is applied. The results are shown in tables.

Introduction

The following is a brief description of computational modeling carried out in order to obtain optimal results from the use of the Fast Fourier Transform (FFT) technique for local geoid computation. These experiments were designed to find the most favorable parameters for local geoid computation using gravity data only. The availability of analytical expressions for the model, both the potential and the gravity, permits us to evaluate the effect of changing any of the parameters introduced when using FFT. It is recognized, that some of the parameters depend very much on the model. Thus these computational experiments are model related and can not be applied blindly for all practical work. Still, the model used in these studies provides the opportunity to test some interesting aspects of the FFT technique.

Model Description

A three-dimensional model of a granitic intrusion (Gibb and van Boeckel,1970), which consists of 64 prisms and covers an area of 80×75 km^2, with a change of about 60 mgal and 75 cm in gravity and geoidal height respectively, was used in these model computations. For details see Nagy(1988). The analytical expressions for the potential, U, and the gravity, Δg, for a single prism are given below (Nagy,1980) :

$$U = k\rho\left[xy\ln(z+r) + yz\ln(x+r) + zx\ln(y+r)\right.$$

$$\left. -\frac{1}{2}x^2\arctan\frac{yz}{xr} - \frac{1}{2}y^2\arctan\frac{zx}{yr} - \frac{1}{2}z^2\arctan\frac{xy}{zr}\right]$$

$$\Delta g = k\rho\left[x\ln(y+r) + y\ln(x+r) - z\arctan\frac{xy}{zr}\right]$$

where $r = \sqrt{x^2 + y^2 + z^2}$.

The negative of the potential divided by the normal gravity, γ, gives the geoidal height for a prism. Summing up the required quantities for all prisms of the model provide the *exact* reference values, with which the result of the various numerical computations can be compared. The difference is clearly the error of the numerical procedure. In this case, the error generated by the FFT method.

Geological Survey of Canada Contribution No. 34788

Effect of Sampling Interval

As the transfer function, i.e. the function used to weigh the gravity anomalies to produce the geoidal height, is relatively flat as compared, for example, with the functions used in calculating the deflections of the vertical, or the vertical derivatives, one expects no large changes associated with the changes in the sampling interval. This has been confirmed with model computations. Different sampling intervals between 1 and 15 km covering the same area produced only 0.3 cm change in geoidal height. For this reason, the sampling interval does not seem to be of major concern in local geoid determinations.

Effect of Padding

The Fourier method assumes periodicity, i.e. the field given in a two-dimensional array is repeated in the frequency domain around the central part in both dimensions and introduces the so called *leakage* into the computations, causing unwanted errors. To partially compensate for this error, the technique known as *padding* is used. Padding consists of putting zeros around the values of the input matrix, practically doubling the dimensions. For the model using 5 km sampling interval and a 26×26 grid, the gravity was practically zero at all boundries. The model geoid over this grid has a span (difference between maximum and minimum) of 74.9 cm. The use of FFT on the corresponding gravity anomaly produced a geoid with the span of 67.3 cm i.e. an error of 7.6 cm. Carrying out the zero padding to generate a matrix of 50×50 resulted in a different geoid with a span of 73 cm. This means that doing only zero padding, the error was reduced from 7.6 cm to 1.9 cm. This is a far greater change then produced by varying the sampling interval. Here the great importance of modeling is stressed. The results of computations without and with padding *are different*. However without the knowledge of the *exact model values*, one would not be able to draw any conclusions. In the case of modeling, the comparison with the exact values makes it obvious which computation gives the better result.

Effect of Tapering

Normally the gravity anomalies at the boundaries are not zero. In order to have a smoother transition, the techique known *tapering* is used. The purpose of tapering is to bring down the non-zero gravity values at the boundary smoothly to zero. There are various ways of achieving this, but model computations show that the particular method used for tapering is not critical. Table 1 summarizes some numerical results with various combinations of tapering with zero padding. The input matrix was generated at a 1 km interval, consisting of an array of 62×62 (used as reference), covering the central part of the anomaly field, with reasonably large non-zero values at the boundaries. All geoidal height related quantities are given in *cm*.

Table 1

Array	Tapering	Padding	Geoidal Heights		Residual Errors	
Size	%	%	min	max	Span	RMS
62	0	0	-24.55	23.89	40.73	7.43
70	6	0	-22.31	26.74	27.30	4.87
90	6	16	-15.98	35.17	22.51	2.96
90	22	0	21.22	34.68	11.98	2.54
110	22	16	-17.38	42.76	8.54	1.77
110	38	0	-21.71	42.34	16.63	2.96
130	38	17	-17.13	49.69	10.97	2.16
110	6	32	-12.22	41.78	20.97	2.66
130	22	33	-13.17	48.99	7.76	1.64

Numerical Errors

It is well known that the computed values toward the border of the area become erroneous. Modeling provides again a unique opportunity to study this question by comparing the analytical and the FFT-derived values and, based upon the residuals, draw some conclusions. On the model used, there is a sharp drop in residual errors after reducing the array size by about 10%, thereafter no significant reduction in errors occur. Obviously, the results are again model dependent.

Practical Application

Based upon the results of model computations, the FFT method has been used to calculate relative geoidal heights for the Franklin County GPS survey. The calculation was done in two steps :

- the regional component was calculated from the **OSU86F** truncated to $n = 36$,

- the local component was derived by applying the FFT technique to the residual gravity field, which was gridded at 5' intervals resulting in an array of 192×192 providing the desired coverage for the area of interest.

The geoidal height difference is the sum of the global geoid and column [1]. This value will be used later in the comparisons listed in Table 3.

The results of some of the computations are shown in Table 2. Column [1] is the direct application of FFT; all other solutions are the changes with respect to this solution. The dramatic reduction of errors by the combined effect of tapering and padding (for example, solution [8] vs. solution [4]) is readily recognizable from Table 2.

Table 2

Base line	Global geoid	FFT [1]	Residual FFT Geoids							
			[2]	[3]	[4]	[5]	[6]	[7]	[8]
Rhodes → Clark	-8	3.3	-.3	.5	2.4	1.1	.4	.6	-.4
18–83 → Clark	-7	-9.2	-.4	-.1	1.6	.9	.3	.2	-.5
18–83 → Rhodes	1	-12.5	-.1	-.6	-.8	-.2	-.1	-.4	-.1
Britton → 18–83	10	-30.9	-.1	-.8	-2.9	-1.0	-.1	-.7	.7
Hoover → Clark	3	9.0	.5	.1	-.8	-1.1	-1.1	-.3	-.5
18–83 → Shannahan	-17	4.1	-.6	1.1	5.0	2.7	.5	.8	-1.3
Jackson → Britton	-20	18.3	-.3	1.9	7.2	2.9	1.1	2.2	-.7
Smith → Jackson	-8	59.0	.4	.9	2.4	.5	-.5	.4	-1.2
Smith → Hoover	-28	28.2	-.9	1.8	9.1	4.4	1.9	2.4	-1.2

Legend :

No.	Array	Remarks
[1]	192	8.0° border around baselines
[2]	144	5.5° border around baselines
[3]	72	3.0° border around baselines
[4]	52	20 rows and columns removed at south and east (simulating lack of data at shore lines)
[5]	72	zero padding for removed data
[6]	144	50% zero padding on [5] all around
[7]	72	20% tapering on [4] all around
[8]	144	50% zero padding on [7]

The relative geoidal height computations were repeated next by truncating the **OSU86F** global model to $n = 180$ and both results (i.e. the $n = 36$ and $n = 180$) were then compared to values derived from GPS surveys and leveling (Table 3). The GPS survey used in these comparisons was reported earlier by Engelis et al. (1984) and Kearsley (1985), and are listed as **OSU** and **AUS** respectively in Table 3. Relative geoid heights (**GPS**) were derived at the National Geodetic Survey of USA (Fury,1985); the old values were given in the above cited references.

Table 3

Base line	Length	Relative Geoid Heights					
		GPS	old	OSU	AUS	36	180
Rhodes → Clark	10	-5	(-7)	-3	-6	-5	-3
18–83 → Clark	11	-18	(-19)	-14	-19	-16	-14
18–83 → Rhodes	4	-13	(-13)	-11	-13	-12	-12
Britton → 18–83	13	-21	(-19)	-21	-19	-21	-22
Hoover → Clark	10	19	(19)	12	15	12	12
18–83 → Shannahan	22	-18	(-25)	-11	-19	-13	-10
Jackson → Britton	24	-4	(1)	0	-5	-2	0
Smith → Jackson	14	58	(32)	50	63	51	52
Smith → Hoover	35	4	(-13)	3	5	0	4

Conclusions

The numerical experiments presented here confirm the effectiveness of the FFT method for local gravimetric computation and show some of the results which can be obtained from model computations for use as guidelines in practical applications to obtain the best result from the FFT technique.

References

[1] Engelis T., Rapp R.H., and Tscherning C.C., 1984, *The Precise Computation of Geoid Undulation Differences with Comparison to Results Obtained from Global Positioning System*. Geophysical Research Letters, Vol.1, No.9, Sept.

[2] Fury R.J., 1985, *Report on Data Analysis of GPS Survey Project, Franklin County GPS Surey*. NGS Report, May

[3] Gibb R.A., and van Boeckel J., 1970, *Three-dimensional gravity inetrpretation of the Round Lake batholith, notheastern Ontario*. Can. J. Earth. Sci. 7

[4] Kearsley, A.H.W., 1985, *Towards the Optimum Evaluation of the Inner Zone Contribution to the Geoid Heights*. Australian Journal of Geodesy, Photog. and Surv., No.42, June

[5] Nagy, D., 1966, *The gravitational attraction of a right rectangular prism*. Geophysics, **XXXI**, No.2, April, 362–371.

[6] Nagy, D., 1980, *Gravity anomalies, deflection of the vertical and geoidal heights for a three-dimensional model*. Acta Geodaet.Geophys. et Mont. Acad. Sci. Hung. Tomus 15 (1), 17–26.

[7] Nagy, D., 1988, *Fast Fourier Transform and Modeling in Geoid Computation*. Bolletino di Geodesia e Scienze Affini No.1, 1988, 33–43.

A Comparison between SEASAT, GEOSAT and Gravimetric
Geoids Computed by FFT and Collocation in the
Central Mediterranean Sea

R. Barzaghi[*], R. Forsberg[**] and C.C. Tscherning[**]
* Politecnico di Milano, Milano, Italy
** Geodetic Institute, Charlottenlund, Denmark

Abstract

Gravimetric geoids have been computed for the central Medi-
terranean Sea between latitude 32^0 and 36^0 and longitude 18^0 and
22^0 using FFT and collocation. A comparison with cross-over ad-
justed SEASAT and GEOSAT data in the area showed for both gravi-
metric geoids the standard deviation of the differences to be
0.20 m and 0.15 m, respectively. The mean and standard deviation
of the difference between the FFT and the collocation geoid
heights were -0.82 and 0.20 m, respectively. This quite large
difference may be due to the different data sampling and noise
weighting used by the two methods, but is not yet fully explain-
ed.

1. Introduction

In the early 1990'ties the ERS-1 and the Topex/Poseidon sa-
tellites will be launched, both equipped with a radar altimeter.
The usefulness of the altimeter data for oceanographic purposes
will be greatly improved, if we are able to compute a precise
height reference surface for an area being investigated, i.e. a
regional, relative, geoid. By this we mean that height differen-
ces are precisely known, but that all the values may be affected
by a common bias. (Clearly, it would be better, if we could com-
pute an absolute geoid, but this will require that e.g. a global
gradiometric satellite mission is carried through).

At the Geodetic Institute there has been developed a softwa-
re package for gravity field modelling "GRAVSOFT", which may be,
and have been, used for geoid determination (Tscherning and
Forsberg, 1986). The package includes programs for gravity mo-
delling using collocation, (GEOCOL), and FFT (GEOFOUR), as well
as programs for the estimation of statistical parameters for the
gravity field (EMPCOV, COVFIT).

It is our intension to use GRAVSOFT for geoid determination
as a part of our participation in the ESA ERS-1 project. There-
fore we wanted to test the programs in a kind of worst-case si-
tuation, namely where the geoid variation was large. On the ot-
her hand, the distribution of the gravity data should be good,
and nearly no oceanographic phenomena should influence the sa-
tellite altimeter data, which we wanted to use in our evalua-
tion. Such a situation is found in the central Mediterranean
Sea, see Fig. 1.

In the following we will describe the data and the result of
the evaluation.

2. Available Data

Gravity data were made available to us by D. Arabelos, University of Thessaloniki, in the form of data in a 0.125° grid digitized from the maps published by Morelli et al.(1975). Data in the sea area shown in Fig. 1 was used.

Since the use of the FFT requires data to be available in a regular grid all the missing values were predicted using a fast collocation procedure implemented in the program module GEOGRID. On the other hand does collocation not permit the use of all the 4194 values, since a full system of equations with this dimension must be solved. Therefore, when using collocation for geoid computation, only the 0.25° grid points were used outside the 4° x4° inner area, where the geoid was computed.

Cross-over adjusted SEASAT-data (Cruz and Rapp, 1982) were made available to us by R.H. Rapp. A local cross-over adjustment, using the data in the 4°x4° area, made the standard deviation of the cross-over values of the six used tracks decrease from 0.05 cm to 0.02 cm. Raw GEOSAT data were also adjusted, and cross errors (mainly due to data over land, see Fig. 1) were removed. The data covered a 1/2 year period, and contained therefore up to 10 repeat tracks. Originally the dataset consisted of 3096 points, which before the removal of gross errors had a standard deviation of 5.53, and with 97 values removed had a standard deviation of 2.87 m. The result of a cross-over adjustment with only bias gave a standard deviation of the cross-over differences of 0.05 m compared to 5.29 m before the adjustment.

3. Gravimetric Geoid Computations

First the contribution of the spherical harmonic expansion GPM2 was subtracted. Using these "reduced" values, empirical auto- and cross -covariance functions were estimated by EMPCOV, using the gravity and the GEOSAT data, regarded as geoid heights. An analytic expression for the covariance function was then determined using COVFIT (Knudsen,1987),

$$C(\psi) = a \cdot \sum_{i=0}^{N} e_i P_i(\cos\psi) + \sum_{i=N+1}^{\infty} \frac{A(i-1)}{(i-2)(i+4)} \left(\frac{R_B}{R}\right)^{2i+4} P_i(\cos\psi).$$

Here ψ is the spherical distance between two gravity anomaly values (at the sea surface), e_i the error degree-variances of GPM2, a, A scale factors and R_B the radius of the so-called Bjerhammar sphere. R is the mean radius of the Earth, and P_i are the Legendre polynomials. Values of $N=120$, $a=0.88$, $A=444$ and $R-R_B=3.75$ km was found to give a nearly perfect agreement between the analytic expression and the empirical auto- and cross covariances.

The gravity data were then used to compute geoid heights for the 4°x4° area. The use of collocation look more than 10 times as long time as the use of FFT. A comparison with the altimeter measurements were then made, and the results are given in Table 1. In Fig. 2 are shown the FFT, collocation and GEOSAT heights along the longest track in the open sea.

97

Table 1. Comparison of FFT and collocation gravimetric geoids with SEASAT and GEOSAT adjusted altimeter heights.

	Mean m	Standard Dev. m
GEOSAT-data with GPM2 subtracted	-1.24	0.62
Difference GEOSAT-FFT geoid	-2.18	0.15
Difference GEOSAT-Collocation geoid	-1.37	0.15
Difference SEASAT-FFT geoid	-0.54	0.20
Difference FFT-Collocation geoid	-0.82	0.20

The difference between the FFT and collocation geoid heights are shown in Fig. 3. The large mean difference and standard deviation may be caused by the way the two methods accounts for the long-wavelength information. Also the standard deviation of the differences is surprisingly large, considering that both methods agree so well with the GEOSAT data.

A detailed analysis of the differences between the GEOSAT heights and the gravimetric geoid heights along the individual tracks, see Fig. 4, showed that altimeter data close to the coast (<50 km distance) have a larger variation than points at the open sea. This indicates a possible coastal current, the existence of which must be verified.

4. Conclusion

The result of the investigation shows (as expected) that the GEOSAT data in this area are slightly superior to the SEASAT data. Also, considering the error in the altimeter data, we have demonstrated that it is possible to compute a regional, relative geoid, at the decimeter level, using the GRAVSOFT programs. It is obvious, that FFT should be used if the data configuration and quality permits it. Otherwise collocation should be used, since it puts few requirements on the data configuration, and also makes it possible to include the adjusted altimeter data as observations. The quite large differences between FFT and collocation must be further studied.

References

Cruz, J.Y. and R.H.Rapp: Sea surface heights in the Mediterranean area from SEASAT altimeter data. Bollettino di Geofisica, Vol. 24, no. 95, pp. 167-174, 1982.

Knudsen, P.: Estimation and Modelling of the Local Empirical Covariance Function using gravity and satellite altimeter data. Bulletin Géodèsique, Vol. 61, pp. 145-160, 1987a.

Morelli, C., M. Pisani and C. Gantar: Geophysical Studies in the Aegean Sea and in the Eastern Mediterranean. Bollettino di Geofisica teoretica ed applicata, Vol. XVIII, pp. 127-168, 1975.

Tscherning,C.C. and R.Forsberg: Geoid determination in the Nordic Countries - a status report. Proc. 10. General Meeting of the Nordic Geodetic Commission, Helsinki, 29.-sept.-3.oct.1986, pp. 279-290. Published by Finnish Geodetic Institute, 1986.
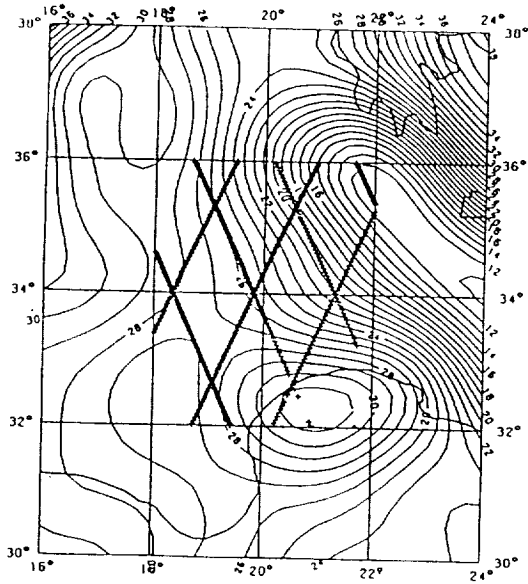
Fig. 1. Geoid heights (contour interval 1 m)
derived from GPM2 with the used GEOSAT tracks.
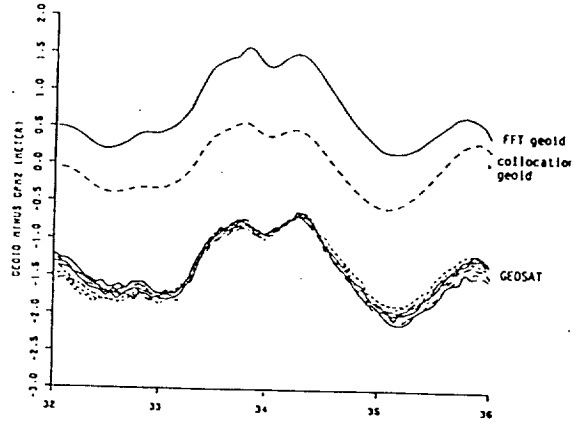
Fig. 2. Adjusted GEOSAT heights and corresponding
FFT and collocation geoid heights along the longest
track. The contribution from GPM2 is subtracted.
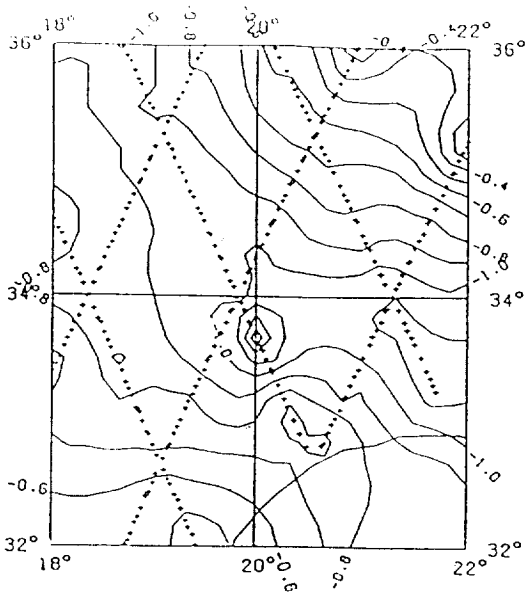
Fig. 3. Difference between geoid heights
computed by FFT and collocation. Contour
interval 0.1 m.
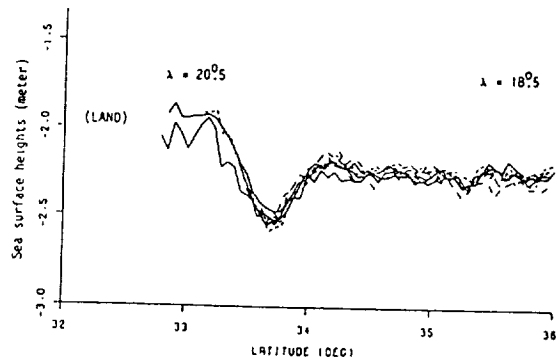
Fig. 4. Sea-surface heights computed as the difference
between the GEOSAT heights and the gravimetric geoid
heights computed by FFT.

Performance of FFT methods in local gravity field modelling

Rene Forsberg **N90-20537**

Geodætisk Institut, Gamlehave Alle 22, Charlottenlund, Denmark

Dag Solheim

Statens Kartverk, Hønefoss, Norway (on leave at Geodætisk Institut)

Abstract and introduction

Fast Fourier transform methods provide a fast and efficient means of processing large amounts of gravity or geoid data in local gravity field modelling. The FFT methods, however, has a number of theoretical and practical limitations, especially the use of flat-earth approximation, and the requirements for gridded data. In spite of this the method often yields excellent results in practice when compared to other more rigorous (and computationally expensive) methods, such as least-squares collocation.

The good performance of the FFT methods illustrate that the theoretical approximations are offset by the capability of taking into account more data in larger areas, especially important for geoid predictions. For best results good data gridding algorithms are essential. In practice "truncated" collocation approaches may be used. For large areas at high latitudes the gridding must be done using suitable map projections such as UTM, to avoid trivial errors caused by the meridian convergence.

In the paper the FFT methods are compared to "ground thruth" data in New Mexico (ξ,η from Δg), Scandinavia (N from Δg, the geoid fits to 15 cm over 2000 km), and areas of the Atlantic (Δg from satellite altimetry using Wiener filtering). In all cases the FFT methods yields results comparable or superior to other methods.

Gravity field modelling by FFT methods

The Fourier transformation methods have become practical tools in geodesy after the advent of high-degree (180x180) spherical harmonic expansions of the geopotential. Using such a geopotential reference model, the residual field may with good approximation be treated within the flat-earth approximation of the Fourier methods.

For the (residual) anomalous potential T, two-dimensional Fourier transformation

$$\tilde{T}(k_x,k_y) = \iint_{-\infty}^{\infty} T(x,y)\, e^{-i(k_x x + k_y y)} dxdy \qquad (1)$$

yields the familiar simple frequency domain relationships

- upward continuation: $\quad \tilde{T}(k_x,k_y,z) = \tilde{T}(k_x,k_y)\, e^{-kz}$

- geoid prediction: $\quad \tilde{N} = \dfrac{1}{\gamma}\dfrac{1}{k}\,\tilde{\Delta g}$ $\qquad\qquad (2)$

- deflections: $\quad \left.\begin{matrix}\tilde{\xi}\\ \tilde{\eta}\end{matrix}\right\} = -\dfrac{i}{\gamma}\dfrac{1}{k}\left\{\begin{matrix}k_x\\ k_y\end{matrix}\right\}\tilde{\Delta g}$

where γ is normal gravity and $k = (k_x^2 + k_y^2)^{1/2}$ the radial wavenumber. The above equations may be evaluated by the Fast Fourier Transform algoritm, and the final results obtained by an inverse transform. The use of FFT requires gridded data, and introduces errors due to periodicity assumptions and aliasing. For details see, e.g., Kearsley et al. (1985).

The "inverse Stokes" transformation N to Δg is a high pass filtering operation, often seriously affected by noise when data is from satellite altimetry. In this case Wiener filtering may be used. Assuming Kaula's rule to

be valid, the PSD of the geoid heights ϕ_{NN} will decay like k^{-4} (Forsberg, 1984). In the presence of white noise w in data, the optimum Δg-estimate will be

$$\widetilde{\Delta g} = k \frac{\phi_{NN}}{\phi_{NN} + \phi_{ww}} \, \gamma\widetilde{N} = k \frac{1}{1 + ck^4} \, \gamma\widetilde{N} = k\alpha(k)\gamma\widetilde{N} \qquad (4)$$

The constant c depends on data noise and local variability of the gravity field. It may be specified indirectly through the wanted <u>resolution</u> of the solution, the resolution here defined as the wavelength corresponding to the wavenumber k_R with $\alpha(k_R)$ = 0.5. Resolutions around 20 km give good results.

The FFT prediction examples in the sequel have been done using the GI programme modules GEOGRID (fast gridding using truncated collocation with a second-order Markov model), GEOFOUR (FFT manipulation), and TCIP (interpolation from result grids with local splines).

Examples of gravity field modelling by FFT

1. Δg to (ξ, η) - White Sands area, New Mexico.

Gravity data was gridded in a 4° x 3° area on a 2' x 2' grid using terrain reduced data. The FFT prediction results were compared to 384 deflection pairs from astrogeodetic observations, yielding

	ξ"	η"
R.m.s. observed deflections	2.69	6.16
Difference FFT minus observed	0.73	0.85

For a comparison r.m.s. prediction accuracies in the range 0.9-1.0" for ξ and 1.1-1.8" for η were reported in Kearsley et al (1985), using the same data with four different prediction methods (ring integration, collocation, collocation/integration, and FFT on 5' mean data)

2. Δg to N for a large area - Scandinavia.

The geoid was computed for the region 54°-71^ON, 4°-32^OE by two FFT solutions gridding the available gravity data on either a 6' x 12' geographical grid, or a 10 km x 10 km UTM grid (zone 33). The FFT results are compared to an earlier comprehensive blocked collocation prediction consisting of 26 3^Ox 6° solution blocks (Tscherning and Forsberg, 1986), and all solutions are compared to 41 GPS derived geoid undulations (fig. 1) observed by the Institut fur Erdmessung, Hannover (Denker, pers.comm.).

The FFT solutions were both based on GPM2 and a thinned out gravity data set (6' x 12' pixels), as for the collocation solution, with some new data added in northern Germany and off northern Norway. A total of some 20000 gravity stations were gridded onto a 210x180 (geographic) or 256x256 point grid (UTM). The comparison of the predicted geoids to the GPS results are shown below and in fig. 2.

Geoid comparison at 41 GPS stations (m):	mean	std.dev.
Difference FFT (geographic) minus GPS	0.07	0.17
- FFT (UTM zone 33) - GPS	-0.09	0.15
- collocation - GPS	-1.31	0.54
Difference FFT (geographic) - FFT (UTM)	0.16	0.04

The FFT solutions are clearly superior to the collocation solution, illustrating the benefit of being able to take more data into account. The UTM

FFT solution provided best results as expected (GRS80 bias uncertain), with the difference between the two FFT solutions being quite large: On 1044 0.5°x1° grid points the difference had a mean value of 15 cm, std.dev. of 12 cm, and a maximal discrepancy of 45 cm, unacceptable for a precision geoid.
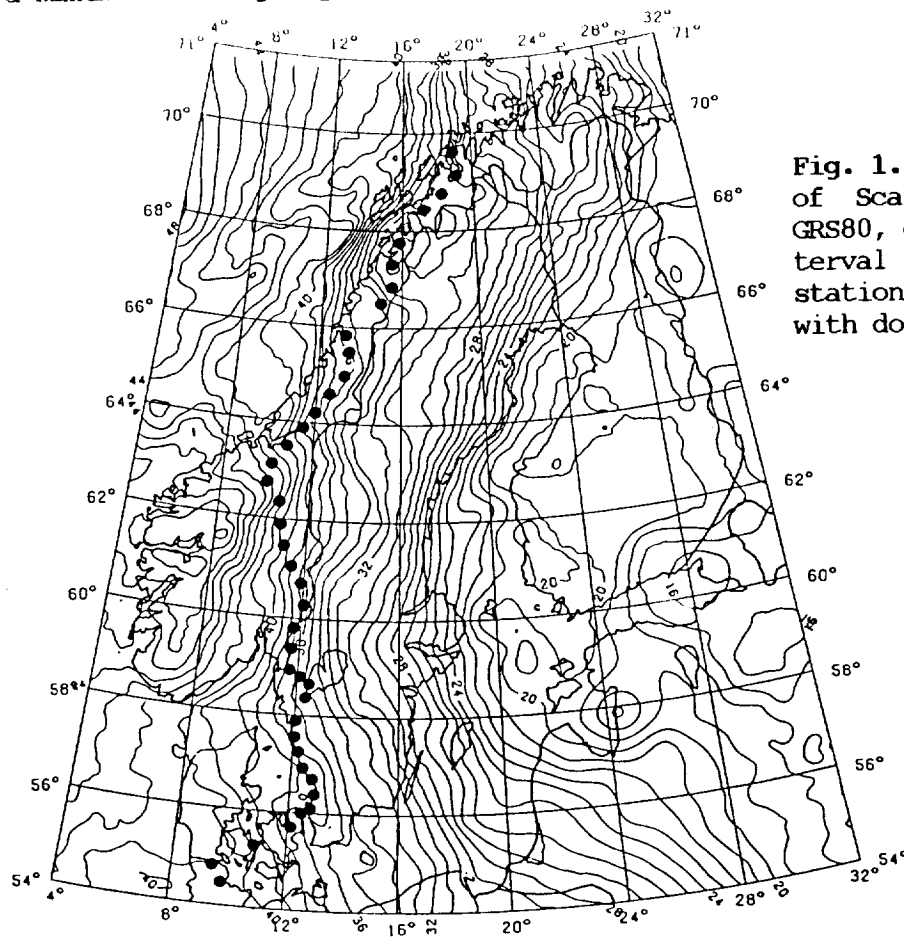
Fig. 1. FFT geoid of Scandinavia in GRS80, contour interval 1.0 m. GPS stations shown with dots.
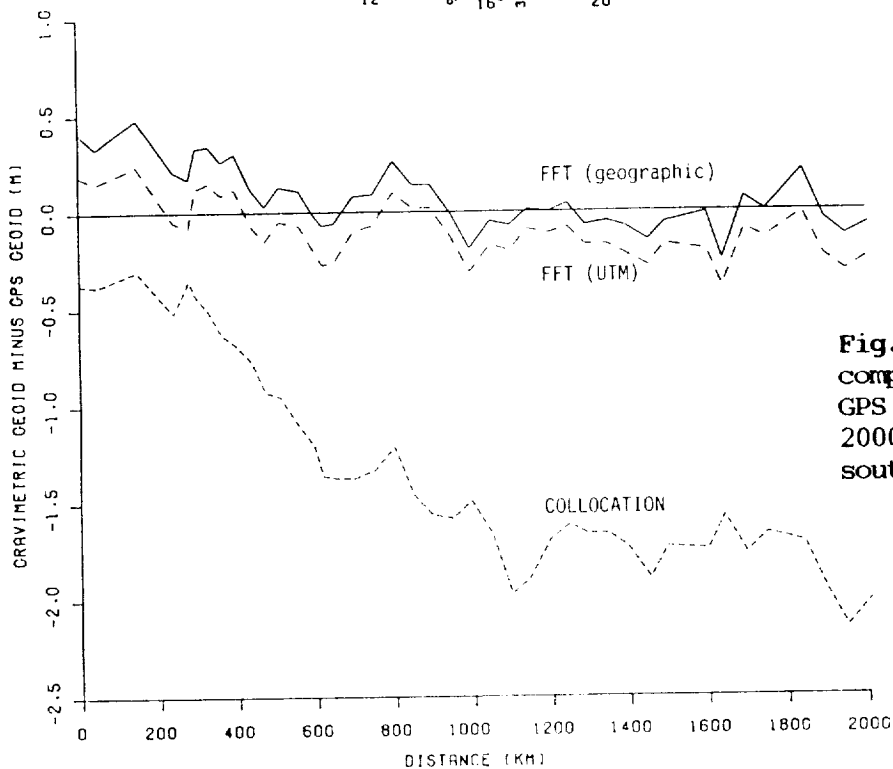
Fig. 2. Comparison of computed geoids versus GPS results along the 2000 km profile from south to north.

3. N to Δg – satellite altimetry off Norway and Puerto Rico trench.

In this example Wiener filtering with resolution k_R^{-1} at 20-30 km is used. With the simple FFT approach useful Δg values were not obtained. In both cases the satellite altimetry data was submitted to a local bias cross-over adjustment prior to gridding and FFT.

The test area S of Lofoten, Norway, is a shelf area. Available SEASAT data within a $5°x\ 8°$ were gridded at 3'x 6' using GPM2 as reference field. The adjusted orbits had r.m.s. cross-overs at 8 cm. The computed gravity anomalies are compared to recent SK gravimetry in a $2.5°x\ 4°$ area (fig. 3). For comparison a collocation solution (GEOCOL) was also done.

In the Puerto Rico area combined SEASAT/GEOS3 data were compared to all ship gravimetry in a $3°x\ 3°$ area over the trench. The r.m.s. crossovers after adjustment was 31 cm. The FFT solution was done by a 6'x 6' grid in a $8°x\ 8°$ area (without reference field). Results are shown below, together with OSU collocation results (Kadir, Knudsen and Rapp, pers.comm).

Area	Δg observed		FFT difference		Collocation diff.	
	mean	std.dev.	mean	std.dev.	mean	stddev.
Norway	12.2	33.8	-1.0	10.9	1.2	12.8
Puerto Rico	-125.8	130.5	-12.7	15.3	-10.5	15.9
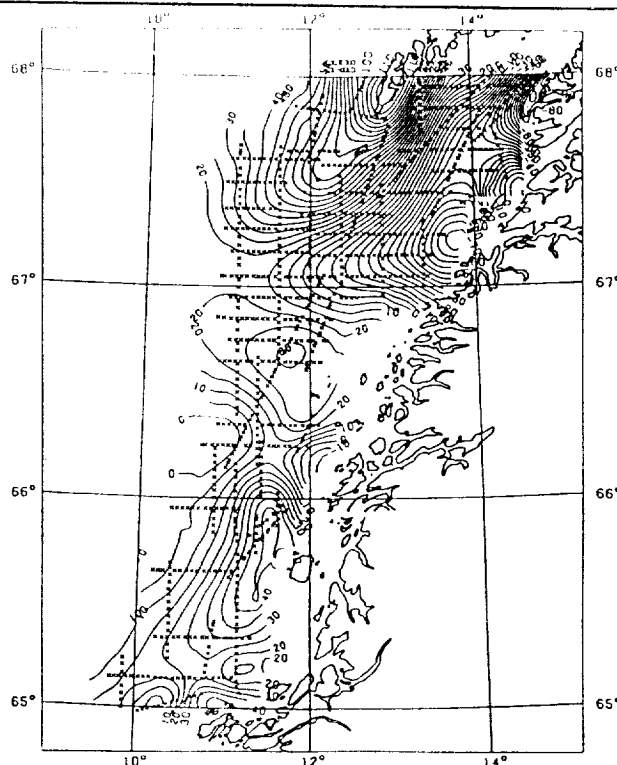
ORIGINAL PAGE IS
OF POOR QUALITY

Fig. 3. Gravity anomalies computed by FFT from SEASAT altimetry south of Lofoten, Norway. 5 mgal contour interval. Comparison gravimetry tracks shown with crosses.

Conclusions

The FFT methods work, theoretical approximations are offset by the ability to handle more data. For large blocks proper map projections must be used.

References

Forsberg, R.: Local Covariance Functions and Density Distributions. Rep. Dept. of Geodetic Science, Ohio State University, no. 356, 1984.

Kearsley, Sideris, Krynski, Forsberg, Schwarz: White Sands revisited. Dept. of Surveying Engineering, University of Calgary, Rep. 30007, 1985.

Tscherning, Forsberg: Geoid Determination in the Nordic Countries from Gravity and Height Data. Boll.geod.sci.aff. 46 no. 1, pp. 21-43, 1987.

N90-20538

J. C. Harrison and M. Dickinson
Geodynamics Corporation
5520 Ekwill Street, Suite A
Santa Barbara, CA 93111

Abstract

New algorithms have been derived for computing terrain corrections, all components of the attraction of the topography at the topographic surface and the gradients of these attractions. These algorithms utilize fast Fourier transforms, but, in contrast to methods currently in use, all divergences of the integrals are removed during the analysis. Sequential methods employing a smooth intermediate reference surface have been developed to avoid the very large transforms necessary when making computations at high resolution over a wide area.

A new method for the numerical solution of Molodensky's problem has been developed to mitigate the convergence difficulties that occur at short wavelengths with methods based on a Taylor series expansion. A trial field on a level surface is continued analytically to the topographic surface, and compared with that predicted from gravity observations. The difference is used to compute a correction to the trial field and the process iterated. Special techniques are employed to speed convergence and prevent oscillations.

Three different spectral methods for fitting a point-mass set to a gravity field given on a regular grid at constant elevation are described. Two of the methods differ in the way that the spectrum of the point-mass set, which extends to infinite wave number, is matched to that of the gravity field which is band-limited. The third method is essentially a space-domain technique in which Fourier methods are used to solve a set of simultaneous equations.

THIN-PLATE SPLINE QUADRATURE OF GEODETIC INTEGRALS

Herman van Gysen

Department of Surveying and Mapping
University of Natal
Durban, South Africa

ABSTRACT

Thin-plate spline functions - known for their flexibilty and fidelity in representing experimental data - are especially well-suited for the numerical integration of geodetic integrals in the area where the integration is most sensitive to the data, i.e. in the immediate vicinity of the evaluation point. Spline quadrature rules are derived for the contribution of a circular innermost zone to Stokes's formula, to the formulae of Vening Meinesz, and to the recursively evaluated operator L_n in the analytical continuation solution of Molodensky's problem. These rules are exact for interpolating thin-plate splines.

In cases where the integration data are distributed irregularly, a system of linear equations needs to be solved for the quadrature coefficients. Formulae are given for the terms appearing in these equations. In case the data are regularly distributed, the coefficients may be determined once-and-for-all. Examples are given of some fixed-point rules. With such rules successive evaluation, within a circular disk, of the terms in Molodensky's series becomes relatively easy.

The spline quadrature technique presented here complements other techniques such as ring integration for intermediate integration zones.

Quadrature rules are sought approximating the contribution of a circular innermost zone to the evaluation of Stokes's formula, the formulae of Vening Meinesz, and the L_1 gradient operator in the series analytical continuation solution of Molodensky's problem. The rules are to be of the form

$$\zeta_I(x) = \frac{r_0}{\gamma_0} \sum_{i=1}^{N} a_i \Delta g(\alpha_i);$$

$$\begin{pmatrix} \xi_I(x) \\ \eta_I(x) \end{pmatrix} = \frac{1}{\gamma_0} \sum_{i=1}^{N} \begin{pmatrix} b_{1i} \\ b_{21} \end{pmatrix} \Delta g(\alpha_i);$$

$$L_{1,I} f(x) = \frac{1}{\gamma_0} \sum_{i=1}^{N} c_i \{f(\alpha_i) - f(x)\};$$

where $x = (x_1, x_2)$, $y = (y_1, y_2)$ are plane co-ordinates (with the 1-axis north and 2-axis east), r_0 is the radius of the innermost zone, and the subscript I indicates innermost zone contribution. $\{r_0\alpha_i\}$, $i=1,..,N$, are distinct points in the innermost zone (not all on a single straight line) where the data are given. The coefficients in each instance are chosen to make the integration exact for thin-plate splines with nodes at the α_i, and exact for constant and linear functions in the nullspace of these splines. The thin-plate spline kernel function associated with function evaluation at α_i is $|y - \alpha_i|^2 \log_e |y - \alpha_i|$.

The quadrature weights for Stokes's formula are obtained from the solution of the linear equations

$$\sum_{i=1}^{N} a_i |\alpha_j - \alpha_i|^2 \log_e |\alpha_j - \alpha_i| + b_0 + b_1\alpha_{1j} + b_2\alpha_{2j} = d_j(x), \quad j = 1, \ldots, N;$$

$$\sum_{i=1}^{N} a_i = e_0(x); \quad \sum_{i=1}^{N} a_i\alpha_{1i} = e_1(x); \quad \sum_{i=1}^{N} a_i\alpha_{2i} = e_2(x);$$

where

$$d_j(x) = \frac{1}{2\pi} \iint_{|x-y| \leq 1} \frac{|y - \alpha_j|^2 \log_e |y - \alpha_j|}{|x - y|} dm(y) = -\frac{1}{9} + \frac{4}{9}|x - \alpha_j|^3;$$

$$e_0(x) = \frac{1}{2\pi} \iint_{|x-y| \leq 1} \frac{1}{|x - y|} dm(y) = 1;$$

$$e_1(x) = \frac{1}{2\pi} \iint_{|x-y| \leq 1} \frac{y_1 - x_1}{|x - y|} dm(y) = 0;$$

$$e_2(x) = \frac{1}{2\pi} \iint_{|x-y| \leq 1} \frac{y_2 - x_2}{|x - y|} dm(y) = 0.$$

Similar looking systems of equations give the quadrature weights for the spline approximation of Vening Meinesz'z formula and the L_1 operator. In the last case non-zero constant functions are not admissable, and the thin-plate spline kernel function needs some modification.

Numerical examples show that thin-plate spline quadrature can be very effective in evaluating the three integrals of Stokes, Vening Meinesz and the L_1 gradient operator.

THE REDUCTION CORRECTION IN NORTH AMERICA

P. D. Martzen and J. C. Harrison
Geodynamics Corporation
5520 Ekwill Street, Suite A
Santa Barbara, CA 93111

Abstract

An inverse Poisson integral technique has been used to determine a gravity field on the geoid which, when continued by analytic free space methods to the topographic surface, agrees with the observed field. The computation is performed in three stages, each stage refining the previous solution using data at progressively increasing resolution (1° x 1°, 5' x 5', 5/8' x 5/8') from a decreasing area of integration. Reduction corrections are computed at 5/8' x 5/8' granularity by differencing the geoidal and surface values, smoothed by low-pass filtering and sub-sampled at 5' intervals. This paper discusses 1° x 1° averages of the reduction corrections thus obtained for 172 1° x 1° squares in western North America.

The 1° x 1° mean reduction corrections are predominantly positive, varying from -3 to +15 mgal, with values in excess of 5 mgal for 26 squares. Their mean and rms values are +2.4 and 3.6 mgal respectively and they correlate well with the mean terrain corrections. The mean and rms contributions from the three stages of computation are; 1° x 1° stage +0.15 and 0.7 mgal; 5' x 5' stage +1.0 and 1.6 mgal; and 5/8' x 5/8' stage +1.3 and 1.8 mgal. These results reflect a tendency for the contributions to become larger and more systematically positive as the wavelengths involved become shorter. The results are discussed in terms of two mechanisms; the first is a tendency for the absolute values of both positive and negative anomalies to become larger when continued downwards and, the second, a non-linear rectification, due to the correlation between gravity anomaly and topographic height, which results in the values continued to a level surface being systematically more positive than those on the topography.

This paper has been submitted to the Bulletin Geodesique for publication; conference preprints are available from the authors.

Downward Continuation of the Free-Air Gravity Anomalies to the Ellipsoid Using the Gradient Solution and Terrain Correction - An Attempt of Global Numerical Computations

Y. M. Wang
Department of Geodetic Science and Surveying
The Ohio State University

Abstract

The formulas for the determination of the coefficients of the spherical harmonic expansion of the disturbing potential of the earth are defined for data given on a sphere. In order to determine the spherical harmonic coefficients, the gravity anomalies have to be analytically downward continued from the earth's surface to a sphere - at least to the ellipsoid. The goal of this paper is to continue the gravity anomalies from the earth's surface downward to the ellipsoid using recent elevation models. The basic method for the downward continuation is the gradient solution (the g_1 term). The terrain correction has also been computed because of the role it can play as a correction term when calculating harmonic coefficients from surface gravity data.

The fast Fourier transformation has been applied to the computations.

1. Introduction

The formulas for the determination of the coefficients of the spherical harmonics of the earth's gravitational potential require the free-air anomalies to be given on a sphere, at least at a simple surface, e.g., ellipsoid or sea level. Thus we have to continue the free-air gravity anomalies downward to a sphere or an ellipsoid.

The validity of the analytically downward continuation of the free-air gravity anomalies inside the earth is guaranteed by Runge's theorem (Moritz, 1980, p. 67). Of course these gravity anomalies are not the original gravity anomalies inside the earth. The downward continuation gives a fictitious gravity anomaly on the ellipsoid that generates a disturbing potential T on and outside the earth.

Moritz (1980) suggested that the free-air anomalies be continued to the point level. We can take also the ellipsoid as the reference surface and use this method to continue the gravity anomalies down to the ellipsoid.

Pellinen (1966) studied the methods for the determination of the coefficients of the spherical harmonics of the earth's gravitational potential and he added a term, which can be easily transformed into terrain correction, to the free-air anomalies.

In this paper we carried out some numerical investigation with the above mentioned methods. The terrain correction and the gradient solution were computed on a global basis.

2. Mathematical formulation

We continue the free-air anomalies downward to the ellipsoid by using the "gradient solution (Moritz, 1966, p. 68):

$$\Delta g^* = \Delta g + g_1 = \Delta g - h \frac{\partial \Delta g}{\partial h} \tag{1}$$

where Δg^*, Δg are the gravity anomalies on the ellipsoid and on the earth's surface, respectively.

The gradient of the gravity anomaly Δg is given by

$$\frac{\partial \Delta g}{\partial h} = \frac{R^2}{2\pi} \iint_\sigma \frac{\Delta g - \Delta g_P}{\ell_0^3} \, d\sigma \tag{2}$$

where $\ell_0 = 2R \sin \psi/2$, ψ is the angular distance between the current point and the computation point p, σ is the unit sphere, and R is the mean radius of the earth.

Pellinen (1966, p. 70) suggested that

$$\Delta g^* = \Delta g + G' \tag{3}$$

where

$$G' = \frac{R^2}{4\pi} \iint_\sigma \frac{(h-h_p)(\Delta g - \Delta g_p)}{\ell_0^3} \, d\sigma \tag{4}$$

The relationship between the gravity anomaly Δg and the elevation h is assumed as

$$\Delta g = a + bh, \qquad b = 2\pi k\rho \approx 0.11 \text{ mgal/meter} \tag{5}$$

a is a constant.

Taking the plane approximation and using the assumption (5) we get

$$g_1 = -h_p k\rho \iint_\tau \frac{h-h_p}{\ell_0^3} \, dxdy \tag{6}$$

$$G' = C = \frac{1}{2} k\rho \iint_\tau \frac{(h-h_p)^2}{\ell_0^3} \, dxdy \tag{7}$$

with $\ell_0 = [(x-x_p)^2 + (y-y_p)^2]^{1/2}$, where τ is the two-dimensional plane.

3. Computations of the Terrain Correction and the Gradient Solution on a global Basis

The elevation data in 5' x 5' mean block values are available from the National Geophysical Data Center, Boulder, Colorado as ETOPO5. This elevation data was used for the computation of the g_1 term and the terrain correction on a global basis.

The integration region is taken as 15° in latitude extent and 30° in longitude. The boundary (or overlap) of the integration is taken 50 km. This satisfies the accuracy for most situations (Noë, 1980). But the boundary is not large enough for the Himalaya Mountains. In the computations we took a 250 km boundary for the high mountain areas and a 50 km boundary for the flat areas.

The g_1 term and the terrain correction are computed in 5' mean block values by using the FFT (fast Fourier transformation) technique. All computations are completed at the Instruction and Research Computer Center at Ohio State University. The CPU time required was about 10^{-3} second for each point on the IBM 3081 at OSU.

The statistics of the g_1 term and the terrain correction are exhibited in Tables 1 and 2.

Table 1. Statistics of the g_1 Term in 5' and 30' Mean Block Values
Unit: mgal

Block Size	Mean Value	Standard Dev.	Max. Value	Min. Value
5'	0.27	±2.56	442.14	-78.88
30'	0.27	±1.54	45.08	-10.47
1°	0.27	±1.24	25.52	- 5.16

Table 2. Statistics of the Terrain Correction in 5' and 30' Mean Block Values
Unit: mgal

Block Size	Mean Value	Standard Dev.	Max. Value	Min. Value
5'	0.23	±1.01	183.57	0.0
30'	0.23	±0.82	25.24	0.0
1°	0.23	±0.74	17.77	0.0

It shows that the mean values of the g_1 term and of the terrain correction are almost the same. Of course, the g_1 term is larger and rougher (larger standard deviation, larger maximum values).

After the computations of the g_1 term and terrain correction in 5' mean block values on a global basis, g_1 and the terrain correction were expanded in the spherical harmonics up to 180th order. The RMS (root mean square) values of the degree variances of the g_1 term and the terrain correction are about 2 percent of the RMS values of the degree variance of the OSU86E gravity model.

The total contributions of the g_1 term and the terrain correction on the geoid and the deflections of the vertical are shown in Table 4.

Table 4. RMS values of the corrections of the geoid undulation and the deflections of the vertical due to the g_1 and TC

correction	RMS of δN	RMS of $\delta\theta$
g_1	0.7071 m	0.1129 secs
TC	0.7065 m	0.0880 secs

4. Conclusion

The g_1 term and the terrain correction were computed in $5'$ mean block values on a global basis. The maximum of the g_1 term is 442 mgal located in the Himalaya Mountains. The maximum of the terrain correction is 184 mgal. The influence of the g_1 term and the terrain correction on the geoid undulation has been considered. It takes the order of 1 meter (RMS of correction of the geoid undulation). For the deflections of the vertical the RMS of the corrections of the g_1 term and the terrain correction is on the order 0.1".

Acknowledgments

References

Bracewell, R., The Fourier Transformation and its Applications, McGraw-Hill, New York, 1965.

Heiskanen, W., and H. Moritz, Physical Geodesy, W.H. Freeman and Co. San Francisco, 1967.

Pellinen, L.P., A Method for Expanding the Gravity Potential of the Earth in Spherical Harmonics, Translated From Russian, ATIC-TC-1282, NTIS: AD-6611819, Moscow, 1966.

Moritz, H., Linear Solutions of the Geodetic Boundary Value Problem, Report No. 79, Dept. of Geodetic Science and Surveying, The Ohio State University, Columbus, 1966.

Noë, H., Numerical Investigations on the Problem of Molodensky. Mitteltungen der Geodatischen Institute der Technischen Universität graz, Folge 36, 1980.

Rapp, R.H., Effect of Certain Anomaly Correction Term on Potential Coefficients Determinations of the Earth's Gravitational Field, Bulletin Geodesique, No. 115, 1975.

Sideris, M.G., A Fast Fourier Transform Method for Computing Terrain Corrections, manuscripta geodaetica, Vol. 10, No. 1, 1985.

Alphonse S. Lwangasi

N90-20542

Dept. of Surveying & Photogrammetry, University of Nairobi, Kenya.

ABSTRACT

The definition of geoidal undulations is given and after summarising the methods of determination of the geoid, computed geoidal undulations by some of the methods for several points in Kenya are compared to the results obtained by the satellite gravimetric solutions.

Results from astrogeodetic levelling and satellite attimetry show some reasonable agreement with the satellite-gravimetric geoids while results by Doppler satellite positioning indicate that good agreement can be obtained if the orthometric heights for the points are adjusted to a uniform system.

INTRODUCTION

This paper gives the geoidal undulations in Kenya computed for the whole country using gravimetric and satellite derived solutions. The gravimetric solution is that of Gachari and Olliver, 1986; and the satellite solution is based on the GEM 10C earth model. Geoidal undulations have been computed at discrete points using results of Doppler satellite positioning and spirit levelling. Geoidal undulations differences have also been computed by astrogeodetic levelling at a few points. A comparison of the results for the discrete points is made with the values estimated from the geoidal maps of the gravimetric and satellite solutions. Comparison is also made for the satellite altimetry results for a few points on the coast.

THEORETICAL CONSIDERATIONS

<u>Definition:</u> The geoid is the equipotential surface of the earth's attraction and rotation that best approximates the mean sea-level over the whole earth. The term was introduced by K.F. GAUSS in 1884 as the mathematical figure of the earth and as such it is a key figure in Geodesy, playing a fundamental role in positioning.

<u>Approximations of the geoid</u>

(i)   Up to an accuracy of a few metres (±2m) the geoid is represented by the mean sea-level.

(ii)   Up to an accuracy of some tens of metres the geoid is represented by a biaxial geocentric ellipsoid whose minor axis coincides with the earth's principal polar axis of inertia. The biaxial ellipsoid is an analytically defined 'normal body of the earth' that best fits the geoid and is often referred to as the 'reference ellipsoid'.

<u>Geoidal height</u> - This is the undulation of the geoid obtained as the separation between the geoid and the reference ellipsoid.

<u>Causes of geoidal undulations:</u>

Geoidal undulations are generally caused by the inaccurate approximation of the geoid by the reference ellipsoid because:

1. From the definition, geoidal undulations are brought about by the differences between the normal gravity field and the actual gravity field of the earth.

2. Where there are irregularities in the mass distribution, the geoidal undulations will be more pronounced even if the best fitting ellipsoid were adopted.

3. With a reference ellipsoid of dimensions (a,f) adopted, its positioning with respect to the geoid will also give rise to geoidal undulations if the positioning is not accurately done.

METHODS OF DETERMINATION OF GEOIDAL UNDULATIONS

The commonly used methods are:

1. Astronomical Levelling: This is suited for a local or regional area. The data required are the astrogeodetic deflections of the vertical. The method will give an accuracy of about ±4m. However the accuracy is not homogeneous and can be very much affected in rough topography.

2. Gravimetric determinations: Geoidal undulations at discrete points can be obtained by use of Stoke's integral. This method is suited for the whole earth but practically suited for limited areas of about 1000kmx1000km. It requires a dense gravity coverage and can give an accuracy of about ±1m.

3. Satellite fixes, e.g. Doppler Positioning – Geoidal undulations at discrete point at which the orthometric heights (H) are known can be determined from N=h-H, with h obtained as the geodetic height from the Doppler positioning. The same principle used on oceans, (in Satellite Altimetry) will give the difference between sea-level height and sea-surface height.

4. Potential coefficients – Potential coefficients together with dynamic form factor uniquely specify the normal gravity field. The coefficients are obtained from the analysis of perturbations of the orbits of several satellites. With the potential coefficients known, other parameters of the gravity field can be determined and hence the disturbing potential and finally by Bruns' formula, the geoidal undulations can be obtained. The accuracy by this method is about ±1m. It gives a globally homogeneous solution, but somewhat not detailed enough.

5. Other methods – Other methods used in geoidal determination are combinations of various data, usually done so as to take advantage of the effectiveness of the various methods as far as homgenuity, accuracy and detail coverage are concerned.

COMPUTED GEOIDAL UNDULATIONS

(i) Gravimetric and satellite geoids: Fig. 1 shows a gravimetric geoid of Kenya computed on the GRS80 ellipsoid computed (by Gachari & Olliver, 1986) using a combination of GEM10B satellite derived potential coefficients and terrestrial gravity data. Fig. 2 shows the satellite derived geoid computed on the WGS72 ellipsoid, using potential coefficients based on GEM10C.

(ii) Geoidal undulations from Doppler positioning – Geoidal undulations have been computed at some stations that are fixed by Doppler positioning. Most of the stations are part of the African Doppler Survey (ADOS) program and all are part of the Kenya geodetic network. With the heights of these points from the vertical control, the geoidal undulations on WGS72 ellipsoid are computed at these stations and shown in Fig. 1 and 2.

(iii) Geoidal undulations from Astrogeodetic levelling – Astronomical levelling was computed at a few astrodeflection points shown in Fig 1 and 2 as A,B,C,..I. The differences in geoidal undulations, ΔNAL, computed on the Clarke 1880 ellipsoid and converted to WGS72 ellipsoid are shown in the table below, alongside the estimated

113
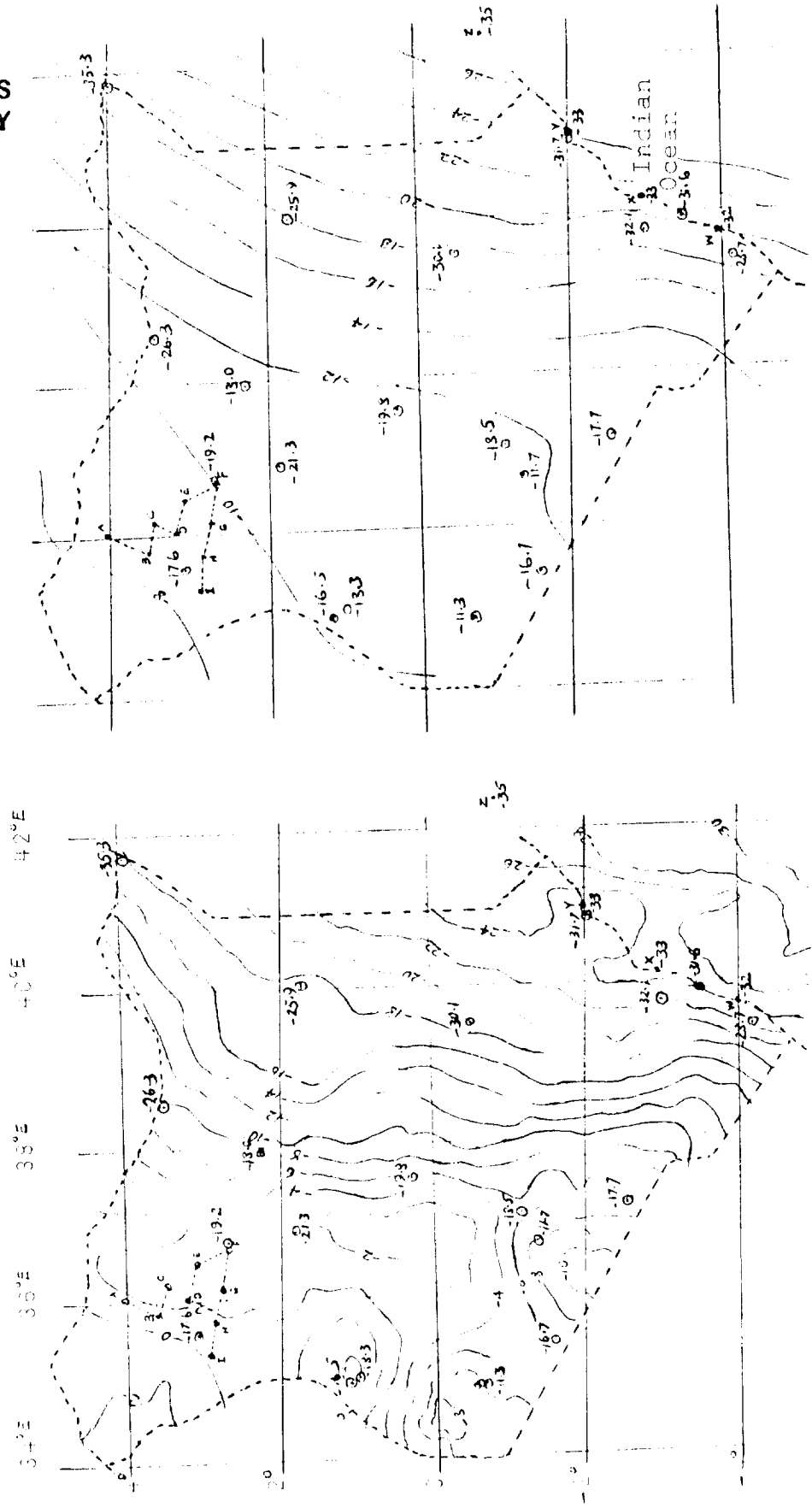
Fig. 2. Satellite derived geoid on
WGS72, 2m interval.

Fig. 1. Gravimetric geoid of Kenya on
WGS72, 2m interval.

114

differences in geoidal undulations from the geoidal maps for the
gravimetric (ΔN_G) and satellite (ΔN_{SD}) geoids.

Line	ΔN_{AL}	ΔN_G	ΔN_{SD}	Line	ΔN_{AL}	ΔN_G	ΔN_{SD}
A-B	0.91m	-0.6m	0.0m	E-F	0.53m	-0.5	-0.6
B-C	-1.13	-0.4	-0.7	F-G	-0.79	-0.1	0.5
C-D	0.28	-0.6	0.0	G-H	0.73	-0.4	0.5
D-E	0.05	-0.8	-0.3	H-I	0.91	0.8	0.7

Table 1: undulations differences by various methods.

(iv) Geoidal undulations from satellite altimetry - For the four points on
the coast line, W,X,Y,Z, the values on GRS80 ellipsoid estimated from
Rapp, 1982 are shown in Figs. 1 and 2.

COMPARISON OF RESULTS

The gravimetric and satellite derived geoids are similar in shape,
particularly for the south-eastern and north-eastern parts of Kenya. However,
the two differ in shape and detail as we go from the central part to the
west and north-western. The differences in detail show up since satellite geoid
is more generalised than the gravimetric geoid, while the similarity in shape
is expected since the gravimetric geoid was computed incorporating potential
coefficients. The differences in values could be due to the different
ellipsoids and the gravity anomalies that were not corrected for terrain,
indirect effect and atmospheric effects.

The Doppler derived undulations, for the points considered, differ from
both the gravimetric and satellite derived geoids by mean values of about
-12.7m and -8.8m respectively. These differences arise mostly due to errors
in the orthometric heights. It is regrettable that the orthometric heights
used to derive the Doppler geoidal undulations are not accurately computed as
the vertical network was poorly observed and computed piecemeal.

The altimeter geoidal undulations estimated for the coastal shore points
differ by about -8.3m and -10.1m from the estimated undulations of the
gravimetric and satellite derived geoids respectively.

The comparison with astronomical levelling is relative as none of the
points used has a fixed (known) geoidal undulation determined astrogeodetic-
ally. However, with mean differences of 0.5m and 0.2m for the relative
geoidal height differences when compared with the gravimetric and satellite
derived geoids respectively, it shows good agreement for the astronomical
levelling method.

CONCLUSION

The gravimetric geoid has good agreement with the satellite derived
geoid for the most parts of the country except for most of the western
half of the country. This is likely to be due to the topography in the
western half - it is mostly rugged and mountainous and in some parts rising
to over 4000m above sea-level.

The Doppler derived undulations show some consistency with either the
gravimetric or satellite derived geoid. If the orthometric heights can be
accurately determined, these can improve on the undulations by Doppler
positioning.

115

Astrogeodetic levelling can also be used to give more information for the geoidal undulations.

REFERENCES

Bomford, G., Geodesy, 4th Ed. Clarendon, Oxford, 1980.

Chodota, M.W.L., African Doppler Survey (ADOS), News Bulletin of the Regional Centre for Services in Surveying, Mapping and Remote Sensing. Nairobi, July/Dec. 1985.

Gachari M.K., & Olliver J.G., The detailed gravimetric geoid of Kenya, Survey Review, Vol. 28 No. 221 July 1986.

Heiskanen, W., & Moritz, H., Physical Geodesy, W.H. Freeman, 1967

Lachapelle, G., Comparison of Doppler derived and gravimetric geoid undulations in North Americ, paper presented at the 2nd Int. Symp. on Satellite Doppler positioning, Univ. of Texas, Austin 1979.

Rapp, R.H., A global atlas of sea surface heights based on the adjusted Seasat Altimeter data, Rep. No. 333 of the Dept. of Geodetic Science and Surveying, Ohio State Univ. Columbus Ohio, August 1982.

Rapp, R.H., & Wechiencharon C., Comparison of Satellite Doppler and gravimetric geoid undulations considering terrain corrected gravity data, J.Geophy. Res., Vol. 89, No. B2, 1984.

Vanicek P. , & Krakiwsky, E.J., Geodesy - The concepts, 2nd Ed., North Holland Publishing Co., 1986.

GEOID '88 : A Gravimetric Geoid for Canada

Dezső Nagy, Geophysics Division, Geological Survey of Canada
1 Observatory Crescent, Ottawa, K1A 0Y3, Canada

Abstract

Using Stokes' formula, a gravimetric geoid has been calculated for Canada. The input data are as follows : $15' \times 15'$ block averages were used for Canada and the USA and $1° \times 1°$ block averages and satellite model (GEM-T1) provided values for the remaining part of the Earth. The geoid was calculated at 6398 points covering the area within the points $p_i(\varphi_i, \lambda_i)$, ($\lambda$ is + west) :

$$p_1(40, 125); \quad p_2(75, 184); \quad p_3(75, 10); \quad \text{and} \quad p_4(40, 60)$$

The computed geoid refers to the GRS1980 and reaches a local minimum of -47.3 metres around the western part of Hudson Bay. A contour map of the geoid is shown.

Introduction

There is a renewed interest in geoid determination in connection with the use of the Global Positioning System (GPS) for geodetic purposes. The demand in this case is for geoidal height differences over relatively short distances (measured in kilometres), with an error of a few parts per million relative accuracy. If the differences in one region are to be connected to those in another region, the need for absolute geoid height will demand a similar accuracy to enable one to join the piece-wise information. Gravity coverage over the entire surface of the Earth has been assembled for the computation. Computation points over continental Canada have been selected at a nearly equidistant interval. The subject of this short note is to report on the geoid computation and show the results in the form of a contour map. Further information is available in Nagy(1988).

Theory

The geoid was calculated from the formula derived by Stokes(1849) :

$$N = \frac{R}{4\pi\gamma} \int_{\sigma} \Delta g S(\psi)\, d\sigma$$

where
	N	is the geoidal height,
	R	is the mean radius of the earth,
	γ	is the mean gravity,
	Δg	is the gravity anomaly, corresponding to $d\sigma$,
	$S(\psi)$	is the Stokes function,
and	$d\sigma$	is the surface element of the unit sphere.

Stokes' function is defined as :

$$S(\psi) = \operatorname{cosec}\tfrac{1}{2}\psi + 1 - 6\sin\tfrac{1}{2}\psi - 5\cos\psi - 3\cos\psi \ln\left(\sin\tfrac{1}{2}\psi + \sin^2\tfrac{1}{2}\psi\right)$$

Thus to calculate the geoidal height, N, the gravity anomaly, Δg, (representative for the surface element), is multiplied by the Stokes function and the area of the surface element, $d\sigma$. This product is then summed up over the entire surface of the Earth. This process requires gravity everywhere. In the following, the input data used in the computations will be described briefly.

117

Input data

For the computations, the following data-sets were assembled :

CANUS15 : 15′×15′ block surface gravity averages for Canada and the continental United States,

WORLD1 : 1°×1° block surface gravity averages outside the CANUS15 data-set,

MISSING : 1° × 1° block satellite gravity model values calculated at the centre of each block where terrestrial gravity coverage is missing.

Each of these data-sets will be discussed briefly and some values associated with each particular data-set will be given in Table 1. Data-sets not originally on the GEODETIC REFERENCE SYSTEM 1980 (Geodesist's Handbook 1980), were transferred to this reference surface during the computations.

CANUS15

This 15′ data-set consists of two files :

CAN15 : 15′ × 15′ block surface gravity averages for Canada,

USA15 : 15′ × 15′ block surface gravity averages for the continental United States.

The CAN15 was calculated from 602 577 point values, available at the begining of 1988 from our National Gravity Data Base. The USA15 block averages were obtained from the National Geodetic Survey of Rockville, Md. Computed from 1 256 119 point values, 44 029 blocks were made available. Parts of this data-set covering Canada were screened out. Also omitted were some offshore values and data over Hawaii. After this data editing, 21 510 blocks were included to represent gravity over the United States. The combination of these files resulted in 65 539 15′ blocks and provides the best possible surface gravity coverage for North America at this resolution.

WORLD1

This 1° × 1° mean world-wide surface gravity data-set was obtained from The Ohio State University and is described in detail in Despotakis(1986). It contains 48 955 values of which 44 203 were used (over North America, the more detailed CANUS15 data-set, described earlier, was used).

MISSING

After assembling the two previously described files, there were still 15,608 1° × 1° blocks over the Earth's surface with no surface gravity values. For these missing blocks the most recent GEM-T1 satellite gravity model values were used. The spherical harmonic coefficients were obtained from the Goddard Space Flight Center (Marsh et al. 1987) and were evaluated at the center of each block.

This completed the preparation of the input, consisting of three files, and provided the required gravity coverage over the entire surface of the Earth.

To conclude this section, Table 1 summarizes some statistics about the input files.

Table 1 : INPUT FILE STATISTICS

	CAN15	USA15	CANUS15	CAN1P	CAN1R	WORLD1	MISSING
min	-135.7	-223.3	-223.3	-112.0	-112.0	-270.0	-40.49
max	239.4	219.7	239.4	98.3	111.8	340.0	46.34
N	44 029	22 444	65 539	3 446	3 446	44 203	15 608

In Table 1, *min* and *max* give respectively, the minimum and maximum value of gravity, for the particular file and N designates the number of blocks in these files. CAN1P and CAN1R refer to $1° \times 1°$ files calculated for Canada : CAN1P was obtained simply by averaging the point values within each $1° \times 1°$ block, CAN1R is the result of averaging all of the available $15' \times 15'$ mean values within each $1° \times 1°$ block with unit weight (up to 16 blocks). This latter value may be more of a regional representation for the block than the average of all values in the block.

Computation

Early estimates of computing time for the CYBER 730 indicated that 100 CPU hours may be needed to compute the geoid at 1 000 points. For a few thousand points, the use of the CYBER was not feasible. In the meantime, the Cray 1-S supercomputer became available for use and all the required programs were transported to this computer. Further program developments with optimization were then carried out in this new environment. For final comparison, the program as used on the Cray was transported back to the CYBER and run for performance comparisons. The test computations indicated a 34-fold speed increase on the Cray.

The computations were always carried out in such a manner that, for each computation point the contribution of each of the three data-sets was also available separately. This allowed each effect to be seen separately when plotted as a partial contribution to the geoidal height. The computation points were selected first at $1°$ intervals along the meridian and at the same *distance* along the parallels. For a denser net of computing points, this *grid* was shifted in both directions. Additional points were inserted where better definition of the geoid was required. Finally about 1 000 points were added to trace out the geoid locally in greater detail. This resulted in a total of 6 398 computation points, from which the present geoid map was prepared. In addition to a colour APPLICON map, a contour map was also prepared, and shown in Figure 1. As mentioned earlier the geoid refers to the GRS1980. It reaches a local minimum of -47.3 m at $\varphi = 59.76°$ and $\lambda = 92.34°$W in Hudson Bay.

The total computation time on the Cray was 8.07 CPU hours, which corresponds to over 275 hours on the CYBER.

References

[1] Despotakis, V.K., 1986, *The Development of the June 1986 $1° \times 1°$ and the August 1986 $30' \times 30'$ Terrestrial Mean Free-Air Anomaly Data Bases*. Internal Report, Department of Geodetic Science and Surveying, The Ohio State University, Columbus, Ohio.

[2] The Geodesist's Handbook 1980, Bulletin Géodésique, v. 54, no. 3.

[3] Marsh, J. G. , Lerch, F.J., Putney, B.H., Christodoulidis, D.C., Felsentreger, T.L., Sanchez, B.V., Smith, D.E., Klosko, S.M., Martin, T.V., Pavlis, E.C., Robbins, S.M., Williamson, R.G., Colombo, O.L., Chandler, N.L., Rachlin, K.E., Patel, G.B., Bhati, S., and Chinn, D.S., 1987, *An Improved Model of the Earth's Gravitational Field : *GEM-T1** NASA Technical Memorandum 4019.

[4] Nagy, D., 1988, GEOID '88 : *A gravimetric geoid for Canada*. Open File Report (in press), Geophysics Division, Geological Survey of Canada.

[5] Stokes, G. G., 1849, *On the variation of gravity on the surface of the earth*. Transactions Cambridge Philosophical Society, v. 8.
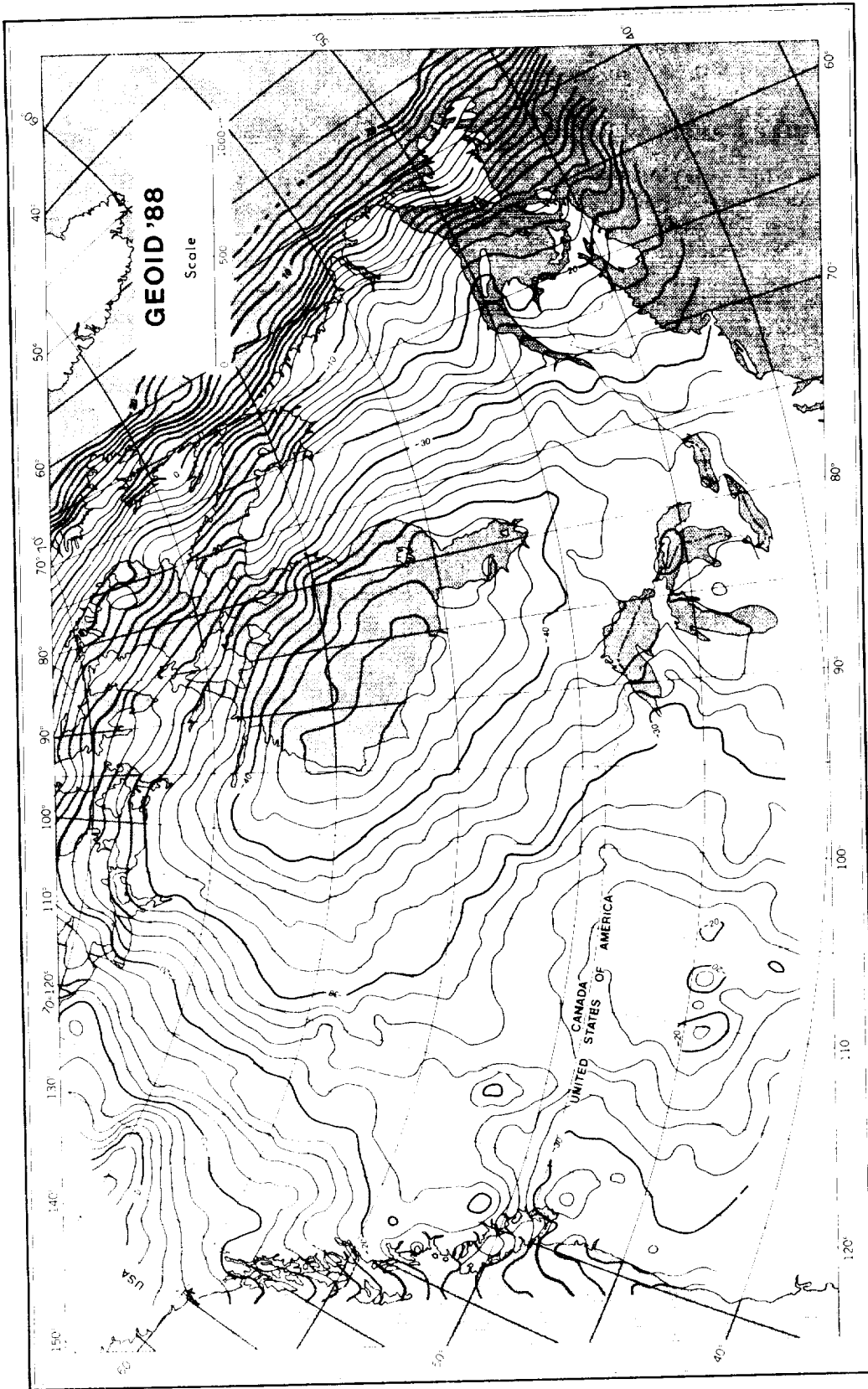
Figure 1 : Gravimetric geoid of Canada

Regional Quasigeoid Determination in Northern Germany And Comparison With GPS

Heiner Denker, Institut für Erdmessung (IFE), Universität Hannover, Federal Republic of Germany

1. Abstract and Introduction

For the northern part of the Federal Republic of Germany, new quasigeoid solutions have been computed by least squares collocation and FFT techniques using point and mean gravity data, a digital terrain model, and a global geopotential model. As severe accuracy limitations for precise regional quasigeoid determination come from global model uncertainties, different geopotential models have been investigated by combining them with gravimetric data and comparing the quasigeoid heights with GPS and leveling. Optimum results have been obtained by a global model tailored to gravity data in Europe. Collocation and FFT results based on this model agree well. The comparison with GPS and leveling yields r.m.s. discrepancies of ± 2 cm over approx. 400 km range.

2. Computation Method

Height anomalies have been determined for the northern part of the Federal Republic of Germany using least squares collocation and FFT techniques. The predicted height anomalies are obtained by

$$\zeta = \zeta_1 + \zeta_2 + \zeta_3 , \tag{1}$$

where ζ_1 is the influence of the spherical harmonic model, ζ_2 is the contribution from a residual terrain model (RTM), and ζ_3 is the contribution from terrestrial gravity field observations. The spherical harmonic model is used as a reference field and yields the major part of the quasigeoid, the terms ζ_2 and ζ_3 being typically less than $0.5 \ldots 1.0$ m.

After subtracting the effect of a global geopotential model and a residual terrain model from all observations, the contribution of terrestrial gravity field observations (ζ_3) has been computed by least squares collocation and integral formulas. The main drawback of collocation, being the solution of a normal equation system with as many unknowns as the number of observations, may be overcome to a certain extent with modern vector computers (see *Denker* and *Wenzel* 1987). On the other hand, the use of integral formulas evaluated by FFT with gridded data is also possible on a mini computer, and thus making this technique very attractive from the computational point of view. The spectral computation of the disturbing potential and its functionals by FFT is based on flat-earth approximations. Thus, Stokes' integral formula may be written as a two-dimensional convolution in the form

$$\zeta_3 = \frac{1}{2\pi\gamma} s * \Delta g' , \qquad s = (x^2 + y^2)^{-\frac{1}{2}} , \tag{2}$$

where $\Delta g'$ are the reduced gravity anomalies. The convolution of the kernel function s with the data $\Delta g'$ is most easily done in the frequency domain. Using the analytical transform of s, formula (4) can be written as

$$\zeta_3 = \frac{1}{2\pi\gamma} \mathbf{F}^{-1} \left\{ \frac{2\pi}{\omega} \widetilde{\Delta g}'(u, v) \right\} , \qquad \omega = \sqrt{u^2 + v^2} , \tag{3}$$

where $\mathbf{F}^{-1}$ denotes the inverse Fourier transform, (u, v) are the frequencies and $\widetilde{\Delta g}'$ is the Fourier transform of $\Delta g'$.

3. Data Collection and Evaluation

For the determination of the long wavelength part of the earth's gravity field, the geopotential models GPM2 complete to degree and order 200 (*Wenzel* 1985), OSU86F complete to degree and order 360 (*Rapp* and *Cruz* 1986), and IFE87E2 complete to degree and order 360 (*Bašić* 1988) have been considered. The third model IFE87E2 is based on GPM2 and has been tailored to available $12' \times 20'$ mean gravity anomalies in Europe (*Bašić* 1988). The computation procedure consists of a spherical harmonic analysis of the non-global distributed differences between start model and terrestrial data, and the obtained potential difference coefficients are then added to the original coefficients resulting in an improved geopotential model fitted to the regional gravity field data.
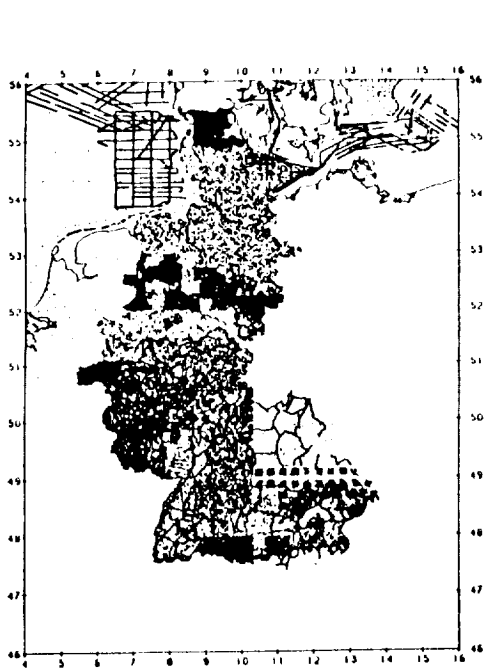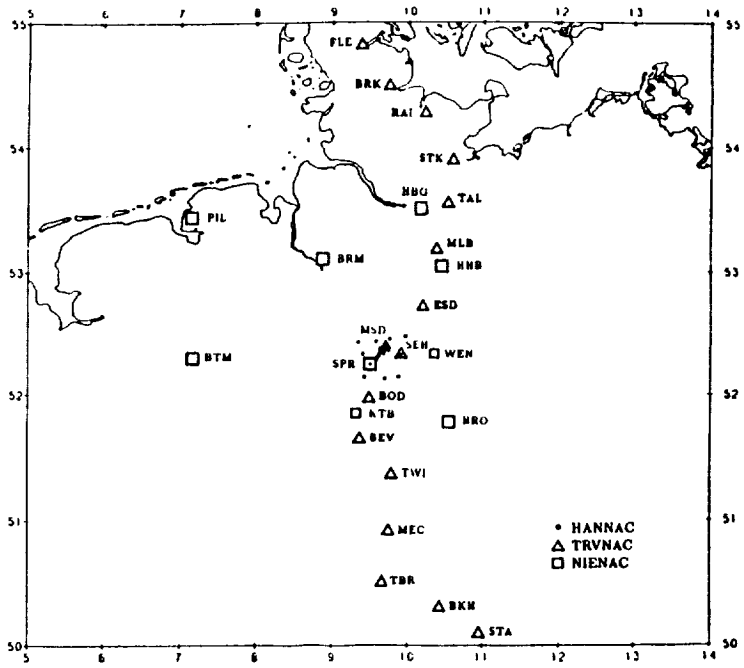
Figure 1: Distribution of Point Gravity Data

Figure 2: Distribution of GPS Stations

For the computation of terrain reductions, $30'' \times 50''$ mean elevations are available for the area of the Federal Republic of Germany.

Point gravity data have been extracted from the standard data base PFA, existing at IFE. Since the collected point values are located mainly in the Federal Republic of Germany (see fig. 1), additionally $6' \times 10'$ and $12' \times 20'$ mean gravity anomalies have been extracted from the IFE gravity data base for the evaluation of the outer zone.

All data sets have been checked carefully for gross errors by applying different procedures, for details see *Denker* and *Wenzel* (1987) and *Denker* (1988).

In addition, GPS results from three different campaigns (HANNAC, NIENAC, TRVNAC) observed with TI 4100 dual frequency receivers are available for northern Germany (see fig. 2). The internal error estimates for ellipsoidal height differences from GPS do not exceed 3 cm. The GPS coordinates are refering to the WGS84 reference system, which can be assumed to coincide with the gravimetric reference frame. The GPS stations have been connected to the national leveling network by spirit leveling to a nearby benchmark for the TRVNAC campaign and partly by the trigonometric method for the other campaigns.

4. Practical Results

In order to study the impact of different geopotential fields on gravimetric quasigeoid determinations, the three models GPM2, OSU86F and IFE87E2 have been tested by comparing the quasigeoid heights derived from GPS and leveling with values computed from these three models as well as from combination solutions with gravimetric and topographic data. For this task, the FFT method was used because of the high speed of this algorithm and the generally good agreement with corresponding collocation solutions.

For the FFT computations, the RTM-reduced gravity data were gridded in a 1.0×1.5 grid for the area $47°5 - 57°5$ N and $3° - 15°$ E using point data and $6' \times 10'$ mean values in areas with no point data available. The gravimetric solutions were performed in one step for the whole area of North Germany yielding a 576×480 grid for FFT. Due to periodicity effects of FFT, a cosine tapered window was used for the outer 10 grid points.

The topography was taken into account by a residual terrain model (RTM) reduction using a $6' \times 10'$ moving average filter for the construction of the reference topography, for details see *Denker* and *Wenzel* (1987).The maximum values of the obtained RTM-effects are approx. 30 mgal for gravity anomalies, $3''$ for vertical deflections resp. 8 cm for height anomalies.

Fig. 3 shows a comparison of quasigeoid heights derived from GPS and leveling for stations of the
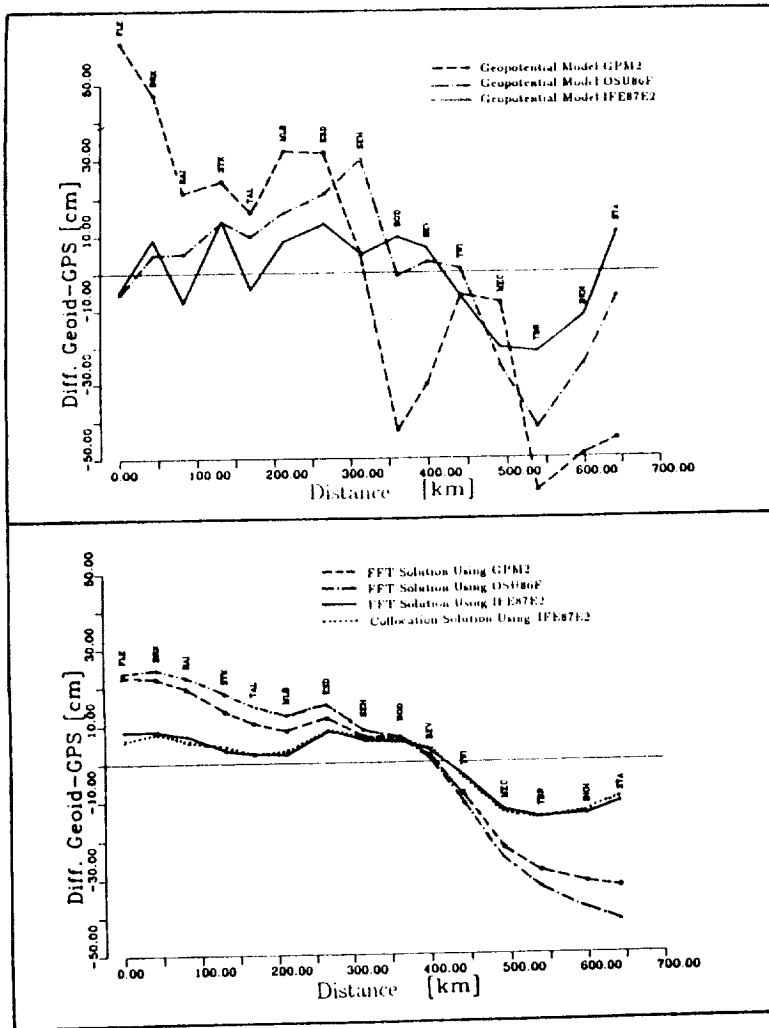
122

Figure 3: Comparison of GPS and Leveling With Quasigeoid Heights From Geopotential Models and From Gravimetric Combination Solutions for Stations of the GPS Traverse (TRVNAC)

Station		ζ	Differences (Bias Fit)	
No.	Name	(Coll.)	Coll.	FFT
1	FLE	40.827	0.063	0.085
2	BRK	40.428	0.082	0.086
3	RAI	40.236	0.058	0.073
4	STK	40.154	0.045	0.033
5	TAL	40.594	0.025	0.026
6	MLB	41.126	0.035	0.023
7	ESD	42.235	0.089	0.084
8	SEH	43.518	0.065	0.058
9	BOD	45.152	0.062	0.054
10	BEV	46.246	0.036	0.033
11	TWI	46.753	−0.043	−0.036
12	MEC	47.738	−0.136	−0.126
13	TBR	48.324	−0.149	−0.146
14	BKH	47.652	−0.134	−0.139
15	STA	47.182	−0.098	−0.109
R.M.S.			±0.084	±0.084
R.M.S.*			±0.020	±0.024
* Only Stations FLE–BEV				

Table 1: Comparison of Gravimetric Height Anomalies With GPS and Leveling for the TRVNAC Campaign (Units are m)

ORIGINAL PAGE IS
OF POOR QUALITY

Station		ζ	Differences (Bias Fit)	Differences (Bias And Tilt Fit)		
No.	Name	(Coll.)	Coll.	FFT	Coll.	FFT
1	SPR	44.228	−0.062	−0.052	−0.004	−0.001
2	WEN	43.323	−0.001	−0.010	0.074	0.054
3	BRO	46.031	−0.205	−0.156	−0.052	−0.023
4	HHB	41.414	0.046	0.038	0.033	0.021
5	BRM	41.202	0.103	0.098	0.028	0.032
6	HBG	40.729	0.036	0.036	−0.047	−0.041
7	PIL	40.971	0.157	0.138	−0.028	−0.021
8	BTM	44.224	0.059	0.043	0.027	0.022
9	KTB	45.767	−0.132	−0.134	−0.030	−0.043
R.M.S.			±0.108	±0.093	±0.040	±0.032

Table 3: Comparison of Gravimetric Height Anomalies With GPS and Leveling for the NIENAC Campaign (Units are m)

Station		ζ	Differences (Bias Fit)	
No.	Name	(Coll.)	Coll.	FFT
1	MSD	43.403	−0.003	−0.004
2	LIN	43.489	0.008	0.008
3	VEL	43.464	0.031	0.031
4	BEN	43.559	−0.006	−0.013
5	RON	43.657	−0.030	−0.042
6	MHL	43.589	−0.015	−0.018
7	LVA	43.444	0.002	0.005
8	GEH	43.833	−0.041	−0.044
9	SPR	44.228	0.014	0.028
10	ALT	43.384	−0.010	−0.023
11	MEY	43.281	0.026	0.031
12	LHG	43.135	0.007	0.014
13	SLG	42.992	0.031	0.039
14	BAN	43.824	−0.030	−0.031
15	SEH	43.518	0.018	0.018
16	HAS	44.633	−0.005	−0.002
17	WIT	44.386	0.007	0.005
18	SOR	44.214	−0.005	−0.002
R.M.S.			±0.020	±0.024

Table 2: Comparison of Gravimetric Height Anomalies With GPS and Leveling for the HANNAC Campaign (Units are m)

123

GPS traverse (TRVNAC) with values computed from three different geopotential models (upper part) as well as values computed by FFT on the basis of these models, gravity data and RTM-contributions (lower part). As expected, the solutions based on model IFE87E2 tailored to gravity data in Europe yields the best agreement with GPS and leveling. Using this model, the contribution of terrestrial gravity data takes a maximum value of about 50 cm. The other two models have larger long to medium wavelength errors, which are essentially presurved in the combination solutions. This problem might be overcome with a larger data collection area, but then the advantages of high-degree geopotential models are lost. However, the computation of tailored models in connection with a small cap size of local gravity field data will in many cases be less expensive than the use of existing geopotential models with a large cap size.

In addition, collocation solutions were computed using the tailored model IFE87E2. Due to the large amounts of data, the computations were blocked in $1° \times 2°$ areas using a larger data collection area (see *Denker* 1988). Altogether, 11 blocks were computed to provide coverage of northern Germany. As compared to the FFT method, the computation time necessary for all 11 collocation blocks is approx. two orders of magnitude larger. The covariance functions required for the computations were assumed the same for all blocks; the model covariance function selected on the basis of empirical data has a gravity anomaly variance of 100 mgal^2 and a correlation length of about 20 km. One unsolved problem in this context is to fit different partial solutions together. In practical tests it was found, that discrepancies between adjacent blocks are mainly dependent on the size of the data collection area, on the quality of the used geopotential model and on the degree variances contained in the covariance model for the low degrees. However, if the used covariance function contains long wavelength components, collocation performs an estimate of corresponding field structures for each block being one of the main reasons for the occuring discrepancies at the block boundaries. In order to keep the discrepancies between adjacent blocks below 1 cm, it was finally decided to assume the reference field to be errorless up to degree 72. Through this assumption, changes in the predicted height anomalies are of long wavelength nature resulting in biases up to 2 cm and tilts < 2 cm/100 km. Formal error estimates from collocation (without the assumption of an errorless reference field up to a certain degree) are in the order of 1 cm/50 km and 2 cm/100 km for height anomalies.

The FFT and the collocation solution have been evaluated by comparing the predicted height anomalies with GPS and leveling from different campaigns, the discrepancies found are listed in tables 1-3 (after subtraction of a common bias for each campaign). As can be seen, the collocation and the FFT results agree well within a few cm. For the TRVNAC campaign, both solutions show jumps of approx. 10 cm between stations BEV/TWI and TWI/MEC (see fig. 3). There are indications that these discrepancies are caused by the GPS data processing, but this remains to be clarified in the future. If only the northern part of the traverse with a length of approx. 400 km is considered, the r.m.s. discrepancy amounts to ±2.0 cm.

For the HANNAC campaign with maximum interstation distances of about 50 km, the r.m.s. discrepancies are approx. ±2.0 cm for the FFT and the collocation solution.

The third GPS data set available in North Germany is the NIENAC campaign with maximum interstation distances of 300 km. The r.m.s. difference is about ±10 cm, but a detailed analysis shows a slope about an axis with an azimuth of approx. 45°, which is probably due to the GPS solution as a similar behaviour is not visible for the GPS traverse (TRVNAC). After taking additional tilts in northern and eastern direction into account, the r.m.s. discrepancy reduces to about ±4 cm.

References

Bašić, T. (1988): Untersuchungen zur regionalen Geoidbestimmung mit "dm"-Genauigkeit. Dr.-Ing. Dissertation, University of Hannover, in preparation.

Denker, H. (1988): Hochauflösende regionale Schwerefeldbestimmung mit gravimetrischen und topographischen Daten. Dr.-Ing. Dissertation, University of Hannover, in preparation.

Denker, H., H.-G. Wenzel (1987): Local Geoid Determination and Comparison With GPS Results. Bulletin Géodésique 61, 349-366, 1987.

Rapp, R.H., J.Y. Cruz (1986): Spherical Harmonic Expansions of the Earth's Gravitational Potential to Degree 360 Using 30' Mean Anomalies. The Ohio State University, Department of Geodetic Science and Surveying, Rep. 376, Columbus/Ohio 1986.

Wenzel, H.-G. (1985): Hochauflösende Kugelfunktionsmodelle für das Gravitationspotential der Erde. Wissenschaftliche Arbeiten der Fachrichtung Vermessungswesen der Universität Hannover, Nr. 137, Hannover 1985.

Long Range Geoid Control
Through the European GPS Traverse
— Final Results —

W. Torge, T. Bašić, H. Denker, J. Doliff, H.-G. Wenzel

Institut für Erdmessung, Universität Hannnover, Nienburger Straße 6,
D-3000 Hannover 1, Federal Republic of Germany

Abstract

The European north-south GPS-traverse proposed by IAG SSG 3.88, should control and improve the European geoid. This traverse follows first order leveling lines, included in the United European Leveling Network. From May to August 1986 and in July 1987, the central and northern part of this traverse (approx. 3000 km) has been observed using up to four TI 4100 receivers, covering Austria, Federal Republic of Germany, Denmark, Sweden and Norway. Both traverse parts contain 71 stations with distances of about 50 km. In addition, 8 stations have been occupied for overlapping connections, and traverse links were established for connecting the fundamental stations Wettzell (VLBI and SLR) and Onsala (VLBI). Final results show a GPS observation precision of a few cm for loops of some 100 km circumference.

After transformation of the GPS results to geoid heights using the leveled heights, comparisons with different existing gravimetric geoid determinations including geopotential models have been performed. In addition, new geopotential models complete to degree and order 360 tailored to gravity data in Europe, and gravimetric geoid solutions using $6' \times 10'$ mean gravity anomalies have been investigated. The comparison with GPS and leveling yields r.m.s. discrepancies of $\pm 0.1 \ldots 0.2$ m over 1000 km traverse sections for the best solutions, but a strong slope is existing in Sweden and southern Norway in almost all solutions, which is probably caused by systematic errors in the available gravity data for Scandinavia. This is confirmed by a new geoid computation at the Danish Geodetic Institute (see *Forsberg* and *Solheim*, these proceed.), where the slope has disappeared. If this new solution is taken for the northern traverse section and our best solution for the central part, the r.m.s. discrepancy reduces to approx. ± 0.2 m over 3000 km. Thus, a $\pm 10^{-7}$ relative height accuracy seems to be achievable over long distances with the GPS/leveling and the gravimetric geoid calculation techniques, applied in this experiment.

Treatment of Geodetic Leveling in the Integrated Geodesy Approach

Dennis G. Milbert
Geodetic Research and Development Laboratory
National Ocean Service, NOAA, Rockville, MD 20852

Abstract and Introduction

Integrated geodesy is a method in which a wide variety of surveying measurements are modeled in terms of geometric positions and the earth's geopotential. Using heterogeneous data, both geometric and gravimetric quantities are simultaneously estimated by a least-squares procedure. Heretofore, geodetic leveling differences have been reduced into pseudo-observables using assumed values of gravity prior to their inclusion into integrated geodesy least-squares adjustments. This study compares the errors in estimates of geometric and gravimetric quantities obtained from integrated geodesy adjustments of geodetic leveling difference, potential differences and Helmert height differences.

Model

If one corrects for atmospheric and instrumental effects, then the lines of sight of a rotatable level describe a plane in space which is normal to the direction of the local gravity vector. This plane can be considered to pass through a point midway along a chord between the bases of the level rods. The level rods are aligned along their own local verticals. These local verticals need not be parallel or possess any special relationships to the local vertical at the level instrument. (In practice, the verticals will be nearly parallel). One may compute a directed distance between the base of a given level rod and the point of intersection of that level rod with the level instrument normal plane. The geodetic level difference is modeled as the difference between the directed distances at the two level rods (BD - AC in Figure 1). A detailed derivation of the geodetic level difference model can be found in Milbert [1988].
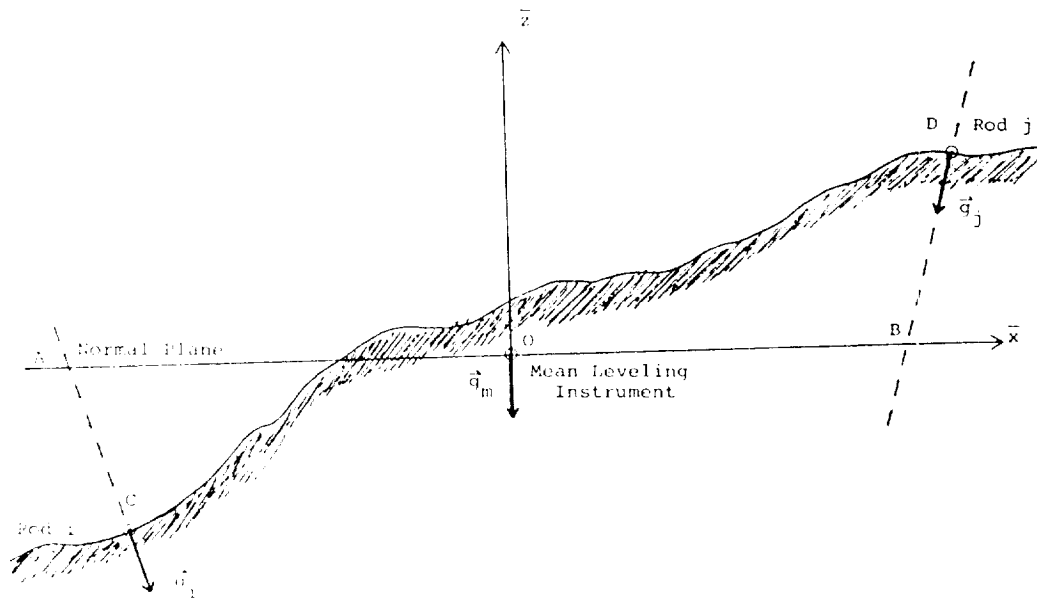

Figure 1. Side View of Level Rods and Mean Normal Plane Relationships.

Computational Procedure

To evaluate the geodetic level difference model, and to compare its behavior to that of potential differences and Helmert height differences, a simulation approach is chosen. An analytic model (a Molodensky mountain) provides prior values of geometric and gravimetric quantities, including gravity, GPS ellipsoidal heights, and level measurements. The geometric part of the model is a conical mountain, one kilometer (km) high, with a base of about 40 km radius, resting on a spherical earth of 6369.4 km. The gravimetric part of the model is composed of a single disturbing point mass imbedded 4 km beneath the spherical earth and the OSU86F geopotential. This combination provides a non-isotropic gravity field that is more realistic than those found in other analytic models. Through the analytic model, 400 geodetic level differences (corresponding to a 40 km level route from the peak of the mountain to the base), 144 gravity measurements arranged in a 1° x 1° grid, and 31 gravity measurements along the level route are obtained. With the exception of one benchmark at the peak of the mountain, the locations of the gravity measurements are not coincident with the benchmarks. In addition to the gravity measurements discussed above, derived data, which correspond to the pseudo-observables, are formed in a process consistent with that found in practice. Derived gravity values are predicted at benchmarks by collocation. Potential differences and Helmert height differences are then derived from the geodetic level differences and gravity interpolated from those values predicted at the benchmarks.

Results

As a baseline example, an integrated geodesy least-squares adjustment was computed using the 175 gravity measurements and the 40 derived potential differences. The ellipsoidal heights of the gravity stations were held fixed at the analytic model values. The ellipsoidal height of the benchmark at the peak of the mountain was fixed to eliminate a datum defect. The integrated geodesy adjustment estimates geometric position and the geopotential field and its derivatives. Figure 2 displays the error in the estimates of ellipsoidal height at the benchmarks using the model data near Denver, Colorado, potential difference pseudo-observables, and the OSU86F model in a "remove/restore" process. The errors are in the sense of estimate minus analytic model. Estimation error is induced by the disturbing point mass, which is not parameterized by the observation equations or the remove/restore process.

The integrated adjustments were repeated using either potential difference, ΔW, Helmert height difference, ΔH, or geodetic level difference data, Δn. In the case of the geodetic level differences, the measurements were fed directly into the adjustment, without any need for reduction in a pre-adjustment computation. The results of these adjustments are virtually identical to those of Figure 2. To illustrate the slight changes, Figure 3 displays differences formed when the adjustment errors of the geodetic level difference model are subtracted from the adjustment errors of the remaining models. Discrepancies due to choice of model are seen to be smaller than the measurement noise of leveling. The upper curve demonstrates that the geodetic level difference model is as effective as the potential difference model.
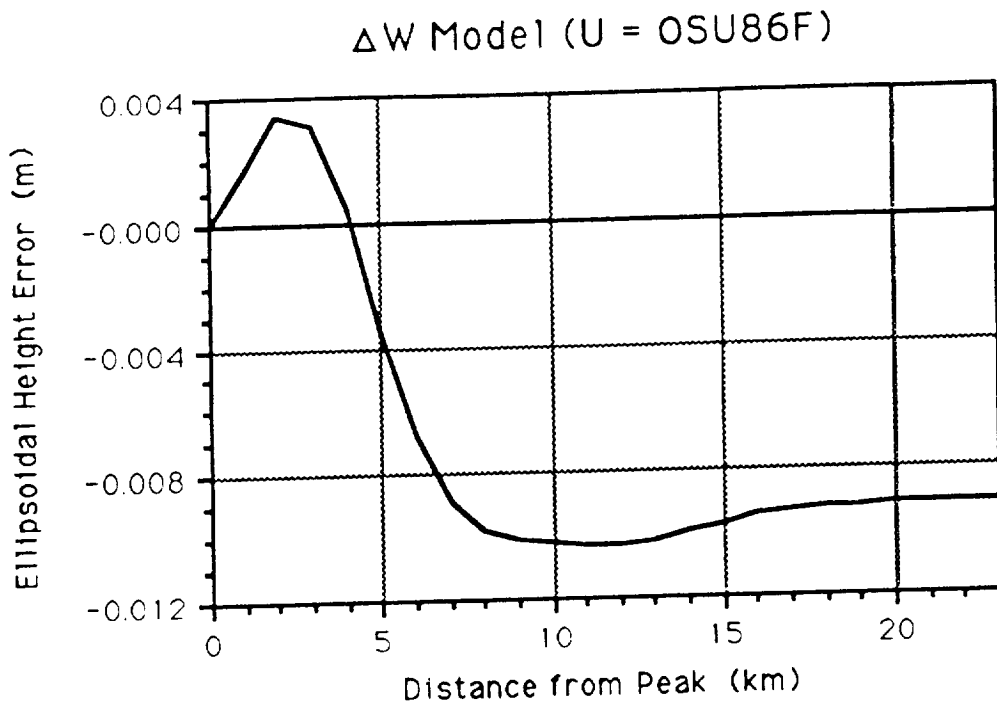
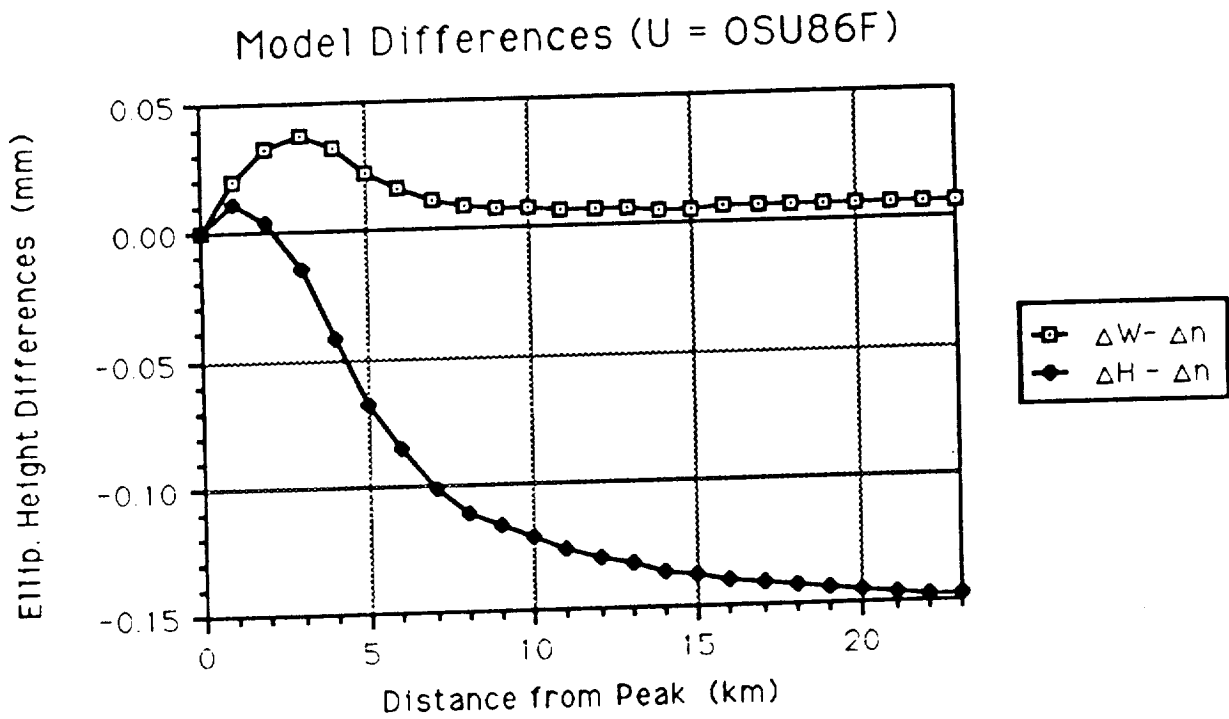Figure 2. Error in Ellipsoidal Height Estimates at Benchmarks, Potential Difference Model, ΔW.

Figure 3. Ellipsoidal Height Errors Compared Between Models
(ΔW model errors - Δn model errors)
(ΔH model errors - Δn model errors)

128

These results were seen to hold throughout a variety of scenarios. Integrated adjustments were computed using GRS80 in place of OSU86F for linearization of the models. The influence of ellipsoidal height difference data, such as obtained from GPS signals, was examined. The analytic model was varied with regard to choice of region and magnitude of the disturbing point mass. Tests were performed to observe the influence of the gravity grid data set. And, the effects of various computational approximations to the observation equations were explored. Greater detail on these tests can be found in Milbert [1988].

Covariance Models

Since a least-squares collocation method was selected to solve the integrated geodesy observation equations, it was necessary to develop a model for the covariances and cross-covariances of components of the disturbing potential. One component of the gravimetric part of the analytic model was a high degree spherical harmonic expansion, OSU86F, complete to degree and order 360. The associated covariance model is based on those potential degree variances. The other component of the gravimetric part of the analytic model was a disturbing point mass. However, the spectrum of the potential degree variances from a point mass generates covariance functions which do not lend themselves to evaluation by the closed forms of Tscherning and Rapp [1974]. A new family of covariance functions (one member of which contains the point mass spectrum) is defined. It is shown that the covariance and cross-covariance functions for a point mass can be expressed in closed formulas by means of incomplete elliptic integrals of the first and second kind. Highly efficient algorithms exist for the evaluation of the elliptic integral functions, allowing rapid computation of the point mass covariance functions.

Conclusions

It has been found possible to model geodetic level differences in an integrated geodesy approach. By means of this model, it is not necessary to reduce geodetic level differences into potential differences or Helmert height differences in a preliminary computation.

References

Milbert, D.G., 1988: Treatment of Geodetic Leveling in the Integrated Geodesy Approach. Report of the Department of Geodetic Science and Surveying, The Ohio State University, Columbus, Ohio.

Tscherning, C.C., and Rapp, R.H., 1974: Closed Covariance Expressions for Gravity Anomalies, Geoid Undulations, and Deflections of the Vertical Implied by Anomaly Degree Variance Models. Report of the Department of Geodetic Science, Nr. 208, The Ohio State University, Columbus, Ohio.

Determination of Mean Gravity Anomalies in the Taiwan Island

Ruey-Gang Chang

N90-20547

Department of Surveying Mapping Engineering, Chung Cheng Institute of
Technology, Ta-Shi, Tao-Yuan, Taiwan (33509), Republic of China

ABSTRACT

In the present paper the fitting and proper regression coefficients have been made of 117 10'x10' blocks with observed gravity data and corresponding elevation in the Taiwan Island. To compare five different predicted models, and the proper one for the mean gravity anomalies were determined. The predicted gravity anomalies of the non-observed gravity blocks were decided when the coefficients obtained through the model with the weighted mean method. It was suggested that the mean gravity anomalies of 10'x10' blocks should be made when comprehensive the observed and predicted data.

1. INTRODUCTION

The purposes of the paper is to understand the relationship of gravity anomaliy with the topography and the area, doing further research, comparing the good and bad points from the most common used mean computing models. Analysising which model is more suitable for Taiwan Island and meatime computing the accuracy of mean gravity anomaly. This paper is mainly stressed on Taiwan area, surrounded by the longitude from 120° E to 122° E, the latitude from 21.5° N to 25.5° N.

2. COMPUTATION MODELS

There are five formulas of the mean gravity anomaly will be discussed [Uotila, 1967a&b ; Kassim, 1980; Sünkel, 1983]:

$$(1) \quad \overline{\Delta g} = a + b\overline{h} , \tag{1}$$

$$(2) \quad \overline{\Delta g} = 1/n \ \Sigma \Delta g_i , \tag{2}$$

$$(3) \quad \overline{\Delta g} = 1/n \ \Sigma \ [\Delta g_i - b \ (h_i - \overline{h})] , \tag{3}$$

$$(4) \quad \overline{\Delta g} = \Sigma \ (\Delta g_i \ /s_i^{3.5})/\Sigma(1/s_i^{3.5}) , \tag{4}$$

$$(5) \quad \overline{\Delta g} = \{\Sigma \ [(\Delta g_i - bh_i)/s_i^{3.5}]/\Sigma(1/s_i^{3.5})\} + b\overline{h} , \tag{5}$$

which $\overline{\Delta g}$ is the mean gravity anomaly of square block; Δg_i is the ith gravity anomaly in square block; $\overline{h}$ is the mean height of square block; h_i is the ith height in square block; a, b are the regression coefficients; s_i is the distance between number the ith point and the centre of the square block; 3.5 is the weighted exponent.

In these five computing models, the needed parameters as Δg_i, h_i, $\overline{h}$, s_i, a, b. And Δg_i, h_i are obtained from the observation values, s_i is the distance betwen the observation point and the centre point in block, $\overline{h}$ is obtained from digital terrain model. Therefore, the regression coefficients a, b are obtained from the first order of the stochastic functions of the gravity anomaly and height. In this paper, they come from two main resources: (1) using more than two points data in every individual block to calculate its

a, b value in block, (2) using all observed gravity materials, setting different groups according to the height of topography then calculate the a, b value in three different topography in Taiwan area (Table 1).

Table 1. The three groups of regression coefficient value of heights

HEIGHT(m)	a (mGal)	b(mGal/m)
h ≤ 100	- 1.8585	0.1091
100 < h ≤1000	13.7330	0.0281
h > 1000	-63.8362	0.1195

Therefore, as long as using mean height in each block, the selected a, b coefficient can be determined. a, b are calculated with data from all over Taiwan, so the stability is very strong. When the height is between 100 metre and 1,000 metre, the value of b is regarding 0.0281 to 0.119, somewhate different in theory but it is due to the effect of topography and area.

3. THE RESULT AND ANALYSIS

Having 117 blocks in observed gravity data, it makes difficult to show them all. We picked 12 block results at random to discuss as a base line. We select different topography - plain, hill, mountain besides chosing each block in different location from the east to west and the south to the north. In keeping with comparing and analysing the effect from five different computing models, the results of above selected 12 blocks is showed in Table 2, and among the five numbered gravity are corresponding with the sequence of computing data.

As following, we point out and explain some results, we compared and analysed: (1) Clearly, the computed result from five models may be devided into three categories: $\overline{\Delta g}_1$ as a independent, $\overline{\Delta g}_2$, $\overline{\Delta g}_4$ as category, $\overline{\Delta g}_3$, $\overline{\Delta g}_5$ is another one. $\overline{\Delta g}_2$, $\overline{\Delta g}_4$ as deficit result of height and gravity anomaly which the relationship between them has not been considered. And $\overline{\Delta g}_3$, $\overline{\Delta g}_5$ as a group result from the effect of height was considered. Then why the result is differentin $\overline{\Delta g}_1$ with the effect of height? The reason in $\overline{\Delta g}_1 =$ a+b$\overline{h}$ within, we set a as fixed value. In the contrary, by using a value for section area to compute $\overline{\Delta g}_1$, the result is unified in mathematical meaning and $\overline{\Delta g}_3$. (2) The different between the group ($\overline{\Delta g}_2$, $\overline{\Delta g}_4$) and $\overline{\Delta g}_3$ $\overline{\Delta g}_5$) is explained by location of height. The difference in these two depend on if there is affecting existance from height to gravity anomaly. Thus inter-relation may very well became greater by increasing the height. In the contrast, the deficit is greater comparing mountain with hill, the hill somewhate larger than the plain. Therefore the relationship between height and gravity anomaly have to be stressed on particularty the mountains areas. Providing standardizesd data in mean gravity anomaly in any topography, we must disregard height in predicted model. Then the group of $\overline{\Delta g}_3$ and $\overline{\Delta g}_4$ is abandoned. (3) Finally, in group $\overline{\Delta g}_3$ and $\overline{\Delta g}_5$, the reason, the deficit existed is if the locations of points can represent the mean position as a whole in any blocks. $\overline{\Delta g}_3$ is computed from any point position, $\overline{\Delta g}_5$ is using the position of the centre point in the block to compute mean value. The closer the points to the centre are, the closer result of $\overline{\Delta g}_3$ and $\overline{\Delta g}_5$ are. Again if the points in block are situated uniformly, the $\overline{\Delta g}_3$ value will be the most accurate. In $\overline{\Delta g}_5$, it is no way to prove if the mean gravity in centre position can represent mean value according to the result obtained from Table 2, there are a small discrepancy and $\overline{\Delta g}_3$ computing model is

simpler and the more idealistic positions are, the more reasonable result are. Therefore, the present paper decided to use $\overline{\Delta g}_3$ as computing method for mean gravity anomaly model.

Table 2. The results of five computation models

NOS. OF BLOCK \ MEAN GRAVITY ANOMALY	$\overline{\Delta g}1$	$\overline{\Delta g}2$	$\overline{\Delta g}3$	$\overline{\Delta g}4$	$\overline{\Delta g}5$
179	-1.86	-31.30	-58.66	-31.3	-58.66
183	6.87	-25.36	-17.81	-24.67	-16.76
63	3.60	-14.39	- 9.79	-14.03	-9.43
260	3.60	2.69	- 4.55	13.04	4.77
165	36.78	50.64	69.65	38.83	58.17
185	24.97	-37.84	-29.51	-41.60	-34.08
53	29.19	65.98	77.14	66.6	77.23
250	28.49	9.76	20.25	17.89	25.56
177	95.10	39.10	166.73	34.68	159.05
162	121.39	-17.88	122.08	-17.88	122.08
113	68.81	19.47	96.11	18.12	95.41
237	82.55	38.59	122.84	36.02	117.97

4. THE ACCURACY OF THE MEAN GRAVITY ANOMALY

Because of being unable to observe the exact mean gravity anomaly in each block, we have no way to discuss the experimental accuracy of the block, we can use the law of propagation of errors to estimate the accuracy of the block. The present paper decided to use the mean gravity anomaly computing model, that

$$\overline{\Delta g} = 1/n \; \Sigma \; [\Delta g_i - b \; (h_i - \overline{h})] \; ,$$

we can predict mean gravity anomaly in block in Taiwan Island with observed data (Table 3).

Table 3 Categorized by topography to determine the
accuracy of the mean anomaly in the block

TOPOGRAPHY \ ACCURACY	PLAIN	HILL	MOUNTAIN
$\sigma \overline{\Delta g}$ (mGal)	4.8	3.5	16.1

5. CONCLUSION

Being the 2/3 of Taiwan Island is mountain, situated on earthquake zone, the gravity anomaly is greatly different by year. At present, Taiwan Island we have just completed the levelling stations to promote gravity observations. Along with doing dense in mountain area, we strongly believer we can obtain more accurate mean gravity anomaly in this area.

REFERENCES

Kassim, F.A., An evaluation of three techniques for the prediction of gravity anomalies in Canada, Technical Report No.73, Department of Surveying Engineering, University of New Brunswick, Fredericton, N.B., 1980.

Sünkel, H. and G. Kraiger, The prediction of free-air anomalies, Proceeding of the IAG Symposium, IUGG, 1, 531, 1983.

Uotial, U.A., Analysis of correlation between free-air anomalies and elevations, Report No.94, Department of Geodetic Science, Ohio State University, Columbus, Ohio, 1967a.

Uotila, U.A., Computation of mean anomalies of 1 x 1 degree blocks, Report No.95, Department of Geodetic Science, Ohio State University, Columbus, Ohio, 1967b.

VERY ACCURATE UPWARD CONTINUATION TO LOW HEIGHTS IN A TEST OF NON-NEWTONIAN THEORY

Anestis J. Romaides and Christopher Jekeli
Air Force Geophysics Laboratory, Hanscom AFB, MA, 01731

Abstract

Recently, gravity measurements were made on a tall, very stable televsion transmitting tower in order to detect a non-Newtonian gravitational force. This experiment required the upward continuation of gravity from the Earth's surface to points as high as only 600 m above ground. The upward continuation was based on a set of gravity anomalies in the vicinity of the tower whose data distribution exhibits essential circular symmetry and appropriate radial attenuation. Two methods were applied to perform the upward continuation - least-squares solution of a local harmonic expansion and least-squares collocation. Both methods yield comparable results, and have estimated accuracies on the order of 50 μGal or better (1 μGal = 10^{-8} m/s^2). This order of accuracy is commensurate with the tower gravity measurements (which have an estimated accuracy of 20 μGal), and enabled a definitive detection of non-Newtonian gravity. As expected, such precise upward continuations require very dense data near the tower. Less expected was the requirement of data (though sparse) up to 220 km away from the tower (in the case that only an ellipsoidal reference gravity is applied).

1. INTRODUCTION

The upward continuation may be summarized as follows. A set of surface gravity anomalies, circularly symmetric about the tower, serves as the set of boundary values. The upward continuation is based on Newtonian theory either through a local harmonic series expansion of the potential or through the use of least-squares collocation. At altitude, the (upward continued) GRS67 normal gravity and attraction of the atmospheric layer are added to the upward continued gravity anomaly. The result is the total gravity as would be observed in a strictly Newtonian world. A comparison with the gravity directly observed using a gravimeter offers a test of the underlying theory.

2. THE MATHEMATICS OF UPWARD CONTINUATION

If V denotes the earth's gravitational potential, then under Newtonian potential theory, V satisfies Laplace's differential equation in free space:

$$\nabla^2 V = 0. \tag{1}$$

One solution to Laplace's equation (1) is a Fourier-Bessel series expansion in cylindrical coordinates, which is appropriate for a local representation of the potential. Thus, since in the planar approximation the gravity anomaly is also a harmonic function (it satisfies Laplace's equation in free space), it may be expressed as the following series (Morse and Feshbach, 1953, pp. 1259-1262):

$$\Delta g(\rho,\theta,z) = \sum_{n=-\infty}^{\infty} \int_0^\infty C_n(k)\, J_n(k\rho)\, e^{-kz-in\theta} dk, \tag{2}$$

where ρ is radial distance in the horizontal plane, θ is azimuth, and z is altitude. J_n is the Bessel function of the first kind and n-th order, k is

the wavenumber in the radial direction, and the C_n are coefficient functions to be determined from gravity anomaly data. Since the final evaluation of (2), once the C_n are known, is along the vertical, $\rho=0$, this problem is simplified by defining an azimuthal average:

$$\overline{\Delta g}(\rho,z) = \frac{1}{2\pi} \int_0^{2\pi} \Delta g(\rho,\theta,z) \, d\theta = \int_0^\infty C_0(k) \, J_0(k\rho) \, e^{-kz} \, dk \ . \tag{3}$$

This average coincides with the unaveraged Δg along the vertical:

$$\overline{\Delta g}(0,z) = \Delta g(0,\theta,z) = \int_0^\infty C_0(k) \, e^{-kz} \, dk \ . \tag{4}$$

The second equality in (4) follows by noting that at $\rho=0$ all J_n's in (2) are zero except J_0 which is one. It remains, therefore, to determine only the function C_0 from azimuthally averaged gravity anomaly data. One can determine at best a finite set of values of C_0 from a discrete and finite data set. The integral (3), therefore, is truncated to some finite limit and discretized. The truncation is optimized if the discretization is in the form of a Fourier-Bessel expansion. After making the appropriate substitutions in replacing the integral (3) with the discrete summation (see Romaides et al., 1988), the least-squares solution is obtained by the following:

$$\sum_{p=1}^{P} \left[f_p - \sum_{m=1}^{M} A_m \, J_0(\xi_p \kappa_m) \, \exp\left[\frac{-\kappa_m}{R} (z_p - z_0)\right] \right]^2 \longrightarrow \min., \tag{5}$$

where P is the number of points, M is the number of zeros, κ_m are the zeros of J_0, $f_p = \Delta g(\xi_p R, \theta_p, z_p) - \overline{\Delta g}(R,z)$, $\xi_p = \rho/R$, R is the maximum radius of surface data, z_0, z_p are the elevations of the tower base and surface points, and A_m are the solution coefficients.

The Fourier-Bessel upward continuation then proceeds in three steps. An initial expansion is done using 23 zeros and approximately 1800 anomalies out to 220 km from the tower. This expansion allows the resolution of half-wavelengths down to about 5 km. A second expansion is then done on only the residuals inside of 5 km (from the tower) allowing resolution of half-wavelengths down to about 100 m. And finally a third expansion is done on the second set of residuals inside of 50 m from the tower resolving half-wavelengths down to about 20 m. Table 1 shows the results of the three steps, and Figure 1 is a contour map of the final set of residuals.

The other upward continuation method used is least-squares collocation which is an optimal estimation method based on the validity of Laplace's equation. All important in LSC estimation is a good representation of the covariance function of Earth's anomalous gravity field. The covariance model employed for the tower experiment consists of the actual degree variances of the Rapp-1981 field up to degree 30 (1300 km wavelengths) plus a sum of 9 reciprocal distance models (see Jekeli, 1984) each covering a specific band of wavelengths shorter than 1300 km. These models are fitted to a sequence of periodograms based on the gravity anomaly data. Figure 2 shows these periodograms along with the power spectral density of the final model. The model psd at wavelengths shorter than 300 m represents a rough

extrapolation. Figure 3 shows a plot of the collocation weights that are applied to ~270 data points; note the increase in the last two sets of weights which could be an artifact of oversampling.

3. CONCLUSION

The upward continuation of the surface gravity anomalies was done using two independent computation methods. The two methods are in excellent agreement (see Table 2) with both results clearly showing a departure from the inverse-square law. The conclusion is that there is a dominantly attractive non-Newtonian component to gravity. Previous experiments had indicated a repulsive component to gravity. This inconsistency can be overcome by postulating the existence of two additional forces, one attractive and one repulsive. Our data do not contain adequate resolution to distinguish between the one force (scalar) and two force (scalar-vector) models but are consistent with both. Figures 4 and 5 show plots of the two models along with our data. The error bars used are those of the first method.

REFERENCES

Jekeli, C., "Analysis of airborne gravity gradiometer survey accuracy," Manuscripta Geodaetica, vol.9, no.4, pp.323-379, 1984.

Morse, P.M., and H. Feshbach, Methods of Theoretical Physics, McGraw-Hill Book Company, Inc., New York, 1953.

Romaides, A.J., C. Jekeli, A.R. Lazarewicz, D.H. Eckhardt, and R.W. Sands, "A Detection of Non-Newtonian Gravity," Journal Of Geophysical Research, accepted for publication, 1988.

Table 1.

Table 2.

FOURIER-BESSEL UPWARD CONTINUATION

OBSERVED MINUS PREDICTED (μGal)

ELEVATION	STEP 1	STEP 2	STEP 3
0.69	.422	.266	.009
7.58	.256	.116	.002
9.38	.233	.098	.008
23.07	.094	-.013	-.013
45.93	-.054	-.121	-.098
68.76	-.159	-.196	-.176
93.92	-.187	-.199	-.184
192.17	-.341	-.306	-.301
283.58	-.455	-.414	-.412
379.54	-.534	-.499	-.498
473.24	-.567	-.541	-.540
562.27	-.566	-.548	-.547

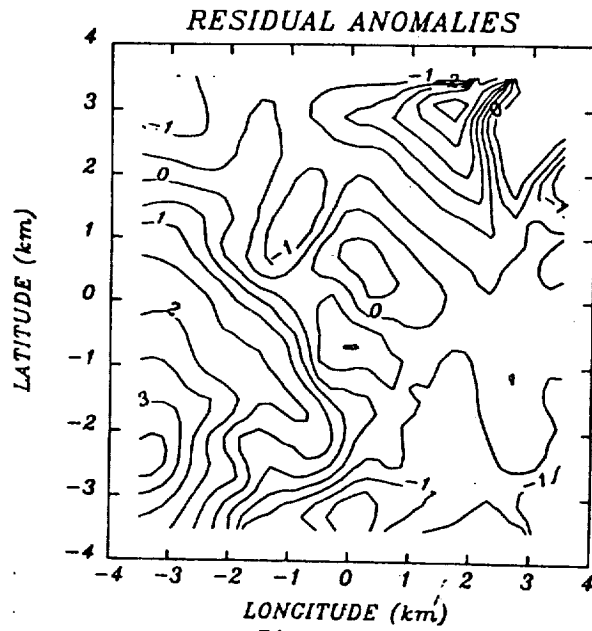| ELEVATION	METH 1	ERROR	METH 2	ERROR
0.69	9	59	35	9
7.58	2	59	-2	13
9.38	8	59	0	16
23.07	-13	58	-27	36
45.93	-98	57	-100	61
68.76	-176	56	-171	80
93.92	-184	54	-179	95
192.17	-301	48	-304	117
283.58	-412	44	-413	120
379.54	-498	38	-493	120
473.24	-540	37	-528	121
562.27	-547	36	-526	121

RESIDUAL ANOMALIES

Figure 1.

Figure 2.

Figure 3.

SCALAR MODEL

Figure 4.

SCALAR-VECTOR MODEL FIT
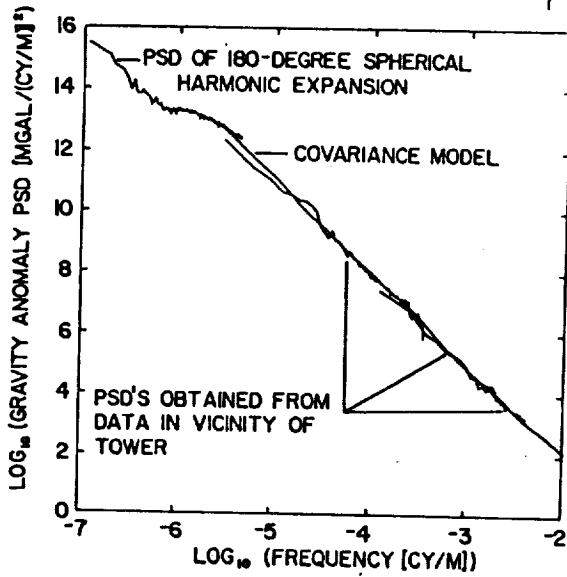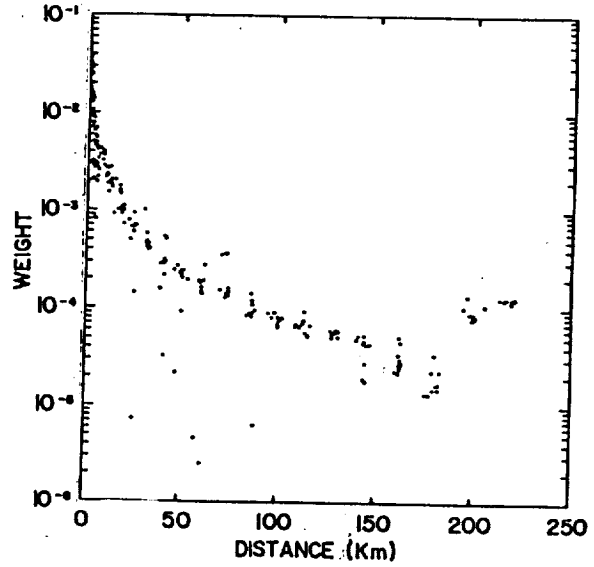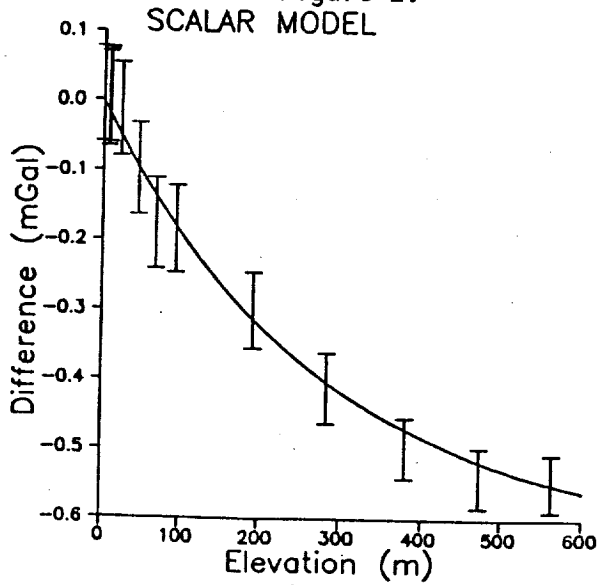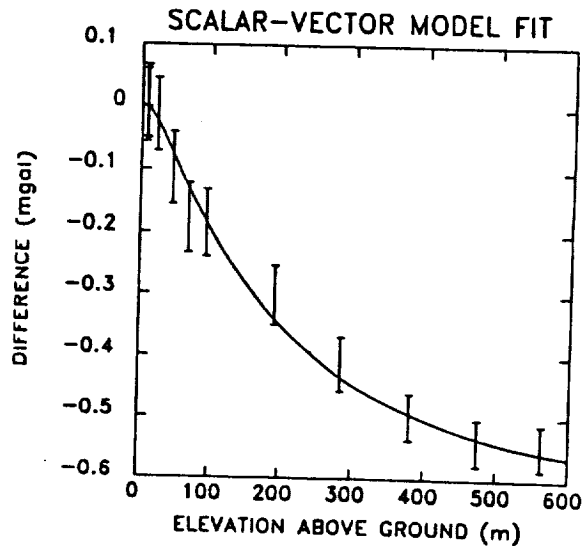

Figure 5.

Global Gravity Field Applications and Requirements in Geophysics and Oceanography

Moderators: Brad Hager

Victor Zlotnicki

✓

Geodynamics and Temporal Variations in the Gravity Field

D. C. McAdoo and C. A. Wagner

National Geodetic Survey, Charting and Geodetic Services
NOS, NOAA, Rockville, Maryland 20852

N90-20549

ABSTRACT

Just as the Earth's surface deforms tectonically, so too does the gravity field evolve with time. Now that precise geodesy is yielding observations of these deformations it is important that concomitant, temporal changes in the gravity field be monitored. Although these temporal changes are minute they are observable: changes in the J2 component of the gravity field have been inferred from satellite (LAGEOS) tracking data; changes in other components of the gravity field would likely be detected by Geopotential Research Mission (GRM), a proposed but unapproved NASA gravity field mission. Satellite gradiometers have also been proposed for high-precision gravity field mapping. Using simple models of geodynamic processes such as viscous postglacial rebound of the solid Earth, great subduction zone earthquakes and seasonal glacial mass fluctuations, we predict temporal changes in gravity gradients at spacecraft altitudes. We find that these proposed gravity gradient satellite missions should have sensitivities equal to or better than 10^{-4} E in order to reliably detect these changes. We also find that satellite altimetry yields little promise of useful detection of time variations in gravity.

1. INTRODUCTION

Because the solid Earth is dynamic, its internal density structure evolves with time. This evolution in density structure produces temporal changes in the gravity field. And, although these changes in gravity are quite small ($dg/g < 10^{-6}$, local) over time spans of years or decades, they could tell us much about dynamics of the Earth's interior. Observations of these time variations will be particularly useful when combined with precise observations of surface deformation.

This paper examines the prospects for detecting these time variations from satellites. Changes in the second zonal harmonic, J2, of the geopotential have been detected [Yoder et al., 1983; Rubincam, 1984] using 6 years of LAGEOS tracking data. These changes have been attributed to ongoing viscous rebound of the Earth's crust and mantle [Wu and Peltier, 1983]. Other high altitude satellites such as Starlette, LAGEOS, II, III, and Stella will help refine estimates of temporal changes in the long-wavelength ($\lambda > 4000$ km) components of the gravity field. A proposed system of two, low-altitude satellites, the GRM [Taylor et al., 1983] would, were it flown successfully, have very likely detected other temporal changes in the gravity field such as those in the nonzonal and intermediate-wavelength components [Wagner and McAdoo, 1986, hereafter WM]. Gradiometer missions which have been proposed [Paik, 1981; Balmino, 1986] for mapping the gravity field could make useful observations of these time variations if these missions are sufficiently high in sensitivity and low in altitude.

2. GEOPHYSICAL RATIONALE

Gravity fields derived from satellite data possess an ever increasing accuracy at longer spatial wavelengths. The importance of this accuracy to geophysicists is not obvious. For most geophysical applications, high spatial resolution (inherently lacking in satellite gravity fields) is more important than accuracy at lower resolution. However, one application does require this very high accuracy: the geodynamical study of active regional deformation in the crust and mantle. Mass motion in these deformation zones produces slow, subtle changes in the gravity field. If we can detect these changes, we can place significant constraints on models of deformation. Figure 1 shows a simple example of how observations of changes in gravity might discriminate between two possible modes of compressional, crustal deformation: swelling and folding, modes which might well be indistinguishable in observations of surface strain.
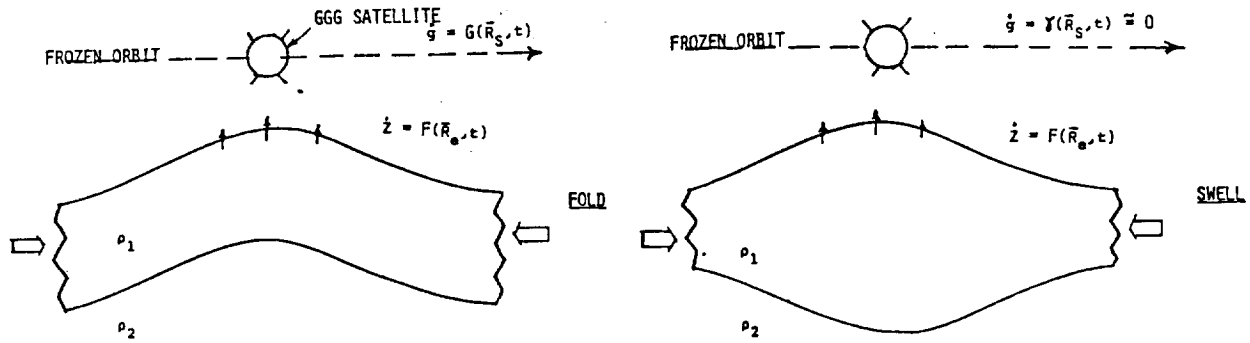
Figure 1. Folding and swelling: a similar vertical motion signal but folding produces greater changes in gravity.

3a. DIP-SLIP EARTHQUAKES

The most energetic earthquakes are the great, thrust faulting events which occur at subduction zones. These, among all earthquakes, should produce the largest changes in the gravity field at satellite elevations. Assume that a gradiometer satellite is operating in a repeating orbit when such an earthquake occurs, and that this orbit lies directly above the epicenter and is orthogonal to the strike of the subduction zone. Characteristics of the great dip-slip event are taken to be identical to those of the 1964 Prince William Sound, Alaska event ($M_o = 8 \times 10^{29}$ dyn cm). Resultant coseismic changes in the gravity gradient field at the spacecraft (Fig. 2) as well as geoid changes are computed using an extension [WM] of a model due to Walsh and Rice, [1979]. This model represents the earthquake as dislocations in a uniform elastic half-space and predicts that the surface free-air gravity anomalies produced by dip-slip events are proportional to the coseismic surface height changes [WM]. We have upward-continued and transformed predicted surface gravity to obtain the horizontal (xz) component of the gradient (z is vertical and x is along-track). The corresponding coseismic geoid change has an amplitude of <2 cm which would be difficult to detect with a satellite altimeter due to omnipresent oceanographic 'noise'. Note also that gradient signals at a spacecraft altitude of 160 km are about 4 $\times 10^{-3}$ Eotvos units or E in amplitude. The 1964 Alaska earthquake was, however, extraordinarily large, perhaps the second largest in seismological history. A more typical great earthquake is the 1985 Michoacan, Mexico event [$M_o = 0.2 \times 10^{29}$ dyn cm; Eissler et al., 1986] which was also a thrusting event but was of smaller spatial extent. Predicted changes in horizontal gravity gradients aloft are shown in Figure 3. Note diminished signal at 160 km as well as the more pronounced attenuation at 230 km altitude. Detection of this event requires that a gradiometer with a sensitivity at least 10^{-4} E be flown at the lowest possible altitude.

— Sea | Land —
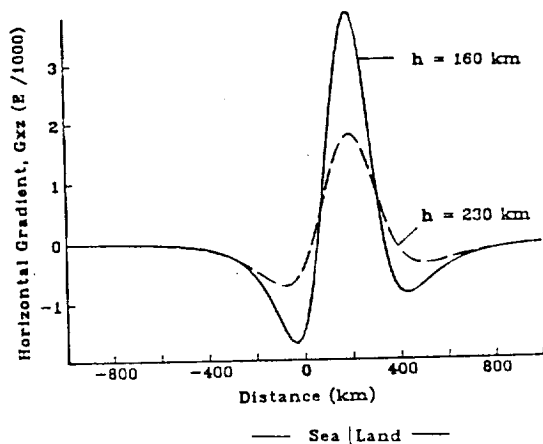
Figure 2. 1964 Prince William Sound, Alaska earthquake. Change in xz component of gravity gradient. Satellite elevation is h.
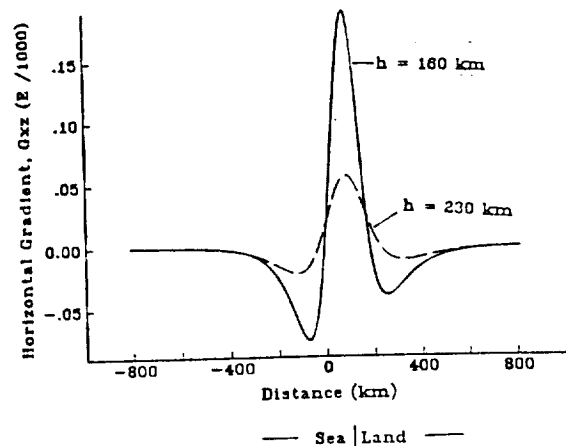

— Sea | Land —

Figure 3. Predicted change in xz component of gravity gradient for 1985 Michoacan, Mexico earthquake.

3b. POSTGLACIAL REBOUND

The Earth's mantle and crust continues to rebound today in response to the last global deglaciation which began 18000 years ago and largely ceased 6000 years ago. Detailed models [Wu and Peltier, 1983] of this process have been developed and extended [Yoder et al., 1983; Rubincam, 1984] to compute concomitant dynamic changes in the gravity field. For this study, we use a simpler model of [WM], which takes the Earth to be a uniform, Maxwell viscoelastic sphere and the ice masses (Laurentide, Fennoscandian and Antarctica) to be circular, spherical caps. This simple model predicts vertical velocities of the solid Earth's surface (Fig. 4) which agree rather well with both observations and predictions of more complex models. Using Hotine (1969) we compute, from geopotential changes, the change in the XZ gradient component (Figure 5: Z is polar and X is equatorial) which will accrue in one year's time at an elevation of 230 km. Note that the amplitude of this change is about 10^{-5} E. So, to detect the long wavelength gravitational effects of postglacial rebound with a satellite gradiometer, one must have an instrument (assumed lifetime of one year) with a sensitivity of 10^{-5} E. Satellite gradiometry (measuring second derivatives of potential) is better suited to detecting shorter wavelength signals.
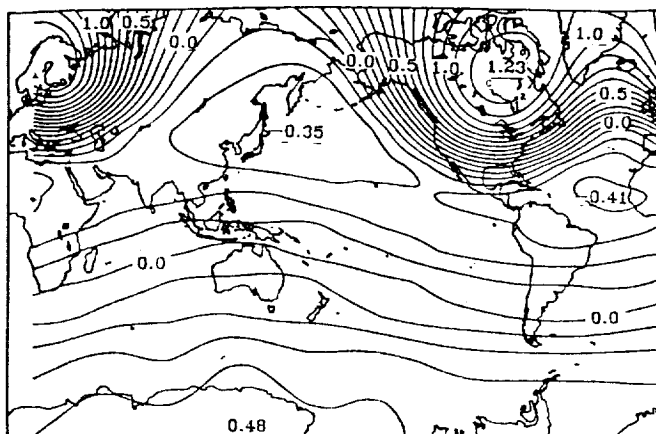

Figure 4. Present-day vertical velocity (cm/yr) of solid Earth's surface from simplified model of postglacial rebound. [WM]
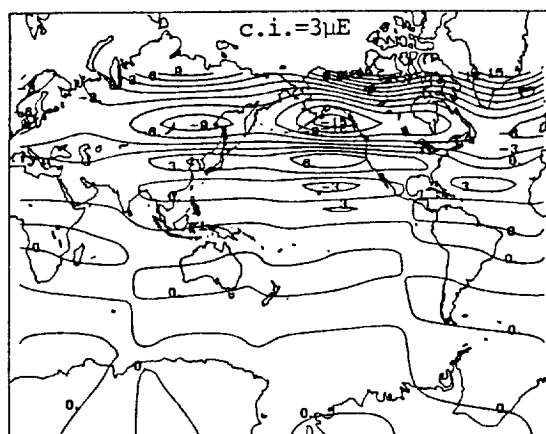
Figure 5. Predicted annual change (μE) in xz component of gravity gradient due to postglacial rebound.

3c. SEASONAL GLACIAL MASS FLUX

Secular and season glacial mass flux is large enough to produce a potentially detectable temporal variation in the gravity field. Meier [1984] suggests that the secular component of mass ablation from smaller glaciers (i.e., Greenland and Antarctica excluded) is the dominant contributor to the nonsteric rise in global sea level. He also estimates season mass flux for each of 25 smaller glacier systems. By far, the largest among these estimates is the 225 km^3 (water equivalent) amplitude annual flux from the Gulf of Alaska Coastal Mountains. This flux occurs as annual accumulation and ablation over 88,400 km^2 with an areal mean amplitude of 2.54 m. The seasonal drop in the geoid (2 cm) produced by this winter-to-summer ablation is estimated (Fig. 6a) by assuming a source body which is a rectangular prism (100 x 884 km x 5.1 m) of density -1.0 x 10^3 kg/m^3. We searched the GEOSAT altimeter data from the Gulf of Alaska for such a geoid change. By averaging in space (over a swath of several groundtracks) and time (over five 17-day repeat cycles), we obtained an ascending and a descending sea surface profile to represent the Gulf in both the summer and winter of 1987. We subtracted the winter results from the summer to estimate seasonal change in the sea surface topography. We found this change (14cm) too large to be geoidal. More likely, it is a steric sea level change. This demonstrates the obstacle which oceanographic variability presents to detection of time variations in gravity from satellite altimeters.
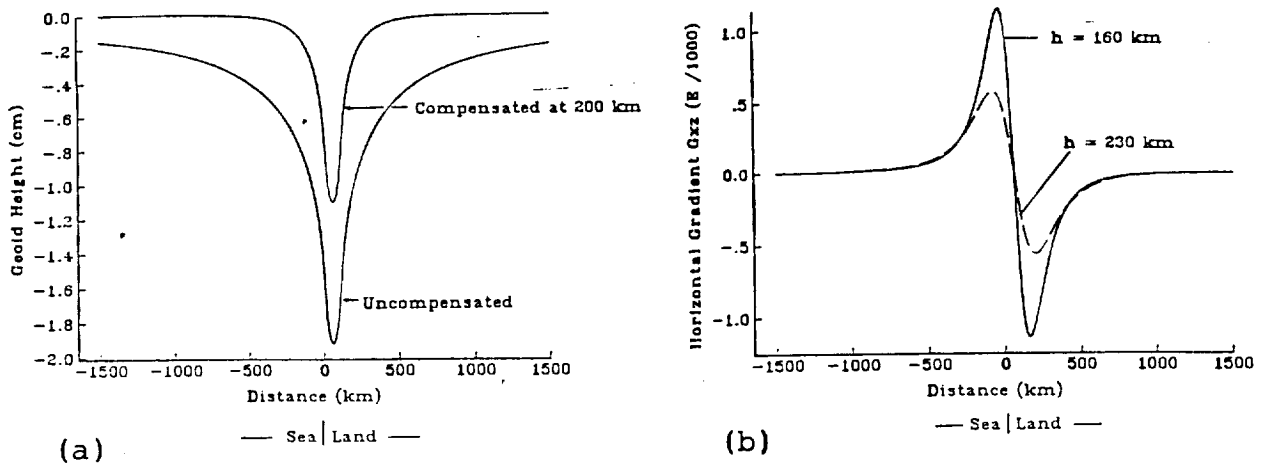
Figure 6. (a) Predicted geoid change (summer minus winter) due to seasonal mass ablation from southern Alaska glaciers. (b) Associated change in xz component of gravity gradient at elevation, h.

We also estimate (Fig. 6b) the change in the horizontal gravity gradients (xz) at satellite elevation for this seasonal glacial mass flux along coastal Alaska. At 160 km elevation, this signal has an amplitude of 10^{-3} E. A gradiometer with a sensitivity, again, of about 10^{-4} E is needed to reliably detect it.

REFERENCES

Balmino, G.; 1986, in *Space Geodesy and Geodynamics*, ed. by A. Anderson and A. Cazenave, p. 19, Academic Press, London.

Eissler, H., L. Astiz and H. Kanamori; 1986, *Geophys. Res. Lett., 13*, 569.

Hotine, M., 1969, *Mathematical Geodesy*, ESSA Monoograph 2, (NOAA/NGS, Rockville MD).

Meier, M.F.; 1984, *Science, 226*, 1418.

Paik, H.J.; 1981, *J. Astronaut. Sci., 29*, 1.

Rubincam, D.P.; 1984, *J. Geophys. Res., 89*, 1077.

Taylor, P.T., T. Keating, W.D. Kahn, R.A. Langel, D.E. Smith and C.C. Schnetzler, 1983, *EOS Trans. AGU*, 64, 09.

Wagner, C.A. and D.C. McAdoo; 1986, *J. Geophys. Res., 91*, 8373.

Walsh, J.B. and J.R. Rice; 1979, *J. Geophys. Res., 84*, 165.

Wu, P. and W.R. Peltier, 1983, *Geophys. J. R. Astron. Soc., 74*, 377.

Yoder, C.F., J.G. Williams, J.O. Dickey, B.E. Schutz, R.J. Eanes and B.D. Tapley, 1983, *Nature, 307*, 757.

A Model of the General Ocean Circulation Determined From a Joint Solution for the Earth's Gravity Field

R. S. Nerem, B. D. Tapley, C. K. Shum, and D. N. Yuan

Center for Space Research, The University of Texas at Austin

Abstract

If the geoid and the satellite position are known accurately, satellite altimetry can be used to determine the geostrophic velocity of the surface ocean currents. The purpose of this investigation is to simultaneously estimate the sea surface topography, ζ, the model for the gravity field, and the satellite orbit. Satellite tracking data from fourteen satellites were used; along with Seasat and Geosat altimeter data as well as surface gravity data for the solution. The estimated model of ζ compares well at long wavelengths with the hydrographic model of ζ. Covariance studies show that the geoid is separable from ζ up to degree 9, at which point geoid error becomes comparable to the signal of ζ.

1. Introduction

The determination of the general ocean circulation is one of the more important applications future satellite altimeter missions will provide. If the height of the ocean surface relative to the geoid can be measured, the absolute geostrophic surface current velocity at a given location can be inferred. The Seasat and Geosat altimeter missions measured the height of the ocean to a precision suitable for this purpose [*Tapley et al.*, 1982; *McConathy and Kilgus*, 1987]. Errors in the gravity field have limited previous determinations of ζ for two reasons: 1. ζ is measured with respect to the geoid, an equipotential surface defined by the gravity field model, and 2. gravity field errors are the primary limitation in the accuracy of the satellite orbit computation.

The radar altimeter carried by Earth orbiting satellites measures the range between the radar antenna and the instantaneous ocean surface. If the geocentric position of the satellite is known, the altimeter measurement can be differenced from the computed satellite height to yield the ocean surface height at the sub-satellite point. If there were no forces acting except the Earth's gravity and centrifugal force, the ocean surface would coincide with an equipotential surface referred to as the geoid, N. However, a number of effects cause the height of the ocean surface to deviate from the geoid height. Among these, ocean currents cause deviations with maximum amplitudes of about one meter. If an accurate estimate of N is available, the measured height of the ocean surface (corrected for tides and other effects [*Tapley et al.*, 1982]) and the geoid height may be differenced to provide an estimate of ζ.

Previous maps of ζ with wavelengths comparable to a degree and order 6 spherical harmonic model (6000 km) have been determined using Seasat altimeter data [*Tai and Wunsch*, 1984; *Engelis*, 1986]. Each of these approaches adopted a mean sea surface computed using Seasat altimeter data which was then differenced with a low degree and order geoid to give an estimate of the long wavelength components of ζ. The error in the gravity field model has been a limiting factor in the accuracy achieved in these investigations.

The results described here were derived as an adjunct to a concentrated effort to determine an improved gravity field model for the Topex/Poseidon altimeter mission [*Tapley et al.*, 1987]. The use of altimeter data in a gravity field solution, without correcting for ζ, can allow the oceanographic signal due to ζ to be aliased into the gravity field. The potential for simultaneously improving the geoid and ζ using satellite altimetry, surface gravity observations, and hydrography has been discussed by *Wunsch and Gaposchkin* [1980]. Since the influence of the gravity field on the geoid and the orbit, and the effect of ζ, are both present in the altimeter measurement, a more rigorous treatment of the problem would involve estimating the parameters which define both models simultaneously. This investigation demonstrates a joint solution for ζ, the gravity field, and the satellite orbit using satellite altimeter and tracking data.

2. Methods

Seasat and Geosat tracking data and altimeter data along with tracking data from twelve additional satellites and surface gravity data were processed in a simultaneous solution using a modified least squares estimator [*Tapley et al.*, 1987]. The estimated parameters included a set of spherical harmonic geopotential coefficients, complete to degree and order 50 with selected higher order terms, the spherical harmonic coefficients of ζ, complete to degree and order 15, and ocean tide parameters. Solar radiation pressure, atmospheric drag, and doppler tracking station coordinates were adjusted as individual satellite parameters. Altimeter biases and scale

factors for the significant wave height correction were estimated for Seasat and Geosat also. In addition to Seasat and Geosat altimeter data, the different types of satellite tracking data included laser range data, doppler data, optical data, and altimeter crossover data.

The stationary ocean surface is composed of the sum of N and ζ. The Earth's gravitational potential can be expressed in spherical harmonic form as:

$$U = \frac{\mu}{r}\left[1 + \sum_{l=2}^{L_{max}} \sum_{m=0}^{l} \left(\frac{r_e}{r}\right)^l \overline{P}_{lm}(\sin\phi)\left[\overline{C}_{lm}\cos m\lambda + \overline{S}_{lm}\sin m\lambda\right]\right] \quad (1)$$

where $\overline{C}_{lm}$, $\overline{S}_{lm}$ are the normalized spherical harmonic coefficients of degree l and order m, μ is the product of the gravitational constant and the total mass of the earth, r_e is the mean equatorial radius of the earth, r, ϕ, λ are the radial distance, geocentric latitude and longitude measured from the zero meridian, $\overline{P}_{lm}(\sin\phi)$ is the normalized associated Legendre function ($m \neq 0$) or the normalized Legendre polynomial of degree l ($m=0$), and L_{max} is the truncation degree of the geopotential. The position vector (x,y,z) of the sub-satellite point, which defines the geoid height, is computed by iteratively solving [Shum, 1983]:

$$W(x,y,z) = W_0 \quad \text{and} \quad \nabla W / |\nabla W| = \hat{u}_h \quad (2)$$

where $W(x,y,z) = U + T$, the total potential at the sub-satellite point, T is the rotational potential, W_0 is value of the total potential corresponding to mean sea level, and $\hat{u}_h$ is a unit vector normal to the geoid and passing through the satellite. Thus the set of constant parameters, $\overline{C}_{lm}$ and $\overline{S}_{lm}$, in Equation (1) are common to both the satellite dynamics and the geoid definition (2). A spherical harmonic model was employed to represent the height of ζ as:

$$\zeta = \sum_{l=1}^{l_{max}} \sum_{m=0}^{l} \left[C'_{lm} \cos m\lambda + S'_{lm} \sin m\lambda\right] \overline{P}_{lm}(\sin\phi) \quad (3)$$

where C'_{lm}, S'_{lm} are the surface spherical harmonic coefficients of the model for ζ. In this investigation, ζ is constrained to be zero over land areas and in polar regions ($|\phi| > 70°$). While the altimeter data with the land constraints do not form an equally spaced data set, the estimate for the coefficients retains the general characteristics of a fully orthogonal parameter set.

Portions of the Seasat and Geosat altimeter data sets were selected to correspond to the time periods when the best ground tracking data was available. Using the Preliminary Topex Gravity Field (PTGF2) [Tapley et al., 1987], reference orbits were computed using tracking data and altimeter crossover data. In all, 30 days of Seasat altimeter data (7/28-8/15, 9/15-9/27, 1978) and 54 days of Geosat altimeter data (11/17/86-12/4/86, 12/21/86-1/24/87) were processed. The altimeter data were edited including the removal of data if the water depth was less than 2000 m (to remove data with large tidal uncertainties) or if the data was over an ocean trench or seamount. The data were corrected for the unmodeled short wavelength features of the geoid (> degree 50) and compressed to form altimeter measurements 10 seconds apart.

There was no a priori variance on the coefficients of ζ. The a priori variance of the geopotential coefficients, v_l^2, were computed using Kaula's rule [Kaula, 1966] which can be stated as $v_l^2 = \alpha \, 10^{-10} \, l^{-4}$, where α is a scale factor equal to 0.04.

3. RESULTS

To evaluate the satellite altimeter solution for ζ, a spherical harmonic model of ζ was constructed from hydrographic data. The Levitus ocean surface referenced to 2250 dbars is adopted for this purpose [Levitus, 1982]. Grid points on land and in the polar regions ($|\phi| > 70°$) were set to zero and a degree and order 15 spherical harmonic model was fit to the data using a minimum variance estimator. Using the estimated values for the spherical harmonic coefficients, ζ can be computed as a function of latitude and longitude using Equation (3). Figure 1 depicts maps of ζ computed from both the altimeter and Levitus derived spherical harmonic coefficients complete to degree and order 6. The major gyres of the ocean circulation are depicted in both solutions. Up to degree and order 6, the altimeter and hydrographic models of ζ compare well. The agreement between the hydrographic and altimetric results is better than in previous altimeter solutions for ζ, suggesting a significant improvement has been achieved by simultaneously solving for the gravity field, the satellite orbit, and ζ. Further details of the solution procedure and the results are given by Tapley et al., [1988].

The improvement in the geoid solution may be evaluated by computing new reference orbits (using the estimated models) and analyzing the residuals from the compressed altimeter data. It

was found that the altimeter residuals improved from 225 cm (for a gravity field without altimeter data) to 30 cm, indicating the geoid model has been substantially improved.

Contour Interval = 0.10 Meters   Longitude   Minimum = -1.00, Maximum = 0.92

Figure 1a. The estimated model of ζ to degree and order 6

Contour Interval = 0.10 Meters   Longitude   Minimum = -1.00, Maximum = 0.84

Figure 1b. The Levitus model of ζ to degree and order 6

4. COVARIANCE ANALYSIS

One benefit of simultaneously estimating both the geopotential coefficients and the coefficients of ζ is that the resulting covariance matrix will describe not only the individual errors in N and ζ, but also the correlation of these errors. Considerable effort was expended to determine the relative weights of the data and the scaling of the covariance matrix.

By examining the degree variance of the ζ and the degree error variance of N (Table 1) it is seen that beyond degree 9, geoid error is larger than the signal of ζ. The covariance matrix for the coefficients of ζ and the geopotential can also be used to compute the standard deviation of the error in N and ζ. The error in N is largest over the land areas (where there is no altimeter data) and in equatorial regions. For terms up to degree 6, the geoid height is accurate to about 8 cm (Table 1). The error in ζ mimics the geoid error, the largest error occurs near the equator and increases with degree. The magnitude of the error in ζ is about 10 cm for terms up to degree 6 (Table 1). In addition to their individual errors, the correlation coefficient for the error in N and ζ can be analyzed to determine if the two quantities are separable. Figure 2 shows the geographical variation of the correlation coefficient for terms in the covariance matrix up to degree 6 in both N and ζ. This figure verifies that the solution for N and ζ are separable, at this degree, since the correlation coefficients are less than 0.6 globally.

Table 1. The degree variance of ζ and the degree error variance of N and ζ

Degree	1	2	3	4	5	6	7	8	9	10	11	12	13	14	15
Signal of ζ (cm)	10	20	11	13	14	17	11	10	12	12	16	12	14	11	7
Error in N (cm)	<1	1	2	4	4	6	8	10	11	14	13	13	16	14	16
Error in ζ (cm)	5	3	4	4	5	5	7	8	9	9	11	11	11	9	9

Contour Interval = 0.05
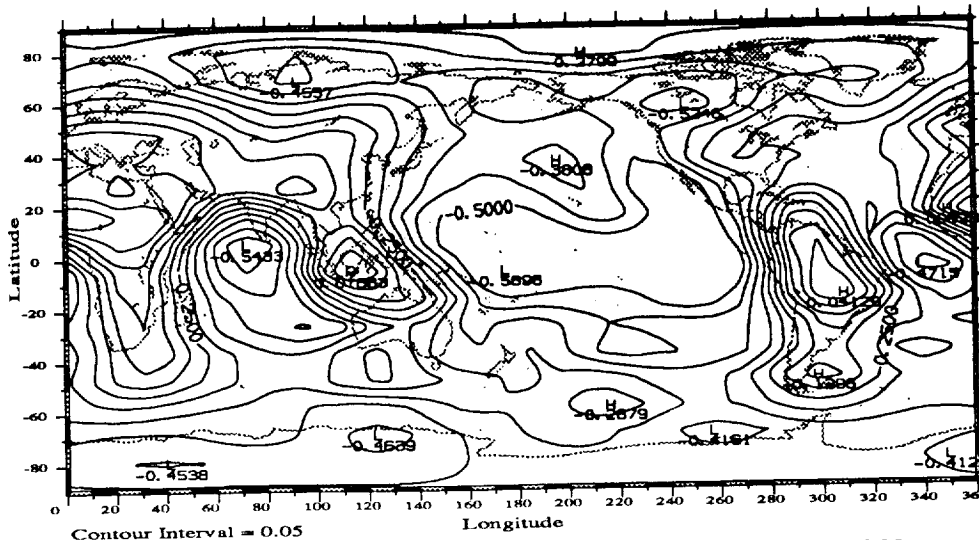
Figure 2. The correlation coefficient of the errors in ζ and N

5. CONCLUSIONS

It has been shown that a global estimate of ζ can be obtained from a joint solution for ζ and the gravity field using multiple satellite tracking data and altimeter data. The simultaneous solution for the ζ, the gravity field, the satellite orbit, and other geophysical parameters provides a substantially improved estimate for the gravity field and the long-wavelength signal of the general ocean circulation. This estimate of ζ compares favorably at long wavelengths with hydrographic determinations of ζ. The accuracy of the solution decreases as shorter wavelength features are examined, primarily due to the influence of geoid error.

REFERENCES

Engelis, T., Global Circulation from Seasat Altimeter Data, *Mar. Geod.*, 9(1), 45-69, 1986.
Kaula, W. M., *Theory of Satellite Geodesy*, 124 pp., Blaisdell, Waltham, Mass., 1966.
Levitus, S., Climatological atlas of the world ocean, NOAA Prof. Pap. 13, 1982.
McConathy, D. R., and C. C. Kilgus, The Navy Geosat Mission:An Overview, *Johns Hopkins APL Technical Digest*, 8(2), 1987.
Shum, C.-K., Altimeter Methods in Satellite Geodesy, Center for Space Research Report, CSR-83-2, The University of Texas at Austin, 1983.
Tai, C.-K. and C. Wunsch, An estimate of global absolute dynamic topography, *J. Phys. Oceanogr.*, 14, 457-463, 1984.
Tapley, B. D., G. H. Born, and M. E. Parke, The SEASAT Altimeter Data and its Accuracy Assessment, *J. Geophy. Res.*, 87(C5), 3179-3188, 1982.
Tapley, B. D., B. E. Schutz, C. K. Shum, J. C. Ries, and D. N. Yuan, An Improved Model for the Earth's Gravity Field, Intern. Assoc. of Geodesy Symposia, 125-143, 1987.
Tapley, B. D., R. S. Nerem, C. K. Shum, J. C. Ries, and D. N. Yuan, Determination of the General Ocean Circulation From a Joint Gravity Field Solution, *Geophys. Res. Lett.*, 15(10), 1109-1112, Sept., 1988.
Wunsch, C. and E. M. Gaposchkin, On using satellite altimetry to determine the general circulation of the ocean with application to geoid improvement, *Rev. Geophys. Space Phys.*, 18, 725-745, 1980.

Geographically Correlated Orbit Error

G. W. ROSBOROUGH

Department of Aerospace Engineering Sciences, University of Colorado, Boulder

ABSTRACT

The dominant error source in estimating the orbital position of a satellite from ground based tracking data is the modeling of the Earth's gravity field. The resulting orbit error due to gravity field model errors are predominantly long wavelength in nature. This results in an orbit error signature that is strongly correlated over distances on the size of ocean basins. *Anderle and Hoskin* [1977] have shown that the orbit error along a given ground track also is correlated to some degree with the orbit error along adjacent ground tracks. This cross track correlation is verified here and is found to be significant out to nearly 1000 kilometers in the case of TOPEX/POSEIDON when using the GEM-T1 gravity model. Finally, it is has been determined that even the orbit error at points where ascending and descending ground traces cross is somewhat correlated. The implication of these various correlations is that the orbit error due to gravity error is geographically correlated. Such correlations have direct implications when using altimetry to recover oceanographic signals.

1. INTRODUCTION

In order to fully exploit the scientific value of satellite altimetry measurements it is necessary to have accurate independent knowledge of the orbital position of the satellite. To date, it has not been possible to determine the position of altimetric satellites to a level of accuracy commensurate with the altimeter measurement accuracy. Thus the determinations of sea surface height above some reference surface are primarily corrupted by the errors in the estimate of the satellite altitude. In turn, these errors in the satellite altitude are primarily caused by errors in the modeling of the Earth's gravity field. Thus, the error spectrum of the sea surface heights is driven by the error spectrum of the satellite orbit altitude errors. This spectrum can be evaluated under some limiting assumptions and if the error spectrum of the Earth's gravity model is known. Evaluation of the spectrum will aid in determining to what extent the sea surface height data can be used in the detection of oceanographic signals.

This paper will principally address the geographic characteristics of the orbit error spectrum. That is, how large is the error in any given geographic region and how much is the orbit error in any one location correlated with the orbit error at another location. This question was originally addressed by *Anderle and Hoskin* [1977] who found a large correlation of the error along the direction of satellite motion and a much smaller though significant correlation of the error for adjacent ground traces. Their results were obtained through a simulation of the SEASAT orbit error based on the difference between two contemporary gravity models. The approach used here is analytic in nature and will be applied to the proposed TOPEX/POSEIDON orbit. Additionally, the gravity model error will be specified by the gravity error covariance of the recent GEM-T1 model [*Marsh, et. al.*, 1988].

2. ANALYTICAL DEVELOPMENT

The objective is to obtain the variance and covariance of sea surface height errors (derived from satellite altimetry) as a function of geographic location. In this development it will be assumed that these errors are solely a result of satellite altitude error due to gravity model error. Thus, the variance and covariance of the sea surface height errors will be equivalently represented by the variance and covariance of the orbit altitude errors. Also, it is assumed that the satellite geodetic altitude error can be accurately approximated by the satellite radial orbit error.

To obtain the variance and covariance of the radial orbit error due to gravity model error requires a relationship between the radial error and the error in the gravity model parameters. Such a relationship can be obtained through application of Kaula's solution [*Kaula*, 1966] which gives the orbit element perturbations based on a spherical harmonic development of the gravity field. The general result for the corresponding radial orbit perturbation is given in *Rosborough and Tapley* [1987]. This result, which gives the radial orbit error as a function of time, also can be expressed as a function of the satellites geographic location if the orbit is assumed to be nearly circular (as in the case of altimetry satellites) [*Rosborough*, 1986; *Engelis*, 1987]. The functional form of this geographic representation of the radial orbit error, δr, due to gravity model error is,

$$\delta r = \sum_{l=2}^{\infty} \sum_{m=0}^{l} [\Phi_{lm}(\phi)(\delta C_{lm} \cos m\lambda + \delta S_{lm} \sin m\lambda) \pm \Phi_{lm}^*(\phi)(\delta C_{lm} \sin m\lambda + \delta S_{lm} \cos m\lambda)]$$

where δC_{lm} and δS_{lm} are the errors in the gravity coefficients of degree l and order m, and Φ_{lm} and Φ_{lm}^* are functions of the satellites body-fixed latitude, ϕ, and mean orbital elements, and λ is the satellites body-fixed longitude. The choice in signs is determined by the satellites directional motion. If the satellite is on an ascending track then the sign is positive, if the satellite is on a descending track then the sign is negative.

This relationship shows the radial orbit error to be stationary along the ascending and descending tracks. That is, the orbit error repeats exactly along any given ground track. This is not the case for actual orbits which have been determined from ground based tracking. To emulate the real case requires this equation to be augmented with additional terms that account for the effect of errors in the initial conditions [*Colombo*, 1984]. These errors will differ for each determination of the initial conditions depending on the distribution of the tracking data. More importantly the resulting radial error due to initial condition error will in general not be stationary in the geographic frame. This effect will certainly augment the results of the next section which are based on the above equation alone. Future studies will attempt to introduce the initial condition error effect.

Given the above linear relationship between the gravity coefficient errors and the radial orbit error it is possible to determine the radial error variance and covariance if the gravity error covariance is known. In this context, the variance of the radial orbit error is the uncertainty in the radial component at any given geographic location, and the covariance is the correlation between the radial error at two different locations. Such variances and covariances have been evaluated using the GEM-T1 gravity error covariance and the mean orbital elements of TOPEX/POSEIDON. These results are given in the following section.

3. RESULTS

The standard deviation of the radial orbit error for TOPEX/POSEIDON due solely to the errors in the GEM-T1 gravity model are given in Figures 1 and 2. These figures show the standard deviation of the error along the ascending and descending tracks respectively. Again it should be emphasized that these results only account for the gravity error. In an actual orbit determination problem the resulting error will differ depending on the accuracy and distribution of tracking data and how much of the gravity induced orbit error can be absorbed through an adjustment of the initial conditions. Nonetheless, these figures illustrate how gravity error, in an ideal case (no initial condition error), is mapped into the radial component of the orbit. There is an obvious strong along track correlation of the error (which will be directly evaluated) and an obvious geographic correlation of the error.

The geographic correlation appears to be a consequence of the non-global distribution of tracking data that was used to construct the GEM-T1 model. Since GEM-T1 was based solely on satellite tracking data this non-global distribution is inevitable. Models which include surface
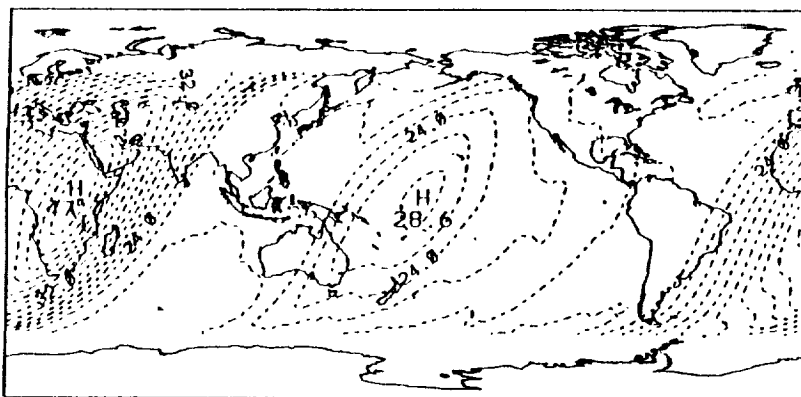
Figure 1: Standard deviation of the TOPEX/POSEIDON radial orbit error along the ascending ground tracks, using the GEM-T1 gravity error covariance. The contour interval is 2 cm.
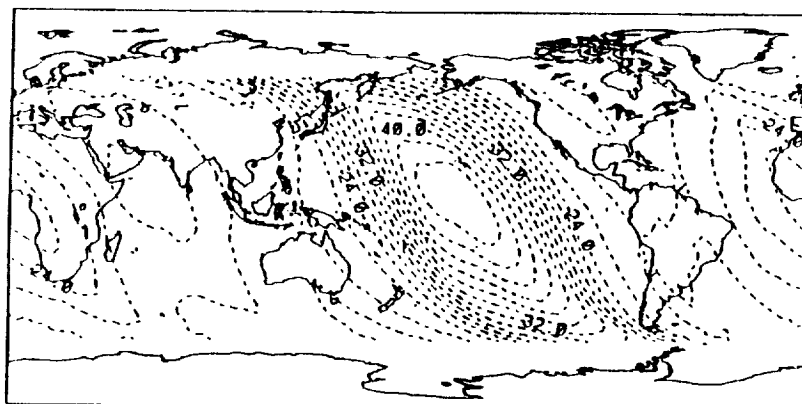

Figure 2: Standard deviation of the TOPEX/POSEIDON radial orbit error along the descending ground tracks, using the GEM-T1 gravity error covariance. The contour interval is 2 cm.

gravity data and altimeter data can be expected to have much better global characteristics and the resulting orbit error would not be expected to be as non-uniform as the case for this satellite only model.

To demonstrate the spatial correlation of the radial orbit error an example is presented that shows how the error at one geographic location is correlated with the errors in the neighboring geographic region. The reference point is located at 200° East longitude on the equator and and corresponds to the radial error along an ascending track passing over that point. The correlation of this error with the errors on all other ascending tracks through the region is given in Figure 3. The correlation value of 1.0 locates the reference orbit error with which all the other errors are correlated against. This plot clearly shows the strong along track correlation and it also shows the significant cross track correlation. That is, the errors on adjacent ascending tracks have significant correlation even when separated by distances of up to a 1000 km. The correlation distances evident in Figure 3 compare with those found by *Anderle and Hoskin* [1977] although the cross track correlation appears stronger here due to the higher altitude of TOPEX/POSEIDON as compared to SEASAT (thus, TOPEX/POSEIDON is not as sensitive to the higher degree coefficient errors which would decorrelate the orbit error at shorter scales).

The spatial correlation of the radial errors at crossover points has also been investigated. In this case, at a given crossover location (where an ascending track crosses a descending track) the correlation between the error on each track is computed. Overall the correlations were found to vary between ±.3 for the case of TOPEX/POSEIDON and using the GEM-T1 gravity error covariance. This is very significant for those applications that attempt to use crossover data to remove the remaining orbit error in an altimetric satellite ephemerides. Due to the correlations of the error along the two tracks (even though widely separated in time) the crossovers do not

148
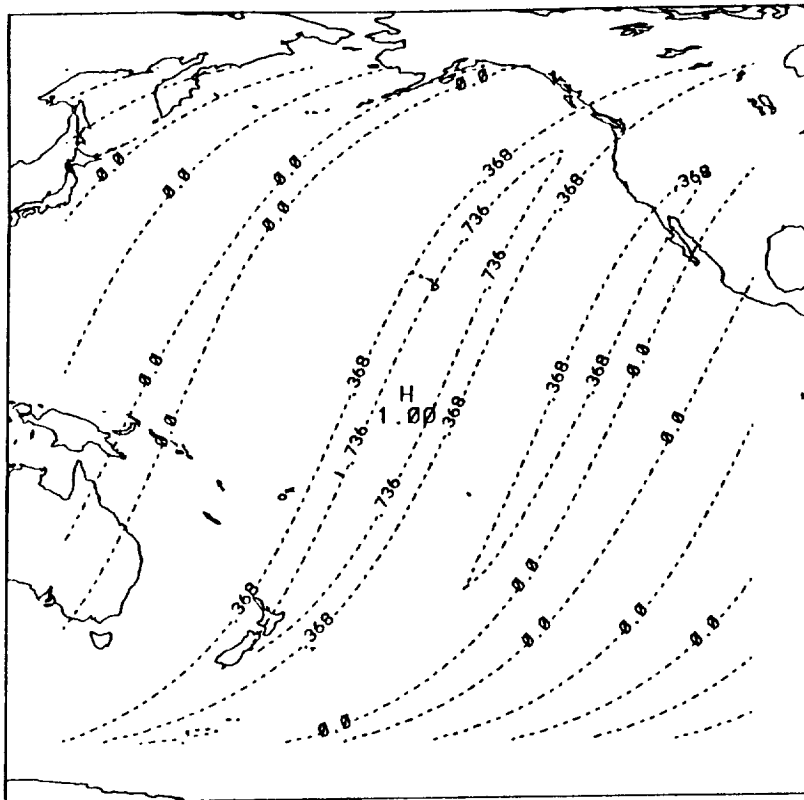
Figure 3: Correlation between the TOPEX/POSEIDON radial orbit error along ascending tracks with the ascending error located at 200° East longitude on the equator. The contour interval is 0.368.

provide an absolute measure of the radial orbit error. In general there is some component of the orbit error (usually referred to as the geographically correlated component) that is unobservable in the crossovers.

4. CONCLUSIONS

Orbit error due to gravity model error is very systematic when examined geographically. This strong geographic dependence is a hindrance in the utilization of satellite altimeter data to measure oceanographic signals. The results presented here are based on some simplifying assumptions (near circular orbit) and do not account for other possible model error sources or the effect of fitting the orbit to a set of tracking data. However, it should be expected that the effects presented here will be manifested into the actual orbital ephemerides at some level. Elimination of these correlations can only be accomplished through the elimination of the gravity model error. Thus, it can be expected that ephemerides for altimetric satellites have errors which are strongly correlated and which can in turn be aliased into the oceanographic signals trying to be recovered from the altimetric data.

REFERENCES

Anderle, R. J. and R. L. Hoskin, *Geophys. Res. Letter, 4*, 421, 1977.
Colombo, O. L., TM 86180, NASA Goddard Space Flight Center, Greenbelt, Maryland, 1984.
Engelis, T., Report No. 377, Dept. of Geodetic Science, Ohio State Univ., Columbus, Ohio, 1987.
Kaula, W. M., *Theory of Satellite Geodesy*, Blaisdell Publ. Co., Waltham, Massachusetts, 1966.
Marsh, J. G., et. al., *J. Geophys. Res., 93*, 6169, 1988.
Rosborough, G. W., Report No. 86–1, Center for Space Research, Univ. of Texas, Austin, Texas, 1986.
Rosborough, G. W. and B. D. Tapley, *Celest. Mech., 40*, 409, 1987.

149

Future Gravity Missions

Moderators: Christopher Reigber

David Smith

$\checkmark$

C-3

Peter J. Melvin
Naval Research Laboratory, Washington, DC

N90-20552

Abstract

A new, geometrical, first order, nonresonant, frozen orbit theory has been developed based on Orlov's uniformly rotating plane of constant inclination. Perturbation spectra generated from a 90th order subset of OSU86F are shown for the ill-fated 1984 JHU/APL SAGE proposal for a pair of TRANSIT satellites at 400km altitude with a 93°5 inclination.

Introduction

To perform the integration for a geodetic satellite a new form has been developed for the geopotential on an orbit as

$$V = \frac{GM}{a} \sum_{k=0}^{\infty} \xi^k \sum_{p=-\infty}^{\infty} \sum_{q=-\infty}^{\infty} e^{i(pu + q\vartheta)} [\bar{R}_{p,q}^{(k)} + \varphi \bar{T}_{p,q}^{(k)}] \ ,$$

where the symbols are defined in [Melvin, 1988a] and an algorithm is derived for the generation of the complex coefficients from a spherical harmonic geopotential model.

The geopotential variation

$$a \sum_{p=-\infty}^{\infty} \sum_{q=-\infty}^{\infty} \bar{R}_{p,q}^{(0)} e^{i(pu+q\vartheta)} \ , \tag{1}$$

is the distance of an equipotential surface from sphere of radius a. The spectrum in Fig. 1 is a log-log bar graph of the amplitudes $2a|\bar{R}_{p,q}^{(0)}|$ where the frequency is $|pn + q\dot{\vartheta}|$. The along-track deflection evaluated on the nominal circular orbit is

$$\frac{1}{a} \frac{\partial V}{\partial u} = \frac{GM}{a^2} \sum_{p=-\infty}^{\infty} \sum_{q=-\infty}^{\infty} ip\bar{R}_{p,q}^{(0)} e^{i(pu+q\vartheta)} \ , \tag{2}$$

and its spectrum is plotted in Fig. 2.

Position Perturbations

The real forms of the series are used for the integration in [Melvin 1988a], but it is apparent from [Melvin, 1988b] that the formulas are much simpler with complex coefficients. In fact the orbit perturbations are of the same form as the disturbing potential

$$\varphi = \sum_{p=-\infty}^{\infty} \sum_{q=-\infty}^{\infty} \varphi_{p,q} e^{i(pu+q\vartheta)} \ , \qquad \eta = \sum_{p=-\infty}^{\infty} \sum_{q=-\infty}^{\infty} \eta_{p,q} e^{i(pu+q\vartheta)} \ ,$$

$$\xi = \sum_{p=-\infty}^{\infty} \sum_{q=-\infty}^{\infty} \xi_{p,q} e^{i(pu+q\vartheta)} \ , \qquad \chi = \sum_{p=-\infty}^{\infty} \sum_{q=-\infty}^{\infty} \chi_{p,q} e^{i(pu+q\vartheta)} \ ,$$
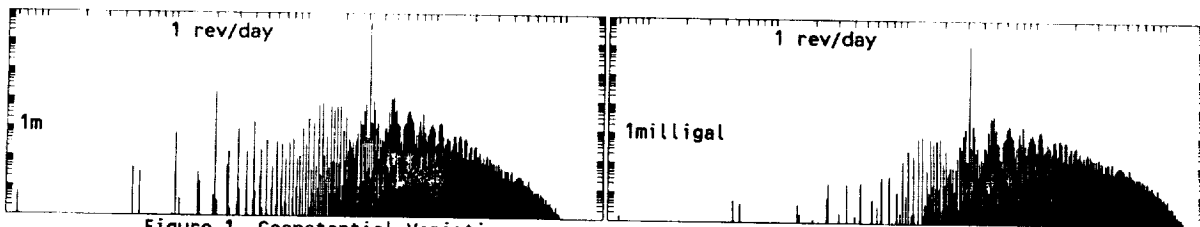
Figure 1. Geopotential Variation

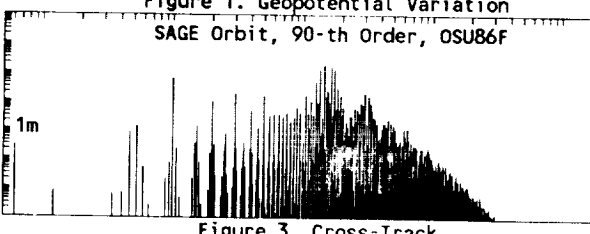Figure 2. Along-Track Deflection
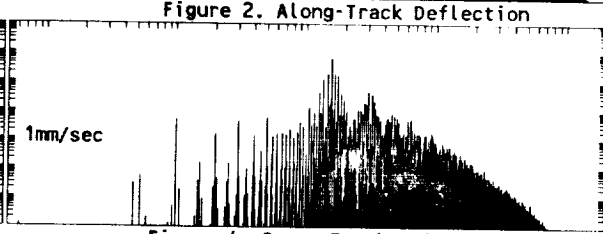
SAGE Orbit, 90-th Order, OSU86F
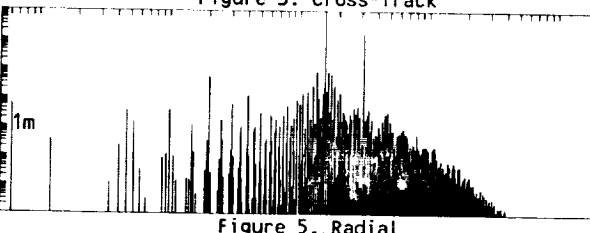
Figure 3. Cross-Track

Figure 4. Cross-Track Velocity
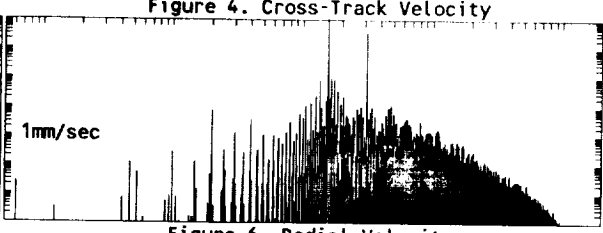
Figure 5. Radial
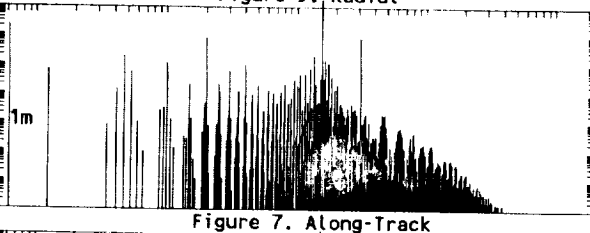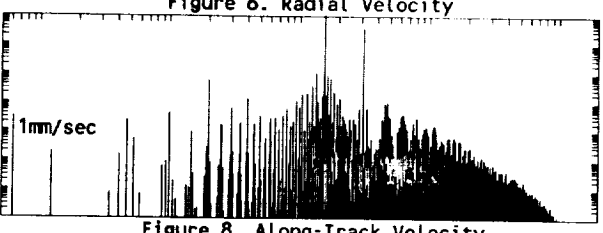
Figure 6. Radial Velocity

Figure 7. Along-Track
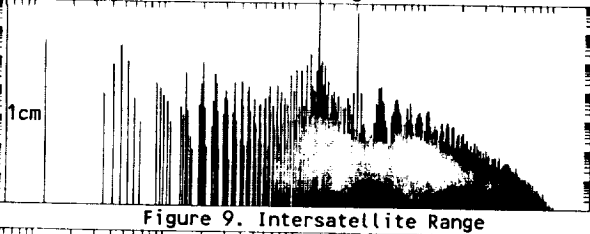
Figure 8. Along-Track Velocity
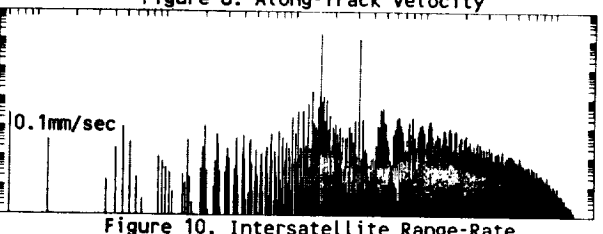
Figure 9. Intersatellite Range
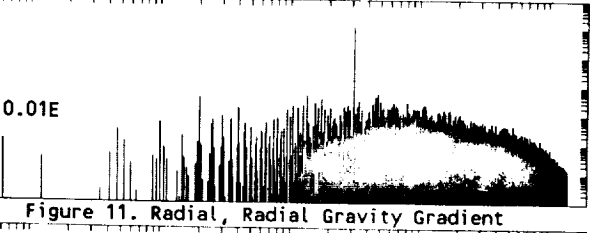
Figure 10. Intersatellite Range-Rate

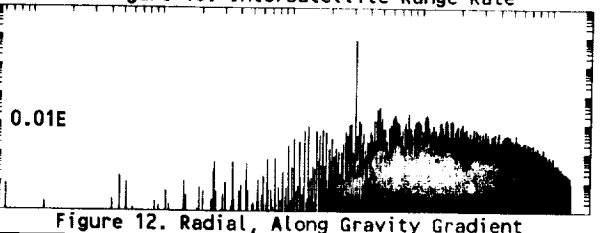Figure 11. Radial, Radial Gravity Gradient
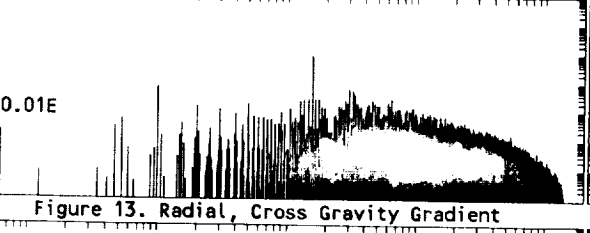
Figure 12. Radial, Along Gravity Gradient

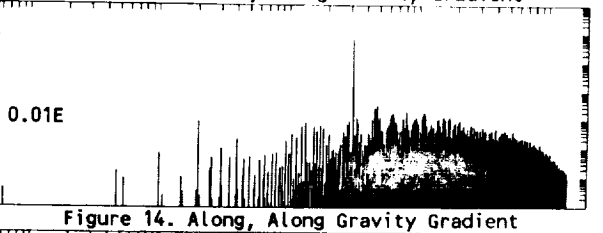Figure 13. Radial, Cross Gravity Gradient

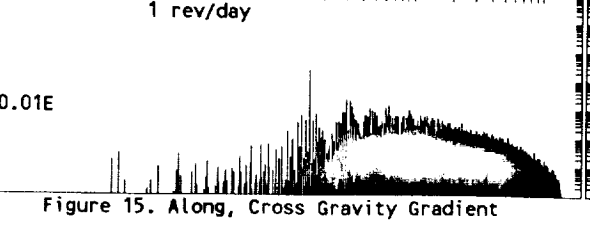Figure 14. Along, Along Gravity Gradient
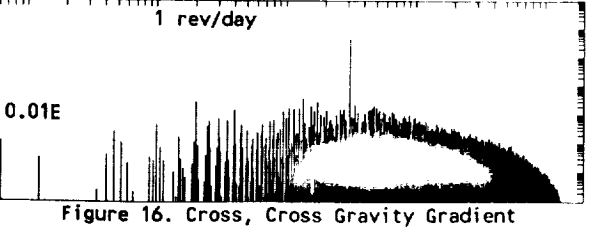
Figure 15. Along, Cross Gravity Gradient

Figure 16. Cross, Cross Gravity Gradient

152

where the coefficients are computed from the algorithm

$$\varphi_{p,q} = -\frac{n_o^2 \bar{T}_{p,q}^{(0)}}{(pn+q\dot{\vartheta})^2 - N^2} \quad , \quad (3), \qquad \eta_{p,q} = \frac{n_o^2 p \bar{R}_{p,q}^{(0)}}{\nu(pn+q\dot{\vartheta})} \quad ,$$

$$\xi_{p,q} = -\frac{n_o^2 \bar{R}_{p,q}^{(1)} + 2\nu^2 \eta_{p,q}}{(pn+q\dot{\vartheta})^2 - N^2} \quad , \quad (5), \qquad \chi_{p,q} = -i\nu \frac{\eta_{p,q} - 2\xi_{p,q}}{pn + q\dot{\vartheta}} \quad . \qquad (7)$$

After multiplication by 2a, the amplitudes of the coefficients of (3), (5) and (7) are plotted in Figs. 3, 5, and 7 from which it is seen that position perturbations accentuate the low and near orbital frequencies and attenuate the high frequencies. Expressions for the cross-track (3), radial (5), and along-track (7) position perturbations from the Kaula-Allan theory are found in [Rosborough and Tapley, 1987].

Velocity Perturbations

By use of coordinates at the nominal satellite position, the cross-track, radial, and along-track velocity components are

$$v_\varphi = a(\dot{\varphi} - \dot{\Omega}\sin\iota\cos u) = a[\sum_{p=-\infty}^{\infty} \sum_{q=-\infty}^{\infty} i(pn+q\dot{\vartheta})\varphi_{p,q} e^{i(pu+q\vartheta)} - \dot{\Omega}\sin\iota\cos u], \quad (4)$$

$$v_r = a\dot{\xi} = a\sum_{p=-\infty}^{\infty} \sum_{q=-\infty}^{\infty} i(pn + q\dot{\vartheta})\xi_{p,q} e^{i(pu+q\vartheta)} \quad , \qquad (6)$$

$$v_u = a\nu + a(\dot{\chi} + \nu\xi) = a\nu[1 + \sum_{p=-\infty}^{\infty} \sum_{q=-\infty}^{\infty} (\eta_{p,q} - \xi_{p,q}) e^{i(pu+q\vartheta)}] \quad . \qquad (8)$$

The amplitudes of the coefficients of (4), (6) and (8) are plotted in Figs. 4, 6, and 8. By comparison of the high frequency fall-off in the position and velocity spectra, it is clear why more geopotential information is obtained from Doppler beacon satellites than from skin tracking even if it is by laser reflectors.

Intersatellite Measurements

For a close satellite pair in same orbit, the intersatellite range is

$$\rho = r\Delta u = a\delta u(1 + \xi + \frac{\partial \chi}{\partial u}) = a\delta u[1 + \sum_{p=-\infty}^{\infty} \sum_{q=-\infty}^{\infty} (\xi_{p,q} + ip\chi_{p,q}) e^{i(pu+q\vartheta)}], \quad (9)$$

A time derivative yields the intersatellite range rate as

$$\dot{\rho} = a\delta u \sum_{p=-\infty}^{\infty} \sum_{q=-\infty}^{\infty} i(pn + q\dot{\vartheta})(\xi_{p,q} + ip\chi_{p,q}) e^{i(pu+q\vartheta)} \quad . \qquad (10)$$

For a nominal separation of aδu=100km the spectra of (9) and (10) are plotted in Figs. 9 and 10. A comparison of the high frequency portions of Figs. 2 and 10 and the foregoing formulas show

$$\dot{\rho} \simeq \frac{a\delta u}{a^2 n} \frac{\partial V}{\partial u} \quad ,$$

from which the result of [Comfort, 1973] is modified to state that at high frequencies for a pair of satellites flying in formation the intersatellite

153

range rate mimics the along track deflection. The paucity of spectral lines near twice per orbit in Fig. 10 indicates that complete geopotential recovery is not possible with only intersatellite range rate.

Gravity Gradient

Equally simple formulas for the gravity gradient tensor along a nominal circular orbit in Orlov's plane are found in [Melvin, 1988b] as

$$\Gamma_{r,r} = 2n_o^2 \sum_{p=-\infty}^{\infty} \sum_{q=-\infty}^{\infty} \overline{R}_{p,q}^{(2)} e^{i(pu+q\vartheta)}; (11), \quad \Gamma_{r,u} = in_o^2 \sum_{p=-\infty}^{\infty} \sum_{q=-\infty}^{\infty} p(\overline{R}_{p,q}^{(1)} - R_{p,q}^{(0)}) e^{i(pu+q\vartheta)}, \quad (12)$$

$$\Gamma_{r,\varphi} = n_o^2 \sum_{p=-\infty}^{\infty} \sum_{q=-\infty}^{\infty} (\overline{T}_{p,q}^{(1)} - \overline{T}_{p,q}^{(0)}) e^{i(pu+q\vartheta)} \quad (13), \quad \Gamma_{u,u} = n_o^2 \sum_{p=-\infty}^{\infty} \sum_{q=-\infty}^{\infty} (-p^2 \overline{R}_{p,q}^{(0)} + \overline{R}_{p,q}^{(1)}) e^{i(pu+q\vartheta)}, \quad (14)$$

$$\Gamma_{u,\varphi} = in_o^2 \sum_{p=-\infty}^{\infty} \sum_{q=-\infty}^{\infty} p\overline{T}_{p,q}^{(0)} e^{i(pu+q\vartheta)} \quad (15), \quad \Gamma_{\varphi,\varphi} = -\Gamma_{r,r} - \Gamma_{u,u}. \quad (16)$$

The gravity gradient spectra computed from (11) through (16) are shown in Figs. 11 through 16.

Geopotential Recovery

Although it is subjective and dependent on the sensitivity of the measuring devices, it became apparent in the generation of the spectrum in Fig. 10 that the claim of 100th order recovery from SAGE, [Pisacane, et al., 1984], could not be substantiated. From intersatellite range rate, about 70th order recovery is more realistic at an altitude of 400km. The abrupt, high frequency cutoff in Figs. 11, 12, and 14 indicates there is information beyond 90th order in the gravity gradient components.

References

Comfort, G.C., "Direct Mapping of Gravity Anomalies by Using Doppler Tracking between a Satellite Pair", J. Geophys. Res., *78*, 6845, 1973

Melvin, P.J., "Satellite Geodesy from Orlov's Plane", (AAS 87-536), Advances in the Astronautical Sciences, eds. Soldner, Misra, Lindberg and Williamson, *65*, 1449, 1988a

Melvin, P.J., "The figure-of-8 librations of the gravity gradient pendulum and modes of an orbiting tether: II. Geodetic, mass distribution and eccentricity effects", AIAA 88-4283-CP, Proc. AIAA/AAS Astrodynamics Conference, Minneapolis, MN, p 503, 1988b

Pisacane, V.L., Yionoulis, S.M., Eisner, A., and Black, H.D., "SAGE - A Two Satellite Experiment for Improving the Gravity Model", EOS, *65*, 858, 1984

Rosborough, G.W., and Tapley, B.D., "Radial, Transverse and Normal Satellite Position Perturbations Due to the Geopotential", Celestial Mechanics, *40*, 409, 1987

Refinement of Earth's Gravity Field with Topex GPS Measurements

SIEN-CHONG WU AND JIUN-TSONG WU

Jet Propulsion Laboratory, California Institute of Technology, Pasadena, CA

1. INTRODUCTION

The NASA Ocean Topography Experiment satellite Topex will carry a microwave altimeter accurate to a few centimeters for the measurement of ocean height. The capability can be fully exploited only if Topex altitude can be independently determined to 15 cm or better [*Born, et al.* 1985]. This in turn requires an accurate gravity model. The gravity will be tuned with selected nine 10-day arcs of laser ranging, which will be the baseline tracking data type, collected in the first six months of Topex flight. Topex will also carry onboard an experimental GPS flight receiver capable of simultaneously observing six GPS satellites above its horizon to demonstrate the capability of GPS carrier phase and P-code pseudorange for precise determination of the Topex orbit. It has been found that sub-decimeter orbit accuracy can be achieved with a mere two-hour arc of GPS tracking data, provided that simultaneous measurements are also made at six or more ground tracking sites [*Yunck, et al.* 1986]. The precision GPS data from Topex are also valuable for refining the gravity model. This paper presents an efficient technique for gravity tuning using GPS measurements. Unlike conventional *global* gravity tuning, this technique solves for far fewer gravity parameters in each filter run. These gravity parameters yield *local* gravity anomalies which can later be combined with the solutions over other parts of the earth to generate a *global* gravity map. No supercomputing power will be needed for such combining. The following describes the approaches used in this study and presents preliminary results of a covariance analysis.

2. GRAVITY ANOMALY INFORMATION CONTENT IN TOPEX GPS MEASUREMENTS

In this section a theoretical formulation is derived for the information content of GPS measurements, in particular carrier phase, from Topex for the recovery of gravity anomalies. The acceleration (force) on Topex in a rotating local $h-c-\ell$ coordinate (Fig. 1), where h is the radial, c the cross-track and ℓ the down-track directions, can be written as

$$\ddot{h} = \frac{\Delta \dot{h}}{\Delta t} - \frac{\dot{\ell}^2}{(r_E + h)} \, ,$$

$$\ddot{c} = \frac{\Delta \dot{c}}{\Delta t} \, ,$$

and

$$\ddot{\ell} = \frac{\Delta \dot{\ell}}{\Delta t} + \frac{\dot{h}\dot{\ell}}{(r_E + h)}$$
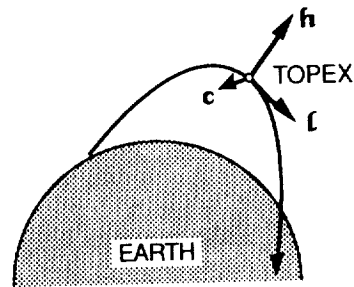
Fig. 1. Rotating $h-c-\ell$ coordinate

where single and double dots denote first and second time derivatives, respectively, and r_E is earth's mean radius. For given uncertainties in Topex velocity and its change over a time increment Δt, the corresponding uncertainty in the determination of the force is

$$\sigma_{\ddot{h}} < \frac{\sigma_{\Delta\dot{h}}}{\Delta t} + \frac{2\dot{\ell}\,\sigma_{\dot{\ell}}}{(r_E + h)} \quad , \qquad \sigma_{\ddot{c}} = \frac{\sigma_{\Delta\dot{c}}}{\Delta t} \qquad \text{and} \qquad \sigma_{\ddot{\ell}} < \frac{\sigma_{\Delta\dot{\ell}}}{\Delta t} + \frac{\dot{\ell}\,\sigma_{\dot{h}}}{(r_E + h)}$$

155

Previous analyses have indicated that Topex orbit determination with GPS measurements yields

$$\sigma_{\dot{h}}, \ \sigma_{\dot{\ell}}, \ \sigma_{\Delta\dot{h}}, \ \sigma_{\Delta\dot{c}}, \ \sigma_{\Delta\dot{\ell}} < 0.5 \, \text{mm/sec}$$

Hence, with an altitude $h = 1{,}334$ km and nominal velocity $\dot{\ell} = 7.2$ km/sec for Topex, and for a sampling time of $\Delta t = 2$ minutes, local gravity anomaly along a Topex flight path can be determined to an accuracy of better than 0.6 mgal in the radial component and better than 0.5 mgal in the other two components.

3. SIMULATION ANALYSIS

Next, a simulation analysis was performed to numerically estimate the accuracy with which a given, but assumed *unknown*, gravity anomaly can be determined by solving for the coefficients of a number of spherical harmonics. In this analysis, a network of six globally distributed tracking sites is used. These include the three NASA Deep Space Tracking (DSN) Sites at Goldstone, California; Madrid, Spain and Canberra, Australia; and three other sites at Japan, Brazil and South Africa. The "truth" model for the gravity anomaly is assumed to consist of a sum of eleven zonal harmonics $J_{15}, J_{16}, ..., J_{25}$, each with a normalized magnitude of 10^{-6}. In the filtering process different subsets of these terms are estimated and the lumped effects of the selected terms are computed and compared with the truth model to assess the accuracy with which the local gravity anomaly can be recovered. Other assumptions used in the analysis are included in Table 1.

Data Type:	0.5-cm GPS Carrier Phase
Data Span:	2 hrs
Data Intervals:	2 minutes
Gravity Anomaly:	$J_{15}, J_{16}, ..., J_{25}$ (10^{-6} each, normalized)
Station Coordinates:	DSN Sites: 3 cm each component (fixed)
	other: 10 cm each component (adjusted)
Clock Bias:	3 μsec (adjusted as white noise)
Carrier Phase Bias:	10 km (adjusted)
GPS Epoch States:	3 m; 0.3 mm/sec (adjusted)
Topex Epoch States:	10 m; 1 cm/sec (adjusted)
Zenith Troposphere:	2 cm

Table 1. Simulation Analysis Model

Fig. 2 shows the results when four different subsets of gravity terms are estimated. Note that good agreement with the truth can be achieved when proper model is used in the estimation (Fig. 2a and 2b). On the other hand, a larger discrepancy occurs if the model is not flexible enough to represent the truth (Fig. 2c and 2d). This leads us to the use of a piecewise constant model for its high flexibility, provided that the step size is fine enough to follow the variation in the truth model. The solution using a piecewise constant model with a 2-minute step size is shown in Fig. 3. Note that the RMS discrepancy between the solution and the truth model (0.54 mgal) is consistent with the theoretical prediction.

4. THE GRAVITY BIN TECHNIQUE

Following the above encouraging findings, a more general and efficient technique was investigated. This technique solves for "gravity bins", which are 3-D positional deviations on Topex, with three parameters at each measurement time point over a period of a few hours. The epoch state of Topex and other pertinent parameters are also simultaneously adjusted. These are related to Topex current state by the following linearized equation.
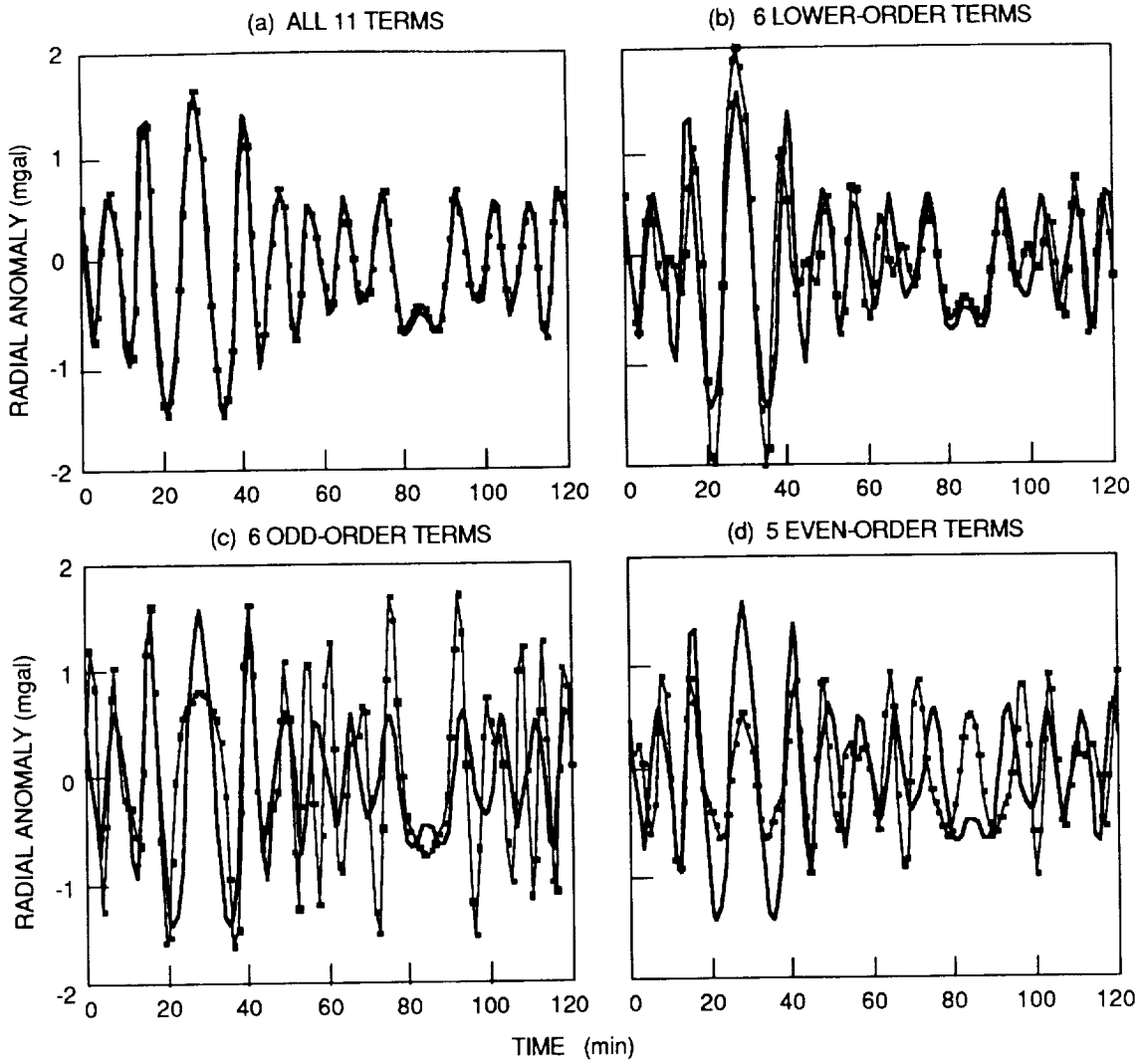
156

(a) ALL 11 TERMS

(b) 6 LOWER-ORDER TERMS

(c) 6 ODD-ORDER TERMS

(d) 5 EVEN-ORDER TERMS

TIME (min)

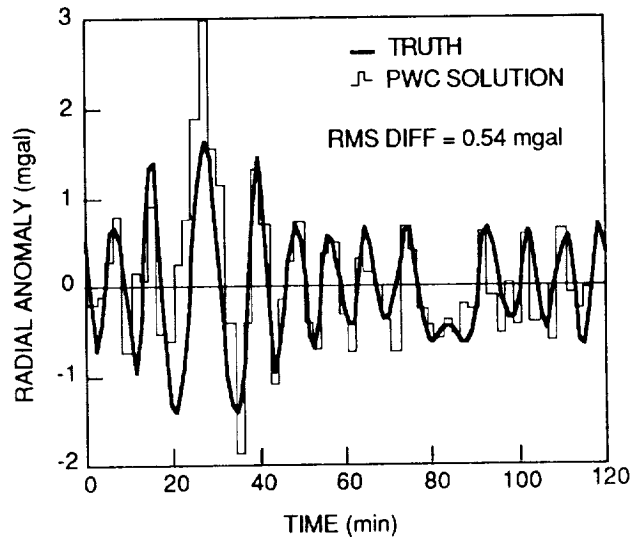Fig. 2. Sample results of simulation analysis (— truth, ⊸ solution)

Fig. 3. Simulation result with piecewise constant model

157

$$r(t) = \frac{\partial r}{\partial r_0} r_0 + \frac{\partial r}{\partial v_0} v_0 + \delta(t)$$

where $r(t)$ is the current position of Topex, r_0 and v_0 are position and velocity at epoch, and $\delta(t)$ is the gravity bin parameter at time t. Since δ remains the same for orbits over repeat ground tracks, which will occur every 10 days for Topex, information from repeat orbits can be combined to increase the estimation accuracy. Gravity bins δ for orbits over different ground tracks are independent from one another and can be determined separately. Hence only moderate number of parameters are estimated in each filter process. Local gravity anomaly Δg can be computed from the solutions of gravity bin parameters δ by

$$\Delta g(t) = \ddot{\delta}(t) - \frac{\partial g}{\partial r}\delta(t)$$

where g is the nominal gravity field. The *global* gravity anomaly expressed in terms of spherical harmonics can be constructed from the *local* gravity anomaly by a process similar to the Fourier transformation.

Fig. 4 shows the result of a covariance analysis using a 2.5-minute bin size over a 2-hour data span which is nearly the Topex orbit period. Note that local gravity anomaly can be determined to an accuracy of 0.2 mgal under most circumstances with GPS measurements over one Topex orbit. This accuracy will improve monotonically by combining multiple data arcs over repeat Topex ground tracks [*Wu and Yunck*, 1988]. It is anticipated that gravity anomalies of medium wavelengths (1,500 to 3,000 km) can be greatly refined with GPS measurements onboard Topex.
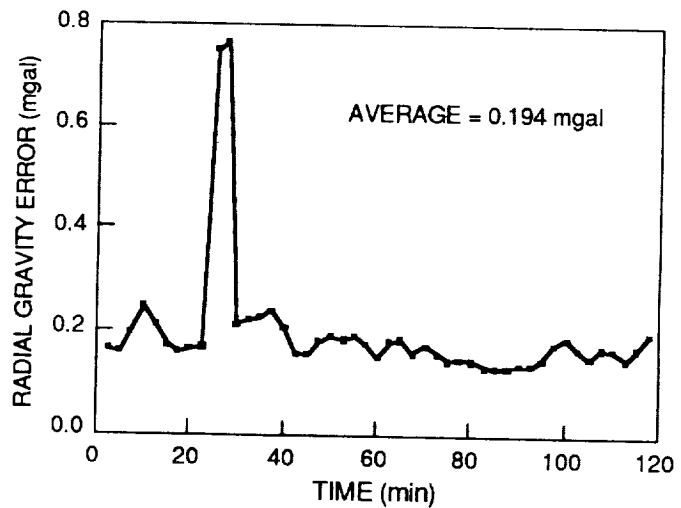
Fig. 4. Performance of gravity bin technique

The computation involved in the transformation of global gravity anomaly from a collection of gravity bins over the entire globe is well known and can be done without the need for a supercomputer. Hence, the gravity bin technique is efficient for global gravity recovery. Note that gravity bins solution can be directly applied as a calibration for the effects of gravity mismodeling on Topex orbit determination. Currently under investigation is the application of the gravity bin technique to Topex with the baseline (laser ranging) tracking data type, where large data gaps exist.

REFERENCES

Born, G. H., R. H. Stewart, and C. A. Yamarone, *Monitoring Earth's Ocean, Land, and Atmosphere from Space — Sensors, Systems, and Applications*, AIAA Inc., 464, 1985.

Wu, J. T., and T. P. Yunck, Paper AIAA-88-0575, AIAA 26th Aerospace Sciences Meeting, 1988.

Yunck, T. P., S. C. Wu, and J. T. Wu, *Proc. IEEE PLANS*, 1986

D.E Smith*, F.J. Lerch*, O.L. Colombo** and C.W.F. Everitt***

*Goddard Space Flight Center, Maryland;
**EG&G, WASC, Inc., Lanham, Maryland; ***Stanford University, Stanford, California.

ABSTRACT

The GRAVITY PROBE-B Mission will carry the Stanford gyroscope relativity experiment into orbit in the mid 1990's, as well as a GPS receiver whose tracking data will be used to study the earth gravity field. This paper presents estimates of the the likely quality of a gravity field model to be derived from the GPS data, and discusses the significance of this experiment to geodesy and geophysics.

I. INTRODUCTION

By 1995, the GRAVITY PROBE-B (GP-B) spacecraft will carry the Stanford gyroscope relativity experiment, to test the theory of general relativity by measuring two effects predicted by this theory. Both should manifest themselves as very slow precessions of the axis of a spinning body (gyroscope) respect to a frame determined by distant stars, when this body moves relative to a massive object, like the earth. They are illustrated in Figure 1: the geodetic precession occurs because the gyroscope is moving in orbit through curved space-time, around the earth; the motional (or frame-dragging) precession, because the earth is spinning about its own axis. Both effects increase as height decreases, so they are easier to measure from lower orbits. Bright stars like Rigel, to which sensors inside the spacecraft will point, will provide the fixed external reference frame. The gyroscopes themselves (four in number) will be made of fused quartz ground into almost perfect spheres, with a coating of niobium. These will spin while electrostatically suspended inside spherical cavities rigidly attached to a solid block of quartz. The whole assembly will be cooled with liquid helium, so the niobium coating is superconducting. A spinning superconductor developes a magnetic field. For each sphere, this field will point in the direction of the spin axis. Once this field is detected with magnetic sensors, the instantaneous direction of the gyroscope's axis in the frame of the stars can be established. The spacecraft will be nearly axially symmetric, spinning about its axis, to maintain a stable attitude in space and to average out effects due to asymmetries in mass distribution.

THE TWO GYRO EFFECTS PREDICTED BY SCHIFF

$\Delta\theta = 6.6$ sec/yr (GEODETIC)

RIGEL

$\Delta\theta = .042$ sec/yr (MOTIONAL)
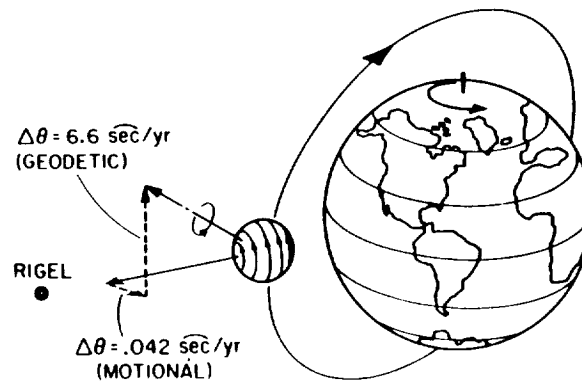
Figure 1. Principle of the Stanford gyroscope experiment. The small spinning sphere is one of the gyroscopes that will orbit the earth on board GP-B.

The spacecraft will also carry a Global Positioning System (GPS) receiver to provide tracking data for studying the earth gravity field and for orbit determination, as well as corner-cube reflectors for geodetic experiments combining GPS and Satellite Laser Ranging (SLR). Also, the spacecraft will have active drag compensation in all three dimensions, to reduce disturbing accelerations on the gyroscopes. To simplify the separation between the relativistic effects, the orbit will be polar. A polar orbit, from the point of view

tribution of the GPS tracking data, provides a complete global coverage, assuming that the full GPS constellation of up to 24 Block II spacecraft is operating. A low, near circular orbit increases the gravitational signal at shorter spatial wavelengths, thus allowing higher resolution in the resulting field model. The drag compensation (which also compensates all the other surface forces, such as solar radiation pressure) will give an orbit shaped purely by gravitation, and thus much "cleaner" from the point of view of geodesy, than those of ordinary, uncompensated, low-orbit satellites.

In coming years, worldwide terrestrial nets of GPS stations are likely to be established for the purpose of providing a framework for geodynamics studies (crustal motion, tides, earth rotation), and for computing very precise GPS ephemerides and satellite clock corrections using tracking data from around the world. The tracking from those stations, or the ephemerides and clock corrections obtained from that tracking, will be needed to analyse the GPS data from the receiver on board GP-B. Conversely, data from a receiver in a relatively low spacecraft like GP-B, obtained simultaneously with that from the ground stations, can be used to improve the geometry of the network by adding to it a moving station high above the ground (Yunk et al., 1985). Therefore, the GPS experiment on GP-B and the operations of the terrestrial network will benefit from each other. Finally, the possibility of tracking GP-B from SLR stations will help to connect and unify the reference frames of the laser and the GPS geodetic networks. At the same time, GP-B will be carrying out its main experiment in relativity. In this way, a single space mission may advance three separate scientific undertakings: one in fundamental physics, and two in geodynamics.

The GP-B mission will follow that of the oceanographic satellite TOPEX, wich will carry a radar altimeter as its main experiment, and will have also a GPS receiver. This receiver will be the first of its kind to operate in space for a prolongued period of time (up to two years). For some studies that can be carried out from the higher orbit of TOPEX as well as from the lower one of GP-B (connection of reference frames, long-wavelength mapping of the gravity field, tidal studies, etc.), the two missions will provide continuity over a period of several years (GP-B is scheduled to begin at about the time when TOPEX is likely to be reaching the end of its useful life).

2. CONCEPT OF A GP-B/GPS GEOPOTENTIAL MAPPING EXPERIMENT

For the purposes of this study, the following assumptions were made:

--- The GP-B spacecraft is drag-free; its orbit is polar, circular, 600 km in altitude, and repeats monthly.

--- The mission lasts for two years, during which an average of 7 GPS satellites from the full constellation of 24 are tracked simultaneously, at all times, from GP-B. The sampling rate is once per second, and there are four simultaneous measurements per GPS satellite: a pseudorange and a carrier phase, in the L1 and also in the L2 bands. The measurements are stored in the spacecraft computer memory and dumped via the TDRSS relay satellites to ground stations, together with telemetry and the relativity experiment data.

--- Mean values of the differences between simultaneous pseudorange and carrier phase measurements, averaged over some tens of minutes (up to a maximum of half a revolution of GP-B, or 40 minutes) are used to estimate the biases in the L1 and L2 carrier phases. The biases are fixed to the integer numbers of wavelengths closest to those averages. If the uncertainty for a given average is much less than one wavelength, the corresponding bias is likely to be resolved. If the uncertainty is large, it is probable that a residual bias remains, which is constant over one averaging interval, but changes value randomly from one interval to the next.

--- The estimated biases are added to the corresponding carrier phase ranges, resulting in full L1 and L2 ranges, which are then combined to correct the effect of ionospheric refraction. The corrected ranges have larger uncertainties than the original L1 and L2 measurements. Next, these corrected ranges are substractd from ranges to the same GPS satellites measured simultaneously from ground receivers. This differencing eliminates the GPS spacecraft clock errors. The resulting single differences are substracted from each other to form double differences, to suppress both the clock errors of the ground receivers and of the receiver on GP-B. At the same time, this double-differencing increases the noise further. Finally, double differences involving four or more GPS satellites altogether, could be combined to estimate geometrically the instantaneous position of GP-B. The uncertainty of the ranges, propagated into those of the x, y, z coordinates (here aligned with the across, along, and radial orbital coordinates), is approximately the uncertainty of the corrected ranges multiplied by the Geometric Dispersion of Precision (GDOP) per coordinate. This quantity depends on the GPS/GP-B geometry at measurement time. The set of measurements can then be compressed, to save work, by estimating from the noisy coordinates of several consecutive points those of a middle (or "normal") point. These normal points then may be used (with their formal accuracies) as

actual data for the orbits/gravity field parameters estimation. Alternatively, the double differences themselves can be used as data (after being compressed into "normal" data points). In either case, errors in the final data (double differences or coordinates) will be affected by the original measurement errors (unresolved biases, noise), and also by the errors in the ephemerides of GPS.

--- The compressed data set is used to estimate corrections to the orbits of both GP-B and of all GPS satellites involved, simultaneously with the potential coefficients of the gravity field up to a high degree and order. This is done by a least squares technique, using a mathematical description of the compressed data linearized about the a priori values of the orbit and gravity field parameters.

3. MISSION ERROR ANALYSIS

The expected accuracies of estimates of potential coefficients obtained from instantaneous x, y, z data, derived from GPS ranges as indicated in the previous section, have been calculated by setting up and inverting the normal matrix of the adjustment of those parameters. An approximate analytical theory described in Colombo (1986, Ch. I), based on the linearized dynamics of a circular orbit, has been used to derive a mathematical model for the gravitational perturbations of the coordinates of GP-B. The theory is based on the trigonometric expansions of the gravitational potential and accelerations, when these are given as functions of time. These expansions become true Fourier series when the orbit repeats precisely, their fundamental frequency being that of this repeat, and the orbital perturbations in x, y, and z are also Fourier series with the same frequencies. As explained in the extended abstract on the analysis of satellite gradiometry (Colombo, this issue), use of this model leads to a normal matrix that is very sparse. Moreover, the non-zero elements can be computed analytically, and with a proper arrangement of the unknowns, the matrix becomes block-diagonal. All this permits the very efficient calculation of the inverse, and thus of the variances and covariances of the estimated coefficients. In practice, the more conventional techniques current today in space geodesy are likely to be used to analyze the GPS data, because of their greater flexibility and accuracy. However, those methods would have to be implemented in a supercomputer, given the unusually large size of the adjustment, and work to this end is underway at GSFC. The approach adopted here is good enough for guessing the uncertainties in the potential coefficients obtained by those methods, and requires little effort and modest computer resources.

Measurement errors have been treated as consisting of 1 cm rms white noise in the carrier phase, after correcting for the ionosphere; residual biases have been treated as 10 cm process noise (before double differencing and making the ionospheric correction), with a triangular covariance function and a 15 minutes' correlation length. This error has been propagated into those of the instantaneous x, y, z coordinates, considering the effect of the ionospheric correction, double differencing, and the geometric dispersion of precision. The GDOP per coordinate was assumed to be, on average, 1.7, based on a study by Martin and McCarthy (1987) for a GPS/space shuttle mission. The GPS antenna on GP-B is supposed to be "looking up" (i.e., not tracking any satellites below the local horizontal plane of the receiver).

A worst and a best case have been studied, too pesimistic and too optimistic, respectively, providing upper and lower bounds for the errors in the coefficients. The worst case assumes the loss of all information with the same frequency content as that of the orbit errors (multiples of once per revolution of GP-B plus/minus multiples of one cycle per twelve hours, which is the orbital frequency of GPS, spread out further over plus/minus one cycle per day, supposing that one-day orbits are estimated). It also assumes residual 10 cm standard deviation for the 15 minutes' residual range biases. The best case assumes that all biases have been resolved and there are no GPS orbit errors. The main reason for obtaining an upper and a lower bound was the difficulty of dealing with the orbit errors of GPS while using the approximate, analytical method adopted here. Figure 2 shows the mean of the expected errors in the normalized potential coefficients, per degree ($[$degree variance$/(2n+1)]^{1/2}$), as a function of the spherical harmonic degree n. The curves for the best and worst cases are very close to each other, narrowly bracketing the actual error, except at very low degrees. Clearly, unresolved biases and orbit errors (both low frequency effects) are the main reason for the low-degree departures. There is a gradual raise followed by a quick exponential one (appearing in the log-linear plot as a straight line), mostly due to attenuation of the signal with height. Where this line intercepts the spectrum of the full gravitational signal (top), the error is 100% of the signal, and the correponding degree n indicates the maximum resolution possible with the data. In this case this degre is close to n = 65, so the size of the smallest detail of the gravity field that can be resolved on the earth's surface is about 300 km, when using GPS data from GP-B. Figure 2 also shows the accuracy spectra of the gravity model GEM-T1, and of those models likely to result from the combination of conventional tracking with altimetry in the early 1990's (dotted line). GP-B/GPS models are likely to be more than two orders of magnitude better through degree and order 20, and substantially better beyond that. The improvement at low degrees looks particularly impressive.

161
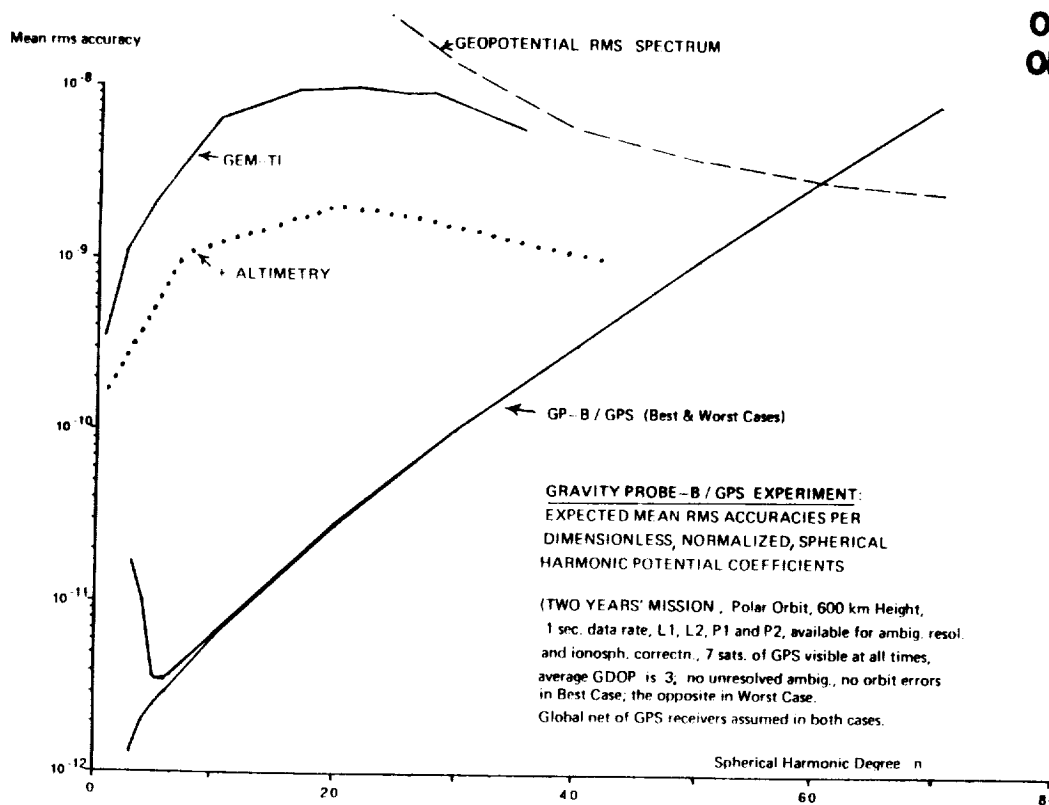
Figure 2. Mean accuracies per degree of normalized potential coefficients estimated with GP-B/GPS data, best and worst cases (as explained in text).

The coefficient errors, translated into rms cumulative geoid errors, are shown in Figure 3. The geoid error grows by about one order of magnitude every ten degrees, reaching 10 cm at about degree 40.
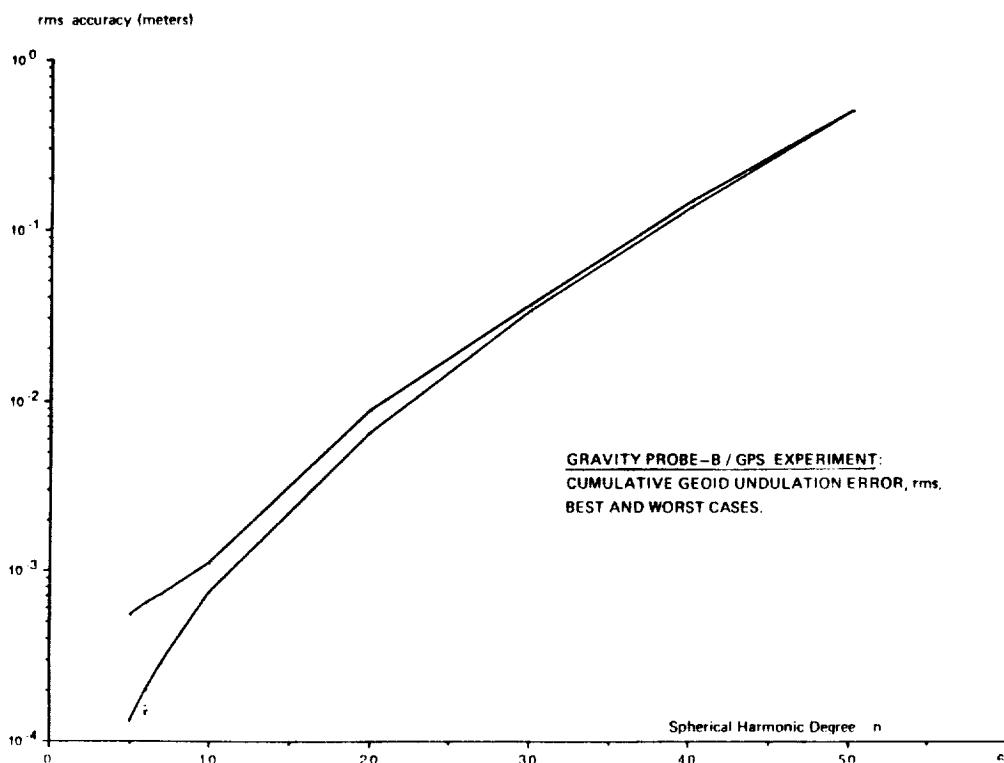
Figure 3. Cumulative geoidal undulation errors per degree, corresponding to the potential coefficient accuracies shown in Figure 1.

162

The accuracies of the spectral powers of various signals of geophysical interest are compared to the accuracies of the potential coefficients in Figure 4. At the top is the spectrum of the mean sea surface topography, associated with the average global circulation (obtained from the charts of Levitus). The spectrum of the gravitational effects of the M2 tide (according to Schwiderski's model), and of two years of post-glacial rebound are shown as well. In all three cases, the accuracy of the geopotential coefficients is considerably smaller than the variance of the signal, suggesting that a good separation of these geophysical signals is possible. The results are, if anything, pesimistic for the tides; even from the much less powerful conventional tracking data used for GEM-T1, a good deal of low-degree information on M2 and other major ocean tidal components has been extracted, mostly from spacecraft in much higher orbits than GP-B. This is possible because there are orbital resonances associated with the tides, and not considered here, that can produce large perturbations in the motions of spacecraft.

mean rms accuracy

MEAN SEA SURFACE TOPOGRAPHY
(LEVITUS)

10^{-2} E FULL TENSOR GRADIOMETER
(6 months, 160 km, 4 sec. data rate)

GP–B/GPS (Best & Worst Cases)
(2 years, 600 km, 1 sec. data rate for
L1, L2, P1, P2 + global terrestrial net
of GPS receivers).

GRAVITY PROBE–B / GPS EXPERIMENT:
COMPARISON OF EXPECTED MEAN RMS
ACCURACIES WITH THOSE OF GRADIOMETERS
AND WITH THE RMS SPECTRA OF IMPORTANT
OCEAN AND SOLID EARTH PHENOMENA.

GLACIAL
REBOUND
(2 YEARS)

M2 TIDE

10^{-4} E GRADIOMETER

Spherical Harmonic Degree   n

Figure 4. Accuracies of potential coefficients from GP-B/GPS data compared to those of conventional models and to the spectra of various geophysical phenomena.

REFERENCES

Colombo, O.L., Admont Summer School, Lecture Notes in Earth Sciences, Vol. 7, Math. and Numer. Techn. in Physical Geodesy, Springer-Verlag, 1986.
Martin, C.F., J.J. McCarthy, EG&G WASC, Planetary Sciences Department Report, Subcontract MCC-86-1002-001, August 1987.
Yunk,T.P., Melbourne, W., C.L. Thorton, IEEE Transactions on Geoscience and Remote Sensing, Vol. GE-23,4, pp. 450-457, July 1985.

Local Gravity Disturbance Estimation from Multiple-High-Single-Low Satellite-To-Satellite Tracking

Christopher Jekeli

Air Force Geophysics Laboratory, Hanscom AFB, Massachusetts

ABSTRACT

The idea of satellite-to-satellite tracking in the high-low mode has received renewed attention in light of the uncertain future of NASA's proposed low-low mission, Geopotential Research Mission (GRM). The principal disadvantage with a high-low system is the increased time interval required to obtain global coverage since the intersatellite visibility is often obscured by Earth. The U.S. Air Force has begun to investigate high-low satellite-to-satellite tracking between the Global Positioning System (GPS) of satellites (high component) and NASA's Space Transportation System (STS), the shuttle (low component). Because the GPS satellites form, or will form, a constellation enabling continuous three-dimensional tracking of a low-altitude orbiter, there will be no data gaps due to lack of intervisibility. Furthermore, all three components of the gravitation vector are estimable at altitude, a given grid of which gives a stronger estimate of gravity on Earth's surface than a similar grid of line-of-sight gravitation components. The proposed Air Force mission is STAGE (Shuttle-GPS Tracking for Anomalous Gravitation Estimation) and is designed for local gravity field determinations since the shuttle will likely not achieve polar orbits. The motivation for STAGE was the feasibility to obtain reasonable accuracies with absolutely minimal cost. Instead of simulating drag-free orbits, STAGE uses direct measurements of the nongravitational forces obtained by an inertial package onboard the shuttle. This paper analyzes the sort of accuracies that would be achievable from STAGE vis-a-vis other satellite tracking missions such as GRM and European Space Agency's POPSAT-GRM.

1. ASSUMPTIONS AND PARAMETERS

The observable in STAGE is the phase of the GPS carrier signal. It is differentiated twice to obtain the line-of-sight (LOS) acceleration of STS with respect to the GPS satellite. For the purpose of the analysis, it is assumed that this is the observed quantity and that it is a component of the difference between the gravity disturbance vectors at the two satellite locations. The actual difference between the LOS acceleration and a component of gravitation is insignificant on the average (see, e.g., Rummel 1980) and is therefore neglected here.

The error analysis is accomplished using the method of least-squares collocation which requires a covariance model for Earth's gravitational field (the Tscherning/Rapp model (Tscherning and Rapp, 1974) is used), the spatial coordinates of the data (sampled from Keplerian orbits), and a model for the noise of the data (assumed to be an uncorrelated process). Errors in the position of the satellites, though important, are not considered in this analysis.

Table 1 lists the adopted Keplerian elements of the satellites entering the analysis. The numbering of the GPS satellites is arbitrary. The two GRM satellites follow each other 300 km apart in the same orbit. Table 2 lists various (potential or fictitious) SST missions which possess the range of parameters to be considered in the analysis. The assumed acceleration accuracy of GRMa-GRMb (0.03 mgal) corresponds (according to an algorithm developed by Rummel (1980)) to the actual range-rate observational accuracy of 10^{-6} m/s (Keating et al., 1986); whereas GRM-POPSAT's assumed 0.7 mgal acceleration accuracy corresponds to 25×10^{-6} m/s (Reigber et al., 1987). All GPS tracking missions have an assumed accuracy in acceleration of 1 mgal for a 75 s integration time. The difference between STS-GPS#1 and STS-GPS#6 is the zenith angle of the LOS; with GPS#1 (#6) it is generally greater (less) than 45°. The designation nGPS means that the full 18-satellite configuration of GPS is used, but only three satellites track the low orbiter at a time. The three chosen satellites have the greatest degree of mutual orthogonality of the LOS vectors. In order to obtain somewhat comparable data distributions, a sampling interval of 75 s was chosen for each mission.

Table 1: SST satellites and their Keplerian elements (e=0, ω=0).

Keplerian Elements	STS	POPSAT	GPS#1	GPS#6	GRMa	GRMb
Altitude [km]	300.	7000.	20189.	20189.	160.	160.
Inclination [deg.]	28.5	98.	55.	55.	90.	90.
R.A. of Asc. Node [deg.]	45.	270.	0.	60.	90.	90.
Time of Perigee Pass. [s]	0.	0.	0.	-33505.	0.	-38.4

Table 2: SST missions and parameters defining resolution at altitude.

Parameters	GRMa-GRMb	GRM-POPSAT	STS-GPS#1	STS-GPS#6	STS-nGPS	GRM-nGPS
Int. Time [s]	4	10	75	75	75	75
Accur. [mgal]	0.03	0.7	1.	1.	1.	1.

The data points are limited to a square region symmetric about the equator and zero meridian. Only those points are included where the zenith angle to the high satellite is less than 100°. The estimated quantity is the 2°-mean gravity disturbance on Earth's surface. The error is estimated for a total of nine such quantities at coordinates in latitude and longitude: (±2°,±2°), (±2°,0°), (0°,±2°), (0°,0°). The error curves shown in the next section represent the root-mean-square (RMS) of these nine error estimates.

2. RESULTS

Figure 1 shows the RMS estimated error in 2°-mean gravity disturbances as a function of data density for the missions of Table 2. The data area is a 10°x10° square (hence a data density of 1 means that it contains 100 points more or less randomly distributed). Since the vertical component of the gravity disturbance is more highly correlated with itself than with the horizontal components, the error with STS-GPS#6 is much less than with STS-GPS#1; and a low-low mission is quite poor in comparison. For similar reasons, there is some, but not an overwhelming improvement in observing all three components of the gravity disturbance vector at altitude (STS-

nGPS). Major improvement comes by reducing the altitude (GRM-nGPS). The low errors of GRM-POPSAT arise from a combination of favorable factors: low altitude, short integration time, low data noise, and complementary orbital parameters.

In Figure 2, the RMS error is a function of data extent. For the high-low STS missions, little is gained by extending the data area beyond a certain size. Because of the longer correlation length of the horizontal gravity disturbance, a wider area is required for the low-low mission.

The instability of the GPS clock frequency dominates the data noise for the GPS tracking missions. It is assumed that all errors in the error budget not associated with this instability have a combined standard deviation of 0.5 mgal. The clock instability is characterized by the Allan variance which is often modelled as inversely proportional to the integration time. It is assumed here that the acceleration noise due to this instability is proportional to the Allan standard deviation divided by the integration time (Upadhyay et al., 1988). By monitoring the short-term fluctuations of these clocks at ground tracking stations having more stable clocks, Upadhyay et al. (1988) estimate that a hundred-fold improvement in the Allan variance can potentially be achieved. Figure 3 shows the RMS error of estimation as a function of integration time for the two multiple-high-single-low SST missions. Increasing the integration time decreases the data noise, but more of the shorter wavelengths of the gravity field are obliterated. Conversely, as the integration time decreases, the observations are more sensitive to the short-term fluctuations in the gravity
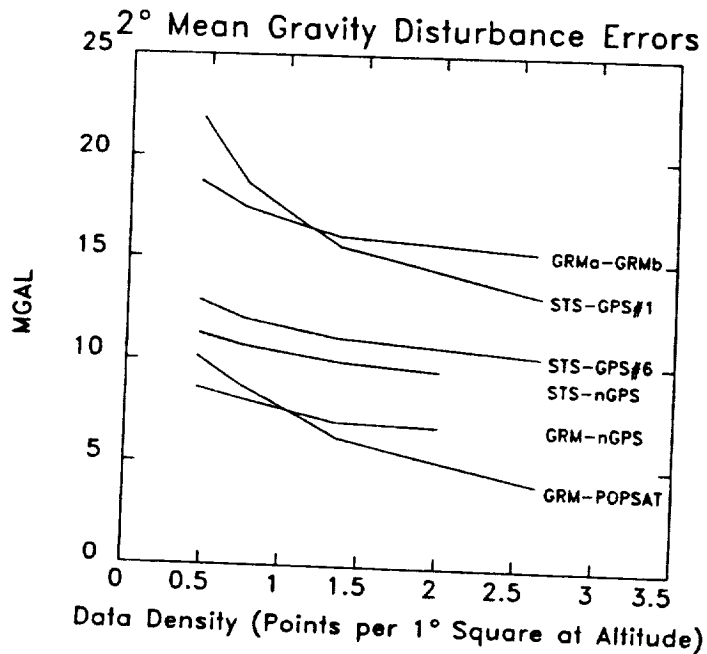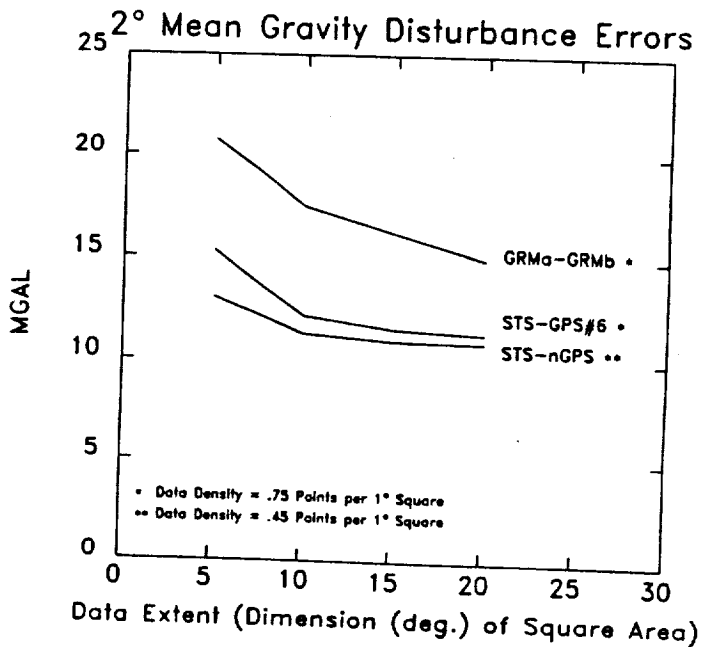

Figure 1

Figure 2

field, but the signal-to-noise ratio is smaller. Therefore, there is a definite optimum integration time for a given Allan variance. An improvement by a factor of 10 in the Allan variance gives a total data noise of 1 mgal at 75 s integration time. A 90-fold improvement implies a total data noise of 1 mgal with a 37 s integration time. The optimal integration time also depends on the altitude of the low orbiter.
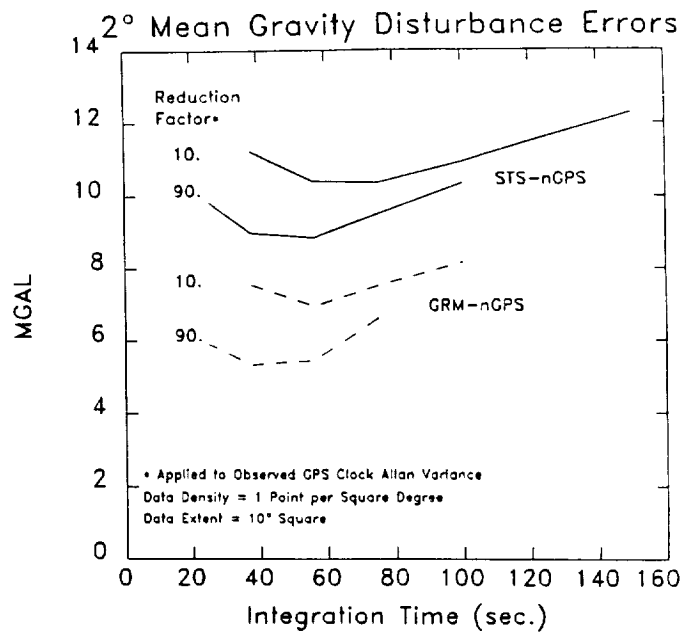

Figure 3

2° Mean Gravity Disturbance Errors

3. CONCLUSION

Although not as accurate as proposed dedicated gravity mapping missions, satellite-to-satellite tracking using the GPS can contribute to an improvement of present models of Earth's gravity. Even STAGE, to be viewed as a demonstration of the concept, would improve the model locally over land areas, such as parts of Asia, Africa, and South America.

REFERENCES

Colombo, O.L. (1981): Global geopotential modelling from satellite-to-satellite tracking. Report No. 317, The Department of Geodetic Science and Surveying, The Ohio State University, Columbus, Ohio.

Keating, T. et al. (1986): Geopotential Research Mission, science, engineering, and program summary. NASA Technical Memorandum No. 86240, NASA Goddard Space Flight Center, Greenbelt, Maryland.

Reigber, C. et al. (1987): Study of a satellite-to-satellite tracking gravity mission. ESA Report, Contract No. 6557/85/NL/PP(SC), Munich.

Rummel, R. (1980): Geoid heights, geoid height differences, and mean gravity anomalies from "low-low" satellite-to-satellite tracking - an error analysis. Report No. 306, The Department of Geodetic Science and Surveying, The Ohio State University, Columbus, Ohio.

Tscherning, C.C. and R.H. Rapp (1974): Closed covariance expressions for gravity anomalies, geoid undulations, and deflections of the vertical implied by anomaly degree variance models. Report No. 208, The Department of Geodetic Science, The Ohio State University, Columbus,Ohio.

Upadhyay, T.N., D.B. Cox, and C. Jekeli (1988): STS-GPS Tracking for Anomalous Gravitation Estimation - STAGE experiment. Presented at the Sixteenth Gravity Gradiometer Conference, Colorado Springs, Colorado

SATELLITE-TO-SATELLITE TRACKING EXPERIMENT FOR
GLOBAL GRAVITY FIELD MAPPING*

Triveni N. Upadhyay
Mayflower Communications Company, Inc., Reading, MA 01867

Christopher Jekeli
Air Force Geophysics Laboratory, Hanscom AFB, MA 01731

Introduction

The satellite-to-satellite (STS) tracking concept for estimating
gravitational parameters offers an attractive means to improve on
regional and global gravity models in areas where data availability is
limited. The extent to which the STS tracking measurements can be
effectively utilized in global field models depends primarily on the
satellite's altitude, number of satellites, and their orbit
constellation. The estimation accuracy of the gravity field recovery
also depends on the measurement accuracy of the sensors employed in the
STS tracking concept. A comparison of the obtainable accuracies in the
gravity field recovery using various STS tracking concepts (e.g., high-
low; low-low) was presented by Jekeli [1].

This paper summarizes the results of a feasibility study for a specific
realization of the STS high-low tracking concept. In this realization,
the high altitude satellites are the GPS satellites (altitude
approximately 20,200 km), and the low orbit satellite is the space
shuttle (orbiter). The GPS satellite constellation consists of 18
satellites in 6 orbital planes inclined at 55° (Kruh, et al [2]), The
shuttle orbit is at approximately 300 km, with an inclination of 30°.
This specific configuration of high-low satellites for measuring
perturbations in the gravity field is named the Air Force STAGE
(Shuttle-GPS Tracking for Anomalous Gravitation Estimation) mission.
The STAGE mission objective is to estimate the perturbations in gravity
vector at the shuttle altitude to an accuracy of 1 mgal or better.
Recent simulation studies (Jekeli [1], Upadhyay and Priovolos [3]) have
confirmed that the 1 mgal accuracy objective is near optimum for the
STAGE mission.

Measurement System Concept

The STAGE measurement system concept involves the measurement of total
forces acting on the shuttle using precision GPS carrier phase
measurements from four or more GPS satellites and the measurement of
non-gravitation forces using a precision IMU accelerometer package.

From these GPS and IMU measurements we estimate the perturbations in gravity vector at the shuttle orbit. There are several advantages of the STAGE mission which makes it attractive, among other STS concepts, for gravity field estimation. These advantages are: (1) the continuous visibility of the low satellite (the shuttle) from the high satellite (GPS satellites); (2) measurement of the estimated line-of-sight accelerations to three or more GPS satellites results in determination of the gravity vector instead of 1 component recovery; (3) low cost of the mission because the major cost items associated with the satellites, i.e., GPS and the shuttle, are already funded. In addition to these advantages of the STAGE mission for gravity estimation, another important benefit of this Air Force mission is that the STAGE data will support other DoD and NASA objectives of precision space navigation and precision pointing and tracking in space, e.g., SDI and Space Station. The STAGE payload for a shuttle flight consists of : (1) a multi-channel GPS receiver utilizing existing upper and lower fuselage installed antennas on the orbiter; (2) an experimental IMU consisting of strapdown RLG (ring laser gyro) and accelerometer assembly; (3) an electronic processing assembly to control the experiment hardware and to integrate the orbit timing buffer; and (4) a flight recorder with ground support equipment provisions.

Results

We have made a preliminary selection of the payload hardware (i.e., GPS receiver, IMU, recorder) to carryout the STAGE mission. A payload integration study for the STAGE mission was carried out by Rockwell International, Space Transportation Systems Division, which has lead to the recommended installation configuration, as shown in Figure 1. In this installation configuration the GPS receiver, the processor and the recorder will be installed in the crew compartment (area L-10), and the IMU will be installed near the C.G. of the shuttle, as shown. The GPS receiver will utilize the existing upper and lower GPS antennae.

The feasibility study for the STAGE mission involved a detailed error analysis to determine whether or not the 1 mgal measurement accuracy can be achieved. The analysis (with support from EG&G Washington Analytical Services Center) considered all the major error sources and their affect on the measurement accuracy. In particular, we considered the GPS receiver measurement noise, phase bias, satellite clock error, GPS orbit errors caused by uncertainty in the geopotential field, solar radiation pressure, tracking station location error, etc., and the IMU errors caused by gyro and accelerometer bias, scale factor errors and misalignment. The results of this analysis, supported by simulation results, indicated that the STAGE mission objective of 1 mgal accuracy at the shuttle orbit can be realized (for a 75 second averaging) provided that certain measures are taken to mitigate the effect of the primary error sources. The primary errors identified in this study are: GPS satellite clock errors, IMU accelerometer bias error, and the IMU misalignment error. Techniques to mitigate the effect of these primary errors are under investigation. An IMU transfer alignment (between the shuttle IMU and the STAGE IMU) technique which employs the shuttle

GRAVITY ANOMALY ESTIMATION USING GPS MEASUREMENTS
ONBOARD THE STS

ORBITER EXPERIMENT INSTALLATION

EIMU

X₀1191

ANTENNA CABLE (EXISTING)

X₀576

EXPERIMENT HARNESS

UPR GPS ANTENNA (EXISTING)

L-10 VOL

LWR GPS ANTENNA (EXISTING)

ANTENNA CABLE (EXISTING)

Rockwell International
Space Transportation
Systems Division

Figure 1

L-10 volume includes
GPS Receiver, Processor
and Recorder - Crew
Module
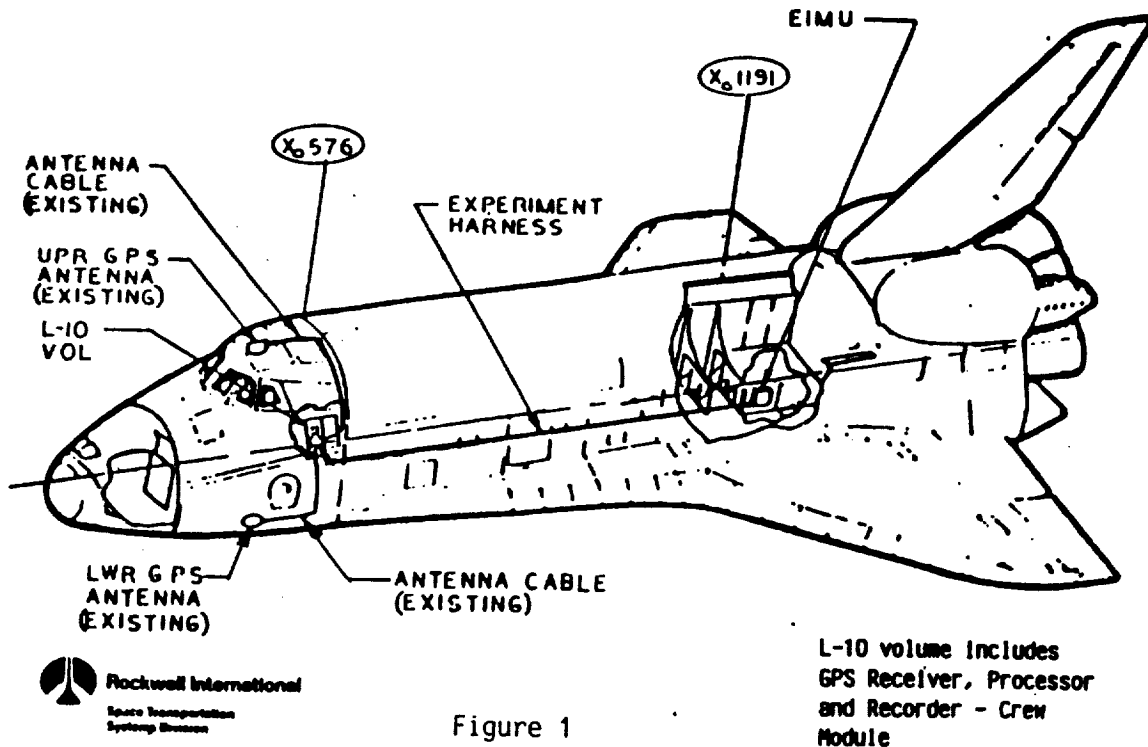
rotation maneuvers has been developed and is being evaluated. We believe that the on-orbit transfer alignment accuracy goal of 1 mrad for the STAGE mission can be achieved. Bias and scale factor errors in the accelerometers are controlled similarly by special on-orbit calibration techniques. These techniques are proven, and we anticipate an accuracy of 0.13 mgal. The largest source of error is the instability of the GPS clock frequency as described by its Allan variance. By monitoring the short-term fluctuations of the GPS clocks at ground stations possessing more stable clocks, it is possible to model corrections to the observed phase and reduce the effective clock error by one to two orders of magnitude. This is an essential component of data processing to bring the gravitational acceleration error below 1 mgal.

While processing techniques to further improve the measurement accuracy for the STAGE mission are in development, we feel very confident in reporting that a payload hardware configuration has been developed and the baseline STAGE configuration is compatible with shuttle mission. The STATE mission can be flown on future shuttle flights on a non-interfering basis.

References

1. Christopher Jekeli, "Local Disturbance Estimation from Multiple High-Single-Low Satellite-to-Satellite Tracking", Paper presented at the Chapman Conference on Progress in the Determination of Earth's Gravity Field, Ft. Lauderdale, Florida, September 1988.

2. P. Kruh, et al, "A Strategy for Buildup to the Operational NAVSTAR/GPS Constellation", Proceedings of the Institute of Navigation, National Aerospace Conference, March 1983.

3. Triveni Upadhyay and George Priovolos, "STS-GPS Tracking Experiment for Gravitation Estimation - Final Program Status Briefing", Air Force Geophysics Laboratory, Hanscom, AFB, MA, Contract No. F19628-86-C-0136, 7 October 1988

A DISCUSSION OF OBSERVATION MODEL, ERROR SOURCES AND SIGNAL SIZE FOR SPACEBORNE GRAVITATIONAL GRADIOMETRY

R. Rummel, R. Koop and E.J.O. Schrama

Faculty of Geodesy, Delft University of Technology, Delft, Netherlands

Various space concepts have been discussed during the past 20 years for a global improvement of our knowledge of the Earth's gravity field. They reach from high-low and low-low satellite-to-satellite tracking via tethered satellite gradiometers to sophisticated super-conducting gradiometers, currently under discussion. The purpose of this article is to show that starting from one basic equation three criteria are sufficient to typify the various concepts and define the underlying observation model. Furthermore the different error sources, in particular the time varying part of self-gravitation, and the expected signal size of all six gravity gradient components shall be discussed.

Assume two proof masses A and B in free fall are observed from a moving ortho-normal triad, see Figure 1. Then the relative acceleration $d\ddot{x}_i$, between A and B relative to their distance dx_j (components i and j = 1,2,3) obey the following conservation law:
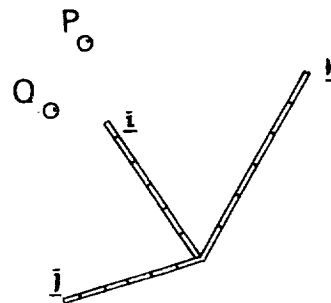

Figure 1.

$$\frac{d\ddot{x}_i}{dx_j} + 2\,\Omega_{ki}\,\frac{d\dot{x}_k}{dx_j} + \dot{\Omega}_{ij} + \Omega_{ik}\,\Omega_{kj} - V_{ij} - \frac{f_i(A)-f_i(B)}{dx_j} = 0 \qquad (1)$$

In eq. (1) it is $2\Omega_{ki}\dfrac{d\dot{x}_k}{dx_j}$, $\dot{\Omega}_{ij}$, and $\Omega_{ik}\Omega_{kj}$ the Coriolis, inertial rotation, and centrifugal term, respectively, with Ω_{ik} the angular velocities; $V_{ij} = \dfrac{\partial^2 V}{\partial x_i \partial x_j}$ are the gravitational gradients, and $f_i(A)$ and $f_i(B)$ non-gravitational accelerations acting on A and B. If the above experiment is carried out at satellite altitude and if the purpose is to determine V_{ij}, we speak of spaceborne gradiometry.

In order to derive V_{ij} as accurate as possible obviously the measurement precision has to be as high (10^{-2} to 10^{-4} E) and the satellite altitude as low as possible (preferably below 200 km). However, three criteria are sufficient to identify the various configurations. These are (1) the orientation of the instrument frame or triad, being either space stable or Earth pointing, (2) the motion of the proof masses, either free drifting or constrained to linear or rotational movement and (3) the shielding against non-gravitational forces, either by an active drag-free system, or by enclosing the proof masses in the satellite but the measurement triad rigidly fixed to its skin, or with no shielding at all. The choices on these three criteria decide about the form eq. (1) takes and what interpretation its terms acquire. Take two examples: In case the instrument frame is maintained space stable the three terms containing Ω and $\dot{\Omega}$ disappear. Or, for an active drag-free system and the proof masses constrained linearly to the triad e.g. by an electric spring, $d\ddot{x}$ and dx become zero and $f(A)$ and $f(B)$ the measured specific forces.

These choices decide as well what the observable accelerometer signal along the three axes will be from which the gradiometer components are derived. Take for example an Earth pointing gradiometer with no active drag-free control, with the x-axis along track, the y-axis cross track, and the z-axis radial and with the proof masses of the orthogonal set of accelerometers constrained to the axes. The dimension of the gradiometer is assumed to be 1 m and its center close to the center of mass of the spacecraft. Then the average accelerations (DC-part) listed in Table 1 shall be typically measured along the three axes. The variations in signal (AC-part) are less than $\dfrac{1}{100}$ of these values.

TABLE 1 : Acceleration Signal (units $10^{-5}ms^{-2}$)

	gravitational	centrifugal	drag
x (along)	0.15	0.15	2
y (across)	0.15	0	0
z (radial)	0.31	0.15	0

We observe that the along track component is heavily affected by the drag, whereas the cross-track component remains largely free from non-gravitational perturbations. This is one of the main reasons, why for the ARISTOTELES mission a plane (y-z)-two dimensional gradiometer is considered.

Once a decision is made about a specific gradiometer design, it is important to develop a realistic error model. In order to get some structure into the various error sources, we divide them into (1) instrument errors, (2) satellite related errors and (3) geodetic gravity recovery model errors. The instrument errors depend largely on the chosen design. Adequate models can only be developed in cooperation with the instrument designer. At this point we refer to (Reinhardt et al.,1982), (Balmino et al., 1985), (Paik & Richard, 1986), or (Sepers, 1986). Satellite related errors are e.g. thermal, electro-magnetic or vibrational effects, deviations from common mode rejection of drag effects due to non-linearities (Barlier & Berger, 1988), self-gravitation, or attitude related errors. We studied the time-varying self-gravitation effect due to fuel consumption. Assuming 1000 kg fuel consumed over half a year the main effect is - depending on the symmetry of the tank configuration - a drift of about 50E per half year. Additional sloshing effects could reach 2-5 E and are to be avoided. Error sources related to the gravity field recovery model reach from the proper modelling of the sampled signal, via the effects of induced symmetries in the adjustment models to stability and convergency problems of downward continuation. Their study requires more attention in the forthcoming years.

In order to get an impression of the size of the gravitational signal, all six gradient components were generated on a global 1^{0}x 1^{0}

174

grid, with the OSU-180 field (Rapp, 1986) at an altitude of 200 km. Then a spherical harmonic analysis was carried out on each of the components separately and the degree variances c_n and degree-order variances c_{nm} were computed. The degree-order variance is defined as $c_{nm} = c_n/(2n+1)$ with n degree and m order and represents the square of the expected average size of an individual spherical harmonic coefficient. The result up to degree 180 is given in terms of the r.m.s. values of c_{nm} in Figure 2. As expected, the (zz)-component is roughly half an order of magnitude greater than the (xx), (yy), (xz), and (yz) component, which are in turn half an order of magnitude greater than (xy). This implies among others that most emphasis should be put on a precise recovery of the (zz) component.
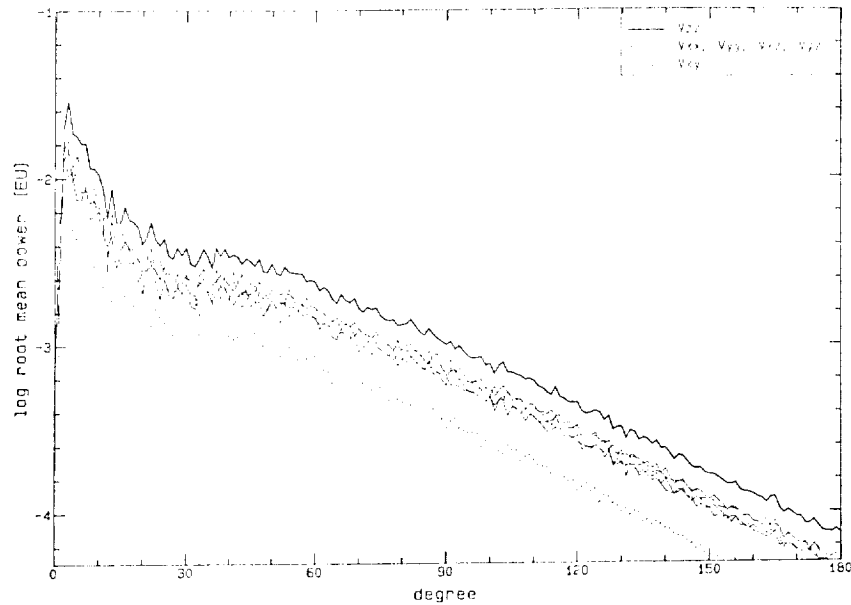
Figure 2.

REFERENCES

Balmino, G., F. Barlier, C. Bouzat, R. Rummel, P. Toubout; proposal to ESA, Toulouse, 1985.

Barlier, F., C. Berger ; CIGAR.CERGA.140/CMTR/1, ESA contract 7521/87/F/FL, 1988.

Paik, H.J., J.P. Richard ; NASA Contractor Report 4011, Univ. of Maryland, 1986

Rapp, R.H.; Dept. Geodetic Science, 322, Ohio State University, Columbus, 1981.

Reinhardt, V.S., F.O. Von Bun, J.P. Turneaure ; proc. IEEE Position Location and Navigation Symposium, 1982.

Sepers, J.; diploma thesis, Delft, 1986.

STUDIES OF AN ORBITAL GRADIOMETER MISSION

B. E. Schutz, J. B. Lundberg, S. Bettadpur, and B. D. Tapley

Center for Space Research, The University of Texas at Austin

Abstract

The goal of using an orbital gradiometer mission to provide an accurate (1-2 mgal), high resolution (1° by 1°), global map of the earth's geopotential is currently being investigated. This investigation involves the simulation of the satellite ephemeris and the corresponding gradiometer measurements which can be used in the study of various techniques and methodologies that have been proposed to recover the parameters used in modeling the geopotential. Also, the effects on the mission of various time varying forces acting on the spacecraft have been included in the studies.

Introduction

The goal of these studies is to create an accurate ephemeris and set of 'perfect' gradiometer measurements to study various techniques to recover the parameters of the geopotential model and to study the effects of various force model, ephemeris, and measurement uncertainties on the recovery of the geopotential parameters. This research effort began by assuming a Geopotential Research Mission (GRM) scenario involving a dual satellite configuration in which the principal measurements are the relative range-rates between the satellites. In the initial simulations, a geopotential model complete through degree and order 180 was used (Schutz et al., 1987). The GRM simulation was extended to include a geopotential model complete through degree and order 360 (Schutz et al., 1988). The satellites in the GRM scenario were assumed to be in 'frozen', polar orbits with a mean altitude of 160 km and a repeat ground track period of 32 sidereal days. For these simulations the earth was assumed to have a constant angular velocity and a static geopotential.

To create as accurate an ephemeris as resources would permit, the equations of motion were solved numerically using Encke's formulation and a class II, fixed mesh multistep algorithm of order 10. The simulations were carried out on the CRAY X-MP/24 computer at the University of Texas using single precision arithmetic which represents floating point numbers using a 48 bit mantissa and a 16 bit exponent. The first simulation (S8705) was carried out using an integration stepsize of five seconds and required 5.6 hours of CPU time. The second simulation (S8703) was carried out using an integration stepsize of four seconds and required 19.2 hours of CPU time. The nearly four fold increase in CPU time reflects the increase in the size of the geopotential model from degree and order 180 to 360. In both simulations the ground track closed to within two kilometers after 32 sidereal days (White, 1987).

In addition to creating these simulations, special studies were carried out on the effects of solid and ocean tides, luni-solar and planetary gravitational forces, and the mass distributions caused by ocean eddies (McNamee, 1986) on the relative range-rate measurements. A study of the disturbance compensation system (DISCOS) was also carried out to verify the proposed control law and estimates of fuel consumption (Antreasian, 1988).

Simulation of a Gradiometer Mission

The products of the GRM simulation have been used to simulate the orbital gradiometer mission. The orbit for the gradiometer mission is assumed to have the same characteristics as GRM, i.e, a polar, frozen orbit with a mean altitude of 160 km and a repeat ground track period of 32 sidereal days. The ephemeris computed for the lead satellite of simulation S8703 is taken to be the true ephemeris for the gradiometer mission. The true gradiometer measurements are simulated by the gravity gradient tensor which is computed using the true ephemeris and a geopotential complete to degree and order 360. The measurement interval is taken to be the same as the ephemeris interval, i.e., four seconds.

Analysis of a Simulated Gradiometer Mission

The simulated true ephemeris and gradiometer measurements can be used to study the orbit determination requirements of the mission, i.e., the effects of orbit uncertainties on the solution for the geopotential parameters, and to study various techniques for recovering the geopotential parameters using gradiometer measurements. The simulation also provides a common data set for the evaluation of results from different researchers and a basis for comparison of gravity gradient computations.

Various tracking systems may be considered for this mission including GPS, satellite laser ranging, PRARE, DORIS, or other suitable systems. Since some form of global tracking will be required for the mission, GPS will probably be part of the overall tracking system (Yunck et al., 1986). Whichever tracking system is used, there are two possible approaches that can be used to determine the orbit of the satellite and recover the geopotential parameters. The first, or gradiometer, approach uses only the tracking system information to establish a nominal orbit for the mission and, once the nominal orbit is computed, uses the gradiometer measurements to recover the geopotential parameters. The second, or dynamical, approach involves using the tracking data along with the gradiometer measurements to determine the orbit and recover the geopotential coefficients simultaneously. The fundamental difference between these two approaches is that the first approach is similar to creating a gravity surface by adjusting the geopotential parameters while the second approach is dependent on the orbit perturbation frequency spectrum including the amplified effects due to resonance.

To illustrate the gradiometer approach, a simulation was carried out in which the observations were the gradiometer measurements computed along the true orbit using only the geopotential coefficients from degree and order 10 through degree and order 15. The gradiometer measurements were used with a least squares algorithm in attempt to recover the geopotential coefficients for arc lengths of up to 60 hours. To represent the effect of orbit uncertainties on the solution, the partial derivatives of the observations with respect to the coefficients were evaluated along a nominal orbit which is randomly perturbed in the radial direction from the true orbit. The accuracy of the solution for the coefficients is evaluated by computing the absolute value of the normalized differences between the estimated coefficients and the true coefficients, i.e.,

$$\delta C = \frac{C_{TRUE} - C_{ESTIMATED}}{C_{TRUE}}$$

Figure 1 shows the results for the solution of $C_{14,12}$ which is typical of all the solutions. The effects of radial orbit uncertainties (1σ) of 0 cm, 5 cm, 30 cm, and 50 cm are represented in

Figure 1. For the case of no orbit error, nine to ten significant figures of $C_{14,12}$ are recovered. For the case of 50 cm radial uncertainty, six to seven significant digits are recovered. This is a very limited example since the solution involved a relatively small number of coefficients and a relatively low degree and order coefficient.

To illustrate the dynamical approach, nominal orbits were determined using the entire 32 day, true ephemeris (S8703) as simulated tracking data and the Goddard Earth Model 10B (GEM-10B) as the *a priori* gravity model while solving for selected resonance coefficients. The selected resonance coefficients were the first two pairs (C_{nm} and S_{nm}) of orders 33, 49, and 82. The results of these solutions are given in Table 1. The results indicate that the resonance terms will have amplified effects in the dynamical solution for the gravity field.

Future Research

Future research of the orbital gradiometer mission includes studies of the gradiometer or dynamical approaches to determine the orbit of the satellite and recover the geopotential parameters, studies of the effects of various error sources on the solutions including tidal errors, nontidal ocean phenomena, and spacecraft attitude errors, and to investigate the adequacy of a six month mission.

Acknowledgements

This research is sponsored under NASA Grant NAG5-528. The authors would like to acknowledge the contributions and support for this project by the Center for High Performance Computing at the University of Texas.

References

Antreasian, P. G., "An Orbit Simulation Study of a Geopotential Research Mission Including Satellite-to-Satellite Tracking and Disturbance Compensation Mechanism," Thesis, Department of Aerospace Engineering and Engineering Mechanics, The University of Texas at Austin, May 1988.

McNamee, J. B., "The Perturbation of Low Altitude Satellite Motion Due to the Presence of Ocean Eddies," Thesis, Department of Aerospace Engineering and Engineering Mechanics, The University of Texas at Austin, December 1986.

Schutz, B. E., B. D. Tapley, J. B. Lundberg, and P. Halamek, "Simulation of a Geopotential Mission for Gravity Studies," *manuscripta geodaetica*, Vol. 12, 1987, pp. 51-63.

Schutz, B. E., J. B. Lundberg, L. K. White, and P. G. Antreasian, "Developments in the Simulation of a Geopotential Research Mission," AIAA/AAS Astrodynamics Conference, Minneapolis, Minnesota, August 15-17, 1988, pp. 323-328.

White, L. K., "Simulation and Analysis of a Geopotential Research Mission," Center for Space Research, Department of Aerospace Engineering and Engineering Mechanics, The University of Texas at Austin, 1987.

Yunck, T. P., S. C. Wu, and J. T. Wu, "Strategies for Sub-decimeter Satellite Tracking with GPS," IEEE Position Location and Navigation Symposium, November 1986, Las Vegas, Nevada, pp. 122-128.

Table 1			
Resonant Effects on the Orbit Residuals			
RMS (meters)	with order 82[*]	with orders 33,82[*]	with orders 33,49,82[*]
radial	64.9	60.4	58.1
transverse	619.5	180.3	148.6
normal	31.8	21.7	33.8

[*] after small adjustments in position vector
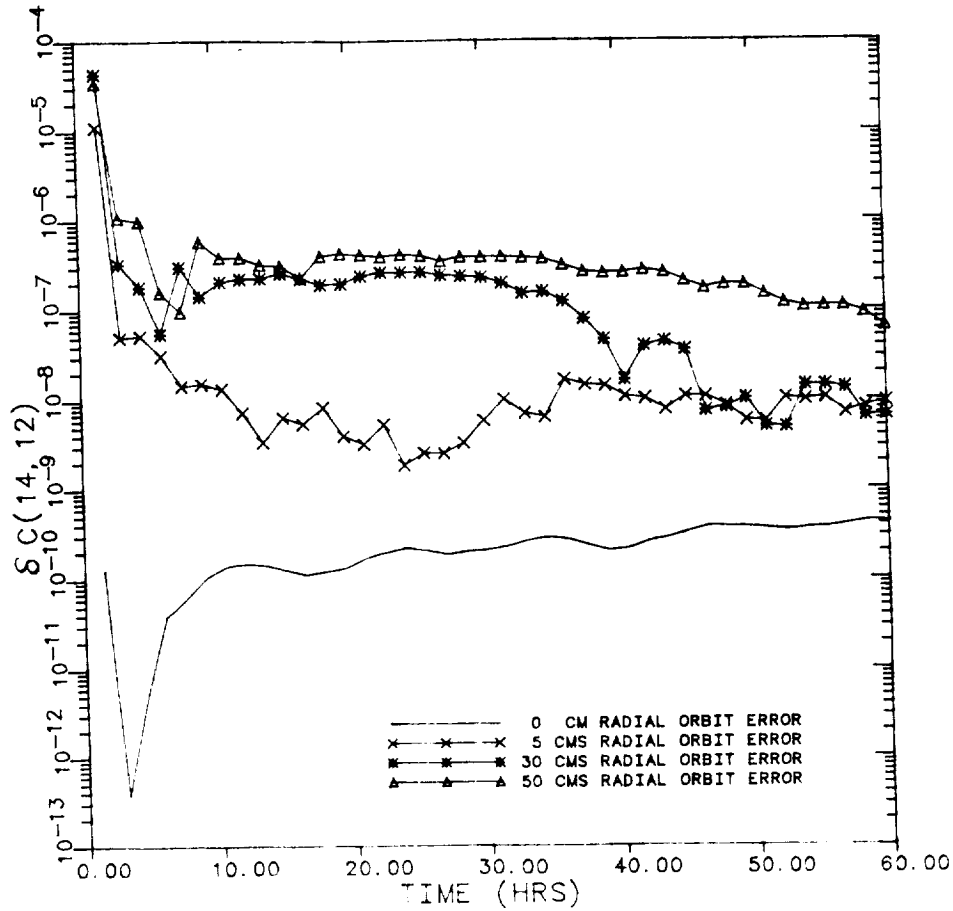

Figure 1

Normalized errors in the solution for $C_{14,12}$ as a function
of radial orbit uncertainty and orbital arc length

179

ARISTOTELES - A EUROPEAN APPROACH FOR AN EARTH GRAVITY FIELD RECOVERY MISSION

R. Benz, H. Faulks, M. Langemann
Dornier-System GmbH, 7990 Friedrichshafen, FRG

Abstract

Under contract of the European Space Agency a system study for a spaceborne gravity field recovery mission has been performed, covering as a secondary mission objective geodetic point positioning in the cm range as well. It was demonstrated that under the given programmatic constraints including dual launch and a very tight development schedule, a six months gravity field mission in a 200 km near polar, dawn-dusk orbit is adequate to determine gravity anomalies to better than 5 mgal with a spatial resolution of 100 x 100 km half wavelength. This will enable scientists to determine improved spherical harmonic coefficients of the Earth gravity field equation to the order and degree of 180 or better.

Introduction

A detailed knowledge of the Earth gravity field is of great interest in geophysical sciences and their applications. In addition orbit determination of satellites will benefit significantly from an improved gravity field model. Although a large amount of local data are available, on a global scale a large part of the Earth has not so far been covered, because of obvious natural, political and cost constraints. A spaceborne system can overcome these constraints and can provide consistent and precise data on a global scale. A comprehensive outline of the benefits of such a mission was given by the SESAME workshop [1] (Solid Earth Science & Application Mission for Europe).

In the framework of the Earth Observation Preparatory Programme (EOPP) of the European Space Agency a system study has been performed to demonstrate the feasibility of such a programme under special constraints including dual launch, a tight development schedule and a limited financial budget. The name of the mission ARISTOTELES stands for 'Application and Research Involving Space Techniques Observing The Earth field from a Low Earth Orbit Satellite' and is a reminder of the great philosopher Aristotle who was the first to speak of gravity forces.

System Requirements

The principal scientific objective of the mission is a global gravity field determination to an accuracy better than 5 mgal in terms of gravity anomalies with a spatial resolution of 100 km half wavelength, where 1 mgal is equivalent to 10^{-5} m/s^2. The operational mission duration for gravity measurements is between 3 and 6 months. The orbit shall be quasi-circular, near polar with a mean altitude between 160 and 240 km, dependent

on the type of payload accommodation. The payload is a gradiometer comprising up to 8 ultrasensitive electrostatic accelerometers, here named GRADIO. As an optional mission part it is intended to raise the orbit after completion of the gravity mission to about 700 km altitude in order to perform point positioning for another 3 years.

The ARISTOTELES satellite is Earth oriented, 3-axis stabilized and shall be launched by an ARIANE 44 as lower passenger within SPELDA 10 together with ERS-2 (ESA Remote Sensing Satellite) or another Earth observation satellite. The nominal launch date is 1994. Kiruna ground station will be used for telemetry and telecommand on a time sharing basis with ERS-2. The gravity field requires an orbit restitution of better than 10 m in the radial direction.

Scientific Evaluation

Within the present study a gravity field recovery analysis has been performed in order to establish the system requirements based on the inter-relations between the instrument accuracy, the orbit altitude, the operational gravity mission duration, the tensor components to be measured and the gravity field accuracy to be met. The results indicate that on the one hand a maximum orbit altitude of 200 km is allowed, assuming a two dimensional instrument accuracy of 10^{-2} E.U. and half a year operational life time (see Figure 1). On the other hand this altitude is the lower limit for a fixed GRADIO accommodation on the non-drag-free satellite because of the maximum allowed acceleration tolerance requirement of $5 \cdot 10^{-5}$ m/s^2 for the accelerometers. A better performance of between 3 and 4 mgal can be expected in a lower altitude of about 180 km or less if a suspended GRADIO accommodation on a drag-free satellite were selected. For this option only a 3 months gravity field mission is required.

However, Figure 1 shows that even with the measurement of the two tensor components across track and radial T_{yy} and T_{zz} respectively, the scientific requirement can be just met from a 200 km orbit. Figure 2 underlines the importance of the instrument accuracy.

Mission Analysis

Using the dual launch with ERS-2, ARISTOTELES will be brought into an 780 km sun synchronous orbit with 10.30 h descending node local time. Within a drift period of about 9 months completed by final descent to 200 km the satellite moves into the operational orbit of the gravity mission. The drift period can also be used for point positioning measurements and is needed to calibrate the GRADIO instrument in space. Because
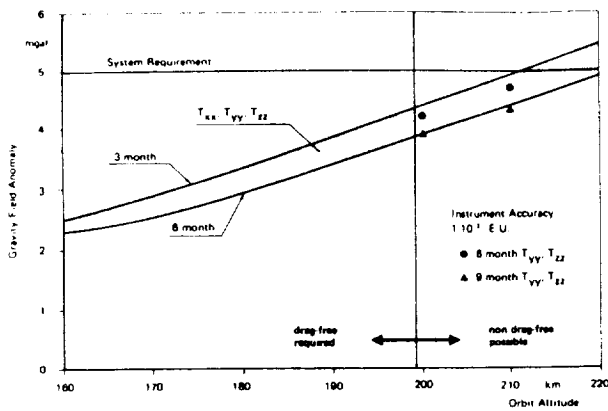
Fig. 1 : Relationship between System Performance and Main System Parameters (Instrument Accuracy 10^{-2} E.U.)
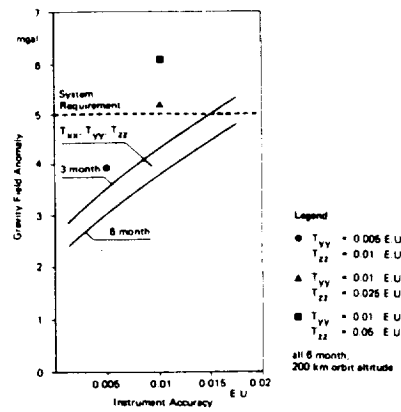
Fig. 2 : Influence of Instrument Accuracy on System Performance

of the Earth's gravity the GRADIO instrument cannot be fully tested on ground, therefore a relatively long period with low drag forces is very attractive to calibrate the instrument under low disturbance conditions.

Because of the large fuel consumption for the transfer and operational phase the originally required polar orbit must be shifted to a near polar, dawn-dusk orbit, advantageous for spacecraft design, but not covering a 600 km circle around the poles.

The optional point positioning mission for another 3 years or more is only possible when flying during the gravity mission above 200 km and using bipropellant fuel without driving the cross section area of the satellite to an unacceptable size and consequently to a higher fuel consumption during the gravity mission phase. A full mission scenario sketch is given by Fig. 3.

by the air drag must be compensated by nearly continuous thrusts with considerable amounts of fuel. Bipropellant fuel is then mandatory, because of the lack of qualified thrusters for hydrazine in this operational mode.

The alternative instrument accommodation option is the so-called non-drag-free version, with the GRADIO mounted isostatically on the satellite structure. Consequently, the maximum acceleration of the satellite has to be below $5 \cdot 10^{-5}$ m/s^2 demanding an orbit altitude above 200 km. In addition via cross coupling effects the air drag variations now impair the measurement and must be compensated by aerodynamic flaps. The proposed design requires that drag variations within the measurement bandwidth are damped out by a factor of one hundred.

Both instrument accommodation options have strong system impacts, and therefore a comprehensive system level trade-off had to be conducted.

Instrument Design

The primary instrument of ARISTOTELES is a gradiometer formed by a set of up to 8 ultrasensitive accelerometers and a calibration device. These accelerometers with a maximum resolution in the pico-g range and sensitive either in 2 or 3 axes, have to be grouped as symmetrically as possible in a 2D or 3D framework.

Each accelerometer itself consists of a proof mass and a caging with 6 pairs of electrodes. Figure 4 shows a laboratory model of a 2D electrostatic accelerometer. The theoretical resolution limit of the proposed device is

$$10^{-2} E.U. /\sqrt{Hz}$$

and the required bandwidth ($5 \cdot 10^{-3}$ Hz to 0.25). The maximum allowed acceleration to avoid saturation of the accelerometers is $5 \cdot 10^{-5}$ m/s^2.

In principle, two different ways of GRADIO accommodation have been studied: A drag-free accommodation, avoiding to the maximum extent the impact of surface forces on the GRADIO. The instrument is then magnetically suspended within the satellite, affected only by gravity forces, while the satellite flies around the instrument, accurately controlled by the attitude control system. In particular this accommodation option avoids air drag forces acting on the accelerometers and therefore allows flight below 200 km. However, the deceleration of the satellite

Major System Options

The dominant system options are related to the GRADIO instrument:

- Drag-free or non-drag-free GRADIO accommodation,
- 2D or 3D GRADIO,
- 2D or 3D accelerometers.

A trade-off dealing with more than 20 different GRADIO designs has resulted in two preferred solutions: Four 2D accelerometers located at the corners of a plate (planar solution) or either 6 or 8 3D accelerometers located at the corners of an octahedron or a cube. While the first solution is associated with a fixed GRADIO accommodation on the satellite, the second should be accommodated suspended to enable achievement of the high theoretical performance of this instrument. Based on the scientific evaluation mentioned above and on the very tight schedule, the planar gradiometer was selected as baseline (see Figure 6). For clarification it must be said that the 2D accelerometers measure in all 3 axis, but with degraded sensitivity in flight direction which is then of no use for gravity gradient measurements. However, this signal can support the attitude control system.

181

Fig. 5 : Layout of the Selected Planar GRADIO

Fig. 6 : ARISTOTELES Satellite Configuration

Fig. 3 : ARISTOTELES Mission Scenario

Fig. 4 : Laboratory Model of 2D Accelerometer

182

Orbit Determination

The restitution of the gravity gradient data requires an accurate knowledge of the orbit position. The 'a posteriori' orbit determination requirement is therefore

　　　10 m　　in radial direction and
　　　1.5 km　across and along track.

This requirement cannot be met by normal S-band tracking, but requires special equipment. For ARISTOTELES a Precise Range and Range Rate Microwave Tracking Equipment named MTS/PRARE similar to the PRARE system to be flown on ERS-1 will be used. Optionally the use of the Global Positioning System (GPS) is under discussion.

When using MTS/PRARE for orbit determination, with the same on-board equipment, geodetic point positioning can be performed by scientists, requiring only additional dedicated PRARE ground stations, to be operated independently by the scientists themselves.

Satellite Configuration

The GRADIO instrument has dictated all of the principal features incorporated in the satellite configuration. The need to fly GRADIO at the minimum possible altitude results in a significant drag force. To provide a mission of long enough duration for recovery of adequate scientific data, the effect of the drag must be minimised. The cross sectional area presented to the 'airflow' is thus reduced resulting in a long slender satellite body limited by accommodation constraints of the AR44 SPELDA 10 payload carrier assembly (see Figure 6). The electrical energy demand is large enough to require solar array wings as well as the body mounted solar arrays, but these must be edge on on the airflow again not only to minimise drag, but also to avoid large disturbance torques on the satellite and thereby affecting GRADIO. In consequence it is only possible to fly in near dawn-dusk orbits, placing a minor restriction on scientific return in relation to tidal effects from the sun.

That the GRADIO instrument measures the gravity field of the satellite as well, has unusual consequences for the satellite internal layout in addition to the above mentioned drag minimisation. The instrument must be placed not only at the centre of gravity of the vehicle, but this centre of gravity must also be the neutral point for the gravitational attractions of all components to minimise their influence. Symmetry is thus of major importance, and the heavier units should be placed as far away from GRADIO as possible. The supporting electronic subsystems contained in pods on the sides of the body meet this requirement in principle, while also assisting thermal stability close to GRADIO since significant variable heat generation is remote from the instrument.

The largest masses are however the fuel (approx. one ton in total) in the 16 tanks. Normally under manoeuvring accelerations the fuel in the tanks moves or 'sloshes'. To almost totally remove this effect, tanks with stable metal diaphragms are used, restraining the fuel to one end of the tank. The fuel used during the period of GRADIO measurements also is contained only in the outer tanks, i.e. furthest from GRADIO. The fuel in the inner tanks is used during initial manoeuvres to place ARISTOTELES in the correct orbit.

In addition, the symmetry requirement can only be met by positively monitoring fuel consumption from the individual tanks, in order to maintain the centre of gravity within fractions of a millimetre of the GRADIO centre.

Tab. 1 :　ARISTOTELES Satellite Properties

o	Satellite Mass	dry	960 kg
		launch	1990 kg
o	GRADIO Mass		65 kg
o	Power at Solar Array		1080 W
o	GRADIO Power Consumption		60 W
o	S-Band Telemetry		1 Mbps
o	Data Storage　(36h)		260 Mb

Subsystem Characteristics

The majority of the subsystems for ARISTOTELES are conventional in character with special attention being paid to satellite structural and thermal effects on GRADIO. However, the performance of the attitude and orbit control system is intimately linked with the orientation and control of GRADIO and thus to the quality of the instrument data output. Because the instrument is attached to the spacecraft structure, it is directly affected by drag forces and spacecraft disturbances, placing high demand on control accuracy.

Conclusions

The ARISTOTELES system study[2] proved that a spaceborne gradiometer can meet an Earth gravity field determination requirement of better than 5 mgal with a spatial resolution of 100 km half wavelength. The required orbit altitude is about 200 km or less with an instrument accuracy of better than 10^{-2} E.U. given that at least the tensor components Tyy (across track) and Tzz (radial) were measured. This is achieved by means of a 2D GRADIO directly attached to the satellite structure. Although a suspended accommodation of a 3D GRADIO with at least 6 3D accelerometers promises better results, the fixed GRADIO solution has been selected as baseline to meet the tight schedule which may not allow the more challenging approach. The lower instrument performance of the 2D fixed GRADIO can be partly compensated for by a gravity mission of six months instead of three and a high performance AOCS subsystem.

References

1) SESAME ESA Special Workshop, ESA SP-1080, Ising, FRG, March 1986

2) Benz, R. et al., ARISTOTELES Phase A Study, Final Report, Dornier-System GmbH, Friedrichshafen, FRG, 1988.

THE GRADIO SPACEBORNE GRAVITY GRADIOMETER:
DEVELOPMENT AND ACCOMMODATION

A. BERNARD

Office National d'Etudes et de Recherches Aérospatiales
BP 72, 92322 Chatillon Cedex, France

ABSTRACT

1. INTRODUCTION

The european ARISTOTELES mission aims at the determination of the Earth Gravity field at short wavelength with a global coverage. Gravity gradient measurements will be achieved during six months by the GRADIO instrument on board a dedicated satellite in a near dawn-dusk sun-synchronous orbit at an altitude of 200 km. The objective is an accuracy of better than 5 mgals for gravity anomalies, at ground level for blocks of $1° \times 1°$.

According to the present knowledge of the potential, the recovery of the higher spherical harmonics (degree and order greater than 30) is of main importance. This leads to focus on the variations of the measured components T_{ij} of the gravity gradient tensor, at frequencies greater than 5×10^{-3} Hz. The resolution, required for the gradiometer, is 10^{-2} Eötvos (i.e. 10^{-11} s^{-2}) with an averaging time of 4 s. [Balmino et al, 1984 ; Balmino and Bernard, 1986].

2. GRAVITY GRADIOMETRY ON BOARD A NON DRAG FREE SATELLITE

The components T_{ij} are determined by means of differential measurements between highly sensitive accelerometers composing the gradiometer [Runavot et al, 1983; Bernard et al, 1983]. Each of them measures the resultant $\overrightarrow{\gamma_i}$ of the effects of gravity gradient [T], angular motion $\left(\overrightarrow{\Omega}, \overrightarrow{\dot{\Omega}}\right)$ and acceleration $\overrightarrow{\Gamma}$ due to drag and radiation pressures.

Linear combinations of the measured $\vec{\gamma}_i$ allow us to determine separately the

components of: $\left[[- T] + [\Omega^2] \right]$, $\dot{\vec{\Omega}}$, $\vec{\Gamma}$.

The variations of $[\Omega^2]$ which cannot be distinguished from those of $[T]$ have to be minimized and estimated. This requires high performances for the attitude control and restitution: over periods of 200 s, the variations of $\vec{\Omega}$ and $\dot{\vec{\Omega}}$ must be less than 10^{-6} rad/s and 10^{-7} rad/s^2.

In practice, the accelerometric measurements are corrupted by mismatchings of the accelerometer scale factors and aligments, non linearities, bias drifts and noise. The gradiometer baseline being about one meter, the accelerometers must be designed in order to achieve a resolution of 5×10^{-12} ms$^{-2}/\sqrt{Hz}$.

To take advantage of such a performance, sufficient rejections of the disturbances, due to drag variations in particular, must be obtained for the differential accelerometric measurements. Accelerometer scale factors and alignments have to be accurately matched. For that purpose, sine wave calibrating accelerations are applied by means of two pairs of unbalanced wheels rotating at constant angular velocities. Synchronous demodulations of the accelerometer outputs at the angular frequencies of the wheels provide the information necessary for the estimations of the deviations. The expected accuracies are 10^{-5} for scale factor matchings and 10^{-5} rad for alignments.

Nevertheless, the instrument being accommodated on board a non drag free and Earth pointed satellite, the acceleration in the along track direction $\vec{x}$ is about 10^{-4} ms^{-2} with variations that can reach 6 % for periods less than 200 s. In these conditions, it appears hopeless to obtain a resolution of 10^{-2} Eötvös in the direction $\vec{x}$. Thus, for the ARISTOTELES mission, the gradiometer is composed of four accelerometers located at the corners of a square in the plane $(\vec{y}, \vec{z})$ perpendicular to the drag. With this configuration, the diagonal component T_{yy} ($\vec{y}$ cross-track direction) can be directly measured; the variations of $[\Omega^2]$ must be rejected for the determination of T_{zz}; T_{yz} is very sensitive to the variations of the roll angle.

3. GRADIO ACCELEROMETER PRE-DEVELOPMENT

This 3-axis accelerometer is based on the electrostatic suspension of a cubic proof-mass which is maintained motionless with respect to a set of electrodes forming a cage around it [Bernard, 1987]. The accelerometric measurements are derived from the drive voltages, applied to the electrodes in order to control the six degrees of freedom of the suspended mass.

GRADIO benefits of the experience acquired in ONERA with the CACTUS accelerometer [Boudon et al, 1978; Bernard et al, 1982] and with further studies of 3-axis electrostatic accelerometers supported by the french ministry of Defence (DRET) and Space Agency (CNES) [Bernard et al, 1985].

The GRADIO accelerometer is designed in order to insure preliminary tests under normal gravity conditions: the vertical axis (drag direction on orbit) is less sensitive but permits the electrostatic suspension of the proof-mass on ground.

Experimental feasability studies have been performed since 1986 with suspensions of 70 gram proof-masses made in silica. The horizontal axes of these laboratory models have, on ground, a measurement full scale range of 10^{-3} G.

A pendulum bench has been realized in order to preserve the accelerometers from the seismic noise in the laboratory. A soft environment of about 10^{-8} G r.m.s in a 0.1 Hz bandwidth is achieved.

The on ground testing of the 2 sensitive horizontal axes is nevertheless, limited by any variation of the coupling with the vertical axis or of the accelerometer orientation. Because of these limitations and of the necessity of testing the final configuration for flight, tests in the ONERA drop tower facility will have also to be performed under microgravity conditions.

In 1988, the pre-development of the GRADIO accelerometer has been undertaken under ESA contract. The design has been optimized to meet the requirements while insuring the compatibility with the on ground testing. The proof-mass is made in platinum-rhodium alloy: its mass is 320 grams for a size of 4 x 4 x 1 cm. The high density minimizes the disturbances due to non gravitational forces. The electrode set, obtained by ultrasonic machining and grinding of three silica plates, exhibits a high geometrical stability.

The feasability of the electrostatic suspension of such an heavy proof-mass under 1 G is demonstrated. The manufacturing of two models is on going and differential tests, rejecting the residual seismic noise, will be done to evaluate their performances.

4. CONCLUSION

The first step of the GRADIO accelerometer development has been achieved through the electrostatic suspension of a 300 gram proof-mass, on ground.

By maintaining our efforts in the next years, the first space gravity gradiometer can be developed for a Solid Earth mission at mid-nineties.

REFERENCES

Balmino G., Letoquart D., Barlier F., Ducasse M., Bernard A., Sacleux B., Bouzat G., Runavot J.J., Le Pichon X., Souriau M., Bull. Géod. 58, pp. 151-179, 1984.

Balmino G., Bernard A., Satellite Gradiometry, Proceedings of an ESA Workshop SESAME, Ising-am-Chiemsee, 1986.

Bernard A., Gay M., Juillerat R., The accelerometer CACTUS, AGARDograph n° 254, 1982

Bernard A., Sacleux B., Touboul P., GRADIO: Orbital Gravity Gradiometry through differential Microaccelerometry, IAF, Budapest, 1983.

Bernard A., Foulon B., Le Clerc G.M., Three-axis electrostatic accelerometer, Symposium Gyro Technology, Stuttgart, 1985.

Bernard A., Triaxial electrostatic accelerometers developed at ONERA, Rech. Aérosp., n° 1987-6, 1987.

Boudon Y, Bernard A., Barlier F., Juillerat R., Mainguy A.M., Walch J.J., Synthèse des résultats en vol de l'accéléromètre CACTUS pour des accélérations inférieures à 10^{-9} g, IAF, Dubrovnik, 1978.

Runavot J.J., Bouzat C., Bernard A., Sacleux B., Acta Astronautica, vol. 10, n° 9, pp. 599-607, 1983.

HIGH RESOLUTION ANALYSIS OF SATELLITE GRADIOMETRY

O.L. Colombo

EG&G, WASC, Inc., Lanham, Maryland, U.S.A.

N90-20561

ABSTRACT

Satellite gravity gradiometry is a technique now under development which, by the middle of the next decade, may be used for the high resolution charting from space of the gravity field of the earth and, afterwards, of other planets. This paper reviews some data analysis schemes for getting detailed gravity maps from gradiometry on both a global and a local basis. It also presents estimates of the likely accuracies of such maps, in terms of normalized spherical harmonics expansions, both using gradiometry alone and in combination with data from a Global Positioning System (GPS) receiver carried on the same spacecraft. It compares these accuracies with those of current and future maps obtained from other data (conventional tracking, satellite-satellite tracking, etc.), and also with the spectra of various signals of geophysical interest.

1. INTRODUCTION

A gravity gradiometer placed in a low, polar, near-circular orbit, will provide within a few months a fine global sampling of the gravity field. From such data, high resolution maps of the anomalous field (through 100 km half-wavelength) are expected, if the accuracy of each component of the gravity tensor measured by the instrument is of the order of 0.01 Eötvos or better (this means detecting a change of 10^{-12} m/sec^2 in gravity acceleration over a 10 cm distance). Both the level of resolution and the homogeneous quality of the results worldwide are beyond what can be obtained by any other space technique, except altimetry. It will have the advantage over altimetry of not being restricted to the oceans and of being more accurate at mid- and long-wavelengths, although fine resolution is likely to be considerably poorer. These conclusions follow from a number of studies (Balmino, 1985, NASA Gravity Workshop, 1987, Colombo, 1987, ESA Report, 1988, etc.). Those studies suggest that the gravitational effects of major oceanographic and geophysical features (such as global ocean circulation, mantle convection, spreading and subduction zones, etc.) could be charted with uncertainties of the order of 10% of their values at the earth's surface. The global character of the data offers the possibility of studying large areas now poorly known (Antarctica, the Artic, parts of South America and Africa), and also regions from which reliable information is not readily available (much of Asia). Employing gradiometers to chart the gravitational fields of other planets and their moons is a further step to take, once the major ones of building and using an earth-mapping instrument have succeeded.

2. DATA ANALYSIS

A successful gradiometer mission should collect millions of measurements over several months. To represent gravity worldwide to the expected resolution of better than 100 km, in the order of 100000 parameters have to be estimated, regardless of the type of base functions used (as long as they are generic functions, such as spherical harmonics, point masses, mean anomalies, and so on). There are two main categories of maps to be considered: global and local. A global map represents the field over the whole earth; a local map, the field over a limited region. Both kinds are complementary: a global map can be used for studies of the planet as a whole; its resolution may be less than the maximum allowed by the data, because the largest number of parameters that can be estimated in practice may not be enough to represent the smallest details everywhere. A local map may reach that maximum resolution over a limited area, because only enough parameters for this geographically restricted representation are needed. A good global map may be used to eliminate trends from the data employed in local maps, to help distinguish small details. Efficient schemes for analysing data, whether global or local, can exploit the uniform geographical distribution of the measurements resulting from the gradiometer's sampling of the field at regular intervals along an orbit with a repeating groundtrack. Such an orbit, with a repeat period comparable to the duration of the mission, provides the finest, most even coverage possible over that period.

2.1 Global Maps

The two most laborious numerical operations involved in estimating the parameters of a global gravity map by a least squares procedure are the formation and the inversion of the normal matrix of the estimator. With a repeating orbit, a regular, uninterrupted sampling of the field by a gradiometer, and the use as base functions of uniformly spaced point masses, or gravity anomalies, or else of spherical harmonics, the elements of the normal matrix can be calculated directly by analytical expressions (instead of being accumulated observation by observation). The matrix also has a very strong structure that allows its fast inversion and

limits roundoff error propagation, in spite of its enormous size (order of 10^{10} elements). This structure may be block-diagonal, and very sparse (with spherical harmonics), or block-Toeplitz circulant, and highly redundant, (with gridded point masses and mean anomalies). In the case of spherical harmonics, the block-diagonal structures occur when the potential coefficients are separated first by order, then by parity (sine or cosine). For a perfectly circular orbit, a third symmetry exists: that of harmonics where n-m is even versus those where n-m is odd (n is the harmonic degree and m the order). This type of structure, as well as the block-Toeplitz one, is not exclusive to gradiometry, but arises whenever these base functions are used together with equispaced gravity data sampled along a repeating orbit. They are discussed in Colombo (1981), (1984), and (1987), and in Wagner (1983). In the case of spherical harmonics, the representation of the potential along a repeating orbit is a Fourier series with the same repeat period as the orbit; in this series, harmonics of different orders, parities, etc., have no common frequencies. This causes many columns of the matrix of observation equations associated with the potential coefficients to become orthogonal when the sampling rate is much higher than the frequency content in the signal. It is also necessary to take care of time-varying components of the signal that do not share the periodicity of the orbit. As explained in Colombo (1984), most of the orbital perturbations due to the anomalous gravity field repeat with the orbit (so they are "geographically correlated": they are the same every time the spacecraft passes over the same place, in each successive repeat). There are, however, deep resonant perturbations (caused mostly by the zonals) that will vary from one repeat to the next; there are also rotational effects, instrumental drift, etc., that lack this periodicity. They can be accomodated by means of additional parameters associated with suitable non-periodical time functions, to be estimated together with the potential coefficients. The result, for spherical harmonics, is an "arrow" normal matrix, as shown in Figure 1. The two edges of the "arrowhead" are non-zero elements associated with both potential coefficients and with the additional parameters; the "shaft" of the arrow is a string of diagonal blocks of decreasing size associated with the potential coefficients alone. This matrix can be inverted efficiently and accurately by the method explained in Colombo (1984).
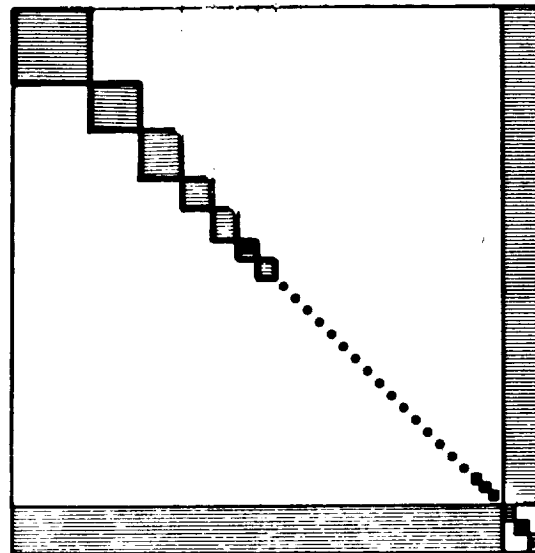

Figure 1. Sparse "arrow" structure of the normal matrix of spherical harmonic potential coefficients for a repeating orbit. White areas show location of zero elements.

2.2 Local Maps

If the data has been sampled without significant interruptions (a few small gaps can be filled by simple interpolation, to restore symmetry, without significant degradation of results), a variety of efficient data analysis techniques can be used; a few examples of these are given here. By separating ascending from descending passes, and chosing a region with parallels of latitude as the northern and southern limits, and groundtracks of passes as the eastern and western edges, equispaced points along the remaining passes define a twisted regular grid on this region. Using this grid to place the point masses or mean anomalies of a local representation leads to an adjustment of their values where the normal matrix is block-Toeplitz. Moreover, in equatorial regions, for sufficiently small areas (where the tracks are virtually straight and parallel, and the earth can be treated as flat), two-dimensional Fourier expansions can be used to represent the field, and fast Fourier transform procedures implemented to estimate the parameters of the local maps.

Mission analyses based on a global data coverage using instruments measuring several components of the gravity tensor over a six-month period, with sampling/averaging data rates of a few seconds, indicate that the sensitivity of the gradiometer initially increases with wavelength, as one would expect from the frequency response of a twice-differenced process (the gravity potential), and then decreases as the spectrum of the potential decays nearly exponentially with frequency, primarily due to the effect of altitude. The spherical harmonic representation of the field has been used in all cases, assuming equispaced measurements along a circular, polar, repeating orbit, to use the efficient methods outlined in section 2.1 for setting up and inverting the normal matrix to obtain the variance-covariance matrix of the estimated potential coefficients.

Figure 2 shows the accuracy of the coefficients estimated with data from a 0.01 Eötvos (E) instrument with a 4 second sampling/averaging rate. A number of spurious effects, mostly of low frequency, such as: orbit errors, instrumental drift, effects of rotation, attitude error, etc., have been supposedly removed by filtering out all information below three cycles per orbital revolution (i.e., only signal with periods shorter than 30 minutes is left). This leads to conservative error estimates. For the gradiometer, two curves, one for an accuracy of 0.01 E, and another of 0.0001 E (the expected accuracy of the supercooled instrument under development for NASA by Ho Paik at the University of Maryland) are shown. Both indicate an initial steep increase in sensitivity, followed by a botttoming-out at about degree 90, and experiencing a nearly exponential increase (approximately straight line in the linear-log graphs shown here) beyond degree 200. The divided curve marked "0.01 E+GPS, best and worst cases" corresponds to the combination of the gradiometer measurements with GPS tracking data in the estimation of the gravity field model. This assumes that a GPS receiver is carried on board of the gradiometer satellite, and that it tracks continuously the GPS spacecraft from the full constellation, simultaneously with a ground GPS network of some 10 globally distributed stations (in order to correct the GPS clocks and orbits, as well as the satellite receiver clock, by double differencing of observations (Yunk et al., 1985)). This not only strengthens the gravity field solution at low degrees (here, through degree 30), but also helps the operation of the ground network (primarily set up for geophysical experiments on geodynamics, according to current expectations for the 1990's) by reinforcing the geodetic connections between the widely separated stations. In this way, two different geodetic and scientific tasks can be combined to mutual advantage. The "worst case", upper curve, assumes large orbit errors, and considerable unresolved carrier-phase biases (order of 10 cm). The "best case", lower curve, corresponds to the ideal situation of no orbit errors either for GPS or for the gradiometer satellite, and no unresolved biases. (For further details on the GPS calculations, see extended abstract on GPS/GP-B by Smith et al., in this issue.) In general, the assumptions were: both the L1 and L2 frequencies are used, with carrier-phase and pseudorange measured; up to seven GPS satellites simultaneously visible from the lower satellite at all times; average GDOP of 3; data corrected for ionospheric refraction and then double differenced; assumed measurement noise: 1 cm for carrier-phase, and 10 cm for pseudorange (after fifteen minutes averaging) in the worst case; 1 cm for carrier-phase, and zero cm for pseudorange in the best case.

Clearly, GPS data and gradiometry complement each other, as the former is more sensitive to lower frequencies, and the latter to higher ones. The 0.0001 E curve is the same as for 0.01 E, but shifted down two decades. At the top of Fig. 2, the broken curve represents the power spectrum of the anomalous field, or full spectrum of the signal. Where the plot of the accuracies of the spherical harmonics intersects this spectrum, signal and noise are equal, and this is usually adopted as the point of highest recoverable frequency. For the 0.01 instrument, this point happens at about degree 360, for a half wavelength of some 70 km.

Figure 3 shows the curves for gradiometry/GPS of Figure 2 against the published accuracies of current, low resolution models such as GEM-T1 (top left corner), and those expected for the improved models planned for the early 1990's, which will include satellite altimetry as well as conventional satellite tracking data. Improvements over such models from the combination of GPS data and gradiometry are shown to be about two orders of magnitude in accuracy, and nearly one order of magnitude in resolution (fields like GEM-T1 and its planned successors are limited to resolutions of some 400 km half wavelength). Also plotted are the accuracies expected from the superconducting gradiometer (0.0001 E) and from satellite-satellite radio-tracking systems like the one designed for the now shelved GRM mission. Figure 3 suggests that a 0.01 E instrument will be better than GRM for features with a harmonic content above degree 120 (i.e., 180 km half wavelength).

The curve at the top of Figure 4 is the spectrum of the stationary sea surface topography (based on the work of Levitus on global circulation). Also shown is the spectrum of the M2 ocean tide based on the model of Schwiderski, and that of changes in the field over the length of the mission due to post-glacial crustal rebound and sea level adjustment. The plots indicate that major ocean tides can be estimated accurately (in fact, due to orbital resonances not considered in the calculations, tides can be estimated better than suggested here). Post-glacial rebound is barely observable over six months with a 0.01 E instrument, and a 0.0001 E device may

be required for its study. The geoid calculated from gradiometry should be good enough to separate most of the stationary ocean topography from the mean sea surface determined with satellite altimetry.
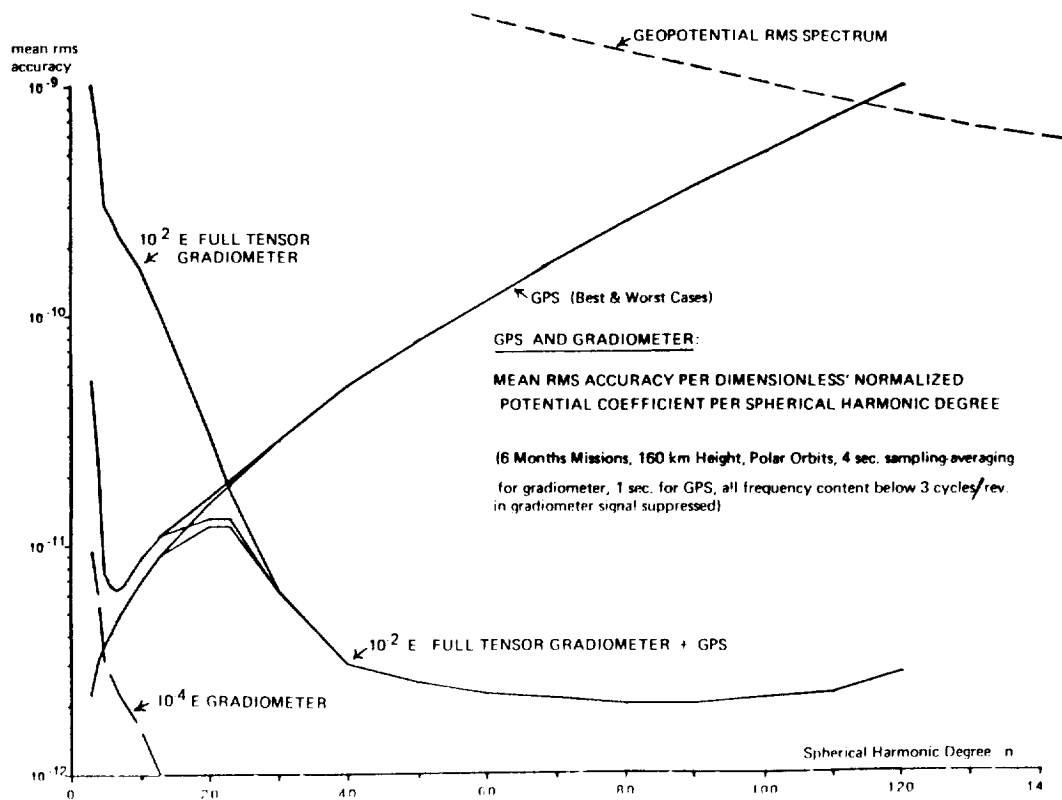

Figure 2. Accuracy per estimated potential coefficient per spherical harmonic degree (the spherical power spectrum of the coefficient errors).
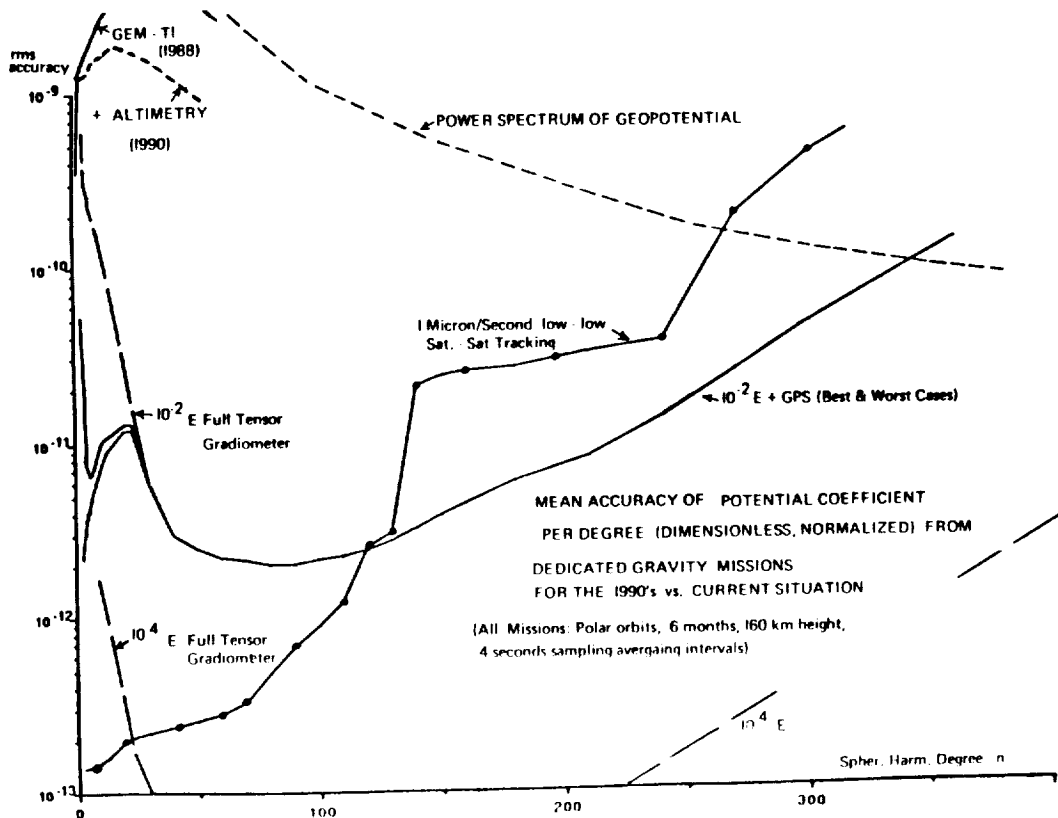

Figure 3. Accuracies of potential coefficients estimated from gradiometry and GPS, compared to present and future results derived from other data.
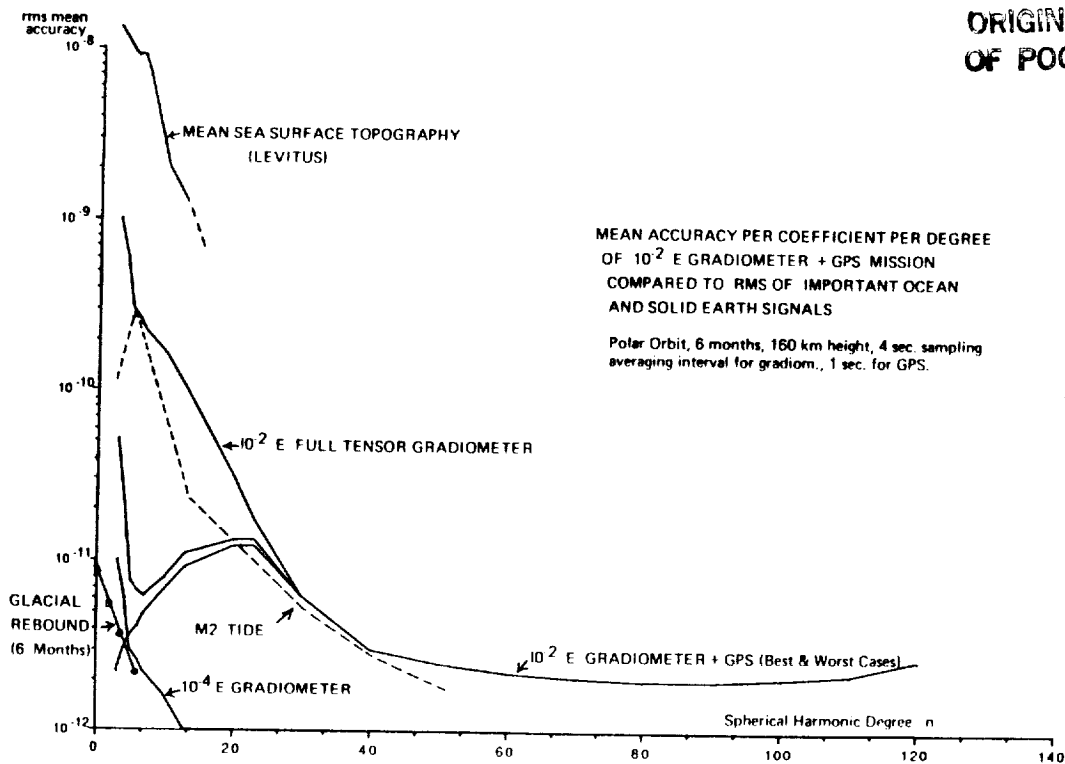
191

Figure 4. Comparing the accuracies of potential coefficients recovered from gradiometry, alone and in combination with GPS data, to the spectra of various phenomena of interest in oceanography and solid earth geophysics.

4. CHARTING THE GRAVITY FIELDS OF OTHER MEMBERS OF THE SOLAR SYSTEM

Gravity and topography can be mapped from space by means of gradiometry and altimetry; jointly, they can help identify the geological structures underlying the surface of a planet. Devices such as radar altimeters and gravity gradiometers may be carried in future space probes destined to orbit other members of the solar system, including the moons of the major planets. Because very little is known about those celestial bodies, instruments many times less sensitive than those needed to gain new information on the earth, may provide nevertheless a wealth of new knowledge. Since many planets and moons have little or no atmosphere, expensive, heavy, complex drag-compensating systems are largely unnecessary, and spacecraft can stay in lower orbits for longer periods than in Earth. Many planets are smaller than our own, but their geophysical features are of the same size or even larger than those on Earth. All these factors tend to compensate for any loss in instrument sensitivity caused by the more stringent limits on weight, size, volume, power consumption, durability, and cost, as well as from a less benign enviroment (e.g., equipment with moving parts in close proximity, etc.), likely to characterize interplanetary missions.

REFERENCES

Colombo, O.L., The Ohio State University, Dept. Geod. Sc. and Surv., Report 310, Columbus, Ohio, 1984.

Colombo, O.L., Netherlands Geodetic Comission, Publications in Geodesy, New Series, Vol. 7, No. 3, Delft, Holland, 1984.

Colombo, O.L., Proceedings IUGG XIX General Assembly, Vancouver, August 1987.

Balmino, G., et al., SESAME report, Executive Summary for ESA, September 1985.

NASA Gravity Worshop, Colorado Springs, Colorado, February 1987.

ESA Executive Report on Aristoteles: A european solid earth mission, Noordwijk, Holland, July 1988.

Wagner, C. A., J.Geophys. Res., Vol. 88, pp. 10309-10322, 1983.

Yunk, T.P, Melbourne, W., C.L. Thorton, IEEE Transactions on Geoscience and Remote Sensing, Vol. GE-23, 4, pp. 450-457, July 1985.

Registrants List
(addresses as of the meeting date)

Trevor Frederick Baker
Proudman Oceanographic Lab
Bidston Observatpru
Birkenhead, Merseyside L43 7RA
England
51-653-8633

Rudolf Benz
Widdum 12
Immenstaad 7997
FR of Germany
7545-81-3250

George Blaha
280 Flamingo Drive
Melbourne Beach, Florida 32951

William D. Braswell
Nichols Research Corp.
P. O. Box 14190
Huntsville, Alabama
205-883-1140

Thomas Camarda
DMA Aerospace Center
Attn: DSG, 3200 South 2nd St.
St. Louis, Missouri
314-263-8462

Ruey-Gang Chang
Rm-4, 7th Fl., No. 100
Fu Kuo Rd., Shih Lin
Taipei, 11121
R.O.C.
02-8340231

Brion Conklin
Bendix Field Engineering Corp.
5719 Rowanberry Dr.
Baltimore, Maryland
301-796-7839

B. Louis Decker
DMA Systems Center/WG
3200 South Second Street
St. Louis, Missouri
314-263-4916

Alan Henry Dodson
University of Nottingham
University Park
Nottingham NG7 2RD
England
602-484848, Ext. 2667

Robin E. Bell
Lamont Doherty Geological Obs.
Palisades, New York
914-359-2900

Alan Bernard
Office National d'Etudes et de Recherches
Aerospatiales
BP72, 92322 Chatillion Cedex
France

Claude Boucher
IGN
2 Avenue Pasteur
St. Mande 94160
France
43741215

John M. Brozena
Naval Research Laboratory
NRL Code 5110
Washington, D. C. 20375-5000
202-767-2024

Archie E. Carlson
Defense Mapping Agency
6500 Brooks Lane
Washington, D.C.
202-227-2152

Oscar L. Colombo
EG&G (WASC) Inc.
5000 Philadelphia Way, Suite J
Lanham, Maryland
301-731-2044

P.A. Cross
Univ. of Newcastle Upon Type
Dept. of Surveying
Newcastle Upon Type NE1 7RU
United Kingdom
091-232-8511, ext. 6348

Heiner Denker
University of Hannover
Institut fuer Ermessung
Nienburger Str. 6
Hannover D-3000
F.R. of Germany
0511-762-3452

Eric F. Engbrecht
MEGA RET, Inc.
1526 North Yeso Circle
P.O. Box 2387
Hobbs, New Mexico
505-393-2464

Registrants List
(addresses as of the meeting date)

C. W. Francis Everitt
Relativity Gyro Program
Stanford University
Via Palou at Serra
Stanford, CA
415-725-4128

Thomas L. Fischetti
Tech. Management Consultants, Inc.
2609 Village Lane
Silver Spring, Maryland
301-871-2425

Rene Forsberg
Geodetic Institute
Gamlehave Alle 22
Charlottenlund 2920
Denmark
45-1631833

Sara Gerrard
University of Nottingham
University Park
Nottingham NG7 2RD
England
602-484848 ext. 2638

Roswitha Grannell
California State Univ., Long Beach
Dept. of Geological Science
Long Beach, California
213-985-4927 or 4809 (msg.)

Bradford H. Hager
California Institute of Technology
Seismologial Laboratory
Pasadena, California
818-356-6938

John C. Harrison
Geodynamics Corp.
5520 Ekwill Street, Suite A
Santa Barbara, California
805-964-2814

Warren G. Heller
The Analytic Sciences Corp. (TASC)
55 Walkers Brook Drive
Reading, Massachusetts 01867
617-942-2000, ext. 2147

Christopher Jekeli
Air Force Geophysics Lab
LWG/Hanscom AFB
Bedford, Massachusetts 01731
617-377-5255

James E. Faller
University of Colorado; JILA
Campus Box 440
Boulder, Colorado
303-492-8509

Edward Flinn
NASA Headquarters
Mail Code EEG
Washington, D.C.
202-453-1675

Rudolf J. Fury
National Geodetic Surveying
11400 Rockville Pike, Room 107
Rockville, Maryland
301-443-3122

Peter Graebner
Chevron Oil Field Res. Co.
1300 Beach Blvd.
La Habra, California
213-694-7435

Erwin Groten
Technology University
IPG, Petersenstrasse 13
Darmstadt
F.R. Germany
06151-163109

Sigmund Hammer
University of Wisconsin
110 S. Henry Street, Apt. 406
Madison, Wisconsin
608-251-3084

Guenter W. Hein
Institute of Astronomical & Physical Geodesy
University FAF Munich,
Werner Heisenberg-Weg 39
Neubiberg D-8014
F.R. Germany
89-6004-3425

James Richard Huddle
Litton Guidance & Control Systems
5500 Canoga Avenue, MS 67/35
Woodland Hills, California
818-715-3264

Majid Kadir
Surveying Department
University of Technology, Malaysia
Gurney Road
Kuala Lumpur, Malaysia 15-01

Registrants List
(addresses as of the meeting date)

William M. Kaula
Univ. of California, Los Angeles
Dept. of Earth and Space Sciences
Los Angeles, California
213-825-4363

Kevin Michael Kelly
Ontario Ministry of Natural Resources
90 Sheppard Ave. East, 4th Floor
North York, Ontario
Canada
416-733-5138

Yeong E. Kim
Purdue University
Dept. of Physics
West Lafayette, Indiana
317-494-3042

Steven Klosko
EG&G
5000 Philadelphia Way
Lanham, Maryland
301-731-2044

Francis J. Lerch
NASA/Goddard Space Flight Center
Code 621
Greenbelt, Maryland 20771
301-286-5005

Andre Mainville
Geodetic Survey of Canada
615 Booth Street
Ottawa
Canada
613-995-4345

David C. McAdoo
N/GS/NOAA
N/CG113, 11400 Rockville Pike
Rockville, Maryland
301-443-8528 or 8529

Peter J. Melvin
Naval Research Laboratory
4555 Overlook Avenue, S.W.
Washington, D.C.
202-767-1899

Dennis G. Milbert
National Geodetic Survey
Code N/CG113, Rm 513
11400 Rockville Pike
Rockville, Maryland 20852
301-443-8528

Arthur Harry William Kearsley
University of New South Wales
School of Surveying, P.O. Box 1
Kensington, New South Wales 2033
Australia
2-697-4188

Paul M. M. Kieniewicz
Exxon Co. Intl.
P.O. Box 146
Houston, TX 77001-0146
713-973-3289

Robert W. King
M.I.T.
Dept. of Earth, Atmospheric and Planetary Sciel
Cambridge, Massachusetts
617-253-7064

Andrew R. Lazarewicz
Air Force Geophysics Laboratory
AWG, Hancom AFB
Bedford, Massachusetts 01731
617-377-5255

Alphonse S. Lwangasi
University of Nairobi
P.O. Box 30197
Nairobi
Kenya 334244

James Marsh
NASA/Goddard Space Flight Center
Code 621
Greenbelt, Maryland 20771
301-286-5324

William Melbourne
Jet Propulsion Laboratory
4800 Oak Grove Drive
Pasadena, California 91109

Burkhard Middel
Stuttgart University
Dept. of Geodetic Science
Keplerstr. 11
Stuttgart D-700
F.R. Germany
071-121-28187

Tilman Muller
Universitat Karlsruhe
Geodatisches Institut
Englerstrasse 7
Karlsruhe D-7500
F.R. Germany

Dezso Nagy
Geological Survey of Canada
1 Observatory Crescent
Ottawa, Ontario
Canada

Robert Steven Nerem
University of Texas, Austin
Center for Space Research
Austin, Texas 78712
512-471-5573

Mrinal Kanti Paul
Geological Survey of Canada
1 Observatory Crescent
Ottawa Ontario
Canada
613-992-9713

George Peter
NOAA/NH Geographic Survey
11164 Boat House Court
Reston, Virginia 22090
703-391-7386

C. H. Poitevin
Observatoire Royal de Belgique
Avenue Circulaire 3
Bruxelles B-1180
Belgium
2-375-2484

Christopher Reigber
DGFI
Marstallplata 8
Muenchen 22
F.R. Germany
089/23037 706

John W. Robbins
EG&G/WASC Inc.
500 Philadelphia Way, Suite J
Lanham, Maryland
301-731-2044

George Rosborough
University of Colorado
Campus Box 429
Boulder, Colorado
303-492-6721

Byron D. Ruppel
U.S. Geological Survey
345 Middlefield Road, MS 999
Menlo Park, California
408-336-8459

Kenneth Nelson
DMA Aerospace Corp.
3200 South Second Street
St. Louis, Missouri
314-263-8410

F. Nouel
CNES
18 Avenue E. Belin
Toulouse 31055
France
61-27-40-67

Nikolaos K. Pavlis
The Ohio State University
1958 Neil Avenue, #404
Cockins Hall
Columbus, Ohio 43210-1247
614-292-6753

Mary Peters
Naval Research Laboratory
4555 Overlook Avenue, S.W.
Washington, D.C.
202-767-2024

Richard H. Rapp
The Ohio State University
Department of Geodetic Science & Surveying
Columbus, Ohio 43210-1247
614-292-6005

Nicholas A. Renzetti
Jet Propulsion Laboratory
4800 Oak Grove Drive
Pasadena, California 91109
818-354-4517

Anestis Romaides
Air Force Geophysics Lab
Hanscom Air Force Base
Bedford, Massachusetts 01731
617-377-3486

Reiner Rummel
Delft University of Technology
Faculty of Geodesy, Thijsseweg 11
JA Delft 2629
The Netherlands
015-785100

Richard Sailor
TASC
55 Walker's Brook Drive
Reading, Massachusetts 01867
617-942-2000

Registrants List
(addresses as of the meeting date)

Fernando Sanso
Instituto di Topografia
Fotogrammetria E. Geofiscia
20133 Piazza Leonardo da Vinci, 32
Milano
Italy

K. P. Schwarz
University of Calgary
2500 University Drive
Dept. of Surveying Engineering
Calgary, Alberta
Canada
403-220-7378

Charles Shaw
U.S. Navy Oceanographic Office
Stennis Space Center
Bay St. Louis, Mississippi
601-688-4378

Michael G. Sideris
The University of Calgary
2500 University Drive, N.W.
Dept. of Surveying Engineering
Calgary, Alberta
Canada
403-220-5874

David E. Smith
NASA/Goddard Space Flight Center
Code 621
Greenbelt, Maryland 20771
301-286-8555

James Strauss
U.S. Navy Oceanographic Office
Stennis Space Center
Bay St. Louis, Mississippi
601-688-4378

Bryon D. Tapley
University of Texas at Austin
Center for Space Research, WRW 402
Austin, Texas 78712
512-471-1356

C.C. Tscherning
Geodetic Institute of Denmark
Gamlehave Alle 022
Charlottenlund
Denmark
45-631833

Hermanus Gerhardus van Gysen
University of Natal
Department of Surveying
King George V. Avenue
Durban
South Africa
031-8161152

Bob Schutz
University of Texas at Austin
Center for Space Research, WRW 402
Austin, Texas 78712
512-471-1356

P. C. Sellers
University of Newcastle Upon Tyne
Dept. of Surveying
Newcastle Upon Tyne NE1 7RU
United Kingdom
091-232-8511, ext. 7833

C. K. Shum
University of Texas, Austin
Center for Space Research
Austin, Texas 78712
512-471-5573

Lars E. Sjoberg
The Royal Institute of Technology
Stockholm S-10044
Sweden
468-7907330

Dag Solhein
Geodetic Institute
Gamlehave Alle 022
Charlottenlund DK2920
Denmark

G. Strykowski
Geodetic Institute of Denmark
Gamlehave Alle 022
Charlottenlund
Denmark

Patrick T. Taylor
NASA/Goddard Space Flight Center
Code 622
Greenbelt, Maryland 20771
301-286-5412

Triveni Upadhyay
Mayflower Communications Co.
384 Lowell Street, Suite 106
Wakefield, Massachusetts
617-245-8100

Petr Vaniček
University of New Brunswick
P.O. Box 4400
Fredericton, New Brunswick
Canada
506-543-5144

Registrants List
(addresses as of the meeting date)

Anthony A. Vassiliou
Mobil Res. and Development Corp.
13777 Midway Road
Dallas, Texas 75244
214-851-8801

Karel F. Wakker
Delft University of Technology
Faculty of Aerospace Engineering
Kluyverweg 1
Delft 2629-HS
The Netherlands
31-15-782065

Zhao Wei
California State University, Long Beach
Department of Geological Sciences
Long Beach, California
213-985-4927

Pascal Willis
IGN
2 Avenue Pasteur
St. Mande 94160
France
43741215

Dah-Ning Yuan
University of Texas, Austin
Center for Space Research
Austin, Texas 78712
512-4871-5573

Paul A. Zucker
Johns Hopkins Applied PHysics Lab.
Johns Hopkins Road
Laurel, Maryland
301-953-5000, ext. 4971

John Wahr
University of Colorado
Department of Physics
Boulder, Colorado
303-492-8349

Yan Ming Wang
Ohio State University
1958 Neil Avenue
408 Cockins Hall
Columbus, Ohio 43210-1247
514-292-6795

Ronald G. Williamson
EG&G
18012 Highfield Road
Ashton, Maryland
731-2044

Jiun-tsong Wu
Jet Propulsion Laboratory
MS 238-640, 4800 Oak Grove Drive
Pasadena, California 91109
818-354-8296

Victor Zlotnicki
JPL/Caltech
4800 Oak Grove Drive/MS 300-323
Pasadena, California 91109
818-354-5519

Joseph Zund
New Mexico State University
Las Cruces, New Mexico
505-646-3901